NUCLEIC ACID POLYMERASES: THE TWO-METAL-ION MECHANISM AND BEYOND,

2nd Edition

EDITED BY: Janice Pata, Indrajit Lahiri and Whitney Yin

PUBLISHED IN: Frontiers in Molecular Biosciences

frontiers Research Topics

ISSN 1664-8714
ISBN 978-2-8325-0382-9
DOI 10.3389/978-2-8325-0382-9

About Frontiers

Frontiers is more than just an open-access publisher of scholarly articles: it is a pioneering approach to the world of academia, radically improving the way scholarly research is managed. The grand vision of Frontiers is a world where all people have an equal opportunity to seek, share and generate knowledge. Frontiers provides immediate and permanent online open access to all its publications, but this alone is not enough to realize our grand goals.

Frontiers Journal Series

The Frontiers Journal Series is a multi-tier and interdisciplinary set of open-access, online journals, promising a paradigm shift from the current review, selection and dissemination processes in academic publishing. All Frontiers journals are driven by researchers for researchers; therefore, they constitute a service to the scholarly community. At the same time, the Frontiers Journal Series operates on a revolutionary invention, the tiered publishing system, initially addressing specific communities of scholars, and gradually climbing up to broader public understanding, thus serving the interests of the lay society, too.

Dedication to Quality

Each Frontiers article is a landmark of the highest quality, thanks to genuinely collaborative interactions between authors and review editors, who include some of the world's best academicians. Research must be certified by peers before entering a stream of knowledge that may eventually reach the public - and shape society; therefore, Frontiers only applies the most rigorous and unbiased reviews.
Frontiers revolutionizes research publishing by freely delivering the most outstanding research, evaluated with no bias from both the academic and social point of view. By applying the most advanced information technologies, Frontiers is catapulting scholarly publishing into a new generation.

What are Frontiers Research Topics?

Frontiers Research Topics are very popular trademarks of the Frontiers Journals Series: they are collections of at least ten articles, all centered on a particular subject. With their unique mix of varied contributions from Original Research to Review Articles, Frontiers Research Topics unify the most influential researchers, the latest key findings and historical advances in a hot research area! Find out more on how to host your own Frontiers Research Topic or contribute to one as an author by contacting the Frontiers Editorial Office: frontiersin.org/about/contact

NUCLEIC ACID POLYMERASES: THE TWO-METAL-ION MECHANISM AND BEYOND,
2nd Edition

Topic Editors:
Janice Pata, Wadsworth Center, United States
Indrajit Lahiri, Indian Institute of Science Education and Research Mohali, India
Whitney Yin, University of Texas Medical Branch at Galveston, United States

Dr. Satwik Kamtekar is currently an employee of Pacific Biosciences of California Limited and holds patents related to the theme of the Topic. All other Topic Editors declare no competing interests.

Publisher's note: In this 2nd edition, the Editorial has been added.

Citation: Pata, J., Lahiri, I., Yin, W., eds. (2022). Nucleic Acid Polymerases: The Two-Metal-Ion Mechanism and Beyond, 2nd Edition. Lausanne: Frontiers Media SA. doi: 10.3389/978-2-8325-0382-9

Table of Contents

frontiers | Frontiers in Molecular Biosciences

EDITORIAL
published: 13 July 2022
doi: 10.3389/fmolb.2022.948326

Editorial: Nucleic Acid Polymerases: The Two-Metal-Ion Mechanism and Beyond

Janice D. Pata[1,2]*, *Y. Whitney Yin*[3] *and Indrajit Lahiri*[4]

[1]Wadsworth Center, New York State Department of Health, Albany, NY, United States, [2]Department of Biomedical Sciences, School of Public Health, University at Albany, Albany, NY, United States, [3]Department of Biochemistry and Molecular Biology, University of Texas Medical Branch, Galveston, TX, United States, [4]Department of Biological Sciences, Indian Institute of Science Education and Research Mohali, Punjab, India

Keywords: DNA polymerase, RNA polymerase, reverse transcriptase, cellular polymerase, viral polymerase

Editorial on the Research Topic

Nucleic Acid Polymerases: The Two-Metal-Ion Mechanism and Beyond

Nucleic acid polymerases are essential for all forms of life, performing diverse functions from genome replication and repair to the transcription of a wide variety of RNAs. Although these enzymes differ widely in substrate specificity, efficiency, accuracy, and evolutionary origin, they all catalyze the same nucleotidyltransferase reaction. This eBook on "*Nucleic Acid Polymerases: The Two-Metal-Ion Mechanism and Beyond*" highlights both the similarities and differences among these enzymes.

The two-metal-ion catalytic mechanism for polymerases was proposed in 1993 by Thomas A. Steitz (Steitz, 1993), based on structural studies of the 3′-5′ exonuclease active site of the Klenow fragment of *E. coli* DNA polymerase I (Beese and Steitz, 1991; Beese et al., 1993) and mutagenesis of the polymerase active site (Polesky et al., 1992). Structural support for this mechanism came over the next several years, when crystal structures were determined with primer-template DNA and dNTP poised for catalysis at the polymerase active sites of several different DNA polymerases and HIV-1 reverse transcriptase (Pelletier et al., 1994; Doublié et al., 1998; Huang et al., 1998; Li et al., 1998). These and subsequent structures show that polymerases have two absolutely conserved aspartate residues that coordinate two divalent cations in the polymerase active site (**Figure 1A**), demonstrating that the two-metal-ion catalytic mechanism is also applicable to DNA synthesis (Brautigam and Steitz, 1998).

More recently, however, a three-metal-ion polymerase mechanism has been proposed based on time-resolved crystallographic studies of translesion and repair DNA polymerases eta and beta, respectively (Nakamura et al., 2012; Gao and Yang, 2016). In fact, Thomas Steitz had initially considered that a third metal ion might be involved (**Figure 1B**). In the first article in this eBook, Wang and Konigsberg review the effects of pH and Mg^{2+} concentration on high-fidelity DNA polymerase activity and argue that the three-metal-ion mechanism may not be universal to all polymerases, suggesting instead that the third metal ion stabilizes pyrophosphate binding after catalysis and thus slows product release (Wang and Konigsberg, 2022).

The review of viral RNA-directed RNA polymerases by Gong highlights the complexities of the nucleotide incorporation cycle, including conformational changes that accompany nucleotide binding and pyrophosphate release, polymerase translocation along the template that is required for processive synthesis, and events outside of the standard catalytic cycle that can impact the fidelity of replication (Gong, 2021).

Carvajal-Maldonado provide a comprehensive review of the other catalytic activities that are frequently associated with DNA polymerases: 3′-5′ exonuclease proofreading that increases replication fidelity, structure-specific 5′-nuclease activity required for Okazaki fragment

Edited and reviewed by:
Adrian Goldman,
University of Helsinki, Finland

***Correspondence:**
Janice D. Pata
janice.pata@health.ny.gov

Specialty section:
This article was submitted to Structural Biology, a section of the journal Frontiers in Molecular Biosciences

Received: *19 May 2022*
Accepted: *16 June 2022*
Published: *13 July 2022*

Citation:
Pata JD, Yin YW and Lahiri I (2022) Editorial: Nucleic Acid Polymerases: The Two-Metal-Ion Mechanism and Beyond. Front. Mol. Biosci. 9:948326. doi: 10.3389/fmolb.2022.948326

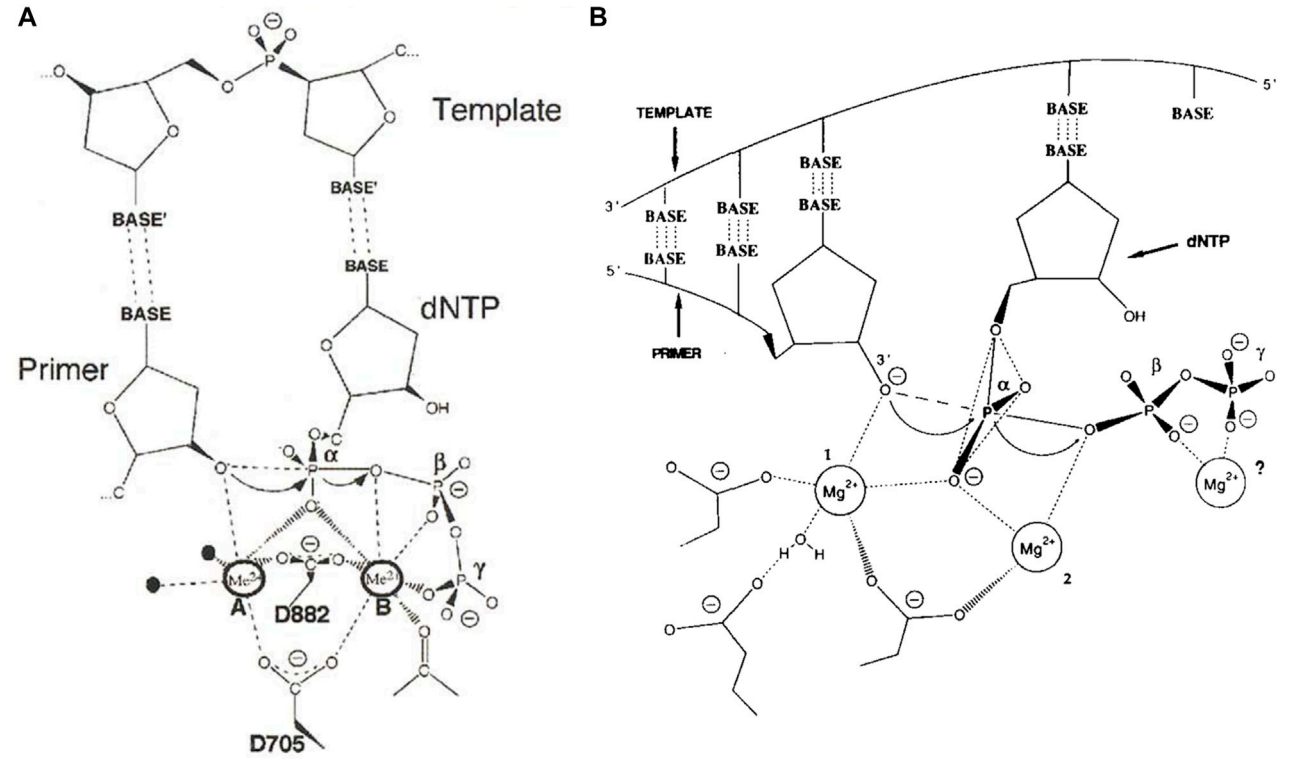

FIGURE 1 | The two-metal-ion catalytic mechanism for nucleic acid polymerases **(A)** Two universally conserved aspartate residues (numbering is for the Klenow fragment of *E. coli* DNA polymerase I) coordinate two divalent cations, usually Mg^{2+}, that facilitate deprotonation of the 3′-hydroxyl of the primer and stabilize the negative charges on the phosphates of the nucleotide and formation of the pentacovalent transition state. Figure is based on the structure of T7 DNA polymerase (Doublié et al., 1998) and is reproduced from Brautigam and Steitz (Brautigam and Steitz, 1998) with permission **(B)** The original mechanism proposed for polymerization based on the structure of the 3′-to-5′ exonuclease active site of Klenow fragment (Beese and Steitz, 1991). The possibility of a third metal ion binding to the beta and gamma phosphates was considered. Figure reproduced from Steitz (Steitz, 1993) with permission.

maturation during lagging strand synthesis, 5′dRP lyase activity required in the base excision repair pathway, and 3′-end-trimming and single-strand extension involved in double-strand break repair (Carvajal-Maldonado et al., 2021).

Kaszubowski and Trakselis focus on the challenges of coordinating multiple polymerases during translesion synthesis where a high-fidelity replicative DNA polymerase encounters DNA damage and is replaced by one of a number of possible specialized enzymes with lower fidelity that allow replication of damaged DNA (Kaszubowski and Trakselis, 2021). The review compares passive and active mechanisms for the handoff of DNA between the polymerases and discusses the role of the sliding clamp processivity factor.

Nucleic acid synthesis is a highly dynamic process and the review by Millar emphasizes how single-molecule Fluorescent Energy Transfer techniques have been able to elucidate the conformational changes that occur during the *E. coli* DNA polymerase I nucleotide incorporation cycle and as the DNA transitions between the polymerase and nuclease active sites–processes that are difficult to resolve using more static structural methods (Millar, 2022).

The original research articles in this eBook emphasize how much there still is to learn about the wide variety of polymerases. Frey et al. use X-ray crystallography and molecular dynamics simulation to describe new non-nucleoside inhibitors of HIV-1 reverse transcriptase that are effective to mutants that are resistant to previously designed compounds (Frey et al., 2022). This work highlights the importance of polymerases as drug targets but also emphasizes the importance of understanding the entire nucleotide incorporation cycle, both kinetically and structurally, in the drug development process.

The work by Park et al. demonstrates that mitochondrial DNA polymerase gamma is capable of efficiently bypassing a CPD lesion at physiological concentrations of Mn^{2+} (Park et al., 2022). This ability is specific to polymerase gamma, not a general property of A-family DNA polymerases, underscoring the diversity of polymerases and emphasizing the role of cellular conditions in regulating activity.

Vaisman et al. address the evolutionary diversity of the translesion DNA polymerases. Biochemical characterization of the four Y-family polymerases (eta, iota, kappa and Rev1) from a lower eukaryote shows that their major properties are very similar to those of their human homologs (Vaisman et al., 2021). This work indicates that polymerase iota evolved earlier than previous sequence analysis had suggested, raising the question of what critical role this enzyme plays in both lower and higher eukaryotes.

In the final research article in this volume, Park et al. present two structures of phage RB69 DNA polymerase in open binary and partially closed ternary complexes that are distinct from previous structures of this enzyme (Park et al., 2021). Since these structures exist in a single crystal form, they suggest that initial binding of the correct incoming nucleotide and the second divalent metal ion are much weaker than expected.

The various articles in this issue demonstrate that, despite decades of seminal work on polymerases in replication and transcription, there are still many unknowns that require future research. We hope this issue will inspire graduate students and postdocs to devote their research to studying these fascinating processes that are fundamental to all life.

We wish to dedicate this special polymerase issue to the memory of Tom Steitz who was a mentor to all of us, both directly (JDP and YWY) and indirectly (IL). His pioneering structural work, insights into catalytic mechanism, and deep appreciation of the connections between biological structure and function continue to inspire our own research. We miss him deeply.

AUTHOR CONTRIBUTIONS

All authors have made a substantial, direct and intellectual contribution to the work, and approved it for publication.

FUNDING

The authors are supported by grants awarded from the NIH to JP (R01GM080573) and to YWY (R01AI134611) and by DBT/Wellcome Trust India Alliance Intermediate Fellowship (IA/I/20/1/504905) awarded to IL.

REFERENCES

Beese, L. S., Derbyshire, V., and Steitz, T. A. (1993). Structure of DNA Polymerase I Klenow Fragment Bound to Duplex DNA. *Science* 260, 352–355. doi:10.1126/science.8469987

Beese, L. S., and Steitz, T. A. (1991). Structural Basis for the 3′-5′ Exonuclease Activity of *Escherichia coli* DNA Polymerase I: a Two Metal Ion Mechanism. *EMBO J.* 10, 25–33. doi:10.1002/j.1460-2075.1991.tb07917.x

Brautigam, C. A., and Steitz, T. A. (1998). Structural and Functional Insights provided by Crystal Structures of DNA Polymerases and Their Substrate Complexes. *Curr. Opin. Struct. Biol.* 8, 54–63. doi:10.1016/s0959-440x(98)80010-9

Carvajal-Maldonado, D., Drogalis Beckham, L., Wood, R. D., and Doublié, S. (2021). When DNA Polymerases Multitask: Functions beyond Nucleotidyl Transfer. *Front. Mol. Biosci.* 8, 815845. doi:10.3389/fmolb.2021.815845

Doublié, S., Tabor, S., Long, A. M., Richardson, C. C., and Ellenberger, T. (1998). Crystal Structure of a Bacteriophage T7 DNA Replication Complex at 2.2 Å Resolution. *Nature* 391, 251–258. doi:10.1038/34593

Frey, K. M., Bertoletti, N., Chan, A. H., Ippolito, J. A., Bollini, M., Spasov, K. A., et al. (2022). Structural Studies and Structure Activity Relationships for Novel Computationally Designed Non-nucleoside Inhibitors and Their Interactions With HIV-1 Reverse Transcriptase. *Front. Mol. Biosci.* 9, 805187. doi:10.3389/fmolb.2022.805187

Gao, Y., and Yang, W. (2016). Capture of a Third Mg 2+ Is Essential for Catalyzing DNA Synthesis. *Science* 352, 1334–1337. doi:10.1126/science.aad9633

Gong, P. (2021). Within and beyond the Nucleotide Addition Cycle of Viral RNA-Dependent RNA Polymerases. *Front. Mol. Biosci.* 8, 822218. doi:10.3389/fmolb.2021.822218

Huang, H., Chopra, R., Verdine, G. L., and Harrison, S. C. (1998). Structure of a Covalently Trapped Catalytic Complex of HIV-1 Reverse Transcriptase: Implications for Drug Resistance. *Science* 282, 1669–1675. doi:10.1126/science.282.5394.1669

Kaszubowski, J. D., and Trakselis, M. A. (2021). Beyond the Lesion: Back to High Fidelity DNA Synthesis. *Front. Mol. Biosci.* 8, 811540. doi:10.3389/fmolb.2021.811540

Li, Y., Korolev, S., and Waksman, G. (1998). Crystal Structures of Open and Closed Forms of Binary and Ternary Complexes of the Large Fragment of Thermus Aquaticus DNA Polymerase I: Structural Basis for Nucleotide Incorporation. *EMBO J.* 17, 7514–7525. doi:10.1093/emboj/17.24.7514

Millar, D. P. (2022). Conformational Dynamics of DNA Polymerases Revealed at the Single-Molecule Level. *Front. Mol. Biosci.* 9, 826593. doi:10.3389/fmolb.2022.826593

Nakamura, T., Zhao, Y., Yamagata, Y., Hua, Y.-j., and Yang, W. (2012). Watching DNA Polymerase η Make a Phosphodiester Bond. *Nature* 487, 196–201. doi:10.1038/nature11181

Park, J., Baruch-Torres, N., Iwai, S., Herrmann, G. K., Brieba, L. G., and Yin, Y. W. (2022). Human Mitochondrial DNA Polymerase Metal Dependent UV Lesion Bypassing Ability. *Front. Mol. Biosci.* 9, 808036. doi:10.3389/fmolb.2022.808036

Park, J., Youn, H.-S., An, J. Y., Lee, Y., Eom, S. H., and Wang, J. (2021). Structure of New Binary and Ternary DNA Polymerase Complexes from Bacteriophage RB69. *Front. Mol. Biosci.* 8, 704813. doi:10.3389/fmolb.2021.704813

Pelletier, H., Sawaya, M. R., Kumar, A., Wilson, S. H., and Kraut, J. (1994). Structures of Ternary Complexes of Rat DNA Polymerase β, a DNA Template-Primer, and ddCTP. *Science* 264, 1891–1903. doi:10.1126/science.7516580

Polesky, A. H., Dahlberg, M. E., Benkovic, S. J., Grindley, N. D., and Joyce, C. M. (1992). Side Chains Involved in Catalysis of the Polymerase Reaction of DNA Polymerase I from *Escherichia coli*. *J. Biol. Chem.* 267, 8417–8428. doi:10.1016/s0021-9258(18)42461-1

Steitz, T. A. (1993). DNA- and RNA-Dependent DNA Polymerases. *Curr. Opin. Struct. Biol.* 3, 31–38. doi:10.1016/0959-440X(93)90198-T

Vaisman, A., McDonald, J. P., Smith, M. R., Aspelund, S. L., Evans, T. C., and Woodgate, R. (2021). Identification and Characterization of Thermostable Y-Family DNA Polymerases η, ι, κ and Rev1 from a Lower Eukaryote, Thermomyces Lanuginosus. *Front. Mol. Biosci.* 8, 778400. doi:10.3389/fmolb.2021.778400

Wang, J., and Konigsberg, W. H. (2022). Two-Metal-Ion Catalysis: Inhibition of DNA Polymerase Activity by a Third Divalent Metal Ion. *Front. Mol. Biosci.* 9, 824794. doi:10.3389/fmolb.2022.824794

Conflict of Interest: The authors declare that the research was conducted in the absence of any commercial or financial relationships that could be construed as a potential conflict of interest.

Publisher's Note: All claims expressed in this article are solely those of the authors and do not necessarily represent those of their affiliated organizations, or those of the publisher, the editors and the reviewers. Any product that may be evaluated in this article, or claim that may be made by its manufacturer, is not guaranteed or endorsed by the publisher.

frontiers in Molecular Biosciences

REVIEW
published: 01 March 2022
doi: 10.3389/fmolb.2022.824794

Two-Metal-Ion Catalysis: Inhibition of DNA Polymerase Activity by a Third Divalent Metal Ion

Jimin Wang and William H. Konigsberg*

Department of Molecular Biophysics and Biochemistry, Yale University, New Haven, CT, United States

Almost all DNA polymerases (pols) exhibit bell-shaped activity curves as a function of both pH and Mg^{2+} concentration. The pol activity is reduced when the pH deviates from the optimal value. When the pH is too low the concentration of a deprotonated general base (namely, the attacking 3′-hydroxyl of the 3′ terminal residue of the primer strand) is reduced exponentially. When the pH is too high the concentration of a protonated general acid (i.e., the leaving pyrophosphate group) is reduced. Similarly, the pol activity also decreases when the concentration of the divalent metal ions deviates from its optimal value: when it is too low, the binding of the two catalytic divalent metal ions required for the full activity is incomplete, and when it is too high a third divalent metal ion binds to pyrophosphate, keeping it in the replication complex longer and serving as a substrate for pyrophosphorylysis within the complex. Currently, there is a controversy about the role of the third metal ion which we will address in this review.

Keywords: two-metal-ion catalysis, third inhibitory divalent metal ion, bell shaped pol activity plots, Hill coefficient, Brønsted equation

OPEN ACCESS

Edited by:
Whitney Yin,
University of Texas Medical Branch at Galveston, United States

Reviewed by:
Vipender Singh,
Novartis Institutes for BioMedical Research, United States
Cheng-Yang Huang,
Chung Shan Medical University, Taiwan
Bret Freudenthal,
University of Kansas Medical Center, United States

***Correspondence:**
Jimin Wang
jimin.wang@yale.edu

Specialty section:
This article was submitted to Structural Biology, a section of the journal Frontiers in Molecular Biosciences

Received: *29 November 2021*
Accepted: *14 January 2022*
Published: *01 March 2022*

Citation:
Wang J and Konigsberg WH (2022) Two-Metal-Ion Catalysis: Inhibition of DNA Polymerase Activity by a Third Divalent Metal Ion. Front. Mol. Biosci. 9:824794. doi: 10.3389/fmolb.2022.824794

INTRODUCTION

The first DNA polymerase (pol) was discovered by Arthur Kornberg and others (Bessman et al., 1958; Lehman et al., 1958), and was shown to be responsible for faithfully copying double-stranded DNA through Watson-Crick basepairing between template and primer strands and between the templating nucleotide and incoming dNTPs. It catalyzed the polymerization reaction with a rate enhancement of over 10^{17}-fold relative to the uncatalyzed reaction (Schroeder et al., 2006; Lassila et al., 2011). This unique ability for rate enhancement can be attributed to the stabilization provided by this enzyme specifically only to the transition state (TS) relative to the enzyme-substrate (ES) or enzyme-product (EP) complexes as shown by the steady-state kinetics (**Figure 1**) (Knowles, 1980; Lassila et al., 2011). The pol-catalyzed reaction absolutely requires divalent Mg^{2+} ions (Goulian et al., 1968; Slater et al., 1972; Kornberg and Baker, 1992). When the logarithm of the steady-state rate was plotted as a function of $[Mg^{2+}]$, the slope was +2.0 (not 3) before $[Mg^{2+}]$ reached the maximal rate (Bolton et al., 2002). Beyond its optimal concentration, the rate decreased linearly with the increasing concentration, with a slope of -1.0 in both linear and log plots (Slater et al., 1972; Sirover et al., 1979; Vashishtha et al., 2016; Vashishtha and Konigsberg, 2016). The slopes of these plots suggest that pols bind two divalent metal ions for catalytic enhancement and a third divalent metal ion for inhibition according to classic enzymology (Fersht, 2017).

Based on extensive biochemical data, Thomas A. Steitz proposed a two-metal-ion catalytic mechanism for phosphoryltransfer (PT) reactions (**Figure 1**) (Steitz, 1999). More recently, the discovery that a third divalent metal ion binds to the two products in the pol EP complex (but

not to the enzyme itself or to the ES complex) led to the proposal of an alternate mechanism that *assumes* that the third divalent metal ion is directly invovled in catalysis of the chemical step of the pol reaction (Nakamura et al., 2012; Gao and Yang, 2016). We have some concerns about this proposed mechanism and about the underlying assumption because we predict that this third metal ion could also bind the two products outside of an enzyme in solution in the uncatalyzed reaction in the same way as it was observed within the pol complex, without directly interacting with the enzyme itself. If this is the case, this metal ion cannot be assigned to be part of the enzyme-catalyzed rate enhancement in the pol reaction.

The pol active site is formed by several negatively charged residues that serve to bind metal ions. These metal ions and positively charged residues bind triphosphate groups or pyrophosphates and phosphate groups from substrates and products. These charged residues are kept apart from each other so that no direct interaction can occur between them. As a result, substrates and products can readily bind to these charged pol active site residues. Whether simple electrostatic potential (ESP) interactions play an important role in the enzyme-catalyzed PT reactions remains debatable because a similar ESP interaction could be generated by the metal ions outside of an enzyme when bound in a similar manner to the substrates in non-enzymatic reaction (Maegley et al., 1996). However, the ESP of an enzyme active site cannot be simply described by positive or negative charges only. Rather, it is composed of many long-range ESP terms from all charged residues of enzymes nearby in so-called local ESP frustration with very steep gradients (Freiberger et al., 2019). It is likely that these unique ESP gradients help to improve the base selectivity of pols on the basis of small energetic differences in basepairing geometry.

TWO-METAL-ION MECHANISM IN ENZYME-CATALYZED PHOSPHOTRANSFER REACTIONS

In 1985 Thomas Steitz and others determined the first polymerase structure, namely, the large fragment of *E. coli* pol I or the Klenow fragment (KF) in complex with dTMP bound in the exonuclease active site (Brutlag et al., 1969; Klenow and Henningsen, 1970; Ollis et al., 1985). Following that in 1991 Lorena Beese and Thomas Steitz provided direct evidence for the two-metal-ion catalysis for a PT reaction at the exonuclease active site of the KF (Beese and Steitz, 1991). In 1992 Thomas Steitz and others published the second DNA polymerase structure, HIV-1 RT in complex with an inhibitor, and suggested that all DNA polymerases exhibit a hand-like architecture and have highly conserved carboxylates for binding of two metal ions (Kohlstaedt et al., 1992). In 1993 Thomas and Joan Steitz further extended the requirement for two metal ions that are necessary for catalytic RNA to have a high catalytic function (**Figure 1**) (Steitz and Steitz, 1993). The two-metal-ion catalytic mechanism has been found to be involved in many known enzymatic processing of nucleic acids (Palermo et al., 2015).

Human/rat pol β and RB69 DNA pol are the three most extensively studied DNA pols using both X-ray crystallography (by Joseph Kraut, Samuel Wilson and others) and biochemistry (by Zucai Suo, Min-Daw Tsai and others), as well as by combined approaches (used by us and

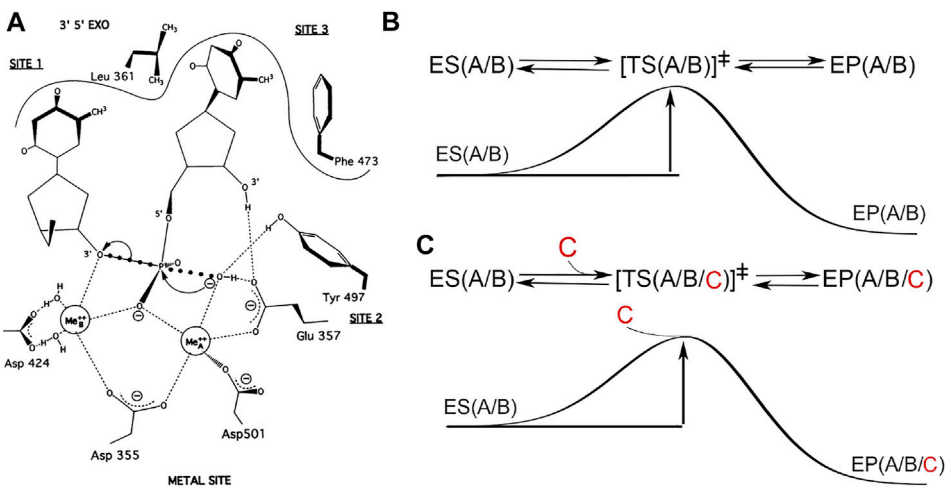

FIGURE 1 | Two-metal-ion catalytic mechanism or three metal ions? **(A)** Hypothetical transition state for the hydrolysis of phosphodiester bond in the 3′,5′-exonuclease active site of Klenow fragment (adapted from Steitz and Steitz, 1993, with permission, ©National Academy of Sciences, 1993). **(B)** Free energy diagram of the classic TS theory involving two metal ions A and B, which are intrisic parts of both ES and EP complexes and remain unchanged during catalysis. Simultaneous bond-breaking and bond-formation at the transition state is a zero order reaction. **(C)** Hypothetical 3-metal ion catalytic mechanism with the third metal ion C entering near or at the TS point, which is not compatabile with the classic TS theory. In this hypothesis, simultaneous bond-breaking and bond formation is a first order reaction, dependent on the occupancy of the third divalent metal ion. This hypothesis predicts a complex dependence of the pol activity on the concentration of divalent metal ions invovling all three sites, which has never been supported by any biochemical data (see text).

others) (Pelletier et al., 1994; Sawaya et al., 1994; Ahn et al., 1997; Wang et al., 1997; Franklin et al., 2001; Batra et al., 2006; Showalter et al., 2006; Xia et al., 2011; Xia et al., 2013; Xia and Konigsberg, 2014; Vyas et al., 2015; Reed et al., 2017; Reed and Suo, 2017; Vyas et al., 2017; Whitaker and Freudenthal, 2020). Other pols that have been extensively studied using both kinetic and structural methods include Dpo4, which binds additional divalent metal ions to the primer/template DNA duplex outside the pol active site (Fiala and Suo, 2004; Irimia et al., 2010). The fact that these metal ions bind makes it very challenging to correlate structures with kinetics, particularly in the chemical step of the pol reaction. In addition to catalysis, divalent metal ions can also modulate noncovalent kinetic behaviors (Dahl et al., 2016).

THE OBSERVATION OF A THIRD METAL ION IN THE ENZYME-PRODUCT COMPLEXES OF DNA POLYMERASES

Wei Yang and others were the first to observe binding of a third divalent metal ion in replication complexes of low-efficiency and low-fidelity lesion-bypass DNA pols (Nakamura et al., 2012; Gao and Yang, 2016). Because the reaction catalyzed by these pols is rather slow, intermediate structures have been characterized by time-resolved X-ray crystallography when crystals were frozen at different times after initiation of the pol reaction (Nakamura et al., 2012; Freudenthal et al., 2013; Gao and Yang, 2016; Jamsen et al., 2017; Reed and Suo, 2017). Yang and others observed a strong correlation between the formation of products and the binding of this third metal ion (Nakamura et al., 2012; Gao and Yang, 2016). In these structures, both ES and EP complexes were simultaneously observed as an inter-convertible mixture at various time points. However, these EP complexes had an extra divalent metal ion bound, which was not found in the other pol complexes discussed above.

One interpretation is that this third metal ion is involved in catalyzing the chemical step in the pol reaction, which would fundamentally change the paradigm of the two-metal-ion catalytic mechanism (Yang et al., 2016; Wu et al., 2017). If, on the other hand, the classic TS theory can fully explain these observations as discussed below, there is no need for revising the original mechanism (Perera et al., 2017; Wu et al., 2017; Yoon and Warshel, 2017; Raper et al., 2018; Stevens and Hammes-Schiffer, 2018). Theoretical calculations can only address whether a given hypothetical chemical mechanism is compatible with chemical principles, but often do not address whether the given mechanism is consistent with existing experimental data. By definition, an enzyme and its cofactors are not reactants or products and not a consumable part of the reaction, thus they remain unchanged in any enzymatic reaction. With this definition, it is hard to classify this third divalent metal ion as a cofactor because it does not directly interact with the enzyme itself but only binds products without an involvement of the enzyme at all (**Figure 1**).

CLASSIC VIEW OF THE ENZYME-CATALYZED REACTION AND ITS APPLICATION TO THE PRESENCE OF A THIRD METAL ION

An enzyme does not change the equilibrium of the reaction it catalyzes (Kraut, 1988). It only accelerates the rate of both forward and reverse reactions by the same amount, i.e., it simply lowers the free energy barrier of the reaction. Joseph Kraut noted in 1988 that the classic TS theory originally proposed by Linus Pauling was simple, and yet many investigators who attempted to revise it often misunderstood it, including Kraut himself before 1988 (Pauling, 1946; Pauling, 1948; Kraut, 1988). All elementary reactions must be fully reversible, including the reactions of the polymerization-pyrophosphorylysis pair (Kraut, 1988). The reason DNA pols catalyze DNA synthesis irreversibly *in vivo* is because the pyrophosphate product is continuously degraded by cellular pyrophosphatases and dNTP substrates are continuously resupplied. However, evidence also exists that *E. coli* pol IV and *S. cerevisiea* Rev1 are capable of directly hydrolyzing pyrophosphate, making the polymerization reaction irreversible (Kottur and Nair, 2018; Weaver et al., 2020). The classic TS theory postulates that the TS is a saddle point on the energy landscape with the spatial gradient being zero, i.e., the highest energy point on the reaction trejactory but also the lowest energy point in all other directions with a fixed chemical composition. At the TS, the vibration frequency of an existing bond being broken for formation of a new bond determines the rate of the chemical reaction for either polymerization or pyrophosphorylysis (Kraut, 1988). This property suggests that rate of the chemical reaction at the TS is independent of the TS concentration and is zero order whereas the experimentally observed rate is proportional to the concentration of the TS. Any metal ion must be part of both the ES and EP complexes before it can be considered as part of the TS along the reaction coordinate.

A new metal ion cannot enter the TS saddle point as part of the EP complexes but not as part of the ES complex. If the third metal ion are indeed part of the TS, as hypothesized by some investigators (Stevens and Hammes-Schiffer, 2018), the concentration of the TS would be proportional to the cube of the metal ion concentration when the metal ion concentration is below the saturation point of the tightest bound catalytically metal ion. The logarithm of the pol activity (which is proportional to the concentration of the TS versus the concentration of metal ions) should have a slope of three (Fersht, 2017). If the third metal ion binds only weakly with a much larger dissociation constant than the first two metal ions, the metal ion-dependent activation phase would be biphasic (Fersht, 2017). The logarithm of the pol activity in the first phase has a slope of three when the metal ion concentration is below the saturation point of the first two metal ions. The second phase occurs when the metal ion concentration is below the saturation point of the third metal ion but above that of the first two metal ions. The slope of this new phase is one. Currently, there are no data to support the hypothesis proposed by Stevens and Hammes-Schiffer for any pol.

For pyrophosphorylysis, this third metal ion may be characterized as part of *substrate*-assisted catalysis as it is part of the ES complex (it should be noted that the terms substrate and product are reversed in the forward and reverse reactions) (**Figure 1**). However, if this third metal ion leaves before the ES complex approaches to the TS (which by definition is at the highest energy point of the reaction coordinate at the saddle point of the energy landscape of the reaction), it cannot contribute to stabilization of the TS. Therefore, it cannot be assigned for any function in pyrophosphorylysis; and if it has no function in pyrophosphorylsis, it cannot have any function in polymerization either, in accordance with the full reversibility principle of any elemental reaction according to the TS theory. Even so, it could still play an indirect role only in the overall reaction of pyrophosphorylysis asymmetrically (but not in polymerization) by retaining the pyrophosphate substrate longer in the ES complex, i.e., increasing the local concentration of the substrate.

When the EP complex of pyrophospholysis is extrapolated from the ES complex, this third metal ion is expected to interact with two phosphate oxygens of Pα of the dNTP product, one with the non-bridging O and the other with the bridging O between the α- and β-phosphate groups. Within an idealized hexacoordination of a Mg^{2+} complex ion (Pavlov et al., 1998), the distance between its two adjacent O ligands is 2.94 Å, which is the distance that the third metal ion is observed in the various pol structures (Nakamura et al., 2012; Gao and Yang, 2016). Within the same Pα phosphate group, the distance between its two O atoms is 2.46 Å (which is shorter by 0.48 Å than the idealized value for simultaneous coordination to any Mg^{2+} ion). If two O atoms of the given phosphate group could become two adjacent ligands for a Mg^{2+} ion with ideal coordination bond length of 2.17 Å, the coordination bond angle O-Mg-O would be 75° (which is a 15° deviation from the ideal value), and if the coordination bond angle to the Mg^{2+} ion would maintain 90°, its coordination bond length would be 1.81 Å (which is a 0.36 Å deviation from the ideal value). With this coordination geometry, other O ligands of Mg^{2+} ion could sterically clash with the O atoms of both α- and β-phosphates of the incoming dNTP. Therefore, on these theoretical grounds, within the energy landscape of the reaction diagram, a Mg^{2+} ion can never be simultaneously coordinate two O atoms of the same phosphate group for stable geometry (particularly if the coordination involves a bridging O atom of reduced charge) as observed in the two products. Because this third Mg^{2+} ion stabilizes only the pyrophosphorylysis ES complex but not the pyrophosphorolysis EP complex, its binding would increase the TS barrier of the reaction. This third metal ion must first leave before pyrophosphorylysis can take place and thus is not part of the catalytic apparatus. The coordination geometry of Mn-O is very similar to Mg-O, although variation of Mn-O coordination bond lengths is larger due to the involvement of its 3*d* electrons compared to that of Mg-O (Sasaki et al., 1979; Pavlov et al., 1998). Due to different rigidities of metal ion coordination octahedra, the two divalent metal ions could have very different degrees of covalency in their coordination bonds.

KINETICS OF BINDING OF THE THIRD DIVALENT ION IN CRYSTAL STRUCTURES

Does the third divalent metal ion bind to the replication complex immediately before the catalysis of the chemical step of the pol reaction or shortly after it? The kinetic consequences in a crystal differ between these two events (Wang and Smithline, 2019). If the metal ion binds before catalysis, the concentration or the occupancy of this metal ion in the crystals will be larger than the fraction of the formed product. This is especially true if the time is extrapolated to $t = 0$. If it binds after catalysis, the situation is reversed when $t = 0$. With increasing time, the situation becomes more complex because the diffusion rates of this third divalent metal ion and the pyrophosphate product away from the replication complex could vary with time.

The fraction of the newly formed bond between the primer-terminal O3′ and Pα of the triphosphate and that of the bond breaking between the Pα and Pβ phosphates of the triphosphate in the complexes can be directly evaluated by the electron density at the midpoint of the corresponding atoms in each pair of the two bonds (**Figure 2**) (Wang and Smithline, 2019). The relative occupancy of the third metal ion relative to the first two metal ions can be quantitatively estimated using analytic procedures (**Figure 3**) (Wang and Smithline, 2019). This analysis shows that the occupancy of this third divalent metal ion is always smaller than that of the product formation at any time point, including when the time is extrapolated to the $t = 0$ point. This result suggests that the third metal ion is not involved directly in catalysis of the chemical step of the pol reaction.

UNIVERSAL BELL-SHAPED POL ACTIVITY CURVES AS A FUNCTION OF DIVALENT METAL IONS AND pH

Min-Daw Tsai noted that many kinetic data generated from his laboratory on pol β could be fully explained using the two-metal-ion catalytic mechanism previously known at the time, but could be equally well explained using the new three metal ion-based catalytic mechanism, i.e., his data cannot distinguish between the two mechanisms (Tsai, 2019; Wang and Smithline, 2019). He suggested that new kinetic experiments might be needed to distinguish these two mechanisms. However, extensive kinetic data already exist in the literature that allow one to discriminate between them, even before the classic two-metal-ion catalytic mechanism was proposed. These results are briefly reviewed below (**Figure 4**), which include data from both pol β and pol η that strongly support the two-metal-ion catalytic mechanism but cannot be explained by a three-metal-ion mechanism.

During the initial partial purification of *E. coli* DNA pol I, it was found that its pol activity absolutely required divalent metal ions and was pH dependent (Goulian et al., 1968; Slater et al., 1972; Kornberg and Baker, 1992). When the pH deviated from its optimal value or when the concentration of divalent metal ions deviated from their optimal value, the pol activity was reduced. Thus the bell-shaped pol activity profile as a function of pH remains universal, and is a hallmark of general acid-general base

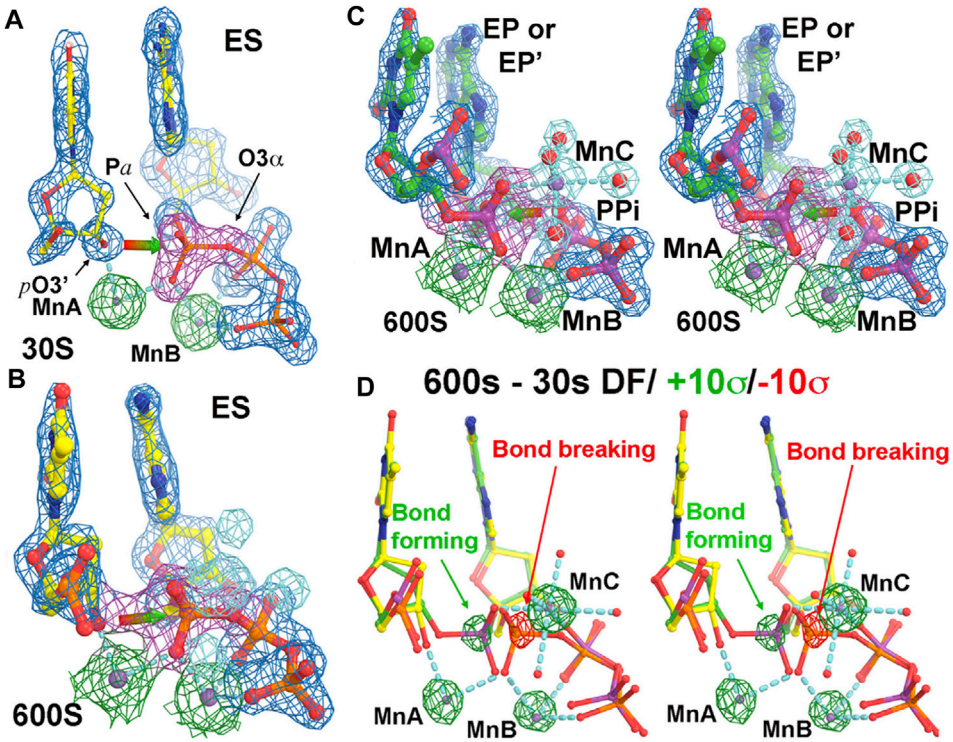

FIGURE 2 | Time-dependent human polymerase η structures (adapted from Wang and Smithline, 2019). **(A)** At 30 s time point. The σ_A-weighted $2F_o$-F_c electron density map contoured at 2σ (blue for overall structure, green for two metal ions A and B, and magenta for the phosphate group). **(B)** At 600 s. New features for MnC and its ligand water molecules (cyan) gradually appear with time. **(C)** Stereodiagram of the 600 s structure. **(D)** Stereodiagram of difference Fourier maps between the 600 s and 30 s structures contoured at +10σ (green) and −10σ (red).

catalysis. If one acid is involved in catalysis, the overall activity is linearly proportional to the concentration of the acid, which would be exponentially reduced with increasing pH. The slope of the log of activity versus pH plot is based on the Brønsted equation (Brønsted and Pedersen, 1924; Dissanayake et al., 2015). If one base is involved, the overall activity is proportional to the concentration of the base, which would decrease with decreasing pH. The bell-shaped pol activity curve as a function of pH for DNA pols suggests that both acid(s) and base(s) are involved in catalysis. The slope of the plot based on the Brønsted equation shows that there is one acid and one base involved in catalysis, which is consistent with hydrogen/dueterium (H/D) effects of the pol reaction catalyzed by DNA pols (Castro et al., 2007; Castro et al., 2009).

Similarly, a bell-shaped pol activity curve as a function of divalent metal ion concentration for DNA polymerases indicates that divalent metal ions act both as an activation cofactor and as an inhibitor in the overall pol reaction (**Figure 4**). The semi-log activity versus log[Mg^{2+}] or log[Mn^{2+}] plot, known as Hill-Langmuir plot, provides the cooperativity Hill coefficients for activation and inhibition of the pol activity, where the coefficient is 2 for the activation phase (Bolton et al., 2002). The optimal metal ion concentration for pol activity is pH dependent, and the optimal pH is dependent on the metal ion concentration because the binding of metal ion can alter the *pKa* value of the general base.

The DNA pol from bacteriophage T4 exhibits pol activity profiles that follow bell-shaped curves for both pH and divalent metal ions (Goulian et al., 1968). In the most recent studies on a DNA pol from a closely-related bacteriophage, RB69, Konigsberg and others showed that the pol activity was reduced by ~ 2-fold when [Mn^{2+}] increased from 10 to 20 mM with the estimated slope of −1 in the plot of log activity versus log[Mn^{2+}] (Vashishtha and Konigsberg, 2016; Vashishtha et al., 2016). The optimal activity of *E. coli* DNA pol I is at 0.07 mM [Mn^{2+}], and was reduced by more than 3-fold when [Mn^{2+}] increased to 0.21 mM (3-fold), highlighting the inhibitory effect of Mn^{2+} ion on its pol activity (**Figure 4A**) (Slater et al., 1972). The estimated slope of the log activity vs log[Mn^{2+}] plot is −1.0 unit, indicating that there is just a single inhibitory binding site. At all pHs, the pol activity on the inhibitory side of the profiles is reduced by approximately 2-fold for every 2-fold increase of divalent metal ion concentration for all DNA pols (**Figure 4**), implying that there is only a single inhibitory divalent metal ion-binding site according to the Hill-Langmuir plot of the log activity-versus-log concentration for divalent metal ions.

Ekaterina Frank and Roger Woodgate have determined the activity profile of human pol η as a function of both Mn^{2+} and Mg^{2+} ions (**Figure 4H**) (Frank and Woodgate, 2007). With Mn^{2+}, the optimal condition is << 0.1 mM in solution. At ~1 mM [Mn^{2+}], the activity is reduced by 3-fold relative to the optimal [Mn^{2+}] condition, and at ~2 mM [Mn^{2+}], the activity

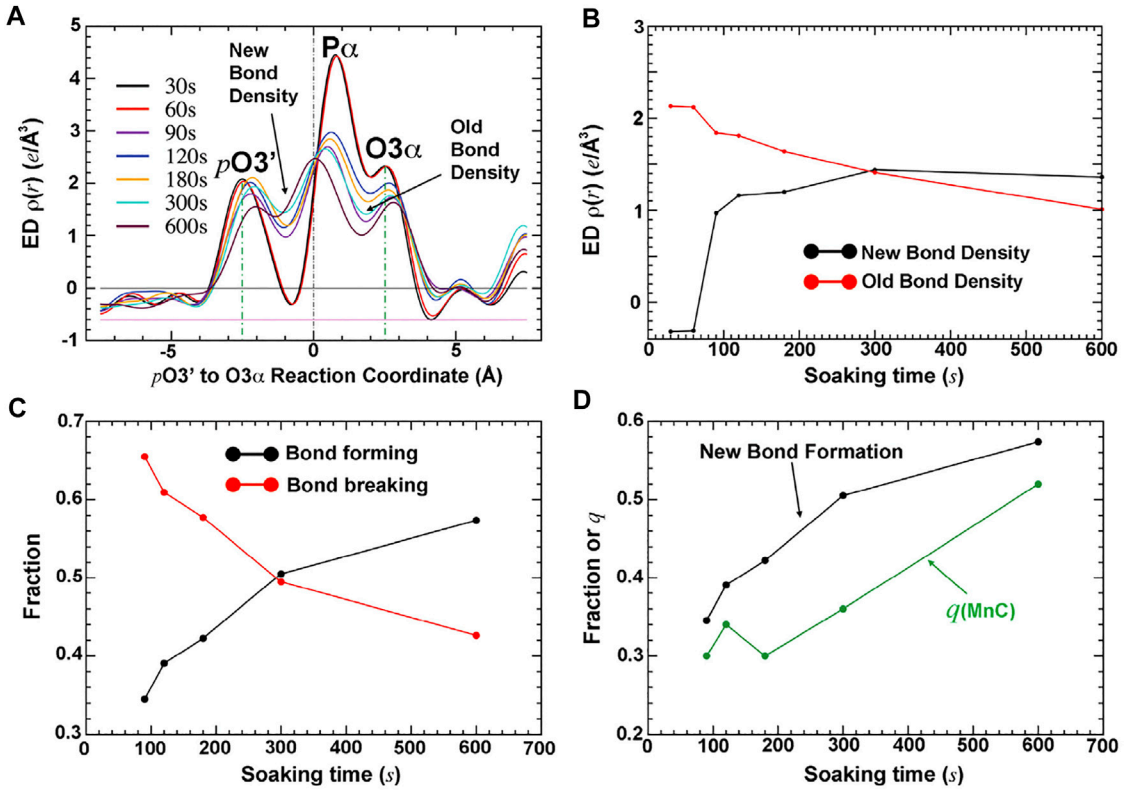

FIGURE 3 | Quantitative analysis of time-dependent electron density for bond formation, bond breaking, and occupancy of the third metal ion MnC (adapted from Wang and Smithline, 2019). **(A)** Plots of the σ_A-weighted F_o-F_c electron density along the reaction coordinate from *pt* O 3′ to Pα to O3α. **(B)** Electron density at the positions defining bond formation and bond breaking. **(C)** Fractions of bond formation and bond breaking. **(D)** Comparison of new bond formation relative to the occupancy of bound MnC helps to establish the relative order of the first bond formation, followed by binding of MnC.

is reduced by 10-fold. Gao and Yang have determined that the binding affinity of MnA and that of MnB in crystal is <0.5 mM, and that of MnC is about 3.2 ± 1.5 mM (Gao and Yang, 2016). Subtle differences in kinetic parameters between solutions and crystals is expected because, in crystals, slower diffusion rates can play a role. The MnC site, with weaker affinity in crystals, likely corresponds to an inhibitory site according to the pol activity profile discussed above (**Figure 4H**). The bell-shaped activity profiles as a function of pH can be readily explained by the deprotonation and protonation processes associated with catalysis. For example, from the maximal activity of rat or zebrafish pol β, the value of log activity versus pH (i.e., –log [H^+]) decreases with increasing or decreasing pH, and the slope of the resulting lines has a unit value (**Figure 4G**) (Ishido et al., 2011).

The bell-shaped pol activity profiles as a function of both pH and divalent metal ions have universally been observed for all DNA polymerases (Kornberg and Baker, 1992). This feature has also been described for human/rat DNA pol α, β, γ, λ, and η, for Taq DNA pol, bacterial and archael DNA pol Dpo4, for T7 DNA pol, T4, and RB69 pol, and for avian myeloblastosis viral DNA pol as well as for Ty1 and HIV-1 RT (**Figure 4**) (Slater et al., 1972; Dube and Loeb, 1975; Sirover et al., 1979; Starnes and Cheng, 1989; Tabor and Richardson, 1989; Lawyer et al., 1993; Bolton et al., 2002; Kokoska et al., 2002; Fiala and Suo, 2004; Castro et al., 2007; Frank and Woodgate, 2007; Ishido et al., 2011; Vashishtha et al., 2016; Vashishtha and Konigsberg, 2016).

KINETIC ASSIGNMENT OF THE THIRD DIVALENT METAL ION AS AN INHIBITOR OF THE POL ACTIVITY

Linda Rehra-Kranz and others have studied the Mn^{2+}-dependent inhibition of the pyrophosphorylysis reaction by the L412M mutant T4 DNA pol using externally supplied pyrophosphate (PPi) (Reha-Krantz et al., 2014). They showed that a high concentration of Mn^{2+} ion clearly inhibited pyrophosphorylysis within the ranges of both the [Mn^{2+}] and [PPi] that they studied. However, the nature of the inhibition could not be easily described using classic kinetic schemes because there was a significant amount of the Mn^{2+}-PPi complex formation, and because Mn^{2+} ion was both an activator and an inhibitor. The half maximal inhibitory concentration (IC_{50}) of Mn^{2+} ion was >3 mM when [PPi] = 4 mM, and IC_{50}([Mn^{2+}]) was ~2 mM when [PPi] = 2 mM, and IC_{50}([Mn^{2+}]) was ~1 mM when [PPi] = 1 mM, and so on.

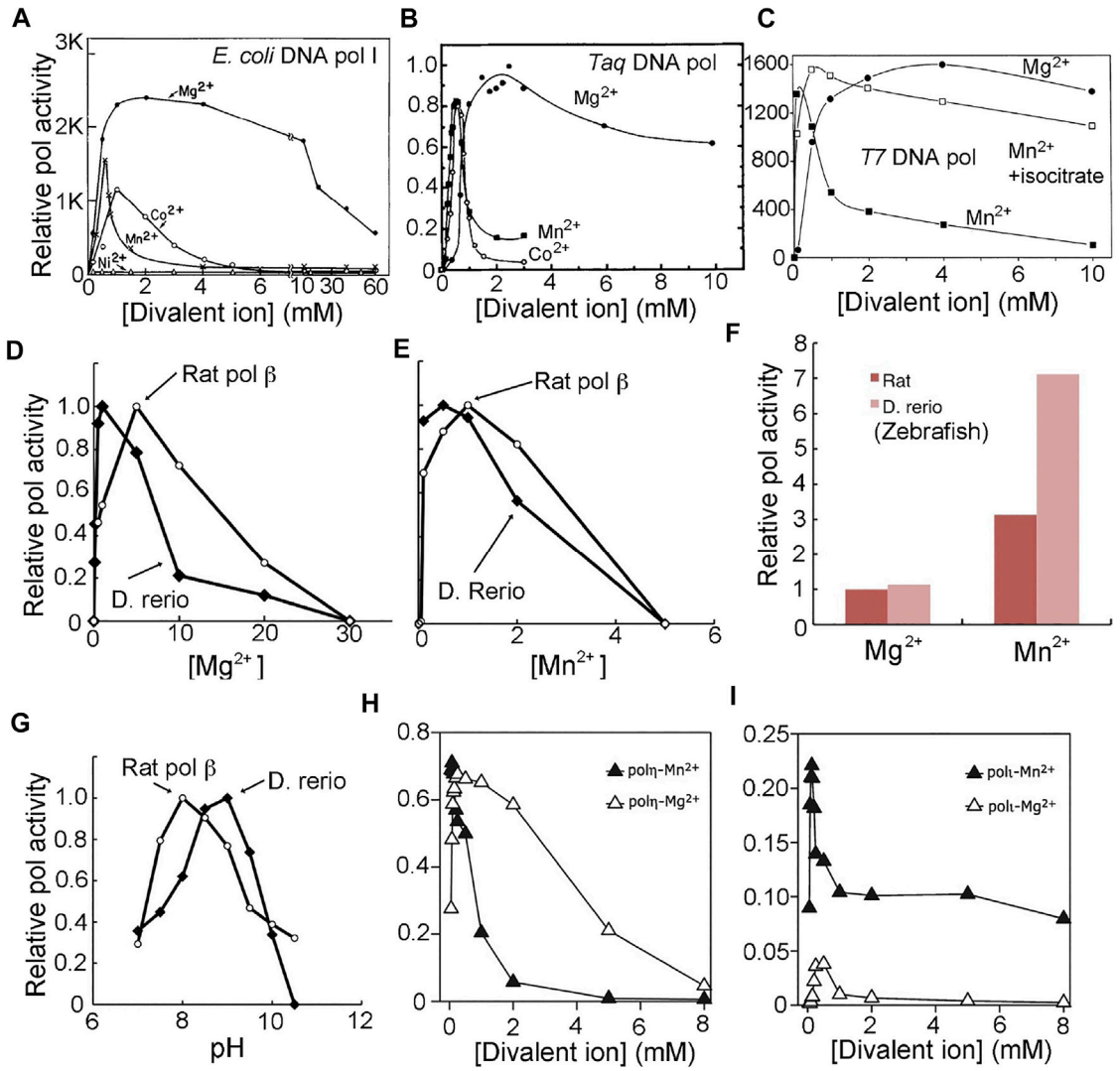

FIGURE 4 | Bell-shaped polymerase activity profiles as a function of divalent metal ions and pH. With the exception of **(A)** and **(C)**, which show nucleotide incorporation under given experimental conditions on the pol product scale, all others are shown on a relative scale. With the exception of **(G)**, which is a pH-activity profile, all others are metal ion-activity profiles. **(A)** *E. coli* DNA polymerase I (adapted from Sirover et al., 1979, J. Biol. Chem.). **(B)** Taq DNA polymerase (adapted from Lawyer et al., 1993, PCR Methods Appl.). **(C)** T7 DNA polymerase (adapted from Tabor and Richardson, 1989, with permission, ©National Academy of Sciences, 1989). **(D–G)** *D. rerio* (zebrafish) pol β and rat pol β (adapted from Ishido et al., 2011, Microbial Cell Factories). **(F)** scale factor between two metal ions and two species. **(H, I)** Human pol η and pol ι (adapted from Frank and Woodgate, 2007, J. Biol. Chem.).

However, these IC_{50} values are not very meaningful because they there was no report on the activation phase of the reaction, nor the maximal activity at the optimal [Mn^{2+}]. Upon comparison with the typical pol activity curves as a function of [Mn^{2+}] for DNA pols (**Figure 4**), the [Mn^{2+}] used in their studies was clearly on the inhibitory side of the curve. Thus, the inhibitory Mn^{2+} ion most likely corresponds to the binding at the third Mn^{2+} site.

Given that the third Mn^{2+} site does not bind to the ES complex of the polymerization reaction but binds only to a non-productive ES complex for pyrophosphorylysis, its apparent inhibition with respect to the pol activity profile of the steady-state reaction is only indirect. We propose that this third Mn^{2+} site helps to retain the pyrophosphate product longer than usual within the ternary complex, thus increasing its local concentration and making pyrophosphorylysis increasingly likely. Our proposal is also based the fact that the unreleased pyrophosphate product is the only source of substrate for pyrophosphorylysis. Consistent with our proposal is the observation that when citrate or isocitrate is included in the Mn^{2+} ion-containing reaction, the third Mn^{2+} ion, which has relatively low affinity, can be removed so that the Mn^{2+}-dependent inhibition can be eliminated and the maximal pol activity can be restored (**Figure 4C**) (Tabor and Richardson, 1989).

CONCLUDING REMARKS

The existing biochemical and structural literature on DNA pols is fully consistent with the generalized mechanism of the two-metal-ion catalysis proposed by Thomas Steitz together with the existing TS theory for enzymatic reactions. This review provides a structural basis for the bell-shaped activity profiles of DNA pols as a function of pH and divalent metal ion concentrations. Weak binding of a third divalent metal ion appears to be responsible for retaining pyrophosphate, allowing extra time for pyrophosphorylysis. This could be important for hydrolysis of incorrectly incorporated nucleotide residues for some DNA pols before mismatches are transferred to the exonuclease site.

AUTHOR CONTRIBUTIONS

JW wrote the draft review. WK and JW finished the final version of the review/prospective manuscript.

FUNDING

Funding was provided by a grant to WK by Franklin Konigsberg.

ACKNOWLEDGMENTS

Authors thank Drs. Satwik Kamtekar, and Soo Hyun Eom for insightful suggestions for this review and Dr. Janice Pata for editing this manuscript.

REFERENCES

Ahn, J., Werneburg, B. G., and Tsai, M.-D. (1997). DNA Polymerase β: Structure–Fidelity Relationship from Pre-steady-state Kinetic Analyses of All Possible Correct and Incorrect Base Pairs for Wild Type and R283A Mutant. *Biochemistry* 36, 1100–1107. doi:10.1021/bi961653o

Batra, V. K., Beard, W. A., Shock, D. D., Krahn, J. M., Pedersen, L. C., and Wilson, S. H. (2006). Magnesium-induced Assembly of a Complete DNA Polymerase Catalytic Complex. *Structure* 14, 757–766. doi:10.1016/j.str.2006.01.011

Beese, L. S., and Steitz, T. A. (1991). Structural Basis for the 3′-5′ Exonuclease Activity of *Escherichia coli* DNA Polymerase I: a Two Metal Ion Mechanism. *EMBO J.* 10, 25–33. doi:10.1002/j.1460-2075.1991.tb07917.x

Bessman, M. J., Lehman, I. R., Simms, E. S., and Kornberg, A. (1958). Enzymatic Synthesis of Deoxyribonucleic Acid. *J. Biol. Chem.* 233, 171–177. doi:10.1016/s0021-9258(19)68049-x

Bolton, E. C., Mildvan, A. S., and Boeke, J. D. (2002). Inhibition of Reverse Transcription *In Vivo* by Elevated Manganese Ion Concentration. *Mol. Cel* 9, 879–889. doi:10.1016/s1097-2765(02)00495-1

Brønsted, J. N., and Pedersen, K. J. (1924). Stöchimetrie und Berwandtschaftslehre. *Z. für Phys Chem.* 108, 185–125.

Brutlag, D., Atkinson, M. R., Setlow, P., and Kornberg, A. (1969). An Active Fragment of DNA Polymerase Produced by Proteolytic Cleavage. *Biochem. Biophys. Res. Commun.* 37, 982–989. doi:10.1016/0006-291x(69)90228-9

Castro, C., Smidansky, E., Maksimchuk, K. R., Arnold, J. J., Korneeva, V. S., Gotte, M., et al. (2007). Two Proton Transfers in the Transition State for Nucleotidyl Transfer Catalyzed by RNA- and DNA-dependent RNA and DNA Polymerases. *Proc. Natl. Acad. Sci.* 104, 4267–4272. doi:10.1073/pnas.0608952104

Castro, C., Smidansky, E. D., Arnold, J. J., Maksimchuk, K. R., Moustafa, I., Uchida, A., et al. (2009). Nucleic Acid Polymerases Use a General Acid for Nucleotidyl Transfer. *Nat. Struct. Mol. Biol.* 16, 212–218. doi:10.1038/nsmb.1540

Dahl, J. M., Lieberman, K. R., and Wang, H. (2016). Modulation of DNA Polymerase Noncovalent Kinetic Transitions by Divalent Cations. *J. Biol. Chem.* 291, 6456–6470. doi:10.1074/jbc.m115.701797

Dissanayake, T., Swails, J. M., Harris, M. E., Roitberg, A. E., and York, D. M. (2015). Interpretation of pH-Activity Profiles for Acid-Base Catalysis from Molecular Simulations. *Biochemistry* 54, 1307–1313. doi:10.1021/bi5012833

Dube, D. K., and Loeb, L. A. (1975). Manganese as a Mutagenic Agent during *In Vitro* DNA Synthesis. *Biochem. Biophys. Res. Commun.* 67, 1041–1046. doi:10.1016/0006-291x(75)90779-2

Fersht, A. (2017). *Structure and Mechanism in Protein Science: A Guide to Enzyme Catalysis and Protein Folding*. New Jersey: World Scientific.

Fiala, K. A., and Suo, Z. (2004). Pre-steady-state Kinetic Studies of the Fidelity of *Sulfolobus Solfataricus* P2 DNA Polymerase IV. *Biochemistry* 43, 2106–2115. doi:10.1021/bi0357457

Frank, E. G., and Woodgate, R. (2007). Increased Catalytic Activity and Altered Fidelity of Human DNA Polymerase ι in the Presence of Manganese. *J. Biol. Chem.* 282, 24689–24696. doi:10.1074/jbc.m702159200

Franklin, M. C., Wang, J., and Steitz, T. A. (2001). Structure of the Replicating Complex of a Pol α Family DNA Polymerase. *Cell* 105, 657–667. doi:10.1016/s0092-8674(01)00367-1

Freiberger, M. I., Guzovsky, A. B., Wolynes, P. G., Parra, R. G., and Ferreiro, D. U. (2019). Local Frustration Around Enzyme Active Sites. *Proc. Natl. Acad. Sci. USA* 116, 4037–4043. doi:10.1073/pnas.1819859116

Freudenthal, B. D., Beard, W. A., Shock, D. D., and Wilson, S. H. (2013). Observing a DNA Polymerase Choose Right from Wrong. *Cell* 154, 157–168. doi:10.1016/j.cell.2013.05.048

Gao, Y., and Yang, W. (2016). Capture of a Third Mg^{2+} Is Essential for Catalyzing DNA Synthesis. *Science* 352, 1334–1337. doi:10.1126/science.aad9633

Goulian, M., Lucas, Z. J., and Kornberg, A. (1968). Enzymatic Synthesis of Deoxyribonucleic Acid. *J. Biol. Chem.* 243, 627–638. doi:10.1016/s0021-9258(18)93650-1

Irimia, A., Loukachevitch, L. V., Eoff, R. L., Guengerich, F. P., and Egli, M. (2010). Metal-ion Dependence of the Active-Site Conformation of the Translesion DNA Polymerase Dpo4 fromSulfolobus Solfataricus. *Acta Acta Crystallogr. Sect. F. Struct. Biol. Cryst. Commun.* 66, 1013–1018. doi:10.1107/s1744309110029374

Ishido, T., Yamazaki, N., Ishikawa, M., and Hirano, K. (2011). Characterization of DNA Polymerase β from *Danio rerio* by Overexpression in *E. coli* Using the *In Vivo*/*In Vitro* Compatible pIVEX Plasmid. *Microb. Cel Fact* 10, 84. doi:10.1186/1475-2859-10-84

Jamsen, J. A., Beard, W. A., Pedersen, L. C., Shock, D. D., Moon, A. F., Krahn, J. M., et al. (2017). Time-lapse Crystallography Snapshots of a Double-Strand Break Repair Polymerase in Action. *Nat. Commun.* 8, 253. doi:10.1038/s41467-017-00271-7

Klenow, H., and Henningsen, I. (1970). Selective Elimination of the Exonuclease Activity of the Deoxyribonucleic Acid Polymerase from *Escherichia coli* B by Limited Proteolysis. *Proc. Natl. Acad. Sci.* 65, 168–175. doi:10.1073/pnas.65.1.168

Knowles, J. R. (1980). Enzyme-catalyzed Phosphoryl Transfer Reactions. *Annu. Rev. Biochem.* 49, 877–919. doi:10.1146/annurev.bi.49.070180.004305

Kohlstaedt, L. A., Wang, J., Friedman, J. M., Rice, P. A., and Steitz, T. A. (1992). Crystal Structure at 3.5 Å Resolution of HIV-1 Reverse Transcriptase Complexed with an Inhibitor. *Science* 256, 1783–1790. doi:10.1126/science.1377403

Kokoska, R. J., Bebenek, K., Boudsocq, F., Woodgate, R., and Kunkel, T. A. (2002). Low Fidelity DNA Synthesis by a Y Family DNA Polymerase Due to Misalignment in the Active Site. *J. Biol. Chem.* 277, 19633–19638. doi:10.1074/jbc.m202021200

Kornberg, A., and Baker, T. A. (1992). *DNA Replication*. 2nd edn. New York: W. H. Freeman.

Kottur, J., and Nair, D. T. (2018). Pyrophosphate Hydrolysis Is an Intrinsic and Critical Step of the DNA Synthesis Reaction. *Nucleic Acids Res.* 46, 5875–5885. doi:10.1093/nar/gky402

Kraut, J. (1988). How Do Enzymes Work? *Science* 242, 533–540. doi:10.1126/science.3051385

Lassila, J. K., Zalatan, J. G., and Herschlag, D. (2011). Biological Phosphoryl-Transfer Reactions: Understanding Mechanism and Catalysis. *Annu. Rev. Biochem.* 80, 669–702. doi:10.1146/annurev-biochem-060409-092741

Lawyer, F. C., Stoffel, S., Saiki, R. K., Chang, S. Y., Landre, P. A., Abramson, R. D., et al. (1993). High-level Expression, Purification, and Enzymatic Characterization of Full-Length Thermus Aquaticus DNA Polymerase and a Truncated Form Deficient in 5' to 3' Exonuclease Activity. *Genome Res.* 2, 275–287. doi:10.1101/gr.2.4.275

Lehman, I. R., Bessman, M. J., Simms, E. S., and Kornberg, A. (1958). Enzymatic Synthesis of Deoxyribonucleic Acid. *J. Biol. Chem.* 233, 163–170. doi:10.1016/s0021-9258(19)68048-8

Maegley, K. A., Admiraal, S. J., and Herschlag, D. (1996). Ras-catalyzed Hydrolysis of GTP: a New Perspective from Model Studies. *Proc. Natl. Acad. Sci.* 93, 8160–8166. doi:10.1073/pnas.93.16.8160

Nakamura, T., Zhao, Y., Yamagata, Y., Hua, Y.-j., and Yang, W. (2012). Watching DNA Polymerase η Make a Phosphodiester Bond. *Nature* 487, 196–201. doi:10.1038/nature11181

Ollis, D. L., Brick, P., Hamlin, R., Xuong, N. G., and Steitz, T. A. (1985). Structure of Large Fragment of *Escherichia coli* DNA Polymerase I Complexed with dTMP. *Nature* 313, 762–766. doi:10.1038/313762a0

Palermo, G., Cavalli, A., Klein, M. L., Alfonso-Prieto, M., Dal Peraro, M., and De Vivo, M. (2015). Catalytic Metal Ions and Enzymatic Processing of DNA and RNA. *Acc. Chem. Res.* 48, 220–228. doi:10.1021/ar500314j

Pauling, L. (1946). Molecular Architecture and Biological Reactions. *Chem. Eng. News Archive* 24, 1375–1377. doi:10.1021/cen-v024n010.p1375

Pauling, L. (1948). Chemical Achievement and hope for the Future. *Am. Sci.* 36, 51–58.

Pavlov, M., Siegbahn, P. E. M., and Sandström, M. (1998). Hydration of Beryllium, Magnesium, Calcium, and Zinc Ions Using Density Functional Theory. *J. Phys. Chem. A.* 102, 219–228. doi:10.1021/jp972072r

Pelletier, H., Sawaya, M. R., Kumar, A., Wilson, S. H., and Kraut, J. (1994). Structures of Ternary Complexes of Rat DNA Polymerase β, a DNA Template-Primer, and ddCTP. *Science* 264, 1891–1903. doi:10.1126/science.7516580

Perera, L., Beard, W. A., Pedersen, L. G., and Wilson, S. H. (2017). Hiding in plain Sight: The Bimetallic Magnesium Covalent Bond in Enzyme Active Sites. *Inorg. Chem.* 56, 313–320. doi:10.1021/acs.inorgchem.6b02189

Raper, A. T., Reed, A. J., and Suo, Z. (2018). Kinetic Mechanism of DNA Polymerases: Contributions of Conformational Dynamics and a Third Divalent Metal Ion. *Chem. Rev.* 118, 6000–6025. doi:10.1021/acs.chemrev.7b00685

Reed, A. J., and Suo, Z. (2017). Time-dependent Extension from an 8-oxoguanine Lesion by Human DNA Polymerase Beta. *J. Am. Chem. Soc.* 139, 9684–9690. doi:10.1021/jacs.7b05048

Reed, A. J., Vyas, R., Raper, A. T., and Suo, Z. (2017). Structural Insights into the post-chemistry Steps of Nucleotide Incorporation Catalyzed by a DNA Polymerase. *J. Am. Chem. Soc.* 139, 465–471. doi:10.1021/jacs.6b11258

Reha-Krantz, L. J., Woodgate, S., and Goodman, M. F. (2014). Engineering Processive DNA Polymerases with Maximum Benefit at Minimum Cost. *Front. Microbiol.* 5, 380. doi:10.3389/fmicb.2014.00380

Sasaki, S., Fujino, K., and Takéuchi, Y. (1979). X-ray Determination of Electron-Density Distributions in Oxides, MgO, MnO, CoO, and NiO, and Atomic Scattering Factors of Their Constituent Atoms. *Proc. Jpn. Acad. Ser. B: Phys. Biol. Sci.* 55, 43–48. doi:10.2183/pjab.55.43

Sawaya, M. R., Pelletier, H., Kumar, A., Wilson, S. H., and Kraut, J. (1994). Crystal Structure of Rat DNA Polymerase β: Evidence for a Common Polymerase Mechanism. *Science* 264, 1930–1935. doi:10.1126/science.7516581

Schroeder, G. K., Lad, C., Wyman, P., Williams, N. H., and Wolfenden, R. (2006). The Time Required for Water Attack at the Phosphorus Atom of Simple Phosphodiesters and of DNA. *Proc. Natl. Acad. Sci.* 103, 4052–4055. doi:10.1073/pnas.0510879103

Showalter, A. K., Lamarche, B. J., Bakhtina, M., Su, M.-I., Tang, K.-H., and Tsai, M.-D. (2006). Mechanistic Comparison of High-Fidelity and Error-Prone DNA Polymerases and Ligases Involved in DNA Repair. *Chem. Rev.* 106, 340–360. doi:10.1021/cr040487k

Sirover, M. A., Dube, D. K., and Loeb, L. A. (1979). On the Fidelity of DNA Replication. Metal Activation of *Escherichia coli* DNA Polymerase I. *J. Biol. Chem.* 254, 107–111. doi:10.1016/s0021-9258(17)30278-8

Slater, J. P., Tamir, I., Loeb, L. A., and Mildvan, A. S. (1972). The Mechanism of *Escherichia coli* Deoxyribonucleic Acid Polymerase I. *J. Biol. Chem.* 247, 6784–6794. doi:10.1016/s0021-9258(19)44655-3

Starnes, M. C., and Cheng, Y. C. (1989). Human Immunodeficiency Virus Reverse Transcriptase-Associated RNase H Activity. *J. Biol. Chem.* 264, 7073–7077. doi:10.1016/s0021-9258(18)83542-6

Steitz, T. A., and Steitz, J. A. (1993). A General Two-Metal-Ion Mechanism for Catalytic RNA. *Proc. Natl. Acad. Sci.* 90, 6498–6502. doi:10.1073/pnas.90.14.6498

Steitz, T. A. (1999). DNA Polymerases: Structural Diversity and Common Mechanisms. *J. Biol. Chem.* 274, 17395–17398. doi:10.1074/jbc.274.25.17395

Stevens, D. R., and Hammes-Schiffer, S. (2018). Exploring the Role of the Third Active Site Metal Ion in DNA Polymerase η with QM/MM Free Energy Simulations. *J. Am. Chem. Soc.* 140, 8965–8969. doi:10.1021/jacs.8b05177

Tabor, S., and Richardson, C. C. (1989). Effect of Manganese Ions on the Incorporation of Dideoxynucleotides by Bacteriophage *T7* DNA Polymerase and *Escherichia coli* DNA Polymerase I. *Proc. Natl. Acad. Sci.* 86, 4076–4080. doi:10.1073/pnas.86.11.4076

Tsai, M. D. (2019). Catalytic Mechanism of DNA Polymerases-Two Metal Ions or Three? *Protein Sci.* 28, 288–291. doi:10.1002/pro.3542

Vashishtha, A. K., and Konigsberg, W. H. (2016). Effect of Different Divalent Cations on the Kinetics and Fidelity of *RB69* DNA Polymerase. *Biochemistry* 55, 2661–2670. doi:10.1021/acs.biochem.5b01350

Vashishtha, A. K., Wang, J., and Konigsberg, W. H. (2016). Different Divalent Cations Alter the Kinetics and Fidelity of DNA Polymerases. *J. Biol. Chem.* 291, 20869–20875. doi:10.1074/jbc.r116.742494

Vyas, R., Reed, A. J., Tokarsky, E. J., and Suo, Z. (2015). Viewing Human DNA Polymerase β Faithfully and Unfaithfully Bypass an Oxidative Lesion by Time-dependent Crystallography. *J. Am. Chem. Soc.* 137, 5225–5230. doi:10.1021/jacs.5b02109

Vyas, R., Reed, A. J., Raper, A. T., Zahurancik, W. J., Wallenmeyer, P. C., and Suo, Z. (2017). Structural Basis for the D-Stereoselectivity of Human DNA Polymerase β. *Nucleic Acids Res.* 45, 6228–6237. doi:10.1093/nar/gkx252

Wang, J., and Smithline, Z. B. (2019). Crystallographic Evidence for Two-metal-ion Catalysis in Human Pol η. *Protein Sci.* 28, 439–447. doi:10.1002/pro.3541

Wang, J., Sattar, A. K. M. A., Wang, C. C., Karam, J. D., Konigsberg, W. H., and Steitz, T. A. (1997). Crystal Structure of a Pol α Family Replication DNA Polymerase from Bacteriophage RB69. *Cell* 89, 1087–1099. doi:10.1016/s0092-8674(00)80296-2

Weaver, T. M., Cortez, L. M., Khoang, T. H., Washington, M. T., Agarwal, P. K., and Freudenthal, B. D. (2020). Visualizing Rev1 Catalyze Protein-Template DNA Synthesis. *Proc. Natl. Acad. Sci. USA* 117, 25494–25504. doi:10.1073/pnas.2010484117

Whitaker, A. M., and Freudenthal, B. D. (2020). History of DNA Polymerase β X-ray Crystallography. *DNA Repair* 93, 102928. doi:10.1016/j.dnarep.2020.102928

Wu, W. J., Yang, W., and Tsai, M. D. (2017). How DNA Polymerases Catalyse Replication and Repiar with Contrasting Fidelity. *Nat. Rev. Chem.* 1, 0068. doi:10.1038/s41570-017-0068

Xia, S., and Konigsberg, W. H. (2014). RB69 DNA Polymerase Structure, Kinetics, and Fidelity. *Biochemistry* 53, 2752–2767. doi:10.1021/bi4014215

Xia, S., Wang, M., Blaha, G., Konigsberg, W. H., and Wang, J. (2011). Structural Insights into Complete Metal Ion Coordination from Ternary Complexes of B Family *RB69* DNA Polymerase. *Biochemistry* 50, 9114–9124. doi:10.1021/bi201260h

Xia, S., Wang, J., and Konigsberg, W. H. (2013). DNA Mismatch Synthesis Complexes Provide Insights into Base Selectivity of a B Family DNA Polymerase. *J. Am. Chem. Soc.* 135, 193–202. doi:10.1021/ja3079048

Yang, W., Weng, P. J., and Gao, Y. (2016). A New Paradigm of DNA Synthesis: Three-Metal-Ion Catalysis. *Cell Biosci.* 6, 51. doi:10.1186/s13578-016-0118-2

Yoon, H., and Warshel, A. (2017). Simulating the Fidelity and the Three Mg Mechanism of Pol η and Clarifying the Validity of Transition State Theory in Enzyme Catalysis. *Proteins* 85, 1446–1453. doi:10.1002/prot.25305

Conflict of Interest: The authors declare that the research was conducted in the absence of any commercial or financial relationships that could be construed as a potential conflict of interest.

Publisher's Note: All claims expressed in this article are solely those of the authors and do not necessarily represent those of their affiliated organizations, or those of the publisher, the editors, and the reviewers. Any product that may be evaluated in this article, or claim that may be made by its manufacturer, is not guaranteed or endorsed by the publisher.

frontiers in Molecular Biosciences

REVIEW
published: 07 January 2022
doi: 10.3389/fmolb.2021.815845

When DNA Polymerases Multitask: Functions Beyond Nucleotidyl Transfer

Denisse Carvajal-Maldonado[1], *Lea Drogalis Beckham*[2], *Richard D. Wood*[1]* and *Sylvie Doublié*[2]*

[1]Department of Epigenetics and Molecular Carcinogenesis, The University of Texas MD Anderson Center, Houston, TX, United States, [2]Department of Microbiology and Molecular Genetics, University of Vermont, Burlington, VT, United States

DNA polymerases catalyze nucleotidyl transfer, the central reaction in synthesis of DNA polynucleotide chains. They function not only in DNA replication, but also in diverse aspects of DNA repair and recombination. Some DNA polymerases can perform translesion DNA synthesis, facilitating damage tolerance and leading to mutagenesis. In addition to these functions, many DNA polymerases conduct biochemically distinct reactions. This review presents examples of DNA polymerases that carry out nuclease (3′—5′ exonuclease, 5′ nuclease, or end-trimming nuclease) or lyase (5′ dRP lyase) extracurricular activities. The discussion underscores how DNA polymerases have a remarkable ability to manipulate DNA strands, sometimes involving relatively large intramolecular movement.

Keywords: DNA polymerases, nucleotidyl transfer, DNA repair, nuclease activity, lyase activity, proofreading

OPEN ACCESS

Edited by:
Janice Pata,
Wadsworth Center, United States

Reviewed by:
Todd Washington,
The University of Iowa, United States
Linlin Zhao,
University of California, Riverside, United States

***Correspondence:**
Sylvie Doublié
sdoublie@uvm.edu
Richard D. Wood
rwood@mdanderson.org

Specialty section:
This article was submitted to Structural Biology, a section of the journal Frontiers in Molecular Biosciences

Received: *15 November 2021*
Accepted: *13 December 2021*
Published: *07 January 2022*

Citation:
Carvajal-Maldonado D, Drogalis Beckham L, Wood RD and Doublié S (2022) When DNA Polymerases Multitask: Functions Beyond Nucleotidyl Transfer. Front. Mol. Biosci. 8:815845. doi: 10.3389/fmolb.2021.815845

INTRODUCTION

DNA polymerases have been intensively studied for decades because of their fundamental importance in DNA replication. Organisms throughout nature possess an array of polymerases encoded by their genomes, specialized for functions in DNA repair, recombination, and DNA damage tolerance. The canonical DNA polymerase reaction is the addition of a nucleotide, usually a deoxynucleoside triphosphate, to the 3′ end of a growing DNA chain, liberating pyrophosphate (**Figure 1**). The reverse reaction, pyrophosphorolysis, catalyzed by some DNA polymerases, is driven backwards by an excess of pyrophosphate. The purpose of this review is to highlight the existence of additional activities associated with DNA polymerases beyond canonical nucleotidyl transfer (**Figure 2**). We briefly summarize each activity, emphasizing recent results and unsolved issues.

3′–5′ Exonuclease Activity

All DNA polymerases share a common polymerase fold, which has been compared to a human right hand, composed of three subdomains: fingers, palm, and thumb (Steitz, 1999). In addition, the DNA polymerase toolbox can include a 3′–5′ exonuclease domain whose main role is to proofread new DNA synthesis to remove nucleotides that have been incorrectly incorporated. This reduces the error rate of DNA polymerases by one or more orders of magnitude during DNA replication (Joyce, 2013). In certain contexts, this 3′–5′ exonuclease activity is essential. Loss of editing activity results in increased incidence of cancer and pronounced genome instability (Shevelev and Hübscher, 2002; Shanbhag et al., 2018).

Multiple families of DNA polymerases harbor a 3′–5′ exonuclease activity: B-, C-, and D-family replicative polymerases (δ and ε in eukaryotes, Pol III in *E. coli,* PolD in euryarchaeota) and A-family

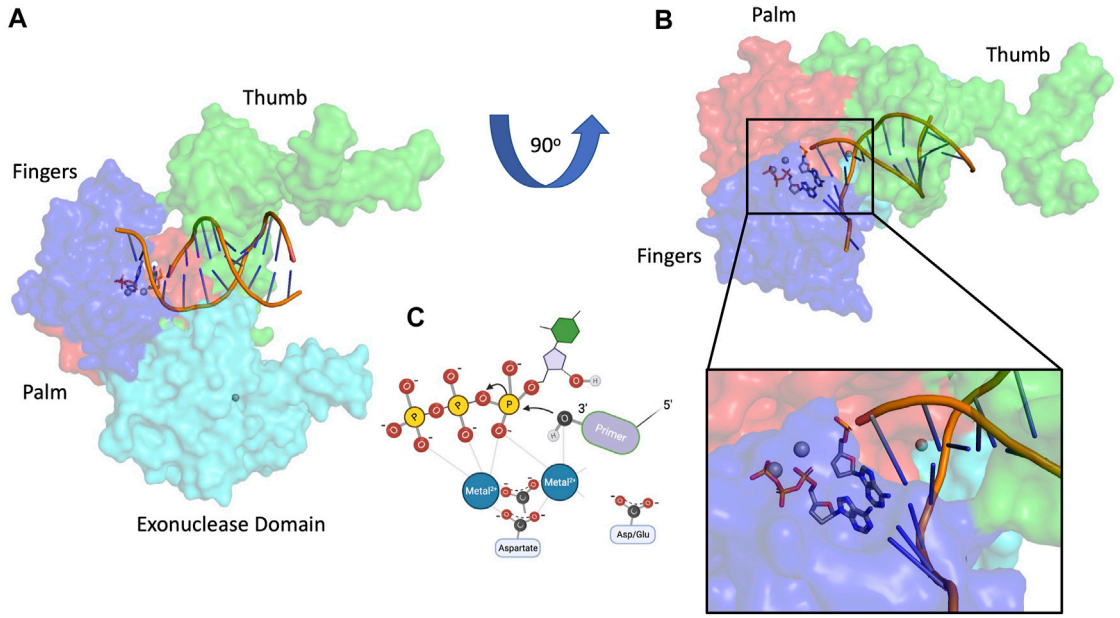

FIGURE 1 | Canonical DNA polymerase nucleotidyl transfer activity. **(A)** T7 DNA polymerase structure 1SKR (Li et al., 2004), **(B)** T7 DNA polymerase rotated 90° with magnified inset, **(C)** two-metal DNA polymerase mechanism. Subdomain color scheme: fingers (blue), palm (red), thumb (green), 3′-5′ exonuclease (cyan).

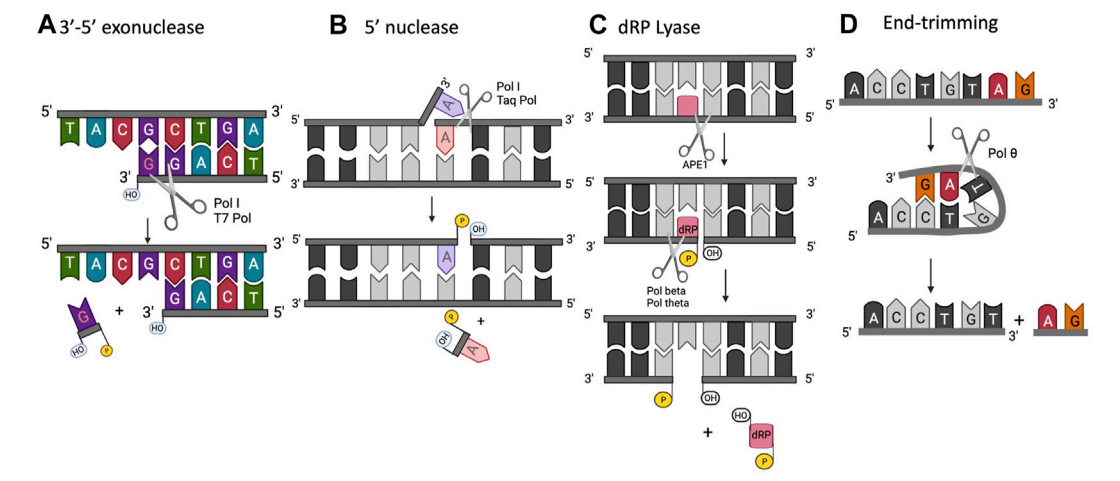

FIGURE 2 | Extracurricular functions of DNA polymerases. **(A)** 3′-5′ exonuclease, **(B)** 5′ structure-specific nuclease, **(C)** dRP lyase, **(D)** end-trimming nuclease.

repair polymerases, such as *E. coli* Pol I (Filée et al., 2002). Many A-family and some B-family polymerases have a conserved 3′–5′ exonuclease domain located in the N-terminal region of the larger polymerase domain (Khare and Eckert, 2002). In other B-family polymerases, the location of the exonuclease domain is found in a structurally distant region. The exonuclease active site in *E. coli* DNA polymerase I, an A-family polymerase, is ~30 Å away from the polymerase active site (**Figure 3A**), whereas the distance between the two active sites is closer to ~40 Å in B-family polymerases (**Figure 3B**) (Franklin et al., 2001; Hogg et al., 2004). Most B-family DNA polymerases have an extended β-hairpin loop that facilitates primer movement by holding the template strand in place as the primer switches into the exonuclease active site, a feature not found in A-family polymerases with 3′–5′ exonuclease activity (Hogg et al., 2007).

Although homology among DNA polymerases varies significantly, the 3′–5′ exonuclease active site itself is very conserved within A-family polymerases. There are three highly conserved amino acid regions containing critical residues that coordinate two divalent metal ions, ssDNA and deoxyribonucleoside monophosphates (dNMPs) (Bernad et al., 1989; Pinz and Bogenhagen, 2000). A key catalytic step required

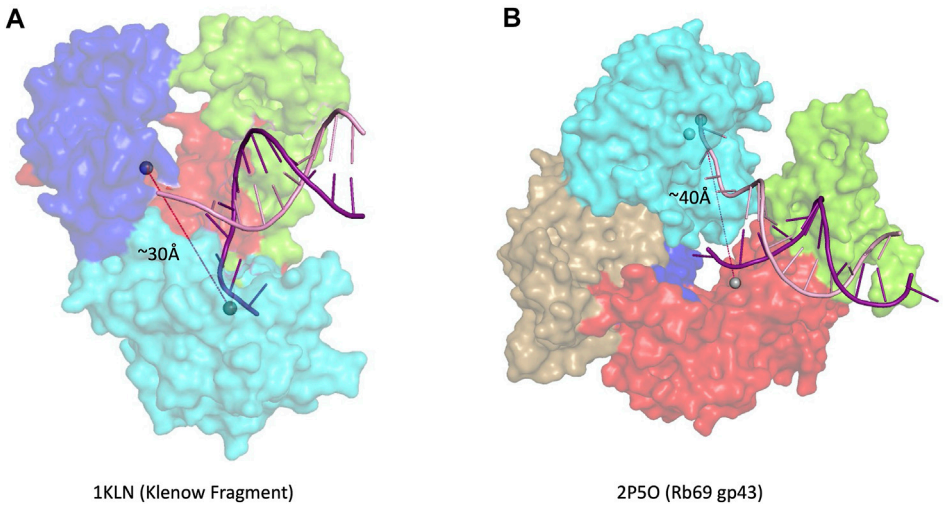

FIGURE 3 | 3′–5′ exonuclease. **(A)** Family- A polymerase Klenow fragment with DNA in the editing site (1KLN) (Beese et al., 1993), **(B)** Family-B polymerase RB69 gp43 with DNA in the editing site (2P5O) (Hogg et al., 2004). Subdomain color scheme same as **Figure 1**, with RB69 gp43 N-terminal domain in gold.

for 3′–5′ exonuclease activity is the chelation of two metal ions by active-site aspartates and glutamates (carboxylates) (Park et al., 1997). The Exo I, Exo II, and Exo III regions are essential for the exonuclease activity, as they contain the carboxylates that directly bind the metal ions required for catalysis (Bernad et al., 1989). Recent studies have identified other residues that help facilitate catalysis in the exonuclease active site. In bacteriophage ϕ29 DNA polymerase, tyrosine, threonine, and glutamine residues help coordinate the binding of DNA to the exonuclease active site. Specifically, Tyr 101 and Thr 189 assist in melting dsDNA to form ssDNA that can bind the active site (Rodriguez et al., 2019). Although *Thermus aquaticus* DNA polymerase (Taq) comprises an exonuclease domain, the enzyme lacks the three aspartates and one glutamate essential for catalysis and therefore has no proofreading activity (Kim et al., 1995); nevertheless exonuclease activity can be conferred to some extent by introducing the four carboxylates into the Taq sequence (Park et al., 1997).

To ensure replication fidelity the exonuclease activity operates in a delicate balance with the polymerase activity, with the exonuclease favored when a mismatch is inserted (Doublié and Zahn, 2014). The enzyme contributes to this regulation by monitoring the newly incorporated bases. The polymerase senses a mismatch by using strategically positioned protein residues that detect the minor groove N3 and exocyclic O2 positions of incorrect base pairs after incorporation, such as Arg 429 and Gln 615 in T7 DNA polymerase, and Tyr 567 and Lys 706 in RB69 gp43, respectively (Doublié et al., 1998; Franklin et al., 2001; Hogg et al., 2004). In Family B DNA polymerase ϵ, conserved Lys 967 and Arg 988 were found essential in regulating the switching of the DNA primer between the polymerase active site and exonuclease active site. Both residues lie between the palm and thumb domains and directly interact with the minor groove (Ganai et al., 2015). When a mismatch is present, the melting temperature of the bases at the 3′ terminus is lower favoring the formation of ssDNA ends. In fact, the binding of at least 3-4 bp ssDNA in the exonuclease active site is required to favor the cleavage reaction over the polymerase reaction, (Derbyshire et al., 1988; Beese et al., 1993). The functional separation of the two active sites also helps in the regulation of the exonuclease activity, to ensure it is used sparingly and only when mismatches are introduced. To achieve proper binding in the exonuclease active site, the enzyme must translocate backwards, leading to sufficient DNA unwinding to allow the primer terminus to leave the polymerase active site and bind the exonuclease active site (Beese et al., 1993). More recent FRET experiments mapped the trajectories recorded by a DNA primer translocating from the polymerase active site to the exonuclease active site of the Klenow fragment of DNA pol I. These data revealed that the enzyme can shuttle the primer between the two sites without dissociating from DNA (intramolecular transfer) (Lamichhane et al., 2013).

In some B-family polymerases, the two domains may be more structurally distant, complicating this active site switching step. To overcome this obstacle, some polymerases can bend the DNA in the active site to bring the exonuclease domain closer to the polymerase domain, facilitating the cleavage reaction. In the bacteriophage ϕ29 DNA pol, the primer terminus moves in one dimension from the polymerization site to the exonuclease site by a 40° rotation in the helix of the DNA (Khare and Eckert, 2002; Del Prado et al., 2018). In addition to the conserved catalytic aspartates in the exonuclease domain discussed above, a non-catalytic conserved aspartate with a regulatory role has recently been identified (Del Prado et al., 2018). In ϕ29 DNA pol, this residue, Asp 121, is located between the Exo II and Exo III motifs. This Asp facilitates the binding of ssDNA substrates at the 3′–5′ exonuclease active site, but, interestingly, it does not come into contact with the metal ions or the ssDNA. Asp 121 facilitates the melting of dsDNA to form the ssDNA primer required to catalyze the cleavage reaction. Similar invariant aspartates have also been identified in other enzymes, such as Asp 150 in *E. coli*

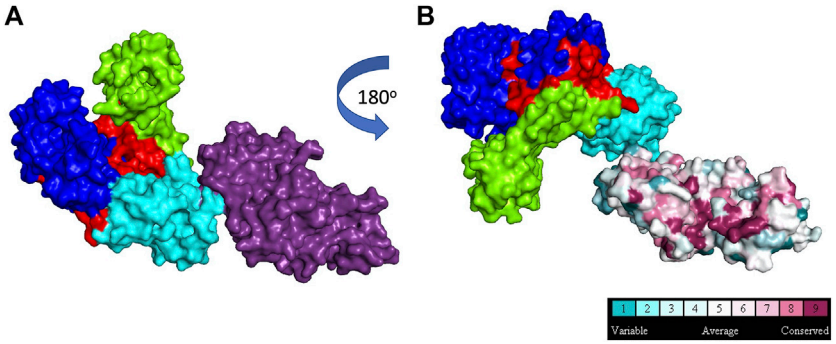

FIGURE 4 | 5′ structure specific nuclease. **(A)**: Taq polymerase with 5′ nuclease domain shown in purple, **(B)**: Taq polymerase rotated 180° to show 5′ nuclease residue conservation across 150 homologs (1TAQ) (Kim et al., 1995). Subdomain color scheme same as **Figure 1**.

RNase T (Zuo and Deutscher, 2002). In bacteriophage T7 DNA pol, mutating the predicted invariant Asp90 in the active site of the exonuclease domain completely ablated the exonuclease activity of the enzyme (Del Prado et al., 2018). The proximity of Asp 90 to multiple residues required for the exonuclease reaction suggested to the authors that this residue functions in a "Romanesque vault" structure, facilitating bending of the DNA to bring the primer into the correct orientation in the active site for cleavage (Del Prado et al., 2018).

Even further redundancies and regulators have been found that facilitate the switch between polymerase activity and exonuclease activity, which is essential for replication fidelity. The switch between polymerase active site and exonuclease active site is also controlled by the concentration of dNTP present in the active site (Beechem et al., 1998). Decreased occupancy of the polymerase active site by incoming dNTP shifts the balance towards exonuclease catalysis. More recently, it was shown that phosphorylation of yeast Pol ε during replication fork stalling can also shift the equilibrium. Checkpoint kinases mediate the phosphorylation of Ser 430 in *S. cerevisiae* pol2, preventing primer DNA switching to exonuclease sites. This post-translational modification regulates the DNA switching between the polymerase active site and the exonuclease site, limiting fork resection and subsequent collapse (Pellicanò et al., 2021).

Beyond proofreading, polymerase 3′–5′ exonuclease activity is important in promoting virus genetic recombination, as seen in Poxviruses. Vaccinia DNA Polymerase mutants lacking 3′–5′ exonucleolytic activity showed a dramatic reduction in recombination (Gammon and Evans, 2009). The authors propose a model in which the polymerase may use 3′–5′ exonuclease activity to rescue a double-strand break (DSB) by exposing sufficient homology in ssDNA to allow annealing at the break, repair by DNA polymerase and ligase, and subsequent resumption of DNA replication (Gammon and Evans, 2009).

5′-Nuclease Activity

Some DNA polymerases, such as Taq, also possess a 5′- nuclease activity located in a separate domain (**Figure 4**) (Longley et al., 1990; Lyamichev et al., 1999). The 5′-nuclease activity was originally referred to as a 5′–3′ exonuclease activity, but it has since been established as a structure specific-cleavage of a 5′-ssDNA end joined to duplex DNA, a structure that is formed during lagging strand DNA synthesis (Joyce, 2013). Conserved residues in the 5' nuclease domain (Gutman and Minton, 1993) share homology with the flap endonuclease (FEN1/XPG) family of proteins (Harrington and Lieber, 1994; Robins et al., 1994; Patel et al., 2001; Tsutakawa et al., 2011). In *E. coli* Pol I, the 5′-nuclease domain is tethered to the polymerase domain by an unstructured 16 amino acid peptide that is susceptible to proteolytic cleavage, allowing isolation of a Pol I "Klenow fragment" that lacks the 5′-nuclease domain (Klenow and Overgaard-Hansen, 1970). As such, the Pol I 5′-nuclease primarily operates during lagging strand synthesis to remove 5′ flaps formed when Pol I encounters Okazaki fragments during synthesis. The 5′-nuclease activity recognizes the 5′ flap and cuts between the first two bases, creating a nick on the DNA that is subsequently filled by DNA ligase (Ceska and Sayers, 1998; Xu et al., 2000).

DNA travels between the polymerase and 5′- nuclease domains through several conformational transitions (Joyce et al., 1992). The 5′-nuclease domain is flexible and adopts different positions within the Pol I-DNA complex to remove 5′ flaps (Ceska and Sayers, 1998). The polymerase and 5′ nuclease active sites compete for access to DNA ends, with dramatic shifts between the two active sites occurring during ongoing lagging strand synthesis. The 5' nuclease activity also requires 2 divalent metal ions for cleavage. The selection of activity is likely intricately regulated by molecular "gates" in the active site, although details of this regulation are unknown (Joyce, 2013). However, the intricate gating mechanisms in FEN family proteins that help discern between different substrates can be used to glean insights into how 5′- nuclease is regulated in Pol I (Grasby et al., 2012; Pauszek et al., 2021).

5′-dRP Lyase Activity

Steps in base excision repair (BER) occur in a coordinated manner and enzymes are sequentially displaced to facilitate the next step in the pathway. During BER, a damaged base (for example, one modified by reactive oxygen species) is removed by a lesion-specific DNA glycosylase. This process

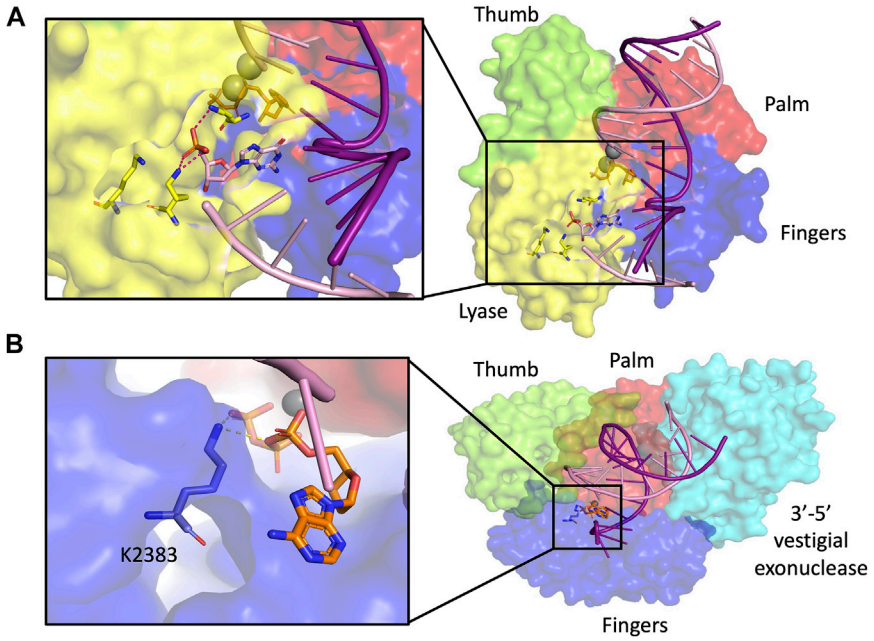

FIGURE 5 | dRP lyase. **(A)** Pol β structure with dRP lyase residues highlighted in yellow in magnified inset (2FMS) (Batra et al., 2006), **(B)** Pol θ structure with dRP lyase residue highlighted in blue in magnified inset (4×0P) (Zahn et al., 2015). Subdomain color scheme same as **Figure 1**.

leaves an apurinic/apyrimidinic (AP) site or abasic site that is recognized and cleaved by an AP endonuclease. This cleavage leaves a 5′-terminal deoxyribophosphate (dRP) residue that must be removed in concert with replacement of the base. In mammalian cells, Pol β is the main DNA polymerase involved in BER, and it is able to carry out both of these enzymatic steps. Pol β removes 5′- dRP and fills the gap (Matsumoto and Kim, 1995; Sobol et al., 1996; Allinson et al., 2001).

The 5′-dRP lyase activity is contained within an 8 kDa N-terminal domain of Pol β (Prasad et al., 1994; Prasad et al., 1998) (**Figure 5A**). A metal ion is required for release of the 5′dRP from double-stranded DNA allowing the gap in the DNA to be filled and subsequently ligated (Matsumoto and Kim, 1995).

A nick adjacent to a 5′-dRP residue is a small target, and Pol β must bind non-specifically along the DNA as it searches for the right substrate to cleave. PARP1 has a high affinity for this substrate and may help recruit pol β (Khodyreva et al., 2010; Prasad et al., 2014). Recently, it was found that three lysines in the lyase active site of Pol β facilitate the search for the 5′- flap substrate on the dsDNA and destabilize non-specific DNA binding. Mutating these three lysine residues to alanines in the lyase active site of Pol β (Lys 35, Lys 68, and Lys 72), increased the binding affinity of Pol β for nonspecific DNA, indicating a role of the 5′dRP lyase in the specificity of lesion recognition (Howard et al., 2020). A tumor-associated variant in the N-terminal 8 kDa domain of Pol β retains polymerase activity but is dRP lyase deficient (Dalal et al., 2008). DNA methylating agents such as methyl methane sulfonate (MMS) create base lesions that are removed by BER. Fibroblasts of Pol β null mice are hypersensitive to MMS. This sensitivity can be rescued by complementation with the 5′dRP lyase activity of Pol β, without requiring the DNA polymerase activity (Sobol et al., 2000). In this case, another DNA polymerase such as pol δ accomplishes gap filling (Klungland and Lindahl, 1997; Fortini et al., 1998). Furthermore, Pol β 5′dRP lyase activity is suggested to be important in preventing trinucleotide repeat instability. Pol β defective in 5′-dRP lyase activity can be tightly bound to a repair site, forcing slippage that can result in deletions of trinucleotides (Lai et al., 2018).

Other polymerases also carry out 5′-dRP lyase activity. Y-Family pol iota (Pol ι) possesses 5′-dRP lyase activity and can alleviate BER deficiency *in vitro* (Bebenek et al., 2001; Prasad et al., 2003). Loss of Pol ι sensitizes the cells to treatment with oxidative damaging agents (Petta et al., 2008). Pol ι accumulates in sites of oxidative DNA damage and associates with BER modulator XRCC1 to facilitate repair. The recruitment of Pol ι to sites of DNA damage in human cells requires the 5-dRP lyase domain of the enzyme. It is not clear whether the dRPase of Pol ι is functionally relevant to its operation in a pathway to counteract DNA replication stress (Wang et al., 2020), involving p53-dependent reactivation of DNA replication forks (Hampp et al., 2016; Biber et al., 2020).

The A-Family polymerase Pol θ also possesses 5′-dRP lyase activity within its polymerase domain. *In vitro*, Pol θ can participate in BER reactions (Prasad et al., 2009). Lys 2383, a residue critical for AP lyase, is also important for the DNA polymerase activity of Pol θ (**Figure 5B**) (Laverty et al., 2018). The 5′-dRP lyase activity of Pol θ can also operate in structurally clustered lesions (Laverty and Greenberg, 2018). In these clustered regions, Pol β is 15–20 fold slower at excising the 5′-dRP lyase compared to Pol θ, which suggests that the two polymerases may have evolved to take care of a larger variety of substrates, with Pol β being favored for excising lesions with

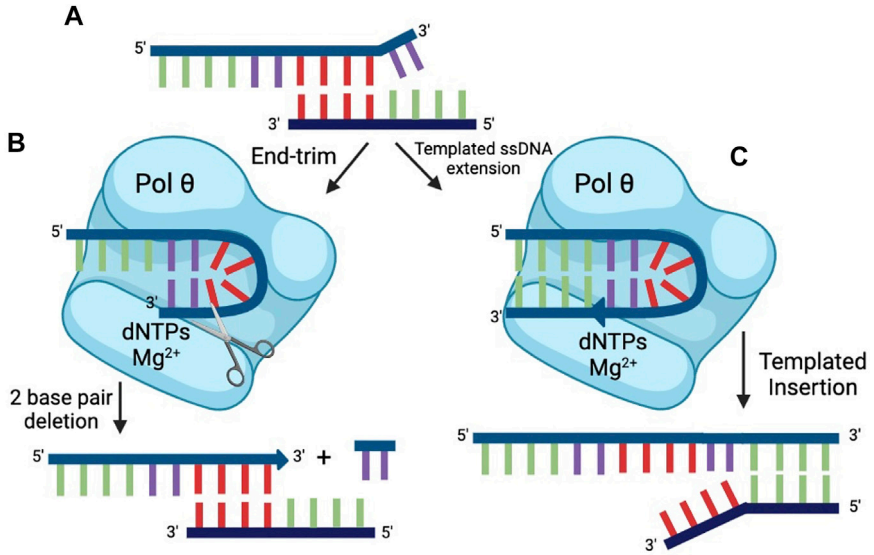

FIGURE 6 | End-trimming. **(A)** The top strand of DNA cannot serve as a primer for successful repair because the microhomology (red) is internal. Two terminal 3′ nt (violet) are unpaired. Pol θ can process ssDNA ends by two modes: **(B)** Transient self-pairing of a 3′ end within pol θ (violet nt) can lead to end-trimming catalysis, resulting in removal of 2 nt (in this case). This allows the internal microhomology (red) to engage in productive priming. **(C)** Transient self-pairing of a 3′ end within pol θ (violet nt) can alternatively result in limited synthesis. In this case, 4 nt (green) that are complementary to an internal microhomology on the bottom strand of DNA are synthesized. The result of this process is a short, templated insertion.

opposite polarity than those excised by Pol θ (Laverty and Greenberg, 2018). BER is also important for repair of oxidative lesions in mitochondrial DNA. Mitochondrial DNA polymerase γ (Pol γ) also possesses 5′-dRP lyase activity, although with a much slower release of the dRP group from the enzyme compared to Pol β. In fact, the 5′-dRP lyase activity in A-family polymerases such as Pol γ, Pol θ, and Pol I is significantly slower than in Pol β, which suggests that this function may not be sufficient to complete repair of abundant AP sites (Pinz and Bogenhagen, 2000).

3′-End-Trimming and Single-Strand Extension

A DNA end-trimming activity, distinct from the nuclease activities discussed above, was identified in human Pol θ (Zahn et al., 2021). The rapid end-trimming activity acts on single-stranded DNA when placed in a transient and appropriate self-pairing conformation within pol θ (**Figure 6**). This end-trimming activity is different from 3′ to 5′ exonuclease activity. Although Pol θ contains a proofreading domain, it lacks two of the conserved amino acids necessary for 3′–5′ exonuclease activity. Further, a short loop in the exonuclease-like domain of pol θ would impede access of DNA to the exonuclease active site (Zahn et al., 2015).

This end-trimming activity shares many of the dependencies and catalytic residues that are required for the DNA polymerase reaction. For example, end-trimming is dependent on the presence of divalent cation (Mg^{2+} or Mn^{2+}), on catalytic residues including invariant aspartate Asp 2330 that coordinates Mg^{2+} in the active site, and on the addition of dNTPs (Zahn et al., 2021). Catalysis of both extension and nuclease activity from the same active site is plausible in principle because the two-metal ion active sites of nucleotidyl transfer enzymes share close similarities with the active sites of many nucleases (Yang et al., 2006).

Experimentally, dNTP-dependent end-trimming activity is observed with some, but not all single-stranded oligonucleotides. For those substrates that are end-trimmed, a unifying feature is that the 3′ terminus is capable of potential self-pairing with a short sequence within the oligonucleotide, suggesting that a hairpin-type configuration is transiently formed within the active site of pol θ (**Figure 6B**). On the most-studied substrate, 2 nt are cleaved from the 3’ terminus in an endonucleolytic reaction; on some substrates 1 nt is removed; on others, possibly more than 2 nt may be end-trimmed. The end-trimming configuration appears to be unimolecular, because all substrate is quickly consumed. Further, the proposed end-trimming configuration explains another activity of pol θ, the ability to extend single-stranded DNA substrate.

Pol θ DNA polymerase can extend some single-stranded DNA molecules, an activity that is not shared by other known A-family polymerases (Hogg et al., 2012). In the presence of Mg^{2+}, the products observed are both primed and largely templated by the same oligonucleotide (**Figure 6C**) (Hogg et al., 2012; Yousefzadeh et al., 2014). It was suggested that the single-stranded extension activity of Pol θ was the result of non-templated terminal transferase activity (Kent et al., 2016). However, Pol θ is not a terminal transferase. Experiments in the study suggesting terminal transferase activity were conducted using Mn^{2+}. This metal leads to promiscuous synthesis and a high rate of mismatch

incorporation, and it is known that Pol θ can extend readily from a 3′-terminal mismatch (Seki and Wood, 2008; He and Yang, 2018). Like other A family polymerases, Pol θ can add an additional dATP to a blunt DNA end, but otherwise shows predictable template requirements in a first round of DNA synthesis (He and Yang, 2018).

DNA polymerase θ is the defining enzyme in a double strand break repair pathway, termed theta-mediated end-joining (TMEJ). During TMEJ, Pol θ engages single stranded 3′ ends by microhomology. It thus makes sense that Pol θ recognizes and processes ssDNA in several ways. Pol θ apparently manipulates the 3′ end of the ssDNA in the active site, forming a transitory hairpin that serves as the intermediate for either cleavage or extension of the 3′-end (Zahn et al., 2021). The factors that dictate the choice between these two activities are being investigated, as well as how processed single-strands are then advanced to a repair stage that uses pairing at microhomologies and primed extension on double-stranded DNA. Statistically, microhomologies will rarely be found at the ends of a double-strand break but will more often occur internal to the break (**Figure 6A**). The two steps of processing of DNA ends and templated extension appear to largely explain the mutational "signature" of TMEJ, involving short sequence insertions and deletions at the site of repair (Schimmel et al., 2019; Carvajal-Garcia et al., 2020; Hwang et al., 2020).

Endonucleolytic cleavage of a polynucleotide chain is also a feature of RNA polymerases, which edit transcripts by cleaving off 1 or 2 nucleotides from the 3′ end (Izban and Luse, 1992; Reines, 1992; Borukhov et al., 1993). This editing reactions are conducted in a Mg^{2+} - dependent manner from the RNA polymerase active site. The regulation of extension vs. cleavage is enhanced by protein cofactors that participate directly in reorganizing the amino acids in the catalytic site, referred to as "active center tuning" (Sosunova et al., 2013). For example, the endonuclease activity of *E. coli* RNA polymerase is stimulated by Gre proteins, and eukaryotic RNA pol II by TFIIS. Stimulated by Gre, RNA polymerase clips off the two terminal nt of a synthetic RNA fragment (Sosunov et al., 2003; Sosunova et al., 2013). In contrast to the pol θ end-trimming reaction, RNA polymerase editing does not seem to be directly dNTP- or NTP-dependent, although it can be modulated by nucleotide concentration. Other nucleotidyl transferases may also engage in a form of end-trimming or editing. For example, telomerase, including highly purified human telomerase, can shorten products as well as extend them (Collins and Greider, 1993; Rubtsova et al., 2012; Fouquerel et al., 2016).

Activity on RNA

Some DNA polymerases perform nucleotidyl transferase reactions that do not involve the usual DNA substrates or primers, and are briefly mentioned here to further illustrate the enzymatic versatility of DNA polymerases.

Reverse Transcriptase

Reverse transcriptases are RNA-dependent DNA polymerases, which use an RNA template to synthesize DNA. Some DNA-dependent DNA polymerases have been reported to have reverse transcriptase activity. Two bacterial A-family polymerases, *Bst* DNA polymerase and the Klenow fragment of *E. coli* Pol I, were successfully used to reverse transcribe RNA *in vitro* (Shi et al., 2015). Taq DNA polymerase can also engage in this activity, after mutating a single aspartate into asparagine (Barnes et al., 2021). Human pol η can use either a DNA duplex or and RNA/DNA mixed duplex during synthesis (Franklin et al., 2004; Su et al., 2017), and was shown to function as a reverse transcriptase in a cellular environment (Su et al., 2019). Pol θ was recently reported to also have a reverse transcriptase activity, although additional studies are warranted to establish the physiological relevance of this finding (Chandramouly et al., 2021).

Primase-Polymerase

Some DNA polymerases, for example eukaryotic DNA pol α, have a separate primase subunit that allows RNA priming for DNA replication. PrimPol is the only known eukaryotic DNA polymerase with intrinsic priming activity. Both primase and DNA synthesis are mediated by the same active site. Recently it was found that a priming activity of DNA polymerase PrimPol is used for replication restart after DNA damage (Garcia-Gomez et al., 2013; Mouron et al., 2013). PrimPol is primarily a TLS polymerase which is found in both the nucleus and the mitochondria, and is capable of bypassing 7,8-dihydro-8-oxoguanine (oxoG) and cyclobutane pyrimidine dimers (CPD) (Mouron et al., 2013; Rechkoblit et al., 2021). PrimPol can synthesize short DNA primers which other polymerases, like mitochondrial polymerase γ, can use to restart replication promoting overall mitochondrial genome maintenance. Recent studies have found that PrimPol repriming activity is used by stalled replication forks to skip DNA lesions and restart replication, leaving behind ssDNA gaps that can be filled by other repair polymerases (Quinet et al., 2020; Tirman et al., 2021).

CONCLUSION

DNA polymerases catalyze the nucleotidyl transfer reaction to generate a DNA polymer. In practice, however, this class of enzymes is able to catalyze a host of other DNA processing reactions that make DNA polymerases a multi-tool of genomic integrity. Redundancy in the activities of DNA polymerases is critical for replication and maintenance of the cell. If a DNA polymerase is unable to perform its function, other DNA polymerases are poised to intervene and assume the role of replication and repair typically filled by the compromised enzyme. These redundancies also facilitate the sheer amount of DNA replication and repair that must continuously occur in the cell throughout its life. It must be noted that the existence of redundant polymerase roles makes targeting DNA polymerases in cancer a challenge due to the ability of the cell to compensate for the loss by employing a different polymerase.

By using a DNA polymerase to execute more than one aspect of DNA processing, the cell can benefit energetically. Requiring a separate enzyme for each step would necessitate a greater energetic commitment from the cell to synthesize and recruit these enzymes than employing an existing polymerase.

Furthermore, repurposing the active site of a DNA polymerase can facilitate spatial organization of enzymatic activities. By utilizing a common active site for multiple reactions, the polymerase becomes a hub where each activity may be performed sequentially. This arrangement is advantageous to the cell as a polymerase can process DNA in multiple ways before diffusing from the DNA, further minimizing the amount of energy required to attain appropriately processed DNA.

While DNA polymerases have been investigated for close to 60 years, we continue to discover noncanonical polymerase activities. From the addition of an enzymatic domain to exploiting an existing active site, DNA polymerases act like Swiss army knives of DNA processing. We can look forward to discovering what other functions these DNA multi-tools utilize to tackle DNA processing errors. Conveniently these multiple functions present additional opportunities to design small molecule inhibitors against these multitasking enzymes.

AUTHOR CONTRIBUTIONS

All authors contributed to planning of the article, writing, designing figures, and editing.

FUNDING

Work on DNA polymerases in our laboratories is funded by National Institutes of Health grant T32 AI055402 (LD), P01 CA247773 (SD and RW), and the J. Ralph Meadows Chair in Carcinogenesis Research (RW).

ACKNOWLEDGMENTS

We acknowledge Prof. Tom Steitz, whose pioneering structural insights into nucleic acid polymerases made the work presented here possible.

REFERENCES

Allinson, S. L., Dianova, I. I., and Dianov, G. L. (2001). DNA Polymerase Beta Is the Major dRP Lyase Involved in Repair of Oxidative Base Lesions in DNA by Mammalian Cell Extracts. *EMBO J.* 20 (23), 6919–6926. doi:10.1093/emboj/20.23.6919

Barnes, W. M., Zhang, Z., and Kermekchiev, M. B. (2021). A Single Amino Acid Change to Taq DNA Polymerase Enables Faster PCR, Reverse Transcription and Strand-Displacement. *Front. Bioeng. Biotechnol.* 8. doi:10.3389/fbioe.2020.553474

Batra, V. K., Beard, W. A., Shock, D. D., Krahn, J. M., Pedersen, L. C., and Wilson, S. H. (2006). Magnesium-induced Assembly of a Complete DNA Polymerase Catalytic Complex. *Structure* 14 (4), 757–766. doi:10.1016/j.str.2006.01.011

Bebenek, K., Tissier, A., Frank, E. G., McDonald, J. P., Prasad, R., Wilson, S. H., et al. (2001). 5'-Deoxyribose Phosphate Lyase Activity of Human DNA Polymerase ι *In Vitro*. *Science* 291(5511), 2156–2159. doi:10.1126/science.1058386

Beechem, J. M., Otto, M. R., Bloom, L. B., Eritja, R., Reha-Krantz, L. J., and Goodman, M. F. (1998). Exonuclease–Polymerase Active Site Partitioning of Primer–Template DNA Strands and Equilibrium Mg2+ Binding Properties of Bacteriophage T4 DNA Polymerase. *Biochemistry* 37 (28), 10144–10155. doi:10.1021/bi980074b

Beese, L. S., Derbyshire, V., and Steitz, T. A. (1993). Structure of DNA Polymerase I Klenow Fragment Bound to Duplex DNA. *Science* 260 (5106), 352–355. doi:10.1126/science.8469987

Bernad, A., Blanco, L., Lázaro, J., Martín, G., and Salas, M. (1989). A Conserved 3′→5′ Exonuclease Active Site in Prokaryotic and Eukaryotic DNA Polymerases. *Cell* 59 (1), 219–228. doi:10.1016/0092-8674(89)90883-0

Biber, S., Pospiech, H., Gottifredi, V., and Wiesmüller, L. (2020). Multiple Biochemical Properties of the P53 Molecule Contribute to Activation of Polymerase iota-dependent DNA Damage Tolerance. *Nucleic Acids Res.* 48 (21), 12188–12203. doi:10.1093/nar/gkaa974

Borukhov, S., Sagitov, V., and Goldfarb, A. (1993). Transcript Cleavage Factors from E. coli. *Cell* 72 (3), 459–466. doi:10.1016/0092-8674(93)90121-6

Carvajal-Garcia, J., Cho, J.-E., Carvajal-Garcia, P., Feng, W., Wood, R. D., Sekelsky, J., et al. (2020). Mechanistic Basis for Microhomology Identification and Genome Scarring by Polymerase Theta. *Proc. Natl. Acad. Sci. USA* 117 (15), 8476–8485. doi:10.1073/pnas.1921791117

Ceska, T., and Sayers, J. R. (1998). Structure-specific DNA Cleavage by 5′ Nucleases. *Trends Biochem. Sci.* 23 (9), 331–336. doi:10.1016/s0968-0004(98)01259-6

Chandramouly, G., Zhao, J., McDevitt, S., Rusanov, T., Hoang, T., Borisonnik, N., et al. (2021). Pol θ Reverse Transcribes RNA and Promotes RNA-Templated DNA Repair. *Sci. Adv.* 7, eabf1771.

Collins, K., and Greider, C. W. (1993). Tetrahymena Telomerase Catalyzes Nucleolytic Cleavage and Nonprocessive Elongation. *Genes Develop.* 7 (7b), 1364–1376. doi:10.1101/gad.7.7b.1364

Dalal, S., Chikova, A., Jaeger, J., and Sweasy, J. B. (2008). The Leu22Pro Tumor-Associated Variant of DNA Polymerase Beta Is dRP Lyase Deficient. *Nucleic Acids Res.* 36 (2), 411–422. doi:10.1093/nar/gkm1053

Del Prado, A., Franco-Echevarría, E., González, B., Blanco, L., Salas, M., and de Vega, M. (2018). Noncatalytic Aspartate at the Exonuclease Domain of Proofreading DNA Polymerases Regulates Both Degradative and Synthetic Activities. *Proc. Natl. Acad. Sci. USA* 115 (13), E2921–E2929. doi:10.1073/pnas.1718787115

Derbyshire, V., Freemont, P. S., Sanderson, M. R., Beese, L., Friedman, J. M., Joyce, C. M., et al. (1988). Genetic and Crystallographic Studies of the 3′,5′-Exonucleolytic Site of DNA Polymerase I. *Science* 240 (4849), 199–201. doi:10.1126/science.2832946

Doublié, S., Tabor, S., Long, A. M., Richardson, C. C., and Ellenberger, T. (1998). Crystal Structure of a Bacteriophage T7 DNA Replication Complex at 2.2 Å Resolution. *Nature* 391 (6664), 251–258. doi:10.1038/34593

Doublié, S., and Zahn, K. E. (2014). Structural Insights into Eukaryotic DNA Replication. *Front. Microbiol.* 5, 444. doi:10.3389/fmicb.2014.00444

Filée, J., Forterre, P., Sen-Lin, T., and Laurent, J. (2002). Evolution of DNA Polymerase Families: Evidences for Multiple Gene Exchange between Cellular and Viral Proteins. *J. Mol. Evol.* 54 (6), 763–773. doi:10.1007/s00239-001-0078-x

Fortini, P., Pascucci, B., Parlanti, E., Sobol, R. W., Wilson, S. H., and Dogliotti, E. (1998). Different DNA Polymerases Are Involved in the Short- and Long-Patch Base Excision Repair in Mammalian Cells. *Biochemistry* 37 (11), 3575–3580. doi:10.1021/bi972999h

Fouquerel, E., Lormand, J., Bose, A., Lee, H.-T., Kim, G. S., Li, J., et al. (2016). Oxidative Guanine Base Damage Regulates Human Telomerase Activity. *Nat. Struct. Mol. Biol.* 23 (12), 1092–1100. doi:10.1038/nsmb.3319

Franklin, A., Milburn, P. J., Blanden, R. V., and Steele, E. J. (2004). Human DNA Polymerase-η, an A-T Mutator in Somatic Hypermutation of Rearranged Immunoglobulin Genes, is a Reverse Transcriptase. *Immunol. Cell Biol.* 82, 219–225.

Franklin, M. C., Wang, J., and Steitz, T. A. (2001). Structure of the Replicating Complex of a Pol α Family DNA Polymerase. *Cell* 105 (5), 657–667. doi:10.1016/s0092-8674(01)00367-1

Gammon, D. B., and Evans, D. H. (2009). The 3′-to-5′ Exonuclease Activity of Vaccinia Virus DNA Polymerase Is Essential and Plays a Role in Promoting Virus Genetic Recombination. *J. Virol.* 83 (9), 4236–4250. doi:10.1128/jvi.02255-08

Ganai, R. A., Bylund, G. O., and Johansson, E. (2015). Switching between Polymerase and Exonuclease Sites in DNA Polymerase ε. *Nucleic Acids Res.* 43 (2), 932–942. doi:10.1093/nar/gku1353

Garcia-Gomez, S., Reyes, A., Martinez-Jimenez, M. I., Chocron, E. S., Mouron, S., Terrados, G., et al. (2013). PrimPol, an Archaic Primase/Polymerase Operating in Human Cells. *Mol. Cell* 52, 541–553.

Grasby, J. A., Finger, L. D., Tsutakawa, S. E., Atack, J. M., and Tainer, J. A. (2012). Unpairing and Gating: Sequence-independent Substrate Recognition by FEN Superfamily Nucleases. *Trends Biochem. Sci.* 37 (2), 74–84. doi:10.1016/j.tibs.2011.10.003

Gutman, P. D., and Minton, K. W. (1993). Conserved Sites in the 5'-3' Exonuclease Domain of *Escherichia coli* DNA Polymerase. *Nucl. Acids Res.* 21 (18), 4406–4407. doi:10.1093/nar/21.18.4406

Hampp, S., Kiessling, T., Buechle, K., Mansilla, S. F., Thomale, J., Rall, M., et al. (2016). DNA Damage Tolerance Pathway Involving DNA Polymerase ι and the Tumor Suppressor P53 Regulates DNA Replication fork Progression. *Proc. Natl. Acad. Sci. USA* 113 (13), E4311–E4319. doi:10.1073/pnas.1605828113

Harrington, J. J., and Lieber, M. R. (1994). The Characterization of a Mammalian DNA Structure-specific Endonuclease. *EMBO J.* 13 (5), 1235–1246. doi:10.1002/j.1460-2075.1994.tb06373.x

He, P., and Yang, W. (2018). Template and Primer Requirements for DNA Pol θ-mediated End Joining. *Proc. Natl. Acad. Sci. USA* 115 (30), 7747–7752. doi:10.1073/pnas.1807329115

Hogg, M., Aller, P., Konigsberg, W., Wallace, S. S., and Doublié, S. (2007). Structural and Biochemical Investigation of the Role in Proofreading of a β Hairpin Loop Found in the Exonuclease Domain of a Replicative DNA Polymerase of the B Family. *J. Biol. Chem.* 282 (2), 1432–1444. doi:10.1074/jbc.m605675200

Hogg, M., Sauer-Eriksson, A. E., and Johansson, E. (2012). Promiscuous DNA Synthesis by Human DNA Polymerase θ. *Nucleic Acids Res.* 40(6), 2611–2622. doi:10.1093/nar/gkr1102

Hogg, M., Wallace, S. S., and Doublié, S. (2004). Crystallographic Snapshots of a Replicative DNA Polymerase Encountering an Abasic Site. *EMBO J.* 23 (7), 1483–1493. doi:10.1038/sj.emboj.7600150

Howard, M. J., Horton, J. K., Zhao, M.-L., and Wilson, S. H. (2020). Lysines in the Lyase Active Site of DNA Polymerase β Destabilize Nonspecific DNA Binding, Facilitating Searching and DNA gap Recognition. *J. Biol. Chem.* 295 (34), 12181–12187. doi:10.1074/jbc.ra120.013547

Hwang, T., Reh, S., Dunbayev, Y., Zhong, Y., Takata, Y., Shen, J., et al. (2020). Defining the Mutation Signatures of DNA Polymerase θ in Cancer Genomes. *NAR Cancer* 2 (3), zcaa017. doi:10.1093/narcan/zcaa017

Izban, M. G., and Luse, D. S. (1992). The RNA Polymerase II Ternary Complex Cleaves the Nascent Transcript in a 3'----5' Direction in the Presence of Elongation Factor SII. *Genes Dev.* 6 (7), 1342–1356. doi:10.1101/gad.6.7.1342

Joyce, C. M. (2013). "DNA Polymerase I, Bacterial," in *Encyclopedia of Biological Chemistry*. Editors W.J. Lennarz and M.D. Lane. Second Edition (Waltham: Academic Press), 87–91. doi:10.1016/b978-0-12-378630-2.00306-6

Joyce, C. M., Sun, X. C., and Grindley, N. D. (1992). Reactions at the Polymerase Active Site that Contribute to the Fidelity of *Escherichia coli* DNA Polymerase I (Klenow Fragment). *J. Biol. Chem.* 267 (34), 24485–24500. doi:10.1016/s0021-9258(18)35792-2

Kent, T., Mateos-Gomez, P. A., Sfeir, A., and Pomerantz, R. T. (2016). Polymerase θ Is a Robust Terminal Transferase that Oscillates between Three Different Mechanisms during End-Joining. *eLife* 5, e13740. doi:10.7554/eLife.13740

Khare, V., and Eckert, K. A. (2002). The Proofreading 3′→5′ Exonuclease Activity of DNA Polymerases: a Kinetic Barrier to Translesion DNA Synthesis. *Mutat. Research/Fundamental Mol. Mech. Mutagenesis* 510 (1–2), 45–54. doi:10.1016/s0027-5107(02)00251-8

Khodyreva, S. N., Prasad, R., Ilina, E. S., Sukhanova, M. V., Kutuzov, M. M., Liu, Y., et al. (2010). Apurinic/apyrimidinic (AP) Site Recognition by the 5'-dRP/AP Lyase in poly(ADP-Ribose) Polymerase-1 (PARP-1). *Proc. Natl. Acad. Sci.* 107 (51), 22090–22095. doi:10.1073/pnas.1009182107

Kim, Y., Eom, S. H., Wang, J., Lee, D.-S., Suh, S. W., and Steitz, T. A. (1995). Crystal Structure of Thermus Aquaticus DNA Polymerase. *Nature* 376(6541), 612–616. doi:10.1038/376612a0

Klenow, H., and Overgaard-Hansen, K. (1970). Proteolytic Cleavage of DNA Polymerase from Escherichia Coli B into an Exonuclease Unit and a Polymerase Unit. *FEBS Lett.* 6 (1), 25–27. doi:10.1016/0014-5793(70)80032-1

Klungland, A., and Lindahl, T. (1997). Second Pathway for Completion of Human DNA Base Excision-Repair: Reconstitution with Purified Proteins and Requirement for DNase IV (FEN1). *EMBO J.* 16 (11), 3341–3348. doi:10.1093/emboj/16.11.3341

Lai, Y., Weizmann, Y., and Liu, Y. (2018). The Deoxyribose Phosphate Lyase of DNA Polymerase β Suppresses a Processive DNA Synthesis to Prevent Trinucleotide Repeat Instability. *Nucleic Acids Res.* 46 (17), 8940–8952. doi:10.1093/nar/gky700

Lamichhane, R., Berezhna, S. Y., Gill, J. P., Van der Schans, E., and Millar, D. P. (2013). Dynamics of Site Switching in DNA Polymerase. *J. Am. Chem. Soc.* 135 (12), 4735–4742. doi:10.1021/ja311641b

Laverty, D. J., and Greenberg, M. M. (2018). Expanded Substrate Scope of DNA Polymerase θ and DNA Polymerase β: Lyase Activity on 5′-Overhangs and Clustered Lesions. *Biochemistry* 57 (42), 6119–6127. doi:10.1021/acs.biochem.8b00911

Laverty, D. J., Mortimer, I. P., and Greenberg, M. M. (2018). Mechanistic Insight through Irreversible Inhibition: DNA Polymerase θ Uses a Common Active Site for Polymerase and Lyase Activities. *J. Am. Chem. Soc.* 140 (29), 9034–9037. doi:10.1021/jacs.8b04158

Li, Y., Dutta, S., Doublié, S., Bdour, H. M. d., Taylor, J.-S., and Ellenberger, T. (2004). Nucleotide Insertion Opposite a Cis-Syn Thymine Dimer by a Replicative DNA Polymerase from Bacteriophage T7. *Nat. Struct. Mol. Biol.* 11 (8), 784–790. doi:10.1038/nsmb792

Longley, M. J., Bennett, S. E., and Mosbaugh, D. W. (1990). Characterization of the 5′ to 3′ Exonuclease Associated with *Thermus aquaticus* DNA Polymerase. *Nucl. Acids Res.* 18 (24), 7317–7322. doi:10.1093/nar/18.24.7317

Lyamichev, V., Brow, M. A. D., Varvel, V. E., and Dahlberg, J. E. (1999). Comparison of the 5' Nuclease Activities of Taq DNA Polymerase and its Isolated Nuclease Domain. *Proc. Natl. Acad. Sci.* 96 (11), 6143–6148. doi:10.1073/pnas.96.11.6143

Matsumoto, Y., and Kim, K. (1995). Excision of Deoxyribose Phosphate Residues by DNA Polymerase β during DNA Repair. *Science* 269 (24), 699–702. doi:10.1126/science.7624801

Mouron, S., Rodriguez-Acebes, S., Martinez-Jimenez, M. I., Garcia-Gomez, S., Chocron, S., Blanco, L., et al. (2013). Repriming of DNA Synthesis at Stalled Replication Forks by Human PrimPol. *Nat. Struct. Mol. Biol.* 20, 1383–1389.

Park, Y., Choi, H., Lee, D. S., and Kim, Y. (1997). Improvement of the 3'-5' Exonuclease Activity of Taq DNA Polymerase by Protein Engineering in the Active Site. *Mol. Cells* 7 (3), 419–424.

Patel, P. H., Suzuki, M., Adman, E., Shinkai, A., and Loeb, L. A. (2001). Prokaryotic DNA Polymerase I: Evolution, Structure, and "base Flipping" Mechanism for Nucleotide Selection. *J. Mol. Biol.* 308 (5), 823–837. doi:10.1006/jmbi.2001.4619

Pauszek, R. F., III, Lamichhane, R., Rajkarnikar Singh, A., and Millar, D. P. (2021). Single-molecule View of Coordination in a Multi-Functional DNA Polymerase. *eLife* 10, e62046. doi:10.7554/elife.62046

Pellicanò, G., Al Mamun, M., Jurado-Santiago, D., Villa-Hernández, S., Yin, X., Giannattasio, M., et al. (2021). Checkpoint-mediated DNA Polymerase ε Exonuclease Activity Curbing Counteracts Resection-Driven fork Collapse. *Mol. Cell* 81 (13), 2778–e4. doi:10.1016/j.molcel.2021.04.006

Petta, T. B., Nakajima, S., Zlatanou, A., Despras, E., Couve-Privat, S., Ishchenko, A., et al. (2008). Human DNA Polymerase iota Protects Cells against Oxidative Stress. *EMBO J.* 27 (21), 2883–2895. doi:10.1038/emboj.2008.210

Pinz, K. G., and Bogenhagen, D. F. (2000). Characterization of a Catalytically Slow AP Lyase Activity in DNA Polymerase γ and Other Family A DNA Polymerases. *J. Biol. Chem.* 275 (17), 12509–12514. doi:10.1074/jbc.275.17.12509

Prasad, R., Beard, W. A., Chyan, J. Y., Maciejewski, M. W., Mullen, G. P., and Wilson, S. H. (1998). Functional Analysis of the Amino-Terminal 8-kDa Domain of DNA Polymerase β as Revealed by Site-Directed Mutagenesis. *J. Biol. Chem.* 273(18), 11121–11126. doi:10.1074/jbc.273.18.11121

Prasad, R., Beard, W. A., and Wilson, S. H. (1994). Studies of Gapped DNA Substrate Binding by Mammalian DNA Polymerase Beta. Dependence on 5'-phosphate Group. *J. Biol. Chem.* 269 (27), 18096–18101. doi:10.1016/s0021-9258(17)32422-5

Prasad, R., Bebenek, K., Hou, E., Shock, D. D., Beard, W. A., Woodgate, R., et al. (2003). Localization of the Deoxyribose Phosphate Lyase Active Site in Human DNA Polymerase ι by Controlled Proteolysis. *J. Biol. Chem.* 278 (32), 29649–29654. doi:10.1074/jbc.m305399200

Prasad, R., Horton, J. K., Chastain, P. D., Gassman, N. R., Freudenthal, B. D., Hou, E. W., et al. (2014). Suicidal Cross-Linking of PARP-1 to AP Site Intermediates in Cells Undergoing Base Excision Repair. *Nucleic Acids Res.* 42 (10), 6337–6351. doi:10.1093/nar/gku288

Prasad, R., Longley, M. J., Sharief, F. S., Hou, E. W., Copeland, W. C., and Wilson, S. H. (2009). Human DNA Polymerase Possesses 5'-dRP Lyase Activity and Functions in Single-Nucleotide Base Excision Repair *In Vitro*. *Nucleic Acids Res.* 37 (6), 1868–1877. doi:10.1093/nar/gkp035

Quinet, A., Tirman, S., Jackson, J., Šviković, S., Lemacon, D., Carvajal-Maldonado, D., et al. (2020). PRIMPOL-Mediated Adaptive Response Suppresses Replication Fork Reversal in BRCA-Deficient Cells. *Mol. Cell* 77, 461–474.

Rechkoblit, O., Johnson, R. E., Gupta, Y. K., Prakash, L., Prakash, S., and Aggarwal, A. K. (2021). Structural Basis of DNA Synthesis Opposite 8-Oxoguanine by Human PrimPol Primase-Polymerase. *Nat. Commun.* 12, 4020.

Reines, D. (1992). Elongation Factor-dependent Transcript Shortening by Template-Engaged RNA Polymerase II. *J. Biol. Chem.* 267 (6), 3795–3800. doi:10.1016/s0021-9258(19)50596-8

Robins, P., Pappin, D. J., Wood, R. D., and Lindahl, T. (1994). Structural and Functional Homology between Mammalian DNase IV and the 5'-nuclease Domain of Escherichia coli DNA Polymerase I. *J. Biol. Chem.* 269 (46) 28535–28538. doi:10.1016/s0021-9258(19)61935-6

Rubtsova, M. P., Vasilkova, D. P., Malyavko, A. N., Naraikina, Y. V., Zvereva, M. I., and Dontsova, O. A. (2012). Telomere Lengthening and Other Functions of Telomerase. *Acta Naturae* 4 (2), 44–61. doi:10.32607/actanaturae.10630

Schimmel, J., van Schendel, R., den Dunnen, J. T., and Tijsterman, M. (2019). Templated Insertions: A Smoking Gun for Polymerase Theta-Mediated End Joining. *Trends Genet.* 35 (9), 632–644. doi:10.1016/j.tig.2019.06.001

Seki, M., and Wood, R. D. (2008). DNA Polymerase θ (POLQ) Can Extend from Mismatches and from Bases Opposite a (6-4) Photoproduct. *DNA Repair* 7 (1), 119–127. doi:10.1016/j.dnarep.2007.08.005

Shanbhag, V., Sachdev, S., Flores, J., Modak, M., and Singh, K. (2018). Family A and B DNA Polymerases in Cancer: Opportunities for Therapeutic Interventions. *Biology* 7 (1), 5. doi:10.3390/biology7010005

Shevelev, I. V., and Hübscher, U. (2002). The 3′-5′ Exonucleases. *Nat. Rev. Mol. Cel Biol* 3 (5), 364–376. doi:10.1038/nrm804

Shi, C., Shen, X., Niu, S., and Ma, C. (2015). Innate Reverse Transcriptase Activity of DNA Polymerase for Isothermal RNA Direct Detection. *J. Am. Chem. Soc.* 137, 13804–13806.

Sobol, R. W., Horton, J. K., Kühn, R., Gu, H., Singhal, R. K., Prasad, R., et al. (1996). Requirement of Mammalian DNA Polymerase-β in Base-Excision Repair. *Nature* 379 (6561), 183–186. doi:10.1038/379183a0

Sobol, R. W., Prasad, R., Evenski, A., Baker, A., Yang, X.-P., Horton, J. K., et al. (2000). The Lyase Activity of the DNA Repair Protein β-polymerase Protects from DNA-Damage-Induced Cytotoxicity. *Nature* 405 (6788), 807–810. doi:10.1038/35015598

Sosunov, V., Sosunova, E., Mustaev, A., Bass, I., Nikiforov, V., and Goldfarb, A. (2003). Unified Two-Metal Mechanism of RNA Synthesis and Degradation by RNA Polymerase. *EMBO J.* 22 (9), 2234–2244. doi:10.1093/emboj/cdg193

Sosunova, E., Sosunov, V., Epshtein, V., Nikiforov, V., and Mustaev, A. (2013). Control of Transcriptional Fidelity by Active Center Tuning as Derived from RNA Polymerase Endonuclease Reaction. *J. Biol. Chem.* 288 (9), 6688–6703. doi:10.1074/jbc.m112.424002

Steitz, T. A. (1999). DNA Polymerases: Structural Diversity and Common Mechanisms. *J. Biol. Chem.* 274 (25), 17395–17398. doi:10.1074/jbc.274.25.17395

Su, Y., Egli, M., and Guengerich, F. P. (2017). Human DNA Polymerase eta Accommodates RNA for Strand Extension. *J. Biol. Chem.* 292, 18044–18051.

Su, Y., Ghodke, P. P., Egli, M., Li, L., Wang, Y., and Guengerich, F. P. (2019). Human DNA Polymerase η has Reverse Transcriptase Activity in Cellular Environments. *J. Biol. Chem.* 294, 6073–6081.

Tirman, S., Quinet, A., Wood, M., Meroni, A., Cybulla, E., Jackson, J., et al. (2021). Temporally Distinct Post-Replicative Repair Mechanisms Fill PRIMPOL-Dependent ssDNA Gaps in Human Cells. *Mol. Cell* 81, 4026–4040.

Tsutakawa, S. E., Classen, S., Chapados, B. R., Arvai, A. S., Finger, L. D., Guenther, G., et al. (2011). Human Flap Endonuclease Structures, DNA Double-Base Flipping, and a Unified Understanding of the FEN1 Superfamily. *Cell* 145 (2), 198–211. doi:10.1016/j.cell.2011.03.004

Wang, R., Lenoir, W. F., Wang, C., Su, D., McLaughlin, M., Hu, Q., et al. (2020). DNA Polymerase ι Compensates for Fanconi Anemia Pathway Deficiency by Countering DNA Replication Stress. *Proc. Natl. Acad. Sci. USA* 117 (52), 33436–33445. doi:10.1073/pnas.2008821117

Xu, Y., Grindley, N. D. F., and Joyce, C. M. (2000). Coordination between the Polymerase and 5′-Nuclease Components of DNA Polymerase I of Escherichia coli. *J. Biol. Chem.* 275 (27), 20949–20955. doi:10.1074/jbc.m909135199

Yang, W., Lee, J. Y., and Nowotny, M. (2006). Making and Breaking Nucleic Acids: Two-Mg2+-Ion Catalysis and Substrate Specificity. *Mol. Cel* 22 (1), 5–13. doi:10.1016/j.molcel.2006.03.013

Yousefzadeh, M. J., Wyatt, D. W., Takata, K.-I., Mu, Y., Hensley, S. C., Tomida, J., et al. (2014). Mechanism of Suppression of Chromosomal Instability by DNA Polymerase POLQ. *Plos Genet.* 10 (10), e1004654. doi:10.1371/journal.pgen.1004654

Zahn, K. E., Averill, A. M., Aller, P., Wood, R. D., and Doublié, S. (2015). Human DNA Polymerase θ Grasps the Primer Terminus to Mediate DNA Repair. *Nat. Struct. Mol. Biol.* 22 (4), 304–311. doi:10.1038/nsmb.2993

Zahn, K. E., Jensen, R. B., Wood, R. D., and Doublié, S. (2021). Human DNA Polymerase θ Harbors DNA End-Trimming Activity Critical for DNA Repair. *Mol. Cel* 81 (7), 1534–1547. doi:10.1016/j.molcel.2021.01.021

Zuo, Y., and Deutscher, M. P. (2002). The Physiological Role of RNase T Can Be Explained by its Unusual Substrate Specificity. *J. Biol. Chem.* 277 (33), 29654–29661. doi:10.1074/jbc.m204252200

Conflict of Interest: The authors declare that the research was conducted in the absence of any commercial or financial relationships that could be construed as a potential conflict of interest.

Publisher's Note: All claims expressed in this article are solely those of the authors and do not necessarily represent those of their affiliated organizations, or those of the publisher, the editors and the reviewers. Any product that may be evaluated in this article, or claim that may be made by its manufacturer, is not guaranteed or endorsed by the publisher.

frontiers in Molecular Biosciences

REVIEW
published: 05 January 2022
doi: 10.3389/fmolb.2021.811540

Beyond the Lesion: Back to High Fidelity DNA Synthesis

Joseph D. Kaszubowski[†] *and Michael A. Trakselis* *[†]

Department of Chemistry and Biochemistry, Baylor University, Waco, TX, United States

High fidelity (HiFi) DNA polymerases (Pols) perform the bulk of DNA synthesis required to duplicate genomes in all forms of life. Their structural features, enzymatic mechanisms, and inherent properties are well-described over several decades of research. HiFi Pols are so accurate that they become stalled at sites of DNA damage or lesions that are not one of the four canonical DNA bases. Once stalled, the replisome becomes compromised and vulnerable to further DNA damage. One mechanism to relieve stalling is to recruit a translesion synthesis (TLS) Pol to rapidly synthesize over and past the damage. These TLS Pols have good specificities for the lesion but are less accurate when synthesizing opposite undamaged DNA, and so, mechanisms are needed to limit TLS Pol synthesis and recruit back a HiFi Pol to reestablish the replisome. The overall TLS process can be complicated with several cellular Pols, multifaceted protein contacts, and variable nucleotide incorporation kinetics all contributing to several discrete substitution (or template hand-off) steps. In this review, we highlight the mechanistic differences between distributive equilibrium *exchange* events and concerted contact-dependent *switching* by DNA Pols for insertion, extension, and resumption of high-fidelity synthesis beyond the lesion.

Keywords: DNA replication, polymerase, switching, translesion synthesis, PCNA, DNA damage, DNA lesion, substitution

OPEN ACCESS

Edited by:
Whitney Yin,
University of Texas Medical Branch at Galveston, United States

Reviewed by:
Linlin Zhao,
University of California, Riverside, United States
Chris Putnam,
University of California, San Diego, United States

***Correspondence:**
Michael A. Trakselis
michael_trakselis@baylor.edu

[†]***ORCID:***
Joseph D. Kaszubowski
0000-0003-0153-9043
Michael A. Trakselis
0000-0001-7054-8475

Specialty section:
This article was submitted to Structural Biology, a section of the journal Frontiers in Molecular Biosciences

Received: *09 November 2021*
Accepted: *16 December 2021*
Published: *05 January 2022*

Citation:
Kaszubowski JD and Trakselis MA (2022) Beyond the Lesion: Back to High Fidelity DNA Synthesis. Front. Mol. Biosci. 8:811540. doi: 10.3389/fmolb.2021.811540

INTRODUCTION

DNA damage can come from a variety of endogenous and exogenous sources and persist within the genome into the synthesis (S) phase of the cell cycle (Hakem, 2008). During S-phase, high fidelity (HiFi) polymerases (Pols) duplicate complementary DNA strands with a rapid rate of synthesis and a low rate of error. However, upon encountering DNA base damage within a template strand, HiFi Pols are unable to continue DNA synthesis and are stalled in place. Specialized Pols capable of bypassing the template-strand lesion, known as translesion synthesis (TLS) Pols, are recruited to the site of the damage, substituted in for the HiFi Pol, and then used to synthesize over and past the lesion (**Figure 1A**). TLS Pols have evolved to ensure error-free synthesis across preferred lesions but have overall lower fidelity than HiFi Pols (Waters et al., 2009; Goodman and Woodgate, 2013; Sale, 2013; Fujii and Fuchs, 2020). Following successful insertion of one or more nucleotides opposite (or past) the lesion, TLS Pols must dissociate from the DNA template and substitute back to the replicative Pol to resume high fidelity genomic synthesis (Trakselis et al., 2017).

Although relatively simple in description, there are many intricate elements of the TLS mechanism. Previously, TLS has been described by a "one-polymerase" or "two-polymerase" process; however, the number and subunit composition of Pols found at TLS sites is expanding, and while some Pols have direct synthesis activities, others act only as scaffolds for assemblies. Therefore, the diversity of TLS processes would be better defined by a "two-substitution" or "three-substitution" mechanism (**Figure 1A**), focusing primarily on the steps required for synthesis instead

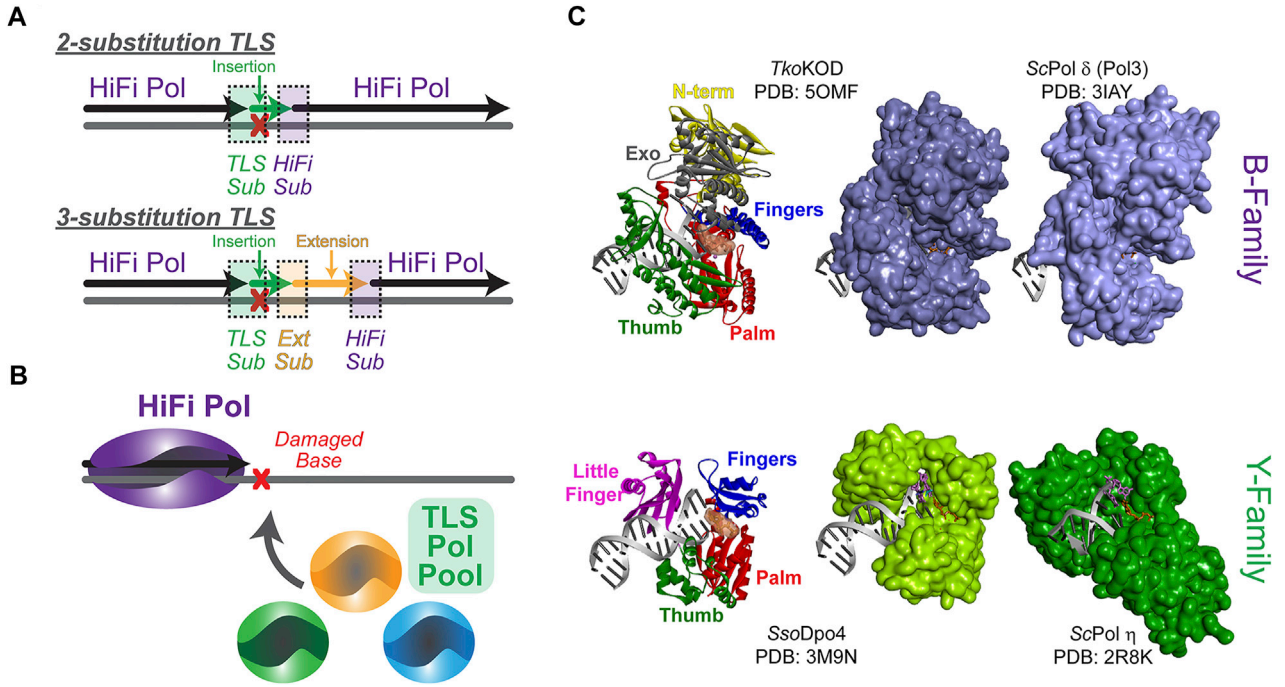

FIGURE 1 | Steps required for the overall translesion synthesis (TLS) process. **(A)** A high fidelity (HiFi) polymerase (Pol) will stall at a lesion requiring two- or three-substitution TLS for bypass. In a two-substitution mechanism, the first TLS substitution (sub) will recruit an inserter TLS Pol (green) for translesion DNA insertion (green) followed by substitution back to a HiFi Pol (purple). In a three-substitution mechanism, an extender (Ext) TLS Pol is substituted after insertion and is required for limited downstream extension (orange) prior to substitution back to the HiFi Pol. **(B)** TLS substitution will be influenced by the available TLS Pol Pool as well as the specificity for a particular lesion. **(C)** Compares the polymerase domain structure (N-term—yellow, Exo—grey, Palm—red, Fingers—blue, Thumb—green, and Little Finger—pink) for the more closed structures of HiFi B-family Pols KOD (*Thermococcus kodakarensis*) (Kropp et al., 2017) and Pol δ (*Saccharomyces cerevisiae*) (Swan et al., 2009) with the more open active sites of TLS Y-family Pols *Sso*Dpo4 (Wong et al., 2010) and Pol η (*Saccharomyces cerevisiae*) (Alt et al., 2007) in complex with DNA, all arranged in the same orientation.

of individual Pols involved. Insertion opposite a lesion requires that an appropriately selected TLS "inserter" Pol is substituted for the HiFi Pol. After TLS insertion, there can be direct substitution back to the HiFi Pol to resume synthesis (i.e., two-substitution) or subsequently an intermediary "extender" Pol can synthesize downstream of the lesion prior to substitution back to the HiFi Pol in a three-substitution mechanism. There are several mechanistic facets that regulate this process to help select TLS Pols from the cellular pool (**Figure 1B**) and restrict their activities after TLS for the benefit of maintaining a stable genome. Although many of these basic principles have been better characterized in prokaryotic systems, where a more limited set of Pols are available, this review will focus primarily on defining the TLS process in more complex eukaryotic systems, culminating with mechanistic hypotheses for limiting lower fidelity TLS Pol synthesis downstream of the lesion to favor resumption of high-fidelity synthesis.

Translesion Synthesis Pol Open Active Site

All DNA Pols resemble a right hand, with a structure consisting minimally of palm, finger, and thumb domains, comprising the catalytic core (**Figure 1C**). This conformation allows for binding of the DNA substrate while simultaneously inserting nucleotides during DNA synthesis. HiFi Pols also include a second exonuclease (Exo) active site that is utilized to proofread insertions and ensure fidelity. While HiFi Pols of the B-family have smaller and more closed active sites to ensure efficient and accurate DNA replication opposite undamaged template strands, TLS Pols of the Y-family have larger and more open active sites that allow insertion of one or more nucleotides opposite a lesion. Y-family TLS Pols generally have small finger domains and have an additional little finger (LF) domain that attenuates lesion bypass abilities and processivities (Boudsocq et al., 2004; Pata, 2010). Varying distances between the LF and the catalytic core, creating a structural gap, add specificity to the size of lesions that each TLS Pol can bypass (Yang and Gao, 2018). As a result of these structural differences, TLS Pols are capable "inserters" opposite specific lesions but are inherently less accurate and can quickly generate errors in the nascent DNA strand when synthesizing opposite undamaged DNA (Vaisman and Woodgate, 2017). Although these Pols have tolerant active sites to accommodate bulky lesions, mutagenesis even during TLS is fairly common (Volkova et al., 2020). Therefore, it is paramount to cellular survival that synthesis by certain TLS Pols be restricted only to base insertion opposite DNA lesions to prevent misincorporations downstream. HiFi Pols with more

discriminative active sites must promptly resume replicating DNA to minimize inaccurate synthesis. To facilitate the end of a TLS event, the DNA replisome needs to *exchange* or *switch* back to the HiFi Pol to proceed with faithful DNA replication.

Translesion Synthesis Pols and Lesion Specificity

DNA damage can lead to genomic instability and carcinogenesis (Hoeijmakers, 2009; Shilkin et al., 2020). TLS serves as a DNA damage tolerance mechanism by allowing DNA replication to persevere in the presence of DNA lesions. By allowing DNA synthesis to continue upon the encountering of a template-strand lesion, TLS Pols reduce the risk of cellular apoptosis and prevent occurrence of double-strand breaks from excessive replisome stalling (Chatterjee and Walker, 2017).

Before discussing the plethora of Pols capable of performing TLS, it is important to understand the types of lesions that are encountered as well as their sources. For DNA-damaging agents that have been prevalent for long periods of time, it is possible that TLS Pols have evolved to specifically bypass the resulting lesions (Livneh et al., 2010). For example, eukaryotic TLS Pol η is capable of perfectly bypassing thymine cyclobutane pyrimidine dimers (CPDs) following UV radiation from sunlight with correctly base-paired adenines (Johnson et al., 2000b; Biertumpfel et al., 2010) (**Figure 1C**). Separately, archaeal DNA polymerase 4 (Dpo4) can synthesize nascent DNA beyond 7,8-dihydro-8-oxoguanine (8-oxoG) lesions generated by reactive oxygen species, as well as many additional lesions (Yang, 2014; Cranford et al., 2020; Jung and Lee, 2020) (**Figure 1C**).

Relatively newer sources of exogenous damage, such as platinating agents used in cancer treatment, have not yielded an evolutionary adaptation in a specific TLS Pol and are instead bypassed by the most suitable (or a combination of multiple) Pol(s). In organisms with multiple available TLS Pols, specificity to lesions is a determining factor for which Pol will perform the bypass (Yang, 2014). Human cells contain four Y-family TLS Pols: Pols η, ι, κ, and Rev1, each with varying active site dimensions and unique bypass capabilities. Pols η, ι, and κ have all been shown to act as the "inserter" Pol opposite a variety of lesions, with the large active site of Pol κ allowing bypass of the bulkiest lesions (Vaisman et al., 2001; Kusumoto et al., 2002; Albertella et al., 2005a; Alt et al., 2007; Yoon et al., 2009; Phi et al., 2019; Jung et al., 2020; Vaisman and Woodgate, 2020; Ghodke et al., 2021). Human Pol ν, an A-family Pol, has also demonstrated an ability to act as an "inserter" TLS Pol opposite lesions (Takata et al., 2006; Gowda and Spratt, 2016; Du et al., 2020). While structurally similar to other Y-family Pols, Rev1 acts less frequently as an "inserter" and more often as a scaffold to facilitate the binding of other Pols through conserved Rev1-interacting regions (RIRs) (Qin et al., 2013; Boehm et al., 2016b; Pustovalova et al., 2016). Recent studies have shown that Pol λ, an X-family Pol, can also perform this scaffolding role during TLS (Yoon et al., 2021). The varying active site structures, activities, and potential contacts of TLS Pols regulate Pol selection for lesion bypass.

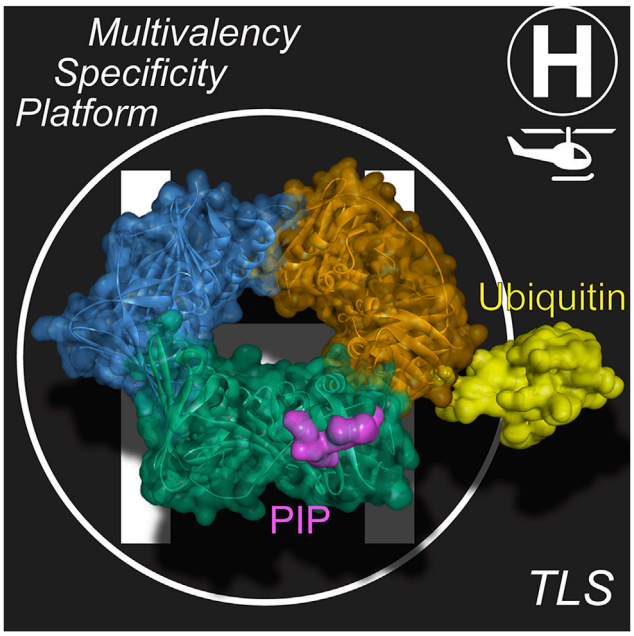

FIGURE 2 | PCNA is a dynamic "landing-pad" (or platform). PIP binding sites at the interdomain connecting loop (IDL) and ubiquitination at K164 are available on each of the three PCNA subunits, providing for multivalency. Structural model derived from PCNA/p21 peptide structure (PDBID: 1AXC) (Gulbis et al., 1996) and monoubiquitinated PCNA structure (PDBID: 3TBL) (Zhang et al., 2012).

POLYMERASE HOLOENZYME COMPLEXES WITH PCNA

A polymerase holoenzyme complex is assembled to provide some stability when bound to DNA that presents biochemically as processivity. Processivity can be defined by an equation that quantifies the probability of a Pol continuing at a specific site based on the k_{pol} for nucleotide incorporation relative to k_{off} for dissociation from the DNA template (Hippel et al., 1994). Several mechanisms have evolved to increase processivities of HiFi Pols and limit processivities of TLS Pols to ensure genome stability. For Pols, the trimeric clamp protein (proliferating cell nuclear antigen, PCNA, in archaea and eukaryotes) encircles duplex DNA and provides a topological link to the DNA, effectively reducing k_{off} (Trakselis and Benkovic, 2001; Boehm et al., 2016a).

The binding affinity of the Pol itself for DNA can also impact the processivity. Interestingly, HiFi Pols generally have a higher affinity for PCNA than DNA, while TLS Pols have a higher affinity for DNA than for PCNA (Lin et al., 2012; Hedglin et al., 2016a). This implies that binding to clamp proteins is often required for high fidelity and processive DNA synthesis, while TLS activity may be more restricted directly by the DNA lesion. This provides a plausible mechanism for limiting TLS, however, the mechanism for releasing a TLS Pol from DNA after translesion synthesis is not well understood.

Pols have several interaction sites with the clamp, but in eukaryotes and archaea, the primary interaction site is through a hydrophobic PCNA-Interacting Protein (PIP) patch, adjacent

to the interdomain connecting loop within a single PCNA monomer (**Figure 2**). This PIP binding site is located on the front (or leading face) of PCNA and interacts with proteins through a specific motif in a partner protein containing the general consensus sequence, *Qxxhxxaa*, where *h* is hydrophobic and *a* is aromatic (Warbrick, 1998). Glutamine binds to a Q-pocket through specific hydrogen bonding contacts, while the aromatic residues lay within the hydrophobic pocket. Although more than 75 proteins, including several DNA repair proteins and cell cycle regulators, contain this consensus PIP motif, TLS Pols generally encode a nonconsensus PIP motif, (K/G)xx(I/L)xx(FY/L)(FY/L) that bypasses the Q-pocket (Slade, 2018; Dash and Hadden, 2021). One to three PIP motifs are located in the unstructured C-terminal extensions of Y-family Pols (Powers and Washington, 2018). The variability within the consensus and nonconsensus PIP motifs can alter the K_d of interaction widely from 10 nM to >30 μM (Slade, 2018; Prestel et al., 2019).

It is well known that upon extreme stalling, PCNA becomes monoubiquitinated (mUB) at K164 (**Figure 2**) (Stelter and Ulrich, 2003; Kannouche et al., 2004; Chang et al., 2006). This additional ubiquitin facet on PCNA can further increase the binding affinity of TLS Pols though a ubiquitin-binding zinc finger (UBZ) motif (Bomar et al., 2007; Pillaire et al., 2014) or a ubiquitin-binding motif (UBM) (McIntyre et al., 2015; Vanarotti et al., 2018) also within the unstructured C-terminal tails of Y-family TLS Pols (Yang and Gao, 2018). mUb-PCNA acts to not only recruit TLS Pols at stalled replication forks but also to increase their residence times to carry out TLS (Sabbioneda et al., 2008; Sabbioneda et al., 2009). The covalent addition of Ub to the back side of $PCNA^{K164}$ and the flexibility inherent within the unstructured C-terminal tails containing these motifs allow these TLS Pols to adopt several conformations on PCNA in inactive carrier or active polymerizing states (Shen et al., 2021). Therefore, based on this multivalency for trimeric mUb-PCNA, there are now at least six specific contact points for recruiting and interacting with Pols, providing a landing platform for assemblies (**Figure 2**) in what has been described previously as a "tool-belt" model (Kath et al., 2014; Boehm et al., 2016b; Cranford et al., 2017). A holoenzyme complex, consisting of the synthesizing Pol bound to PCNA, or a supraholoenzyme complex, comprised of multiple Pols bound to PCNA, contain many protein-protein interactions (PPIs) for added stability during DNA synthesis.

MECHANISMS FOR THE TRANSLESION SYNTHESIS SWITCH OR EXCHANGE

Substitution of a HiFi Pol for a TLS Pol to hand off the primer opposite a damaged template is required to insert opposite a variety of template lesions, however, the exact mechanism for the polymerase *exchange* or *switch* is uncharacterized. Moreover, the diversity of lesion types and abundance of Pols within the cell would not suggest that a single mechanism is utilized. Instead, it is likely that several mechanisms are employed dependent on the specific lesion, the DNA context, and the signaling pathways. Conceptually, substitution of one Pol for another that relies primarily on kinetic modulation (i.e., k_{off}) can be considered equilibrium *exchange* events, while those that are mediated through PPIs directly between Pols or through PCNA in a "tool-belt" or "landing-pad" fashion are *switches* (**Figure 3**). It is probable that aspects of both of these basic mechanisms are employed. For example, recruitment of a TLS Pol to a stalled HiFi holoenzyme may be brought in by specific contacts with PCNA (**Figure 2**) or combined with Pol-Pol interactions creating a transient supraholoenzyme to initiate a *switch* only to then have the HiFi Pol and/or PCNA dissociate in a subsequent *exchange* for insertion opposite a lesion.

A Distributive Mechanism of Polymerase "Exchange"

Stalling of a DNA Pol at a lesion or template-blocking event will render it catalytically inactive. In that case, k_{pol} becomes extremely slow, and the k_{off} event will predominate, dissociating the Pol from DNA. k_{off} can be increased further by minor DNA distortions caused by the lesion itself (Broyde et al., 2008) or from shuttling between polymerase and exonuclease active sites within the HiFi Pol (Khare and Eckert, 2002). In this situation, multiequilibrium processes will predominate, and depending on the affinity of an exchanged Pol for the lesion and the concentration of Pols within the cell, a new TLS Pol would be selected (**Figure 3**). In the *exchange* model, very little, if any, contacts are retained between an incoming TLS Pol and either the HiFi Pol or PCNA. Instead, the template becomes accessible after a k_{off} event, and a new TLS Pol can bind the damaged template for an insertion event. After insertion, the same TLS Pol can extend for several bases past the lesion, dependent on its own processivity and synthesis properties. Alternatively, another Pol substitution event can be utilized to synthesize past the lesion functioning as an "extender" Pol. Thus, the "hand-off" is indirect and is more consistent with an external equilibrium Pol active site *exchange* of the primer/template.

A Concerted Polymerase 'Switching' Mechanism

There is also evidence for several PPIs or contacts within a Pol holoenzyme. This occurs primarily through multivalency of binding to the trimeric PCNA clamp but can also be through direct Pol-Pol interactions. Several Pol interactions have been discovered between B- and Y-family Pols (designated YB sites) (Baldeck et al., 2015; Cranford et al., 2017). The key to a successful *switch* is that enzyme dissociation-association events from DNA are restricted in favor of pre-bound Pols releasing and swapping active-site binding to the damaged template (**Figure 3**). The affinity of TLS Pols for PCNA or the HiFi Pol itself effectively increases the local concentrations of TLS Pols at the replication fork, allowing for a more coordinated *switch*. To be clear, there can be several k_{off} events involved in a switch. The first, and more traditional event, would be $k_{off\text{-}DNA}$ of the HiFi Pol from DNA, but in that case, localized binding can be retained by PCNA. Should the HiFi Pol dissociate from PCNA, a second $k_{off\text{-}PCNA}$ event can occur. Of course, further contacts such as $k_{off\text{-}Pol}$

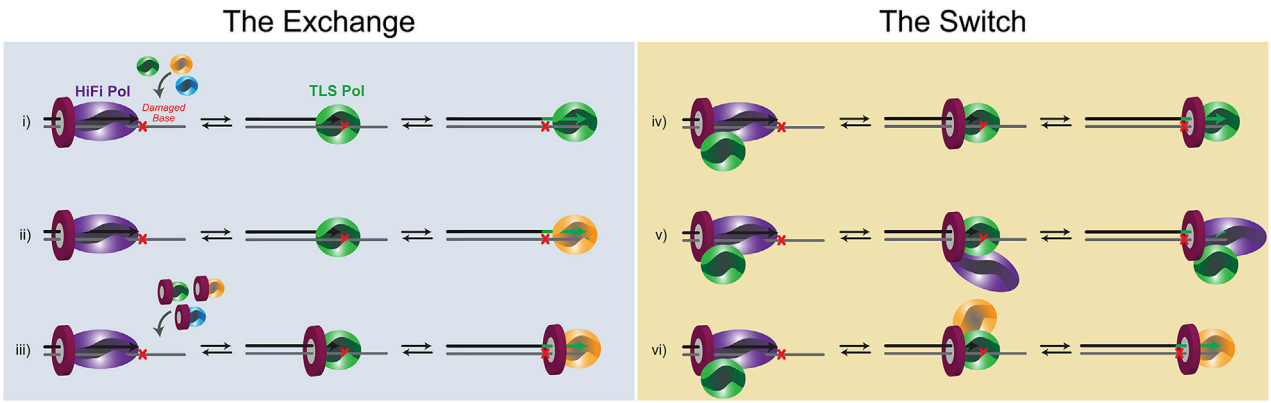

FIGURE 3 | Schematic of the potential equilibrium *exchanges* and PCNA-directed *switches* that occur for TLS. **(i)** a distributive Pol exchange before two-substitution TLS. **(ii)** A distributive Pol *exchange* before three-substitution TLSs.**(iii)** a distributive PCNA/Pol *exchange* before two (or three)-substitution TLS. **(iv)** A concerted Pol *switch* with a pre-associated TLS Pol. **(v)** A concerted Pol *switch* with the HiFi Pol remaining bound to PCNA throughout TLS. **(vi)** Concerted Pol *switches* during three-substitution TLS.

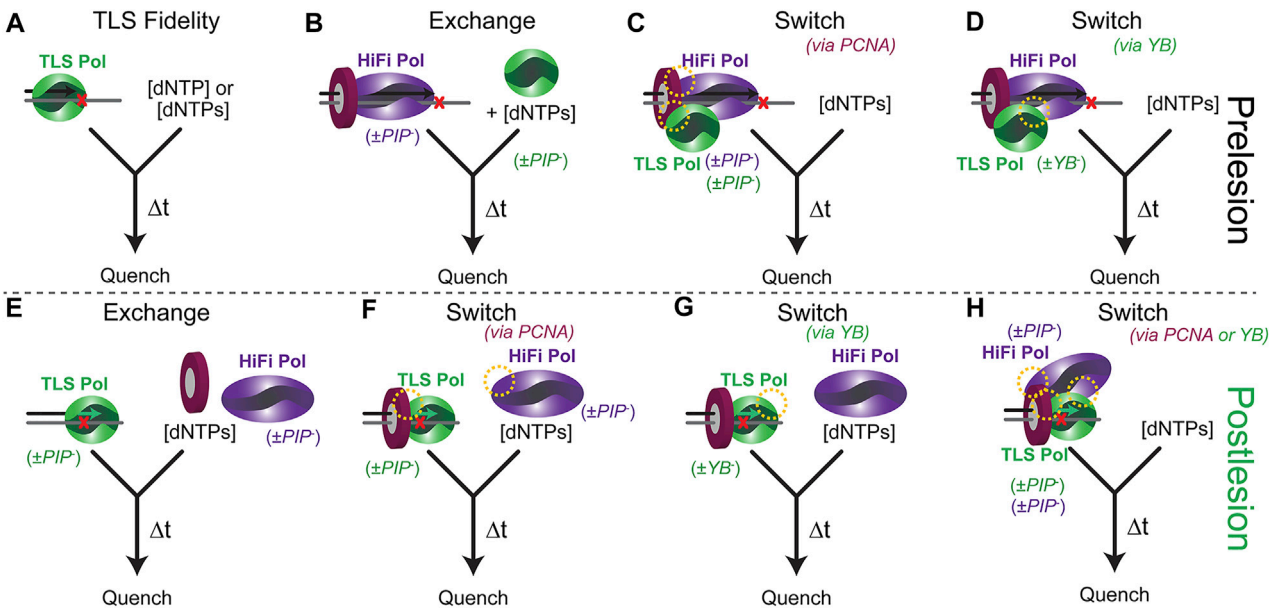

FIGURE 4 | Experimental presteady-state schemes to examine the TLS process both pre and post lesion. **(A)** TLS Pol and various DNA template lesions to examine inherent fidelity in isolation. **(B)** Prebound HiFi Pol with PCNA stalled to examine a kinetic *exchange* process. Preassembled supraholoenzyme complex with HiFi and TLS Pols bound to DNA to examine kinetics of *switching* directed **(C)** by interactions with PCNA (PIP sites) or **(D)** through Pol-Pol interactions (YB site) (yellow circles). **(E)** A TLS Pol with a primer that is a defined number of bases past a lesion is used to examine a distributive *exchange*, **(F)** a PCNA directed *switch*, or **(G)** a YB directed *switch*. **(H)** The kinetics of a preassembled PCNA/TLS/HiFi Pol directed *switch* back to high fidelity synthesis can be validated by utilizing PIP^{-} or YB^{-} mutants of all Pols.

between Pols (i.e., YB site) can also help mediate a *switching* event. In support, mutation of the YB site in the archaeal *Saccharalobus solfataricus* (*Sso*)Dpo4 enzyme results in decreased processivity of DNA synthesis suggesting that the supraholoenzyme complex is a more stable synthesizer (Cranford et al., 2017). Upon successful *switching*, the fate of the HiFi Pol is not always clear. It can dissociate from PCNA and the DNA template and be lost to solution, or it can be held in check within the supraholoenzyme complex. In a TLS *switch*, the "hand-off" is direct with contacts between Pols or coordinated through multivalent PCNA contacts facilitating primer/template binding to a preassociated Pol.

The kinetics of the entire TLS process from stall, substitution, insertion, and extension will be influential in determining whether an *exchange* or *switch* is more likely. For example, weaker PPI contacts and slower rates of insertion opposite

more difficult lesions may favor a more distributive *exchange* of Pols from solution. However, stronger interactions and faster insertion kinetics may allow a concerted *switch* to be more likely, through the confines of a supraholoenzyme complex. Therefore, the PPI affinities, the equilibria concentrations of Pols, and the catalytic efficiency of an insertion (dependent on the lesion type) will be linked, making this highly dynamic process difficult to measure and accurately characterize.

Limitations for Biochemical Assays Designed to Examine Polymerase Substitutions

There are several inherent complexities for a biochemical experiment to fully examine Pol substitutions preceding, during, or after a TLS event. Typically, an *in vitro* dynamic biochemical kinetic characterization can be performed with only a limited and feasible number of biological components in a single experiment. Countless kinetic fidelity measurements have been made for many DNA Pols for even more DNA lesions in a single enzyme—single substrate experiment (**Figure 4A**), providing valuable quantitative understanding of lesion bypass and fidelity (Berdis, 2009; Liu et al., 2016; Powers and Washington, 2017; Raper et al., 2018). As the overall TLS process can include several proteins, numerous PPIs, differing kinetics, and variable equilibria, this experimental setup can be complicated. It is common to mutate the exonuclease proofreading site of the HiFi Pol to eliminate the degradation of the primer strand that complicates the extension kinetics, but the shuttling between Pol and Exo sites may be influential in directing the TLS process (Reha-Krantz, 2010). Moreover, it is also common to truncate TLS Pols to their core polymerase domain, removing important PIP/RIR/UBM/UBZ motifs in the unstructured C-terminal tails and making the examination of *switching* impossible.

The presteady-state kinetics of TLS insertions and extensions can be monitored to better understand the impact of various *exchange* or *switch* processes using a rapid quench setup (**Figures 4B–D**). The experimental design is important as it impacts the desired measured outcome. For example, the k_{on} for a TLS pol is usually diffusion-limited and rapid. However, if that is not the case then the method used to examine an exchange (**Figure 4B**) may be affected. Addition of a TLS Pol after a stalled HiFi Pol will simulate an incoming (or recruited) TLS Pol. The TLS Pol concentration can be varied to examine critical aspects of competitive binding *exchange*. Preincubation of HiFi and TLS Pols with PCNA and DNA can simulate and test a "tool-belt" model of concerted Pol *switching*. The kinetics of insertion and extension may vary depending on whether the TLS Pol is included initially or subsequently to help validate one particular model. The DNA primer length can also be altered to examine any kinetic differences of an approaching DNA Pol holoenzyme with a pre-stalled one in a "running start" assay. Catalytically deficient mutations (cat^{-}) in either the HiFi or TLS Pol active sites can be used to distinguish extension products when multiple Pols are included. PPIs can be disrupted through site-specific mutations of the PIP (PIP^{-}) or YB (YB^{-}) sites for each Pol to test the impact of these contacts in facilitating a TLS *switch*. To fully understand the implications of Pol interactions with PCNA in a *switch*, full length, and not truncated core forms, of TLS Pols should be utilized.

After insertion, the stability and processivity of the TLS Pol can be examined. The design of these experiments will again test whether there is a second distributive *exchange* or facilitated *switch* to resume processive synthesis (**Figures 4E–H**). The DNA primer is systematically lengthened to determine whether there is a position of inherent destabilization of the TLS Pol that limits further extension. PCNA can be excluded or included with the TLS Pol (+/− Rev1) to initiate extension with mixing the HiFi Pol. The resulting product distributions and maximal kinetics of extension will inform on the preferred scheme. For eukaryotic systems, Ub can be covalently added to PCNA through several chemical biology approaches (Freudenthal et al., 2010; Hibbert and Sixma, 2012; Yang et al., 2016; Gong et al., 2018). Combined with UBM/UBZ mutations in the C-termini of TLS Pols, the role for mUb-PCNA in the TLS process can also be explored through the kinetics of extension.

PRELESION: STALLING OF THE HIGH FIDELITY POLYMERASE

Upon encountering a template lesion or a difficult to replicate region from secondary structure or physical impediments, the HiFi Pol will stall (Marians, 2018; Maiorano et al., 2021). The HiFi Pol will attempt insertion of a nucleotide opposite the lesion, however it is almost always unsuccessful (McCulloch and Kunkel, 2008). If insertion opposite a lesion is successful, then further extension is severely inhibited because of distortion in the duplex that is sensed, and the terminal nucleotide is removed at the exonuclease proofreading active site of the HiFi Pol. This stalling (or shuttling between active sites) will set in motion a series of events that act to either stabilize the replication fork for downstream repair or initiate TLS to rapidly continue (Aguilera and Gomez-Gonzalez, 2008; Marechal and Zou, 2013).

After stalling, the HiFi Pol will decouple from the replication helicase causing a buildup of single-strand DNA (ssDNA) (Byun et al., 2005; Chang et al., 2006; Guilliam and Yeeles, 2020). ssDNA alone is fragile and must be protected from breakage by RPA or Rad51 to prevent loss of genetic material and can be a checkpoint signal for repair through the ATR kinase signaling pathway (Cimprich and Cortez, 2008; Blackford and Jackson, 2017; Lanz et al., 2019). Transient stalls, where no direct DNA damage is present, may be relieved by a host of fork stabilizers, accessory factors, and restart proteins that can remove a physical block and allow synthesis and coupling to resume (Lopes et al., 2006; Rickman and Smogorzewska, 2019; Qiu et al., 2021). It has even been shown that the eukaryotic lagging strand Pol δ can efficiently substitute for a decoupled leading strand Pol ε when smaller lesions such as 8-oxoG or thymine glycol are present (Guilliam and Yeeles, 2021). However, if a template lesion is more severe and unsurpassable by the HiFi Pol, then other TLS Pols will be recruited to attempt bypass (Ma et al., 2020).

PRELESION: THE FIRST TRANSLESION SYNTHESIS POLYMERASE SUBSTITUTION

After stalling of the HiFi Pol at a lesion, it must dissociate from the primer/template DNA through one of the above substitution mechanisms (**Figure 3**). The replicative Pol will either fully dissociate from the primer-template junction into solution, following a distributive *exchange* mechanism, or it will remain bound to PCNA in accordance with a concerted *switching* mechanism. For both the archaeal Pol B1 and eukaryotic Pol δ HiFi Pol holoenzyme systems, it was found that the HiFi Pol readily dissociates in a distributive exchange mechanism even during normal DNA synthesis (Bauer et al., 2013; Hedglin et al., 2016b). The lagging strand HiFi Pol in humans, Pol δ, has PIP-sites on three of its four subunits, however only mutation of the PIP-site in the large catalytic subunit significantly reduces Pol activity (Lancey et al., 2020). This potentiates multiple Pols being bound to other PCNA subunits simultaneously in a supraholoenzyme, or at least that multiple PCNA subunits can facilitate *exchange* of Pols (as a landing pad) during TLS. Aside from specific contacts with PCNA, there are several other factors regulating TLS Pol recruitment and selection prior to lesion bypass.

Translesion Synthesis Pol Recruitment and Selection

In mammalian cells, Pol δ is known to convert from a four-subunit to a three-subunit enzyme complex both upon S-phase entry (Zhang et al., 2013) and specifically in response to DNA damage (Zhang et al., 2007; Lee et al., 2014a). Degradation of the smallest subunit, p12, serves as a regulatory mechanism to activate Pol δ for synthesis normally and is further directed by ATR signaling (Zhang et al., 2007; Lee et al., 2019). From here, TLS Pol recruitment and selection can depend on a multitude of factors, including the aforementioned PIP or UBZ/UBM interactions with (Ub-)PCNA (**Figure 2**), Pol affinity for the damaged DNA substrate, and Pol-Pol interactions. Various types of DNA-damaging conditions have been shown to localize TLS Pols in replication foci in nuclei, indicating that Pol concentration is an early contributor of selection for TLS (Maiorano et al., 2021). Once TLS Pols are in the vicinity of the damage site, Pol affinity for the DNA substrate becomes a driver of Pol selection. Accommodation of lesions by TLS Pols can be influenced by template-strand sequence and steric hindrance between bulkier lesions and Pol active sites (Zhao and Washington, 2017; Thomforde et al., 2021). Sequence context has also been shown to affect Pol efficiency and accuracy during TLS opposite various lesions, however the molecular basis for this effect is not well understood (Shriber et al., 2015; Bacurio et al., 2021).

Despite these qualifications for TLS by certain Pols to occur, it should be noted that backup TLS pathways exist in eukaryotes. Certain lesions deter recruitment of some TLS Pols in favor of more suitable inserters, however in the absence of the favored Pol, a less-favored TLS Pol(s) can bypass these lesions. Secondary TLS mechanisms have been demonstrated both *in vivo*, through Pol knockdowns, and *in vitro*, by examining multiple TLS Pol bypass capabilities opposite an assortment of lesions (Yoon et al., 2009; Livneh et al., 2010; Jha and Ling, 2018; Inomata et al., 2021). The presence of backup TLS pathways indicates that steric effects may not fully regulate Pol selection, but likely contribute significantly.

POSTLESION: EXTENSION PAST THE LESION, A POSSIBLE SECOND SUBSTITUTION

After insertion of a base opposite a lesion, the TLS Pol can continue synthesizing and extending downstream until inherent enzymatic properties, PPIs, or multiequilibria processes allow for substitution of other Pols. TLS Pols have no exonuclease proofreading domains and lower fidelities compared to HiFi Pols (**Figure 1C**), and so, their lower processivities serve a vital function to limit further DNA synthesis past a lesion to maintain genome integrity. However, the mechanisms for extension and reestablishing the HiFi holoenzyme past a TLS event are not well studied.

Translesion Synthesis Polymerases: From Inserters to Extenders

Beyond the lesion, "inserter" TLS Pols extend the nascent DNA strand to a position where either an "extender" TLS Pol, such as eukaryotic Pol ζ, can continue TLS or where the HiFi Pol can resume synthesis. A TLS mechanism in which an "inserter" Pol is the only Pol required for TLS can be termed "two-substitution" TLS. In the event both an "inserter" and "extender" Pol is required for TLS, the term "three-substitution" TLS can be used. The vocabulary of "substitution" is preferred over other vague describers including "one-" or "two-polymerase" TLS (Johnson et al., 2000a) to focus more on the mechanistic process. With Rev1 potentially being involved as a scaffold in both two- and three-substitution mechanisms, defining the TLS by the number of Pols may be inaccurate and confusing. Therefore, nomenclature referring to the number of "substitutions" is preferred. Pol ζ has been shown to function as the primary "extender" Pol after the "inserter" in a "three-substitution" TLS process for certain lesions (Shachar et al., 2009; Lee Y.-S. et al., 2014). A-family Pol θ has also displayed some "extender" activity, although its exact role is still not fully defined (Seki et al., 2004; Bacurio et al., 2021). Recently, *Sulfolobus islandicus* B-family polymerase Dpo2 has been shown to act as the "extender" Pol in combination with "inserter" Pol Dpo4 during bypass of abasic sites (Feng et al., 2021).

Pol ζ Recruitment and Assembly

Assembly of the five-subunit extender Pol ζ is facilitated by HiFi Pol δ and the Y-family Rev1. Although the precise timing of this mechanism is not clear, Pol δ can rearrange and share subunits with Pol ζ to form the active Pol ζ complex. Pol δ shares subunits Pol31 and Pol32 in yeast and subunits p50 (Polδ2) and p66 (Polδ3) in humans with Pol ζ (Baranovskiy et al., 2012; Malik et al., 2020).

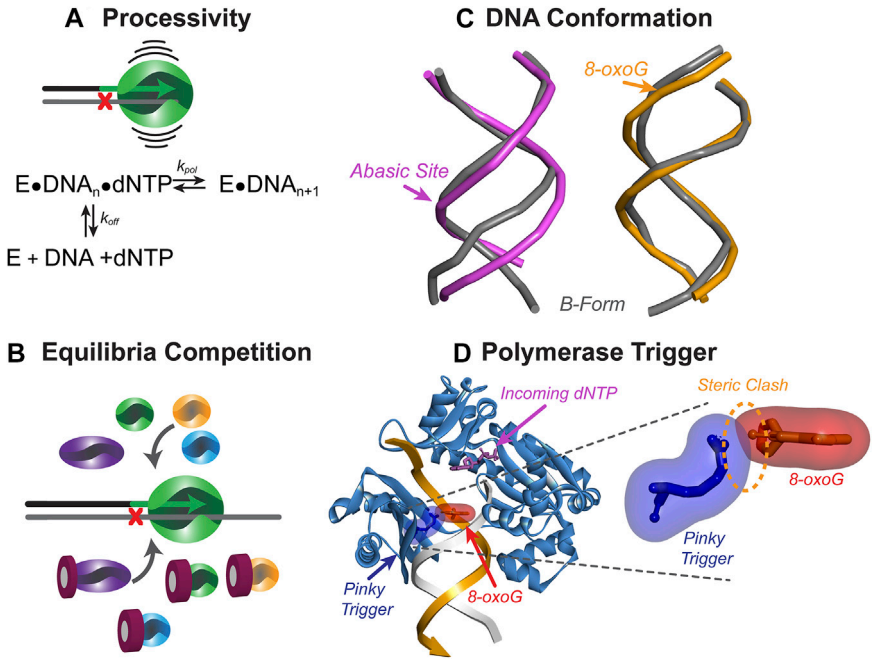

FIGURE 5 | Mechanisms to initiate resumption of high-fidelity synthesis. **(A)** The processivity of a Pol represents the number of nucleotides inserted before dissociating from DNA and calculated as a ratio of k_{pol} to k_{off}. TLS Pols have lower processivity than HiFi Pols and can readily dissociate from DNA when the bypassed lesion is no longer in the active site. **(B)** DNA-damaging events can cause upregulation of TLS Pols, leading to concentration-dependent competition between Pols in solution for access to the DNA substrate. **(C)** DNA lesions can alter the conformation of the DNA, making extension of the nascent strand more difficult for the synthesizing Pol. Abasic site duplex (pink, PDB: 2HSS (Chen et al., 2007)) show more distortion than 8-oxo-G duplex (orange, PDB: 5IZP (Hoppins et al., 2016)) compared to B-form DNA (grey). Arrow shows the position of the lesion **(D)** Template-strand lesions are bypassed by TLS Pols, however as the lesion is exiting the active site, a steric clash may occur between a specific amino acid residue (i.e., Pinky Trigger) and the damaged template base to destabilize binding and further extension. Shown is the ternary *Sso*Dpo4 complex (PDB:ID 1JX4) with oxygen modelled in the 8-position of the guanine in the –3 position on the primer strand.

Aside from the shared subunits, Pol ζ is comprised of Rev3, the catalytic subunit, simultaneously bound to two Rev7 subunits (Rizzo et al., 2018). The entire Pol ζ complex interacts in a 1:1 ratio with the scaffold TLS Pol Rev1. Rev1 is presumably bound to the replisome during an initial response to DNA damage and is soon thereafter able to recruit Pol ζ to the primer/template junction, coordinating the inserter-to-extender three-substitution mechanism (Makarova and Burgers, 2015; Liu et al., 2018). In a two-substitution mechanism, such as Pol η bypass of a UV-induced CPD, there is no requirement for an extender Pol. Under such circumstances, Pol ζ recruitment and assembly would likely not occur, even though the initial DNA damage response may generate mUb-PCNA and recruit Rev1. Interestingly, when Pol η is absent, Pol ζ functions in subsequence to Pol ι or Pol κ in TLS opposite this exact lesion (Ziv et al., 2009). The ability of the extender Pol ζ to function in a backup TLS mechanism when it is not required in the primary bypass mechanism for a certain lesion indicates that Pol ζ recruitment and assembly may always occur in response to DNA damage. Another possibility is that Pol ζ assembly does not occur until after the "inserter" Pol has performed the first step of TLS, at which time synthesis is stalled until a suitable "extender" can be recruited to the DNA substrate. Further experimentation needs to be performed to ascertain the exact timing of Pol ζ recruitment and assembly.

POSTLESION: RESUMING HIGH FIDELITY SYNTHESIS, A FINAL SUBSTITUTION

While most TLS studies have focused on the capability of TLS Pols to insert nucleotides opposite a template-strand DNA lesion, less focus has been placed on resumption of high-fidelity synthesis beyond the lesion. As TLS Pols are often inaccurate and less processive for synthesis opposite an undamaged DNA template, they are limited in their extension capabilities after lesion bypass (Vaisman and Woodgate, 2017). Limiting extension by TLS Pols requires a mechanism for substitution back to a HiFi Pol. The length of extension beyond the lesion by TLS Pols can vary, and likely has to do with the native processivity of the TLS Pol on DNA templates (**Figure 5A**), additional Pols in the vicinity of the primer/template junction (**Figure 5B**), the contacts that the TLS Pol active site residues make with the DNA substrate (**Figure 5C**), and possibly even structural impediments to extension (**Figure 5D**). After TLS has been completed, the TLS Pols extend to a position beyond the lesion, which is now outside of the Pol active site. At this point, structural characteristics of the TLS Pol can cause dissociation from the DNA substrate and initiate a substitution back to the HiFi Pol.

TABLE 1 | The position of substitution back to high fidelity synthesis.

DNA lesion	Species	Inserter	Extender	*Exchange* or *Switch* back position	Reference
Benzo(a)pyrene diol epoxide(BPDE)-dG	*Hs*	Pol κ	Pol ζ	+30	Suzuki et al. (2021)
Cyclobutane pyrimidine dimer (CPD)	*Hs*	Pol η	N/A	+2	Kusumoto et al. (2004), McCulloch et al. (2004)
8-oxoguanine (8-oxoG)	*Sso*	Dpo4	N/A	+3	Cranford et al. (2020)
N^2-dG-peptide	*E. coli*	Pol IV	N/A	+3	Minko et al. (2008)

Inherent Translesion Synthesis Pol Processivity

A primary reason for why TLS Pol synthesis is limited is due to low processivity on undamaged substrates (**Figure 5A**). TLS Pols have the structural features to allow bulky lesions into the active site (**Figure 1C**), but they dissociate readily from undamaged DNA (Raper et al., 2016). The large, tolerant active sites of TLS Pols are optimal for TLS but make the TLS Pol inherently less stable, less processive, and more mutagenic on undamaged substrates. "Extender" Pols have slightly increased processivity compared to "inserter" Pols but remain limited in synthesis capability once far enough downstream from the lesion. Recent structural studies have identified the position of the N-terminal domain-palm domain linker in the catalytic subunit of human Pol ζ as paramount in allowing the extender to tolerate distorted templates (Malik et al., 2020). Beyond active-site recognition of the DNA damage, Pol ζ processivity is greatly reduced. This finding is supported *in vivo* by examination of human Pol ζ mutational signatures in extension past damaged DNA. Recently, human Pol ζ was found to extend the nascent strand of DNA roughly 30 nucleotides from BPDE-induced damage (**Table 1**) (Suzuki et al., 2021). The mutational frequency data also indicated that Pol ζ may be recruited multiple times during extension, even after Pol δ has performed some synthesis. Therefore, further research needs to be performed to confirm the exact mechanism of limiting "extender" Pols in TLS. Adding to this complexity are the shared subunits (PolD2 and D3) between replicative Pol δ and extender Pol ζ. It also remains unclear the exact position of the *exchange* or *switch* back following Pol ζ extension, and whether or not this position is the same for extension past all types of DNA lesions.

Direct contacts between the TLS Pol active site and the damaged DNA template also contribute to the position of the hand-off to a replicative Pol. Likely contributing to processivity, the ability of a TLS Pol to interact with the lesion as it leaves the active site can dictate how many additional nucleotides the Pol will synthesize before dissociating from DNA. For certain Pols, such as human Pol η and its bypass of UV-induced TT-dimers, the TLS mechanism has been thoroughly examined. Crystal structures of Pol η in complex with CPD-containing DNA have shown that the Pol η active site can easily accommodate two template-strand nucleotides (Biertumpfel et al., 2010). Having the dimer within the Pol η active site is crucial to maintaining interaction with the DNA and allows for efficient TLS across dimerized lesions in eukaryotes (Prakash and Prakash, 2002). During bypass of a CPD, it has been shown that Pol η inserts nucleotides opposite the dimer, extends two positions beyond the lesion, and then destabilizes from DNA (Kusumoto et al., 2004; McCulloch et al., 2004). When Pol η is three nucleotides from the template-strand dimer it becomes deprived of these stabilizing contacts (Biertumpfel et al., 2010). This correlates with the position at which the HiFi Pol is able to resume synthesis after TLS. For bypass of this particular DNA lesion in humans, an "extender" Pol is not necessary, confirming +2 nucleotides past the lesion as the position for the HiFi substitution (**Table 1**).

Equilibrium Competition for DNA Binding

The concentrations of TLS Pols are generally kept lower than HiFi Pols to prevent their equilibrium association and low fidelity synthesis. In fact, altered expression of the TLS Pols have been linked with increased mutation rates (Pavlov et al., 2001; Qi et al., 2012; Sasatani et al., 2017), correlated with various cancers (O-Wang et al., 2001; Albertella et al., 2005b; Flanagan et al., 2007; Wang et al., 2010), and give rise to chemotherapeutic resistance (Saha et al., 2021). There is evidence that TLS Pols are cell cycle regulated under normal conditions, peaking in G2 phase to facilitate any required TLS prior to cell division (Waters and Walker, 2006; Plachta et al., 2015; Sobolewska et al., 2020). Even reorganization of Pol δ in eukaryotes from a three to four subunit enzyme (Zhang et al., 2007; Lee et al., 2019) or exchanging with Rev3/7 to form Pol ζ (Rizzo et al., 2018) can impact activity. The return of the p12 subunit to reestablish a four subunit Pol δ is influential in providing greater processivity and strand displacement activity possibly reserved for other DNA repair pathways (Meng et al., 2010; Lin et al., 2013).

Several eukaryotic TLS Pols, including Pol η (Tomicic et al., 2014), Rev1 (Uchiyama et al., 2015), and Pol κ (Velasco-Miguel et al., 2003) are upregulated after specific DNA damage, however the prototypical upregulation of TLS Pols occurs during the SOS response in bacteria to overcome substantial DNA damage and induce DNA mutagenesis for survival (Kenyon and Walker, 1980; Napolitano et al., 2000; Yeiser et al., 2002). Deubiquitination of PCNA may also serve to recruit HiFi Pols back after insertion/extension events, although this may be more influential in the yeast system (Zhuang et al., 2008) compared to mammalian systems (Niimi et al., 2008; Brown et al., 2009). Therefore, with all of these potential expression changes occurring normally during the cell cycle and more specifically in response to DNA damage and in cells with multiple TLS Pols, it is likely that even small changes in the cellular multiequilibrium will affect Pol binding and selection (**Figure 5B**).

Altered DNA Conformation

Some TLS Pols have active sites evolved for specific lesions (Sale et al., 2012; Sale, 2013) either to recognize the lesion itself or the alternative conformation of the primer-template DNA duplex induced by the lesion. Of the most common lesions, 8-oxoG does not induce significant structural duplex distortion (Plum et al., 1995), unlike that for an abasic site (Bignon et al., 2016) (**Figure 5C**). Other lesions such as benzopyrene dG adducts (Menzies et al., 2015), CPDs (Mcateer et al., 1998), or cis-Pt (Hartog et al., 1983) also induce major structural distortions (Pages and Fuchs, 2002; Lukin and De los Santos, 2006; Zhao et al., 2012). After insertion of a base across these lesions, the "inserter" Pol will move to the +1 position. From there, the "inserter" or "extender" will continue to synthesize downstream of the lesion. The structural perturbations that these Pols encounter past the lesions has not been studied in great detail and provide a plausible model for binding destabilization that limits further extension. Interestingly, the extender Pol ζ includes structural features to tolerate lesion-distorted DNA upstream (Malik et al., 2020).

Steric Impediments to Extension

While the aforementioned contacts with DNA stabilize the Pol during TLS, some interactions between the Pol active site and the lesion can promote dissociation from the substrate. Recent studies on the bypass of 8-oxoG lesions by *Sso*Dpo4 have indicated that this Pol is able to insert a nucleotide opposite the lesion and extend three bases beyond the lesion before becoming catalytically inefficient (**Table 1**) (Cranford et al., 2020). This coincided with the exact position (+3) that the replicative Pol B1 is capable of reengaging and efficiently extending the primer to resume high fidelity synthesis. Upon structural examination of Dpo4 in complex with DNA, specific residues of the little finger domain may be directly clashing with the 8-oxoG lesion as it exits the active site. This hypothetical "pinky trigger" may dictate the position where HiFi synthesis resumes for the archaeal system (**Figure 5D**). The ability of TLS Pols to sense the template lesion outside of the active site may destabilize binding of the TLS Pol downstream and provide an opportunity for a HiFi Pol to resume synthesis.

THERAPEUTIC STRATEGIES TARGETING TLS STEPS

Polymerase inhibitors have become part of the ever-growing list of chemotherapeutics. As accurate and complete replication of DNA is vital to cellular growth and viability, inhibition of this process can block growth and promote apoptosis of aberrant cells. By specifically targeting cancer cells with molecules designed to impede DNA replication, one could limit tumor growth. Chain-terminating nucleoside analogs are among the most popular in this class of therapeutics (Berdis, 2017). These nucleotide mimics are inserted by Pols to a nascent strand of DNA during replication and promptly conclude extension of that strand. The potential impact of these chain terminators can be escalated when combined with DNA-damaging agents. TLS Pols are known to bypass lesions generated by platinum chemotherapeutics (Albertella et al., 2005a) and are upregulated in multiple cancer cell lines (Tomicic et al., 2014). The overzealous activity of these TLS Pols desensitizes cancer cells to chemotherapeutics by enabling cell survival amid DNA-damaging conditions. By inhibiting these TLS Pols and preventing insertions opposite chemotherapy-induced lesions or other steps in the TLS process, the efficacy of the treatment is amplified overall.

In accordance with this principle, alternate methods of TLS Pol inhibition would suffice for ameliorated chemotherapy. Pol-Pol and PCNA-Pol contacts that are involved in TLS Pol recruitment, stabilization, and substitutions make ideal targets for cancer drug research (Altieri and Kelman, 2018). TLS in humans across cisplatin-induced intrastrand crosslinks is a three-substitution mechanism requiring Pol η as the inserter, Pol ζ as the extender, and Rev1 as a scaffold. Recently, JH-RE-06, a small molecule inhibitor of this bypass, has been shown to dimerize Rev1 and prevent Pol ζ from binding (Wojtaszek et al., 2019). Without an efficient extender, TLS opposite Pt-GG lesions is reduced, and cisplatin becomes more effective at counteracting tumors. JH-RE-06, along with other small molecule inhibitors of protein-protein interactions, serve to block a specific element of TLS mechanisms in order to minimize obstructions to DNA-damaging agents (Wojtaszek et al., 2019; Dash and Hadden, 2021).

DISCUSSION

All of the examples described in the Postlesion: Resuming High Fidelity Synthesis, a Final Substitution section are mechanisms used to limit synthesis by a TLS Pol after insertion to maintain downstream genome fidelity. The same structural features of TLS Pols that allow bulky lesions to enter the Pol active site are the features that make TLS Pols inaccurate and unstable on undamaged DNA substrates. TLS Pols are more mutagenic on undamaged templates than on suitable damaged substrates; so strict regulation outside of a specific TLS insertion is necessary. Thus, TLS Pols must insert nucleotides opposite the lesion, extend beyond the lesion, and then hand the DNA back to a HiFi Pol at a position that is both favorable to TLS Pol dissociation and subsequent HiFi Pol extension. Integral to the positioning of the resumption of HiFi synthesis are direct Pol-DNA, Pol-PCNA, and Pol-Pol interactions. Pol-Pol binding has been shown to stabilize the replicating Pol throughout TLS (Cranford et al., 2017). Pol-PCNA contacts through PIP motifs, UBZ/UBM contacts, and Rev1 bridges are also known to improve Pol stability and processivity (Boehm et al., 2016b; Acharya et al., 2020). These precise interactions that provide stability during TLS may also be involved in regulation of steps after TLS insertion. Further experimentation needs to be performed to identify the exact substitution mechanism(s) and steps that occur during lesion bypass.

Many *in vitro* experiments examine the TLS lesion bypass capability of truncated core TLS Pols in isolation. However, these absent regions are precisely the ones that facilitate Pol-

Pol and PCNA-Pol binding and are needed to examine the entire TLS process. Full-length TLS and HiFi Pols, in the presence of PCNA and a suitable "extender" Pol will allow for interactions that may influence extension beyond the lesion, thus providing confidence in the kinetic characterizations required to determine a position where high fidelity synthesis resumes. Ultimately, translesion synthesis needs to be rapid, but distributive, to limit successive nucleotide incorporations so that replicative Pols can resume high fidelity synthesis and recouple with the replisome. The entire TLS mechanism, from the initial HiFi Pol stalling, "inserter" Pol recruitment, and TLS Pol(s) selection to the second (and possibly third) Pol substitutions to an "extender" Pol or HiFi Pol, respectively, remains to be fully understood. Location of the substitution positions and identification of the kinetically favored TLS mechanisms for bypass of DNA damage has direct applications in drug discovery. Future experiments should seek to expand our understanding of the complete TLS process to identify additional therapeutic targets within TLS.

AUTHOR CONTRIBUTIONS

All authors listed have made a substantial, direct, and intellectual contribution to the work and approved it for publication.

FUNDING

Work in the Trakselis laboratory is generously supported by the NSF (MCB 2105167 and CHE 2104242 to MT), the NIH R15 (GM13791 to MT), and Baylor University.

REFERENCES

Acharya, N., Patel, S. K., Sahu, S. R., and Kumari, P. (2020). 'PIPs' in DNA Polymerase: PCNA Interaction Affairs. *Biochem. Soc. Trans.* 48, 2811–2822. doi:10.1042/bst20200678

Aguilera, A., and Gómez-González, B. (2008). Genome Instability: A Mechanistic View of its Causes and Consequences. *Nat. Rev. Genet.* 9, 204–217. doi:10.1038/nrg2268

Albertella, M. R., Green, C. M., Lehmann, A. R., and O'connor, M. J. (2005a). A Role for Polymerase η in the Cellular Tolerance to Cisplatin-Induced Damage. *Cancer Res.* 65, 9799–9806. doi:10.1158/0008-5472.can-05-1095

Albertella, M. R., Lau, A., and O'Connor, M. J. (2005b). The Overexpression of Specialized DNA Polymerases in Cancer. *DNA Repair* 4, 583–593. doi:10.1016/j.dnarep.2005.01.005

Alt, A., Lammens, K., Chiocchini, C., Lammens, A., Pieck, J. C., Kuch, D., et al. (2007). Bypass of DNA Lesions Generated during Anticancer Treatment with Cisplatin by DNA Polymerase η. *Science* 318, 967–970. doi:10.1126/science.1148242

Altieri, A. S., and Kelman, Z. (2018). DNA Sliding Clamps as Therapeutic Targets. *Front. Mol. Biosci.* 5, 87. doi:10.3389/fmolb.2018.00087

Bacurio, J. H. T., Yang, H., Naldiga, S., Powell, B. V., Ryan, B. J., Freudenthal, B. D., et al. (2021). Sequence Context Effects of Replication of FapydG in Three Mutational Hot Spot Sequences of the P53 Gene in Human Cells. *DNA Repair* 108, 103213. doi:10.1016/j.dnarep.2021.103213

Baldeck, N., Janel-Bintz, R., Wagner, J., Tissier, A., Fuchs, R. P., Burkovics, P., et al. (2015). FF483-484 Motif of Human Polη Mediates its Interaction with the POLD2 Subunit of Polδ and Contributes to DNA Damage Tolerance. *Nucleic Acids Res.* 43, 2116–2125. doi:10.1093/nar/gkv076

Baranovskiy, A. G., Lada, A. G., Siebler, H. M., Zhang, Y., Pavlov, Y. I., and Tahirov, T. H. (2012). DNA Polymerase δ and ζ Switch by Sharing Accessory Subunits of DNA Polymerase δ. *J. Biol. Chem.* 287, 17281–17287. doi:10.1074/jbc.m112.351122

Bauer, R. J., Wolff, I. D., Zuo, X., Lin, H.-K., and Trakselis, M. A. (2013). Assembly and Distributive Action of an Archaeal DNA Polymerase Holoenzyme. *J. Mol. Biol.* 425, 4820–4836. doi:10.1016/j.jmb.2013.09.003

Berdis, A. J. (2017). Inhibiting DNA Polymerases as a Therapeutic Intervention against Cancer. *Front. Mol. Biosci.* 4, 78. doi:10.3389/fmolb.2017.00078

Berdis, A. J. (2009). Mechanisms of DNA Polymerases. *Chem. Rev.* 109, 2862–2879. doi:10.1021/cr800530b

Biertümpfel, C., Zhao, Y., Kondo, Y., Ramón-Maiques, S., Gregory, M., Lee, J. Y., et al. (2010). Structure and Mechanism of Human DNA Polymerase η. *Nature* 465, 1044–1048. doi:10.1038/nature09196

Bignon, E., Gattuso, H., Morell, C., Dehez, F., Georgakilas, A. G., Monari, A., et al. (2016). Correlation of Bistranded Clustered Abasic DNA Lesion Processing with Structural and Dynamic DNA helix Distortion. *Nucleic Acids Res.* 44, 8588–8599. doi:10.1093/nar/gkw773

Blackford, A. N., and Jackson, S. P. (2017). ATM, ATR, and DNA-PK: The trinity at the Heart of the DNA Damage Response. *Mol. Cel* 66, 801–817. doi:10.1016/j.molcel.2017.05.015

Boehm, E. M., Gildenberg, M. S., and Washington, M. T. (2016a). The many Roles of PCNA in Eukaryotic DNA Replication. *Enzymes* 39, 231–254. doi:10.1016/bs.enz.2016.03.003

Boehm, E. M., Spies, M., and Washington, M. T. (2016b). PCNA Tool Belts and Polymerase Bridges Form during Translesion Synthesis. *Nucleic Acids Res.* 44, 8250–8260. doi:10.1093/nar/gkw563

Bomar, M. G., Pai, M. T., Tzeng, S. R., Li, S. S. C., and Zhou, P. (2007). Structure of the Ubiquitin-Binding Zinc finger Domain of Human DNA Y-Polymerase η. *EMBO Rep.* 8, 247–251. doi:10.1038/sj.embor.7400901

Boudsocq, F., Kokoska, R. J., Plosky, B. S., Vaisman, A., Ling, H., Kunkel, T. A., et al. (2004). Investigating the Role of the Little Finger Domain of Y-Family DNA Polymerases in Low Fidelity Synthesis and Translesion Replication. *J. Biol. Chem.* 279, 32932–32940. doi:10.1074/jbc.m405249200

Brown, S., Niimi, A., and Lehmann, A. R. (2009). Ubiquitination and Deubiquitination of PCNA in Response to Stalling of the Replication Fork. *Cell Cycle* 8, 689–692. doi:10.4161/cc.8.5.7707

Broyde, S., Wang, L., Rechkoblit, O., Geacintov, N. E., and Patel, D. J. (2008). Lesion Processing: High-Fidelity Versus Lesion-Bypass DNA Polymerases. *Trends Biochem. Sci.* 33, 209–219. doi:10.1016/j.tibs.2008.02.004

Byun, T. S., Pacek, M., Yee, M.-c., Walter, J. C., and Cimprich, K. A. (2005). Functional Uncoupling of MCM Helicase and DNA Polymerase Activities Activates the ATR-Dependent Checkpoint. *Genes Dev.* 19, 1040–1052. doi:10.1101/gad.1301205

Chang, D. J., Lupardus, P. J., and Cimprich, K. A. (2006). Monoubiquitination of Proliferating Cell Nuclear Antigen Induced by Stalled Replication Requires Uncoupling of DNA Polymerase and Mini-Chromosome Maintenance Helicase Activities. *J. Biol. Chem.* 281, 32081–32088. doi:10.1074/jbc.m606799200

Chatterjee, N., and Walker, G. C. (2017). Mechanisms of DNA Damage, Repair, and Mutagenesis. *Environ. Mol. Mutagen.* 58, 235–263. doi:10.1002/em.22087

Chen, J., Dupradeau, F.-Y., Case, D. A., Turner, C. J., and Stubbe, J. (2007). Nuclear Magnetic Resonance Structural Studies and Molecular Modeling of Duplex DNA Containing Normal and 4'-Oxidized Abasic Sites,. *Biochemistry* 46, 3096–3107. doi:10.1021/bi6024269

Cimprich, K. A., and Cortez, D. (2008). ATR: An Essential Regulator of Genome Integrity. *Nat. Rev. Mol. Cel Biol.* 9, 616–627. doi:10.1038/nrm2450

Cranford, M. T., Chu, A. M., Baguley, J. K., Bauer, R. J., and Trakselis, M. A. (2017). Characterization of a Coupled DNA Replication and Translesion Synthesis Polymerase Supraholoenzyme from Archaea. *Nucleic Acids Res.* 45, 8329–8340. doi:10.1093/nar/gkx539

Cranford, M. T., Kaszubowski, J. D., and Trakselis, M. A. (2020). A Hand-Off of DNA between Archaeal Polymerases Allows High-Fidelity Replication to Resume at a Discrete Intermediate Three Bases Past 8-Oxoguanine. *Nucleic Acids Res.* 48, 10986–10997. doi:10.1093/nar/gkaa803

Dash, R. C., and Hadden, K. (2021). Protein-Protein Interactions in Translesion Synthesis. *Molecules* 26, 5544. doi:10.3390/molecules26185544

Du, H., Wang, P., Wu, J., He, X., and Wang, Y. (2020). The Roles of Polymerases ν and θ in Replicative Bypass of O6- and N2-Alkyl-2′-Deoxyguanosine Lesions in Human Cells. *J. Biol. Chem.* 295, 4556–4562. doi:10.1074/jbc.ra120.012830

Feng, X., Zhang, B., Xu, R., Gao, Z., Liu, X., Yuan, G., et al. (2021). Enzymatic Switching Between Archaeal DNA Polymerases Facilitates Abasic Site Bypass. *Front. Microbiol.* 12, 802670. doi:10.3389/fmicb.2021.802670

Flanagan, A., Rafferty, G., O'neill, A., Rynne, L., Kelly, J., Mccann, J., et al. (2007). The Human POLH Gene Is Not Mutated, and Is Expressed in a Cohort of Patients with Basal or Squamous Cell Carcinoma of the Skin. *Int. J. Mol. Med.* 19, 589–596. doi:10.3892/ijmm.19.4.589

Freudenthal, B. D., Gakhar, L., Ramaswamy, S., and Washington, M. T. (2010). Structure of Monoubiquitinated PCNA and Implications for Translesion Synthesis and DNA Polymerase Exchange. *Nat. Struct. Mol. Biol.* 17, 479–484. doi:10.1038/nsmb.1776

Fujii, S., and Fuchs, R. P. (2020). A Comprehensive View of Translesion Synthesis in *Escherichia C. Microbiol. Mol. Biol. Rev.* 84, e00002–20. doi:10.1128/MMBR.00002-20

Ghodke, P. P., Mali, J. R., Patra, A., Rizzo, C. J., Guengerich, F. P., and Egli, M. (2021). Enzymatic Bypass and the Structural Basis of Miscoding Opposite the DNA Adduct 1,N2-Ethenodeoxyguanosine by Human DNA Translesion Polymerase η. *J. Biol. Chem.* 296, 100642. doi:10.1016/j.jbc.2021.100642

Gong, P., Davidson, G. A., Gui, W., Yang, K., Bozza, W. P., and Zhuang, Z. (2018). Activity-Based Ubiquitin-Protein Probes Reveal Target Protein Specificity of Deubiquitinating Enzymes. *Chem. Sci.* 9, 7859–7865. doi:10.1039/c8sc01573b

Goodman, M. F., and Woodgate, R. (2013). Translesion DNA Polymerases. *Cold Spring Harb. Perspect. Biol.* 5, a010363. doi:10.1101/cshperspect.a010363

Gowda, A. S. P., and Spratt, T. E. (2016). DNA Polymerase ν Rapidly Bypasses O6-Methyl-dG but Not O6-[4-(3-Pyridyl)-4-Oxobutyl-dG and O2-Alkyl-dTs. *Chem. Res. Toxicol.* 29, 1894–1900. doi:10.1021/acs.chemrestox.6b00318

Guilliam, T. A., and Yeeles, J. T. (2021). The Eukaryotic Replisome Tolerates Leading-Strand Base Damage by Replicase Switching. *EMBO J.* 40, e107037. doi:10.15252/embj.2020107037

Guilliam, T. A., and Yeeles, J. T. P. (2020). Reconstitution of Translesion Synthesis Reveals a Mechanism of Eukaryotic DNA Replication Restart. *Nat. Struct. Mol. Biol.* 27, 450–460. doi:10.1038/s41594-020-0418-4

Gulbis, J. M., Kelman, Z., Hurwitz, J., O'donnell, M., and Kuriyan, J. (1996). Structure of the C-Terminal Region of p21WAF1/CIP1 Complexed with Human PCNA. *Cell* 87, 297–306. doi:10.1016/s0092-8674(00)81347-1

Hakem, R. (2008). DNA-Damage Repair; the Good, the Bad, and the Ugly. *EMBO J.* 27, 589–605. doi:10.1038/emboj.2008.15

Hartog, J. H. J., Altona, C., Boom, J. H., Marcelis, A. T. M., Marel, G. A., Rinkel, L. J., et al. (1983). Cis-Platinum Induced Distortions in DNA. Conformational Analysis of d(GpCpG) and cis-Pt(NH3)2{d(GpCpG)}, Studied by 500-MHz NMR. *Eur. J. Biochem.* 134, 485–495. doi:10.1111/j.1432-1033.1983.tb07593.x

Hedglin, M., Pandey, B., and Benkovic, S. J. (2016a). Characterization of Human Translesion DNA Synthesis across a UV-Induced DNA Lesion. *Elife* 5, e19788. doi:10.7554/elife.19788

Hedglin, M., Pandey, B., and Benkovic, S. J. (2016b). Stability of the Human Polymerase δ Holoenzyme and its Implications in Lagging Strand DNA Synthesis. *Proc. Natl. Acad. Sci. USA* 113, E1777–E1786. doi:10.1073/pnas.1523653113

Hibbert, R. G., and Sixma, T. K. (2012). Intrinsic Flexibility of Ubiquitin on Proliferating Cell Nuclear Antigen (PCNA) in Translesion Synthesis. *J. Biol. Chem.* 287, 39216–39223. doi:10.1074/jbc.m112.389890

Hippel, P. H. V., Fairfield, F. R., and Dolejsi, M. K. (1994). On the Processivity of Polymerases. *Ann. N.Y. Acad. Sci.* 726, 118–131. doi:10.1111/j.1749-6632.1994.tb52803.x

Hoeijmakers, J. H. J. (2009). DNA Damage, Aging, and Cancer. *N. Engl. J. Med.* 361, 1475–1485. doi:10.1056/nejmra0804615

Hoppins, J. J., Gruber, D. R., Miears, H. L., Kiryutin, A. S., Kasymov, R. D., Petrova, D. V., et al. (2016). 8-Oxoguanine Affects DNA Backbone Conformation in the *EcoRI* Recognition Site and Inhibits its Cleavage by the Enzyme. *Plos One* 11, e0164424. doi:10.1371/journal.pone.0164424

Inomata, Y., Abe, T., Tsuda, M., Takeda, S., and Hirota, K. (2021). Division of Labor of Y-Family Polymerases in Translesion-DNA Synthesis for Distinct Types of DNA Damage. *PLoS One* 16, e0252587. doi:10.1371/journal.pone.0252587

Jha, V., and Ling, H. (2018). Structural Basis for Human DNA Polymerase Kappa to Bypass Cisplatin Intrastrand Cross-Link (Pt-GG) Lesion as an Efficient and Accurate Extender. *J. Mol. Biol.* 430, 1577–1589. doi:10.1016/j.jmb.2018.04.023

Johnson, R. E., Washington, M. T., Haracska, L., Prakash, S., and Prakash, L. (2000a). Eukaryotic Polymerases ι and ζ Act Sequentially to Bypass DNA Lesions. *Nature* 406, 1015–1019. doi:10.1038/35023030

Johnson, R. E., Washington, M. T., Prakash, S., and Prakash, L. (2000b). Fidelity of Human DNA Polymerase η. *J. Biol. Chem.* 275, 7447–7450. doi:10.1074/jbc.275.11.7447

Jung, H., and Lee, S. (2020). Promutagenic Bypass of 7,8-Dihydro-8-Oxoadenine by Translesion Synthesis DNA Polymerase Dpo4. *Biochem. J.* 477, 2859–2871. doi:10.1042/bcj20200449

Jung, H., Rayala, N. K., and Lee, S. (2020). Translesion Synthesis of the Major Nitrogen Mustard-Induced DNA Lesion by Human DNA Polymerase η. *Biochem. J.* 477, 4543–4558. doi:10.1042/bcj20200767

Kannouche, P. L., Wing, J., and Lehmann, A. R. (2004). Interaction of Human DNA Polymerase η with Monoubiquitinated PCNA. *Mol. Cel* 14, 491–500. doi:10.1016/s1097-2765(04)00259-x

Kath, J. E., Jergic, S., Heltzel, J. M. H., Jacob, D. T., Dixon, N. E., Sutton, M. D., et al. (2014). Polymerase Exchange on Single DNA Molecules Reveals Processivity Clamp Control of Translesion Synthesis. *Proc. Natl. Acad. Sci.* 111, 7647–7652. doi:10.1073/pnas.1321076111

Kenyon, C. J., and Walker, G. C. (1980). DNA-damaging Agents Stimulate Gene Expression at Specific Loci in *Escherichia C. Proc. Natl. Acad. Sci.* 77, 2819–2823. doi:10.1073/pnas.77.5.2819

Khare, V., and Eckert, K. A. (2002). The Proofreading 3′→5′ Exonuclease Activity of DNA Polymerases: A Kinetic Barrier to Translesion DNA Synthesis. *Mutat. Research/Fundamental Mol. Mech. Mutagenesis* 510, 45–54. doi:10.1016/s0027-5107(02)00251-8

Kropp, H. M., Betz, K., Wirth, J., Diederichs, K., and Marx, A. (2017). Crystal Structures of Ternary Complexes of Archaeal B-Family DNA Polymerases. *PLoS One* 12, e0188005. doi:10.1371/journal.pone.0188005

Kusumoto, R., Masutani, C., Iwai, S., and Hanaoka, F. (2002). Translesion Synthesis by Human DNA Polymerase η across Thymine Glycol Lesions. *Biochemistry* 41, 6090–6099. doi:10.1021/bi025549k

Kusumoto, R., Masutani, C., Shimmyo, S., Iwai, S., and Hanaoka, F. (2004). DNA Binding Properties of Human DNA Polymerase η: Implications for Fidelity and Polymerase Switching of Translesion Synthesis. *Genes Cells* 9, 1139–1150. doi:10.1111/j.1365-2443.2004.00797.x

Lancey, C., Tehseen, M., Raducanu, V.-S., Rashid, F., Merino, N., Ragan, T. J., et al. (2020). Structure of the Processive Human Pol δ Holoenzyme. *Nat. Commun.* 11, 1109. doi:10.1038/s41467-020-14898-6

Lanz, M. C., Dibitetto, D., and Smolka, M. B. (2019). DNA Damage Kinase Signaling: Checkpoint and Repair at 30 Years. *EMBO J.* 38, e101801. doi:10.15252/embj.2019101801

Lee, M. Y. W. T., Zhang, S., Hua Lin, S., Wang, X., Darzynkiewicz, Z., Zhang, Z., et al. (2014a). The Tail that Wags the Dog: P12, the Smallest Subunit of DNA Polymerase δ, Is Degraded by Ubiquitin Ligases in Response to DNA Damage and during Cell Cycle Progression. *Cell Cycle* 13, 23–31. doi:10.4161/cc.27407

Lee, M. Y. W. T., Zhang, S., Wang, X., Chao, H. H., Zhao, H., Darzynkiewicz, Z., et al. (2019). Two Forms of Human DNA Polymerase δ: Who Does what and Why? *DNA Repair* 81, 102656. doi:10.1016/j.dnarep.2019.102656

Lee, Y.-S., Gregory, M. T., and Yang, W. (2014b). Human Pol Purified with Accessory Subunits Is Active in Translesion DNA Synthesis and Complements Pol in Cisplatin Bypass. *Proc. Natl. Acad. Sci.* 111, 2954–2959. doi:10.1073/pnas.1324001111

Lin, H.-K., Chase, S. F., Laue, T. M., Jen-Jacobson, L., and Trakselis, M. A. (2012). Differential Temperature-Dependent Multimeric Assemblies of Replication and Repair Polymerases on DNA Increase Processivity. *Biochemistry* 51, 7367–7382. doi:10.1021/bi300956t

Lin, S. H. S., Wang, X., Zhang, S., Zhang, Z., Lee, E. Y. C., and Lee, M. Y. W. T. (2013). Dynamics of Enzymatic Interactions during Short Flap Human Okazaki Fragment Processing by Two Forms of Human DNA Polymerase δ. *DNA Repair* 12, 922–935. doi:10.1016/j.dnarep.2013.08.008

Liu, B., Xue, Q., Tang, Y., Cao, J., Guengerich, F. P., and Zhang, H. (2016). Mechanisms of Mutagenesis: DNA Replication in the Presence of DNA Damage. *Mutat. Research/Reviews Mutat. Res.* 768, 53–67. doi:10.1016/j.mrrev.2016.03.006

Liu, F., Yang, Y., and Zhou, Y. (2018). Polymerase delta in Eukaryotes: How Is it Transiently Exchanged with Specialized DNA Polymerases during Translesion DNA Synthesis? *Curr. Protein Pept. Sci.* 19, 790–804. doi:10.2174/1389203719666180430155625

Livneh, Z., Z, O., and Shachar, S. (2010). Multiple Two-Polymerase Mechanisms in Mammalian Translesion DNA Synthesis. *Cell Cycle* 9, 729–735. doi:10.4161/cc.9.4.10727

Lopes, M., Foiani, M., and Sogo, J. M. (2006). Multiple Mechanisms Control Chromosome Integrity after Replication fork Uncoupling and Restart at Irreparable UV Lesions. *Mol. Cel* 21, 15–27. doi:10.1016/j.molcel.2005.11.015

Lukin, M., and De Los Santos, C. (2006). NMR Structures of Damaged DNA. *Chem. Rev.* 106, 607–686. doi:10.1021/cr0404646

Ma, X., Tang, T. S., and Guo, C. (2020). Regulation of Translesion DNA Synthesis in Mammalian Cells. *Environ. Mol. Mutagen.* 61, 680–692. doi:10.1002/em.22359

Maiorano, D., El Etri, J., Franchet, C., and Hoffmann, J. S. (2021). Translesion Synthesis or Repair by Specialized DNA Polymerases Limits Excessive Genomic Instability upon Replication Stress. *Int. J. Mol. Sci.* 22, 3924. doi:10.3390/ijms22083924

Makarova, A. V., and Burgers, P. M. (2015). Eukaryotic DNA Polymerase ζ. *DNA Repair* 29, 47–55. doi:10.1016/j.dnarep.2015.02.012

Malik, R., Kopylov, M., Gomez-Llorente, Y., Jain, R., Johnson, R. E., Prakash, L., et al. (2020). Structure and Mechanism of B-Family DNA Polymerase ζ Specialized for Translesion DNA Synthesis. *Nat. Struct. Mol. Biol.* 27, 913–924. doi:10.1038/s41594-020-0476-7

Marechal, A., and Zou, L. (2013). DNA Damage Sensing by the ATM and ATR Kinases. *Cold Spring Harb. Perspect. Biol.* 5, a012716. doi:10.1101/cshperspect.a012716

Marians, K. J. (2018). Lesion Bypass and the Reactivation of Stalled Replication Forks. *Annu. Rev. Biochem.* 87, 217–238. doi:10.1146/annurev-biochem-062917-011921

Mcateer, K., Jing, Y., Kao, J., Taylor, J.-S., and Kennedy, M. A. (1998). Solution-State Structure of a DNA Dodecamer Duplex Containing a Cis-Syn Thymine Cyclobutane Dimer, the Major UV Photoproduct of DNA. *J. Mol. Biol.* 282, 1013–1032. doi:10.1006/jmbi.1998.2062

McCulloch, S. D., Kokoska, R. J., Masutani, C., Iwai, S., Hanaoka, F., and Kunkel, T. A. (2004). Preferential Cis-Syn Thymine Dimer Bypass by DNA Polymerase η Occurs with Biased Fidelity. *Nature* 428, 97–100. doi:10.1038/nature02352

McCulloch, S. D., and Kunkel, T. A. (2008). The Fidelity of DNA Synthesis by Eukaryotic Replicative and Translesion Synthesis Polymerases. *Cell Res.* 18, 148–161. doi:10.1038/cr.2008.4

McIntyre, J., Mclenigan, M. P., Frank, E. G., Dai, X., Yang, W., Wang, Y., et al. (2015). Posttranslational Regulation of Human DNA Polymerase ι. *J. Biol. Chem.* 290, 27332–27344. doi:10.1074/jbc.m115.675769

Meng, X., Zhou, Y., Lee, E. Y. C., Lee, M. Y. W. T., and Frick, D. N. (2010). The P12 Subunit of Human Polymerase δ Modulates the Rate and Fidelity of DNA Synthesis. *Biochemistry* 49, 3545–3554. doi:10.1021/bi100042b

Menzies, G. E., Reed, S. H., Brancale, A., and Lewis, P. D. (2015). Base Damage, Local Sequence Context andTP53mutation Hotspots: a Molecular Dynamics Study of Benzo[a]pyrene Induced DNA Distortion and Mutability. *Nucleic Acids Res.* 43, 9133–9146. doi:10.1093/nar/gkv910

Minko, I. G., Harbut, M. B., Kozekov, I. D., Kozekova, A., Jakobs, P. M., Olson, S. B., et al. (2008). Role for DNA Polymerase κ in the Processing of N2-N2-Guanine Interstrand Cross-Links. *J. Biol. Chem.* 283, 17075–17082. doi:10.1074/jbc.m801238200

Napolitano, R., Janel-Bintz, R., Wagner, J., and Fuchs, R. P. (2000). All Three SOS-Inducible DNA Polymerases (Pol II, Pol IV and Pol V) Are Involved in Induced Mutagenesis. *EMBO J.* 19, 6259–6265. doi:10.1093/emboj/19.22.6259

Niimi, A., Brown, S., Sabbioneda, S., Kannouche, P. L., Scott, A., Yasui, A., et al. (2008). Regulation of Proliferating Cell Nuclear Antigen Ubiquitination in Mammalian Cells. *Proc. Natl. Acad. Sci.* 105, 16125–16130. doi:10.1073/pnas.0802727105

O-Wang, J., Kawamura, K., Tada, Y., Ohmori, H., Kimura, H., Sakiyama, S., et al. (2001). DNA Polymerase Kappa, Implicated in Spontaneous and DNA Damage-Induced Mutagenesis, Is Overexpressed in Lung Cancer. *Cancer Res.* 61, 5366–5369.

Pagès, V., and Fuchs, R. P. (2002). How DNA Lesions Are Turned into Mutations within Cells? *Oncogene* 21, 8957–8966. doi:10.1038/sj.onc.1206006

Pata, J. D. (2010). Structural Diversity of the Y-Family DNA Polymerases. *Biochim. Biophys. Acta (Bba) - Proteins Proteomics* 1804, 1124–1135. doi:10.1016/j.bbapap.2010.01.020

Pavlov, Y. I., Nguyen, D., and Kunkel, T. A. (2001). Mutator Effects of Overproducing DNA Polymerase η (Rad30) and its Catalytically Inactive Variant in Yeast. *Mutat. Research/Fundamental Mol. Mech. Mutagenesis* 478, 129–139. doi:10.1016/s0027-5107(01)00131-2

Phi, K. K., Smith, M. C., Tokarsky, E. J., and Suo, Z. (2019). Kinetic Investigation of Translesion Synthesis across a 3-Nitrobenzanthrone-Derived DNA Lesion Catalyzed by Human DNA Polymerase Kappa. *Chem. Res. Toxicol.* 32, 1699–1706. doi:10.1021/acs.chemrestox.9b00219

Pillaire, M.-J., Bétous, R., and Hoffmann, J.-S. (2014). Role of DNA Polymerase κ in the Maintenance of Genomic Stability. *Mol. Cell Oncol.* 1, e29902. doi:10.4161/mco.29902

Plachta, M., Halas, A., Mcintyre, J., and Sledziewska-Gojska, E. (2015). The Steady-State Level and Stability of TLS Polymerase Eta Are Cell Cycle Dependent in the Yeast *S. C. DNA Repair* 29, 147–153. doi:10.1016/j.dnarep.2015.02.015

Plum, G. E., Grollman, A. P., Johnson, F., and Breslauer, K. J. (1995). Influence of the Oxidatively Damaged Adduct 8-oxodeoxyguanosine on the Conformation, Energetics, and Thermodynamic Stability of a DNA Duplex. *Biochemistry* 34, 16148–16160. doi:10.1021/bi00049a030

Powers, K. T., and Washington, M. T. (2017). Analyzing the Catalytic Activities and Interactions of Eukaryotic Translesion Synthesis Polymerases. *Methods Enzymol.* 592, 329–356. doi:10.1016/bs.mie.2017.04.002

Powers, K. T., and Washington, M. T. (2018). Eukaryotic Translesion Synthesis: Choosing the Right Tool for the Job. *DNA Repair* 71, 127–134. doi:10.1016/j.dnarep.2018.08.016

Prakash, S., and Prakash, L. (2002). Translesion DNA Synthesis in Eukaryotes: A One- or Two-Polymerase Affair. *Genes Dev.* 16, 1872–1883. doi:10.1101/gad.1009802

Prestel, A., Wichmann, N., Martins, J. M., Marabini, R., Kassem, N., Broendum, S. S., et al. (2019). The PCNA Interaction Motifs Revisited: Thinking outside the PIP-Box. *Cell. Mol. Life Sci.* 76, 4923–4943. doi:10.1007/s00018-019-03150-0

Pustovalova, Y., Magalhães, M. T. Q., D'Souza, S., Rizzo, A. A., Korza, G., Walker, G. C., et al. (2016). Interaction between the Rev1 C-Terminal Domain and the PolD3 Subunit of Polζ Suggests a Mechanism of Polymerase Exchange upon Rev1/Polζ-Dependent Translesion Synthesis. *Biochemistry* 55, 2043–2053. doi:10.1021/acs.biochem.5b01282

Qi, H., Zhu, H., Lou, M., Fan, Y., Liu, H., Shen, J., et al. (2012). Interferon Regulatory Factor 1 Transactivates Expression of Human DNA Polymerase η in Response to Carcinogen N-Methyl-N′-nitro-N-Nitrosoguanidine. *J. Biol. Chem.* 287, 12622–12633. doi:10.1074/jbc.m111.313429

Qin, Z., Lu, M., Xu, X., Hanna, M., Shiomi, N., and Xiao, W. (2013). DNA-Damage Tolerance Mediated by PCNAUb Fusions in Human Cells Is Dependent on Rev1 but Not Polη. *Nucleic Acids Res.* 41, 7356–7369. doi:10.1093/nar/gkt542

Qiu, S., Jiang, G. X., Cao, L. P., and Huang, J. (2021). Replication fork Reversal and Protection. *Front. Cel Dev. Biol.* 9, 670392. doi:10.3389/fcell.2021.670392

Raper, A. T., Gadkari, V. V., Maxwell, B. A., and Suo, Z. (2016). Single-Molecule Investigation of Response to Oxidative DNA Damage by a Y-Family DNA Polymerase. *Biochemistry* 55, 2187–2196. doi:10.1021/acs.biochem.6b00166

Raper, A. T., Reed, A. J., and Suo, Z. (2018). Kinetic Mechanism of DNA Polymerases: Contributions of Conformational Dynamics and a Third Divalent Metal Ion. *Chem. Rev.* 118, 6000–6025. doi:10.1021/acs.chemrev.7b00685

Reha-Krantz, L. J. (2010). DNA Polymerase Proofreading: Multiple Roles Maintain Genome Stability. *Biochim. Biophys. Acta (Bba) - Proteins Proteomics* 1804, 1049–1063. doi:10.1016/j.bbapap.2009.06.012

Rickman, K., and Smogorzewska, A. (2019). Advances in Understanding DNA Processing and protection at Stalled Replication forks. *J. Cel Biol.* 218, 1096–1107. doi:10.1083/jcb.201809012

Rizzo, A. A., Vassel, F.-M., Chatterjee, N., D'Souza, S., Li, Y., Hao, B., et al. (2018). Rev7 Dimerization Is Important for Assembly and Function of the Rev1/Polζ Translesion Synthesis Complex. *Proc. Natl. Acad. Sci. USA* 115, E8191–E8200. doi:10.1073/pnas.1801149115

Sabbioneda, S., Gourdin, A. M., Green, C. M., Zotter, A., Giglia-Mari, G., Houtsmuller, A., et al. (2008). Effect of Proliferating Cell Nuclear Antigen Ubiquitination and Chromatin Structure on the Dynamic Properties of the Y-Family DNA Polymerases. *Mol. Biol. Cel.* 19, 5193–5202. doi:10.1091/mbc.e08-07-0724

Sabbioneda, S., Green, C. M., Bienko, M., Kannouche, P., Dikic, I., and Lehmann, A. R. (2009). Ubiquitin-Binding Motif of Human DNA Polymerase η Is Required for Correct Localization. *Proc. Natl. Acad. Sci. U. S. A.* 106, E20. doi:10.1073/pnas.0812744106

Saha, P., Mandal, T., Talukdar, A. D., Kumar, D., Kumar, S., Tripathi, P. P., et al. (2021). DNA Polymerase Eta: A Potential Pharmacological Target for Cancer Therapy. *J. Cel. Physiol.* 236, 4106–4120. doi:10.1002/jcp.30155

Sale, J. E., Lehmann, A. R., and Woodgate, R. (2012). Y-family DNA Polymerases and Their Role in Tolerance of Cellular DNA Damage. *Nat. Rev. Mol. Cel Biol.* 13, 141–152. doi:10.1038/nrm3289

Sale, J. E. (2013). Translesion DNA Synthesis and Mutagenesis in Eukaryotes. *Cold Spring Harbor Perspect. Biol.* 5, a012708. doi:10.1101/cshperspect.a012708

Sasatani, M., Xi, Y., Kajimura, J., Kawamura, T., Piao, J., Masuda, Y., et al. (2017). Overexpression of Rev1 Promotes the Development of Carcinogen-Induced Intestinal Adenomas via Accumulation of point Mutation and Suppression of Apoptosis Proportionally to the Rev1 Expression Level. *Carcinogenesis* 38, 570–578. doi:10.1093/carcin/bgw208

Seki, M., Masutani, C., Yang, L. W., Schuffert, A., Iwai, S., Bahar, I., et al. (2004). High-Efficiency Bypass of DNA Damage by Human DNA Polymerase Q. *EMBO J.* 23, 4484–4494. doi:10.1038/sj.emboj.7600424

Shachar, S., Ziv, O., Avkin, S., Adar, S., Wittschieben, J., Reissner, T., et al. (2009). Two-Polymerase Mechanisms Dictate Error-Free and Error-Prone Translesion DNA Synthesis in Mammals. *EMBO J.* 28, 383–393. doi:10.1038/emboj.2008.281

Shen, S., Davidson, G. A., Yang, K., and Zhuang, Z. (2021). Photo-Activatable Ub-PCNA Probes Reveal New Structural Features of the *Saccharomyces C* Polη/PCNA Complex. *Nucleic Acids Res.* 49, 9374–9388. doi:10.1093/nar/gkab646

Shilkin, E. S., Boldinova, E. O., Stolyarenko, A. D., Goncharova, R. I., Chuprov-Netochin, R. N., Khairullin, R. F., et al. (2020). Translesion DNA Synthesis and Carcinogenesis. *Biochem. Mosc.* 85, 425–435. doi:10.1134/s0006297920040033

Shriber, P., Leitner-Dagan, Y., Geacintov, N., Paz-Elizur, T., and Livneh, Z. (2015). DNA Sequence Context Greatly Affects the Accuracy of Bypass across an Ultraviolet Light 6-4 Photoproduct in Mammalian Cells. *Mutat. Res.* 780, 71–76. doi:10.1016/j.mrfmmm.2015.08.002

Slade, D. (2018). Maneuvers on PCNA Rings during DNA Replication and Repair. *Genes (Basel)* 9, 416. doi:10.3390/genes9080416

Sobolewska, A., Halas, A., Plachta, M., Mcintyre, J., and Sledziewska-Gojska, E. (2020). Regulation of the Abundance of Y-Family Polymerases in the Cell Cycle of Budding Yeast in Response to DNA Damage. *Curr. Genet.* 66, 749–763. doi:10.1007/s00294-020-01061-3

Stelter, P., and Ulrich, H. D. (2003). Control of Spontaneous and Damage-Induced Mutagenesis by SUMO and Ubiquitin Conjugation. *Nature* 425, 188–191. doi:10.1038/nature01965

Suzuki, T., Sassa, A., Grúz, P., Gupta, R. C., Johnson, F., Adachi, N., et al. (2021). Error-prone Bypass Patch by a Low-Fidelity Variant of DNA Polymerase Zeta in Human Cells. *DNA Repair* 100, 103052. doi:10.1016/j.dnarep.2021.103052

Swan, M. K., Johnson, R. E., Prakash, L., Prakash, S., and Aggarwal, A. K. (2009). Structural Basis of High-Fidelity DNA Synthesis by Yeast DNA Polymerase δ. *Nat. Struct. Mol. Biol.* 16, 979–986. doi:10.1038/nsmb.1663

Takata, K.-I., Shimizu, T., Iwai, S., and Wood, R. D. (2006). Human DNA Polymerase N (POLN) Is a Low Fidelity Enzyme Capable of Error-free Bypass of 5S-Thymine Glycol. *J. Biol. Chem.* 281, 23445–23455. doi:10.1074/jbc.m604317200

Thomforde, J., Fu, I., Rodriguez, F., Pujari, S. S., Broyde, S., and Tretyakova, N. (2021). Translesion Synthesis Past 5-Formylcytosine-Mediated DNA-Peptide Cross-Links by hPolη Is Dependent on the Local DNA Sequence. *Biochemistry* 60, 1797–1807. doi:10.1021/acs.biochem.1c00130

Tomicic, M. T., Aasland, D., Naumann, S. C., Meise, R., Barckhausen, C., Kaina, B., et al. (2014). Translesion Polymerase η Is Upregulated by Cancer Therapeutics and Confers Anticancer Drug Resistance. *Cancer Res.* 74, 5585–5596. doi:10.1158/0008-5472.can-14-0953

Trakselis, M. A., and Benkovic, S. J. (2001). Intricacies in ATP-Dependent Clamp Loading: Variations across Replication Systems. *Structure* 9, 999–1004. doi:10.1016/s0969-2126(01)00676-1

Trakselis, M. A., Cranford, M. T., and Chu, A. M. (2017). Coordination and Substitution of DNA Polymerases in Response to Genomic Obstacles. *Chem. Res. Toxicol.* 30, 1956–1971. doi:10.1021/acs.chemrestox.7b00190

Uchiyama, M., Terunuma, J., and Hanaoka, F. (2015). The Protein Level of Rev1, a TLS Polymerase in Fission Yeast, Is Strictly Regulated during the Cell Cycle and after DNA Damage. *PLoS One* 10, e0130000. doi:10.1371/journal.pone.0130000

Vaisman, A., Tissier, A., Frank, E. G., Goodman, M. F., and Woodgate, R. (2001). Human DNA Polymerase ι Promiscuous Mismatch Extension. *J. Biol. Chem.* 276, 30615–30622. doi:10.1074/jbc.m102694200

Vaisman, A., and Woodgate, R. (2020). Mysterious and Fascinating: DNA Polymerase ι Remains Enigmatic 20 Years after its Discovery. *DNA Repair* 93, 102914. doi:10.1016/j.dnarep.2020.102914

Vaisman, A., and Woodgate, R. (2017). Translesion DNA Polymerases in Eukaryotes: What Makes Them Tick? *Crit. Rev. Biochem. Mol. Biol.* 52, 274–303. doi:10.1080/10409238.2017.1291576

Vanarotti, M., Grace, C. R., Miller, D. J., Actis, M. L., Inoue, A., Evison, B. J., et al. (2018). Structures of REV1 UBM2 Domain Complex with Ubiquitin and with a Small-Molecule that Inhibits the REV1 UBM2-Ubiquitin Interaction. *J. Mol. Biol.* 430, 2857–2872. doi:10.1016/j.jmb.2018.05.042

Velasco-Miguel, S., Richardson, J. A., Gerlach, V. L., Lai, W. C., Gao, T., Russell, L. D., et al. (2003). Constitutive and Regulated Expression of the Mouse Dinb (Polκ) Gene Encoding DNA Polymerase Kappa. *DNA Repair* 2, 91–106. doi:10.1016/s1568-7864(02)00189-1

Volkova, N. V., Meier, B., González-Huici, V., Bertolini, S., Gonzalez, S., Vöhringer, H., et al. (2020). Mutational Signatures Are Jointly Shaped by DNA Damage and Repair. *Nat. Commun.* 11, 2169. doi:10.1038/s41467-020-15912-7

Wang, H., Wu, W., Wang, H.-W., Wang, S., Chen, Y., Zhang, X., et al. (2010). Analysis of Specialized DNA Polymerases Expression in Human Gliomas: Association with Prognostic Significance. *Neuro. Oncol.* 12, 679–686. doi:10.1093/neuonc/nop074

Warbrick, E. (1998). PCNA Binding through a Conserved Motif. *Bioessays* 20, 195–199. doi:10.1002/(sici)1521-1878(199803)20:3<195:aid-bies2>3.0.co;2-r

Waters, L. S., Minesinger, B. K., Wiltrout, M. E., D'souza, S., Woodruff, R. V., and Walker, G. C. (2009). Eukaryotic Translesion Polymerases and Their Roles and Regulation in DNA Damage Tolerance. *Microbiol. Mol. Biol. Rev.* 73, 134–154. doi:10.1128/mmbr.00034-08

Waters, L. S., and Walker, G. C. (2006). The Critical Mutagenic Translesion DNA Polymerase Rev1 Is Highly Expressed during G2/M Phase rather Than S Phase. *Proc. Natl. Acad. Sci.* 103, 8971–8976. doi:10.1073/pnas.0510167103

Wojtaszek, J. L., Chatterjee, N., Najeeb, J., Ramos, A., Lee, M., Bian, K., et al. (2019). A Small Molecule Targeting Mutagenic Translesion Synthesis Improves Chemotherapy. *Cell* 178, 152–159. doi:10.1016/j.cell.2019.05.028

Wong, J. H., Brown, J. A., Suo, Z., Blum, P., Nohmi, T., and Ling, H. (2010). Structural Insight into Dynamic Bypass of the Major Cisplatin-DNA Adduct by Y-Family Polymerase Dpo4. *EMBO J.* 29, 2059–2069. doi:10.1038/emboj.2010.101

Yang, K., Li, G., Gong, P., Gui, W., Yuan, L., and Zhuang, Z. (2016). Chemical Protein Ubiquitylation with Preservation of the Native Cysteine Residues. *ChemBioChem* 17, 995–998. doi:10.1002/cbic.201600042

Yang, W. (2014). An Overview of Y-Family DNA Polymerases and a Case Study of Human DNA Polymerase η. *Biochemistry* 53, 2793–2803. doi:10.1021/bi500019s

Yang, W., and Gao, Y. (2018). Translesion and Repair DNA Polymerases: Diverse Structure and Mechanism. *Annu. Rev. Biochem.* 87, 239–261. doi:10.1146/annurev-biochem-062917-012405

Yeiser, B., Pepper, E. D., Goodman, M. F., and Finkel, S. E. (2002). SOS-induced DNA Polymerases Enhance Long-Term Survival and Evolutionary Fitness. *Proc. Natl. Acad. Sci.* 99, 8737–8741. doi:10.1073/pnas.092269199

Yoon, J.-H., Prakash, L., and Prakash, S. (2009). Highly Error-fFee Role of DNA Polymerase in the Replicative Bypass of UV-Induced Pyrimidine Dimers in Mouse and Human Cells. *Proc. Natl. Acad. Sci.* 106, 18219–18224. doi:10.1073/pnas.0910121106

Yoon, J. H., Basu, D., Sellamuthu, K., Johnson, R. E., Prakash, S., and Prakash, L. (2021). A Novel Role of DNA Polymerase Lambda in Translesion Synthesis in Conjunction with DNA Polymerase Zeta. *Life Sci. Alliance* 4, e202000900. doi:10.26508/lsa.202000900

Zhang, S., Zhao, H., Darzynkiewicz, Z., Zhou, P., Zhang, Z., Lee, E. Y. C., et al. (2013). A Novel Function of CRL4Cdt2. *J. Biol. Chem.* 288, 29550–29561. doi:10.1074/jbc.m113.490466

Zhang, S., Zhou, Y., Trusa, S., Meng, X., Lee, E. Y. C., and Lee, M. Y. W. T. (2007). A Novel DNA Damage Response. *J. Biol. Chem.* 282, 15330–15340. doi:10.1074/jbc.m610356200

Zhang, Z., Zhang, S., Lin, S. H. S., Wang, X., Wu, L., Lee, E. Y. C., et al. (2012). Structure of Monoubiquitinated PCNA. *Cell Cycle* 11, 2128–2136. doi:10.4161/cc.20595

Zhao, L., and Washington, M. T. (2017). Translesion Synthesis: Insights into the Selection and Switching of DNA Polymerases. *Genes (Basel)* 8, 24. doi:10.3390/genes8010024

Zhao, Y., Biertumpfel, C., Gregory, M. T., Hua, Y.-J., Hanaoka, F., and Yang, W. (2012). Structural Basis of Human DNA Polymerase -Mediated Chemoresistance to Cisplatin. *Proc. Natl. Acad. Sci.* 109, 7269–7274. doi:10.1073/pnas.1202681109

Zhuang, Z., Johnson, R. E., Haracska, L., Prakash, L., Prakash, S., and Benkovic, S. J. (2008). Regulation of Polymerase Exchange between Pol and Pol by Monoubiquitination of PCNA and the Movement of DNA Polymerase Holoenzyme. *Proc. Natl. Acad. Sci.* 105, 5361–5366. doi:10.1073/pnas.0801310105

Ziv, O., Geacintov, N., Nakajima, S., Yasui, A., and Livneh, Z. (2009). DNA Polymerase ζ Cooperates with Polymerases κ and ι in Translesion DNA Synthesis across Pyrimidine Photodimers in Cells from XPV Patients. *Proc. Natl. Acad. Sci. U. S. A.* 106, 11552–11557. doi:10.1073/pnas.0812548106

Conflict of Interest: The authors declare that the research was conducted in the absence of any commercial or financial relationships that could be construed as a potential conflict of interest.

Publisher's Note: All claims expressed in this article are solely those of the authors and do not necessarily represent those of their affiliated organizations, or those of the publisher, the editors and the reviewers. Any product that may be evaluated in this article, or claim that may be made by its manufacturer, is not guaranteed or endorsed by the publisher.

frontiers in Molecular Biosciences

PERSPECTIVE
published: 10 January 2022
doi: 10.3389/fmolb.2021.822218

Within and Beyond the Nucleotide Addition Cycle of Viral RNA-dependent RNA Polymerases

Peng Gong[1,2]*

[1]Key Laboratory of Special Pathogens and Biosafety, Wuhan Institute of Virology, Center for Biosafety Mega-Science, Chinese Academy of Sciences, Wuhan, China, [2]Drug Discovery Center for Infectious Diseases, Nankai University, Tianjin, China

Nucleotide addition cycle (NAC) is a fundamental process utilized by nucleic acid polymerases when carrying out nucleic acid biosynthesis. An induced-fit mechanism is usually taken by these polymerases upon NTP/dNTP substrate binding, leading to active site closure and formation of a phosphodiester bond. In viral RNA-dependent RNA polymerases, the post-chemistry translocation is stringently controlled by a structurally conserved motif, resulting in asymmetric movement of the template-product duplex. This perspective focuses on viral RdRP NAC and related mechanisms that have not been structurally clarified to date. Firstly, RdRP movement along the template strand in the absence of catalytic events may be relevant to catalytic complex dissociation or proofreading. Secondly, pyrophosphate or non-cognate NTP-mediated cleavage of the product strand 3′-nucleotide can also play a role in reactivating paused or arrested catalytic complexes. Furthermore, non-cognate NTP substrates, including NTP analog inhibitors, can not only alter NAC when being misincorporated, but also impact on subsequent NACs. Complications and challenges related to these topics are also discussed.

Keywords: RNA virus, RNA-dependent RNA polymerase, nucleotide addition cycle, translocation, cleavage, misincorporation, nucleotide analog

OPEN ACCESS

Edited by:
Whitney Yin,
University of Texas Medical Branch at Galveston, United States

Reviewed by:
David Douglas Boehr,
The Pennsylvania State University (PSU), United States
Georgiy Belogurov,
University of Turku, Finland

***Correspondence:**
Peng Gong
gongpeng@wh.iov.cn

Specialty section:
This article was submitted to Structural Biology, a section of the journal Frontiers in Molecular Biosciences

Received: *25 November 2021*
Accepted: *21 December 2021*
Published: *10 January 2022*

Citation:
Gong P (2022) Within and Beyond the Nucleotide Addition Cycle of Viral RNA-dependent RNA Polymerases. Front. Mol. Biosci. 8:822218. doi: 10.3389/fmolb.2021.822218

INTRODUCTION

RNA viruses are a large collection of diverse, rapidly evolving viruses with a wide host range covering bacteria and eukaryotes (Krupovic et al., 2018). In recent years, emerging and re-remerging RNA viruses causing human and animal diseases have posed a great impact to our daily life. Understanding the fundamental features of RNA viruses has become an attractive and rapid growing research area ever since the emergence of severe and acute syndrome coronavirus 2 (SARS-CoV-2) causing the coronavirus disease 2019 (COVID-19) (Zhou et al., 2020). Effective antivirals and vaccines are in urgent need for prevention and control of known and future RNA virus pathogens. One unique feature of RNA viruses is that their genome replication and transcription processes are DNA-independent, thus requiring a virally-encoded RNA-dependent RNA polymerase (RdRP) to carry out these essential processes of the virus life cycle (Wolf et al., 2018). Due to their essentialness and highest conservation level, RdRPs have become attractive targets to develop antivirals with high potency and/or broad-spectrum potential. Although being considered the most conserved protein of RNA viruses, RdRPs are still quite diverse with respect to their global structure organization (Lesburg et al., 1999; Thompson and Peersen, 2004; Lu and Gong, 2013; Pflug et al., 2014; Liang et al., 2015; Jia and Gong, 2019; Kirchdoerfer and Ward, 2019), initiation mechanisms

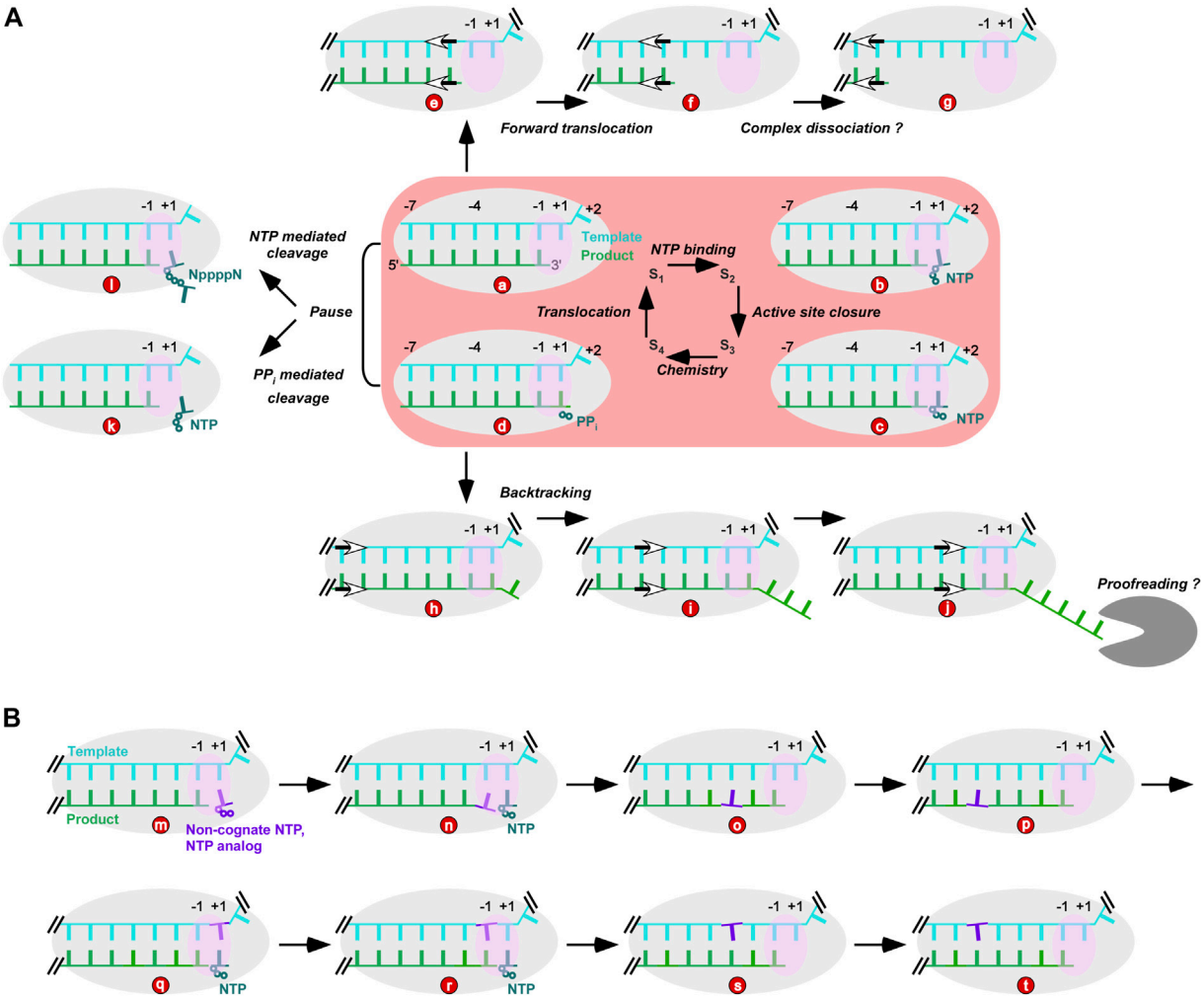

FIGURE 1 | Viral RdRP NAC and possibly related processes. **(A)** RdRP NAC and its relationship with nucleotide addition-free translocation events and intrinsic product cleavage activities. (a–d): four reference states of NAC; e–g: states derived from RdRP forward translocation; (h–j): states derived from polymerase backtracking; d to k: PP_i mediated product cleavage; d to l: non-cognate NTP-mediated cleavage. The gray "pacman" represents a virally encoded exonuclease. **(B)** NAC intervention by incorporation of non-cognate NTP or NTP analogs. Gray and pink ovals represent RdRP and its active site, respectively. Wherever necessary, double slashes were used to indicate continuation of an RNA strand.

(Butcher et al., 2001; Reich et al., 2014; Appleby et al., 2015; Zhang et al., 2021), and regulation by host and viral factors (Kidmose et al., 2010; Liu et al., 2018; Chen et al., 2020; Yan et al., 2021a). Nucleotide addition cycle (NAC), a process shared by all nucleic acid polymerases carrying out NTP/dNTP-driven phosphodiester bond formation (Huang et al., 1998; Li et al., 1998; Yin and Steitz, 2004; Kornberg, 2007; Gong and Peersen, 2010), may thus be the most conservative part of viral RdRP working mechanisms. Understandings of common features in RdRP NAC can help describe the viral genome replication and transcription processes that are composed of thousands of NACs and can benefit development of nucleot(s)ide analog drugs targeting viral RdRPs (Gong, 2021; Johnson and Dangerfield, 2021).

NAC of nucleic acid polymerase typically contain four microsteps: NTP/dNTP binding, active site closure, phosphoryl transfer reaction (chemistry), and translocation, while four structural reference states (S_1-S_4) are usually used to help depict these microsteps (**Figure 1A**, central part with pink background). Critical conformational changes have been found accompanying active site closure (S_2 to S_3) and translocation (S_4 to S_1) (Temiakov et al., 2004; Yin and Steitz, 2004; Wang et al., 2006). In viral RdRPs, a unique palm-domain-based conformational change takes place upon active site closure (Zamyatkin et al., 2008; Gong and Peersen, 2010; Appleby et al., 2015). By contrast, A-family polymerases represented by bacteriophage T7 RNA polymerase and *Thermus aquaticus* (Taq) DNA polymerase close the active site through a large-scale conformational change of their fingers domain (Li et al., 1998; Yin and Steitz, 2004). S_3 and S_4 structures that both have a closed active site have been solved in multiple polymerase systems, and consistently demonstrate the critical role of two divalent metal

ions in forming the transition state of the phosphoryl transfer reaction (Steitz and Steitz, 1993). Two types of RdRP translocation intermediate structures both highlight an asymmetric movement of the template-product RNA strands and stringent control of the template RNA movement by the RdRP-specific template-interacting motif G (Shu and Gong, 2016; Wang et al., 2020a). Similar intermediates have been observed with transcriptional pausing-related multi-subunit DNA-dependent RNA polymerases (DdRPs) (Guo et al., 2018; Kang et al., 2018), suggesting that this phenomenon may be shared even by structurally unrelated polymerase families.

Although numerous NAC-state-related structures from various viral RdRPs have provided a relatively complete structural view of the cognate NTP-driven NAC, several aspects directly or indirectly related to NAC have rarely been addressed structurally in RdRPs including nucleotide addition-free translocation, intrinsic product cleavage activities, and perturbation of NAC by non-cognate NTPs and NTP analogs. As discussed below, these events are possibly related to important events including but not limited to RdRP catalytic complex dissociation, proofreading, reactivation, fidelity control, and effective intervention. In the following sections, a synoptic introduction of these events and structural challenges to approach them are discussed.

RDRP TRANSLOCATION BEYOND NAC

S_1 and S_4 represent the post- and pre-translocation states, respectively. In a classic NAC, a post-translocation S_1 complex directs the binding of the incoming NTP, while the polymerase in the pre-translocation S_4 complex needs to translocate to the next register and reopen its active site for the next NAC (**Figure 1A**, central panel with pink background). By contrast, "forward" movement from the post-translocation S_1 and "backward" movement from the pre-translocation S_4 of the polymerase can move the polymerase out of an NAC. The former, if occurs successively, makes the 3′-end of the product RNA move toward the upstream. The template-product duplex in contact with the polymerase thus shortens and may lead to dissociation of the complex (**Figure 1Aa,e–g**). These forward-translocated states occur in DdRPs during intrinsic transcription termination or in halted transcription elongation complexes, both resulting in dissociation of the polymerase complex (Yarnell and Roberts, 1999; Zhou et al., 2007). Similar situations may also be induced by other nucleic acid binding proteins or nucleic acid elements such as bacterial translocase Rho, bacterial transcription-repair coupling factor Mfd, or the class I transcription termination signal in T7 RNA polymerase transcription (Kassavetis and Chamberlin, 1981; Macdonald et al., 1994; Deaconescu et al., 2006; Murphy et al., 2009; Roberts, 2019). However, dissociation routes unrelated to RdRP forward translocation cannot be ruled out. Furthermore, a Brownian ratchet model applied to DdRPs suggests that polymerase can slide along the nucleic acid template driven by thermal motion with the binding of incoming NTP serving as the "ratchet" to favor the forward-translocated state (Guajardo and Sousa, 1997; Vassylyev and Artsimovitch, 2005). Therefore, RdRP may forward translocate simply through "diffusing" along the template even without *cis*-acting elements or *trans*-acting factors.

The "backward" movement of the polymerase, better known as backtracking in DdRP transcription, results in unraveling of the template-product duplex downstream of the +1 site (the position where incoming NTP binds during NAC). In DdRPs, there is a channel to accommodate the single-stranded 3′-portion of the product RNA and transcription factors such as bacterial GreA/GreB and eukaryotic TFIIS can facilitate intrinsic endonuclease activity of DdRP to reactivate transcription (Abdelkareem et al., 2019; Bradley et al., 2019; Wang et al., 2009). Proofreading activities in viral RdRPs have been found in CoVs, with the virally encoded nsp14 protein utilizing its exonuclease module to excise the 3′-nucleotide(s) of the product RNA (Subissi et al., 2014) (**Figure 1Ad,h–j**). Backtracking-related proofreading models were proposed in SARS-CoV-2 RdRP studies, in which the viral helicase hypothetically facilitates RdRP backtracking upon misincorporation and the 3′-end of the product therefore is delivered to the exonuclease active site for cleavage after multiple rounds of translocation events (Chen et al., 2020; Yan et al., 2021b).

Except for recently reported backtracked SARS-CoV-2 RdRP structures obtained using RNA scaffolds with designed mismatches at the 3′-portion of the product RNA (Malone et al., 2021), structures with the 3′-end of the product strand poise upstream of position −1 (the position of the priming nucleotide of the product strand) or downstream of position +1 have rarely been captured in viral RdRPs. Nevertheless, these nucleotide-addition-free translocation events likely occurs and may indeed play important roles under certain circumstances. On one hand, assembling an RdRP-RNA complex with other factors may help visualize the forward translocated or backtracked states. On the other hand, RdRP variants (i.e., from different viruses or virus strains) or mutants with altered nature in controlling the movement of either the template or the product strand may have different odds in capturing these states by structural biology approaches.

RDRP INTRINSIC CLEAVAGE ACTIVITIES AND THEIR RELEVANCE TO REACTIVATION

Pyrophosphate (PP_i) is the byproduct of the NTP/dNTP-driven phosphoryl transfer reaction in NAC. Under certain circumstances (e.g., high PP_i concentration in polymerase assays), PP_i can reverse the reaction through pyrophosphorolysis (**Figure 1Ac,d–k**). Pyrophosphorolysis can not only participate in proofreading by excising the non-cognate nucleotide, but also play regulatory roles by modulating the overall progress of nucleic acid synthesis (Imashimizu et al., 2019). While PP_i can be observed in pre-translocation polymerase complex structures (Yin and Steitz, 2004; Gong and Peersen, 2010), it has not been observed in polymerase structures that has completed translocation, suggesting that PP_i release and translocation likely coincide in timing. Starting

from a post-translocation S_1 complex crystal, an interesting reverse translocation intermediate structure was captured in an enterovirus RdRP with PP_i present in the soaking solution (Wang et al., 2020a). In such a structure, the 3′-nucleotide of the product moved from position −1 to almost position +1. Although pyrophosphorolysis did not occur in the crystal, solution trials mimicking the crystal soaking condition led to observation of PP_i-mediated cleavage (Wang et al., 2020a) (**Figure 1Ad–k**), suggesting reverse translocation as a prerequisite of the cleavage of a post-translocation complex. Another interesting observation in this structure is the "slippage" between the template-product RNA, resulting in a duplex only partially matched. Completion of this reverse translocation thus requires realigning of the two strands. Such a slippage-and-realigning process was not observed in regular forward translocation, in which basepairing interactions between the two strands were maintained (Shu and Gong, 2016; Peersen, 2017; Wang et al., 2020a). Hence, the reverse translocation is relatively energetically-unfavorable.

Another known polymerase activity cleaving the 3′-nucleotide of the product strand is mediated by non-cognate NTPs. First reported in human immunodeficiency virus 1 (HIV-1) reverse transcriptase (RT), a non-cognate NTP can induce the cleavage of the product strand 3′-nucleotide, forming a dinucleotide with a 5–5′ poly-phosphate (tetra- or tri-phosphate) linkage when the incoming cognate dNTP is not available (Meyer et al., 1998). Similar activities were subsequently observed in hepatitis C virus (HCV) RdRP (Jin et al., 2013a). In both systems, a chain terminating nucleotide can be cleaved by this NTP-mediated activity to yield an extendable 3′-end, and thus implying its potential role in proofreading.

Unlike CoVs, many other RNA viruses do not encode an exonulease and thus sometimes are considered error-prone. However, PP_i- and NTP-mediated cleavage activities by RdRP itself may play key roles in maintaining viral genome stability and keeping the virus away from the error-catastrophe threshold (Crotty et al., 2001). Furthermore, RdRP pausing or arrest caused by RNA elements or regulatory proteins can in principle also be resolved by these activities. As polymerases can pause at either pre- or post-translocation NAC states (**Figures 1Aa,d**) but both cleavage activities likely occur at pre-translocation state (**Figure 1Ad–l**), polymerase backtracking to the pre-translocational position for cleavage may increase the opportunity of rescuing the complex from a "trapped" status. To date, the structural basis of the NTP-mediated cleavage has remained elusive, while structural understandings of pyrophosphorolysis can be readily achieved through its reverse steps of nucleotide addition and the preceding reverse translocation.

RDRP NAC REGULATION BY NON-COGNATE NTP OR NTP ANALOGS

As the major source of nucleotide mutations, misincorporation by nucleic acid polymerases and its mechanisms are of great interest in understanding evolution of species. Misincorporations, often considering basepairing mismatch derived events, occur at a rate of 10^{-3}–10^{-5} if not considering proofreading (Drake and Holland, 1999; Chen et al., 2000; Johnson et al., 2000; Zhang et al., 2000). Therefore, it is generally difficult to capture misincorporation-related polymerase structural states. A classic work in this aspect is from a systematic study in *Bacillus stearothermophilus* DNA polymerase I fragment (BF), a high-fidelity DNA polymerase (Johnson and Beese, 2004). By attempting every possible mismatched base pair combination, multiple mismatch-containing crystal structures were solved at atomic resolution, depicting various types of mismatches and their direct impact on NAC. By solving a set of structures with extension of a G:T mismatch in successive NACs, distortion of a mismatch up to six register from the 3′-end of the product was found to have an impact on the active site through long-range transmission. By contrast, systematic structure determination of mismatch-containing RdRP catalytic complexes is lacking.

The successful usage (Rubin et al., 2020) of nucleotide/nucleoside analog (NA) drugs in treating RNA virus related disease have emphasized the importance of this class of compounds in prevention and control of existing and future pathogens (Furuta et al., 2013; Gane et al., 2013; Rubin et al., 2020). However, multiple factors including but not limited to the differences among RdRP active sites, differences in optimal prodrug forms targeting certain cell types, and emergence of drug-resistant virus strains determine the effectiveness of an NA on a certain virus and its broad-spectrum potential (Feng and Ray, 2021; Jia et al., 2021; Seley-Radtke et al., 2021). Understanding the intervention mechanism of the NTP form of NA (the effective molecule *in vivo*) at enzymology and structural levels is a key not only to identify repurposed NA drugs, but also to design new NA drugs (Appleby et al., 2015; Xu et al., 2017). As an example, remdesivir (RDV), a ribose 1′-substituted adenosine analog, was first developed for Ebola treatment and was found effective on other viruses including various CoVs (Cho et al., 2012; Jacobs et al., 2016; Agostini et al., 2018; Gordon et al., 2020a). A delayed intervention by the NTP form of RDV (RDV-TP) likely at the third NAC after the first incorporation was found in CoVs and subsequently in enterovirus 71 (EV71) (Gordon et al., 2020b; Wu et al., 2021), demonstrating both uniqueness and diversity of this compound in RdRP intervention. Further characterizations revealed that structurally equivalent S861 and S417 in SARS-CoV-2 and EV71 RdRPs are responsible for this delayed intervention likely through steric hindrance of the RDV 1′-cyano group, and under certain circumstances the incorporated RDV (i.e., the monophosphate form of RDV) can overcome this serine roadblock (Tchesnokov et al., 2020; Kokic et al., 2021; Seifert et al., 2021; Wu et al., 2021). The non-terminating feature of RDV intervention awaits further investigation considering the entire replication/transcription process as well as viral protein translation if RDV-containing transcripts are utilized to direct protein synthesis. The 1′-substitutions are therefore endowed with broad-spectrum and delayed intervention potentials in NA drug development. Another notable NA type is represented by ribavirin, favipiravir, and molnupiravir, all with ambiguous basepairing

capability (Crotty et al., 2000; Jin et al., 2013b; Gordon et al., 2021). For example, the N4-hydroxyl cytosine of molnupiravir was structurally captured to direct the incorporation of either a GMP or an AMP in SARS-CoV-2 RdRP (Kabinger et al., 2021). Unlike immediate chain-terminating NAs or RDV, these mutagenic NAs likely generate antiviral effects by driving the viral population beyond the error-catastrophe threshold.

To date, structures of RdRP-RNA complexes containing non-cognate NTP-derived mismatches are rarely reported, while related structures depicting intervention mechanisms of representative NAs have been emerging with the fast growing of RNA virus research (Ferrer-Orta et al., 2007; Appleby et al., 2015; Wang et al., 2020b; Kabinger et al., 2021; Kokic et al., 2021). NAs with immediate chain terminating features may directly interfere with the NAC at the +1 or -1 site (**Figure 1Aa–d,Bm–n**); those are not immediately terminating can possibly propagate its impact on NAC from remote sites (**Figure 1Bo,p**); incorporated NAs that eventually become part of the full-length product may affect NAC when reaching the active site and the template-product binding regions as a template nucleotide (**Figure 1Bq–t**). Together with enzymology characterizations, solving more NA-containing RdRP-RNA structures with representative modifications and intervention mechanisms will provide key references for cell- and animal model-based NA effectiveness assessment and a comprehensive pre-clinical evaluation of NA drug candidates.

DISCUSSION

Representative NAC-related RdRP-RNA complex structures have been reported in picornaviruses, HCV, influenza viruses, bacteriophage ϕ6, and more recently in bunyaviruses and CoVs (Butcher et al., 2001; Gong and Peersen, 2010; Gong et al., 2013; Appleby et al., 2015; Arragain et al., 2020; Wang et al., 2020b; Wandzik et al., 2020). However, a comprehensive structural understanding of NAC requires much more representative RdRP systems and determination of RdRP structures at different phases of its replication and transcription. In most cases, the replication/transcription complex (RTC) works as a multi-subunit machinery and its components vary in different processes and at different stages of a certain process (Reed and Rice, 2000; Bollati et al., 2010; Smith and Denison, 2013). Therefore, structures building on RdRP-RNA complex with other RTC components in the assembly are also highly valuable and in some cases more functionally relevant. Continuing progress in cryo electron microscopy (cryo-EM)-related techniques and deep learning-based structure prediction of biological macromolecule and its complexes have been providing a boost in understanding the RTC as well as the NAC carried out by it (Frank, 2018; Tunyasuvunakool et al., 2021).

DATA AVAILABILITY STATEMENT

The original contributions presented in the study are included in the article/supplementary material, further inquiries can be directed to the corresponding author.

AUTHOR CONTRIBUTIONS

PG surveyed the literature and wrote the manuscript.

FUNDING

National Key Research and Development Program of China (2018YFA0507200); National Natural Science Foundation of China (32070185); Advanced Customer Cultivation Project of Wuhan National Biosafety Laboratory, Chinese Academy of Sciences (2021ACCP-MS10); Key Biosafety Science and Technology Program of Hubei Jiangxia Laboratory (JXBS001).

REFERENCES

Abdelkareem, M. m., Saint-André, C., Takacs, M., Papai, G., Crucifix, C., Guo, X., et al. (2019). Structural Basis of Transcription: RNA Polymerase Backtracking and its Reactivation. *Mol. Cel.* 75, 298–309. doi:10.1016/j.molcel.2019.04.029

Agostini, M. L., Andres, E. L., Sims, A. C., Graham, R. L., Sheahan, T. P., Lu, X., et al. (2018). Coronavirus Susceptibility to the Antiviral Remdesivir (GS-5734) Is Mediated by the Viral Polymerase and the Proofreading Exoribonuclease. *mBio* 9. doi:10.1128/mBio.00221-18

Appleby, T. C., Perry, J. K., Murakami, E., Barauskas, O., Feng, J., Cho, A., et al. (2015). Structural Basis for RNA Replication by the Hepatitis C Virus Polymerase. *Science* 347, 771–775. doi:10.1126/science.1259210

Arragain, B., Effantin, G., Gerlach, P., Reguera, J., Schoehn, G., Cusack, S., et al. (2020). Pre-initiation and Elongation Structures of Full-Length La Crosse Virus Polymerase Reveal Functionally Important Conformational Changes. *Nat. Commun.* 11, 3590. doi:10.1038/s41467-020-17349-4

Bollati, M., Alvarez, K., Assenberg, R., Baronti, C., Canard, B., Cook, S., et al. (2010). Structure and Functionality in Flavivirus NS-Proteins: Perspectives for Drug Design. *Antivir. Res.* 87, 125–148. doi:10.1016/j.antiviral.2009.11.009

Bradley, C. C., Gordon, A. J. E., Halliday, J. A., and Herman, C. (2019). Transcription Fidelity: New Paradigms in Epigenetic Inheritance, Genome Instability and Disease. *DNA Repair* 81, 102652. doi:10.1016/j.dnarep.2019.102652

Butcher, S. J., Grimes, J. M., Makeyev, E. V., Bamford, D. H., and Stuart, D. I. (2001). A Mechanism for Initiating RNA-dependent RNA Polymerization. *Nature* 410, 235–240. doi:10.1038/35065653

Chen, J., Malone, B., Llewellyn, E., Grasso, M., Shelton, P. M. M., Olinares, P. D. B., et al. (2020). Structural Basis for Helicase-Polymerase Coupling in the SARS-CoV-2 Replication-Transcription Complex. *Cell* 182, 1560–1573. doi:10.1016/j.cell.2020.07.033

Chen, X., Zuo, S., Kelman, Z., O'Donnell, M., Hurwitz, J., and Goodman, M. F. (2000). Fidelity of Eucaryotic DNA Polymerase δ Holoenzyme fromSchizosaccharomyces Pombe. *J. Biol. Chem.* 275, 17677–17682. doi:10.1074/jbc.m910278199

Cho, A., Saunders, O. L., Butler, T., Zhang, L., Xu, J., Vela, J. E., et al. (2012). Synthesis and Antiviral Activity of a Series of 1′-substituted 4-Aza-7,9-Dideazaadenosine C-Nucleosides. *Bioorg. Med. Chem. Lett.* 22, 2705–2707. doi:10.1016/j.bmcl.2012.02.105

Crotty, S., Cameron, C. E., and Andino, R. (2001). RNA Virus Error Catastrophe: Direct Molecular Test by Using Ribavirin. *Proc. Natl. Acad. Sci.* 98, 6895–6900. doi:10.1073/pnas.111085598

Crotty, S., Maag, D., Arnold, J. J., Zhong, W., Lau, J. Y. N., Hong, Z., et al. (2000). The Broad-Spectrum Antiviral Ribonucleoside Ribavirin Is an RNA Virus Mutagen. *Nat. Med.* 6, 1375–1379. doi:10.1038/82191

Deaconescu, A. M., Chambers, A. L., Smith, A. J., Nickels, B. E., Hochschild, A., Savery, N. J., et al. (2006). Structural Basis for Bacterial Transcription-Coupled DNA Repair. *Cell* 124, 507–520. doi:10.1016/j.cell.2005.11.045

Drake, J. W., and Holland, J. J. (1999). Mutation Rates Among RNA Viruses. *Proc. Natl. Acad. Sci.* 96, 13910–13913. doi:10.1073/pnas.96.24.13910

Feng, J. Y., and Ray, A. S. (2021). HCV RdRp, Sofosbuvir and beyond. *The Enzymes* 49, 63–82. doi:10.1016/bs.enz.2021.06.003

Ferrer-Orta, C., Arias, A., Perez-Luque, R., Escarmis, C., Domingo, E., and Verdaguer, N. (2007). Sequential Structures Provide Insights into the Fidelity of RNA Replication. *Proc. Natl. Acad. Sci.* 104, 9463–9468. doi:10.1073/pnas.0700518104

Frank, J. (2018). Single-Particle Reconstruction of Biological Molecules-Story in a Sample (Nobel Lecture). *Angew. Chem. Int. Ed.* 57, 10826–10841. doi:10.1002/anie.201802770

Furuta, Y., Gowen, B. B., Takahashi, K., Shiraki, K., Smee, D. F., and Barnard, D. L. (2013). Favipiravir (T-705), a Novel Viral RNA Polymerase Inhibitor. *Antivir. Res.* 100, 446–454. doi:10.1016/j.antiviral.2013.09.015

Gane, E. J., Stedman, C. A., Hyland, R. H., Ding, X., Svarovskaia, E., Symonds, W. T., et al. (2013). Nucleotide Polymerase Inhibitor Sofosbuvir Plus Ribavirin for Hepatitis C. *N. Engl. J. Med.* 368, 34–44. doi:10.1056/nejmoa1208953

Gong, P., Kortus, M. G., Nix, J. C., Davis, R. E., and Peersen, O. B. (2013). Structures of Coxsackievirus, Rhinovirus, and Poliovirus Polymerase Elongation Complexes Solved by Engineering RNA Mediated crystal Contacts. *PloS one* 8, e60272. doi:10.1371/journal.pone.0060272

Gong, P., and Peersen, O. B. (2010). Structural Basis for Active Site Closure by the Poliovirus RNA-dependent RNA Polymerase. *Proc. Natl. Acad. Sci.* 107, 22505–22510. doi:10.1073/pnas.1007626107

Gong, P. (2021). Structural Basis of Viral RNA-dependent RNA Polymerase Nucleotide Addition Cycle in Picornaviruses. *The Enzymes* 49, 215–233. doi:10.1016/bs.enz.2021.06.002

Gordon, C. J., Tchesnokov, E. P., Feng, J. Y., Porter, D. P., and Götte, M. (2020). The Antiviral Compound Remdesivir Potently Inhibits RNA-dependent RNA Polymerase from Middle East Respiratory Syndrome Coronavirus. *J. Biol. Chem.* 295, 4773–4779. doi:10.1074/jbc.ac120.013056

Gordon, C. J., Tchesnokov, E. P., Schinazi, R. F., and Götte, M. (2021). Molnupiravir Promotes SARS-CoV-2 Mutagenesis via the RNA Template. *J. Biol. Chem.* 297, 100770. doi:10.1016/j.jbc.2021.100770

Gordon, C. J., Tchesnokov, E. P., Woolner, E., Perry, J. K., Feng, J. Y., Porter, D. P., et al. (2020). Remdesivir Is a Direct-Acting Antiviral that Inhibits RNA-dependent RNA Polymerase from Severe Acute Respiratory Syndrome Coronavirus 2 with High Potency. *J. Biol. Chem.* 295, 6785–6797. doi:10.1074/jbc.ra120.013679

Guajardo, R., and Sousa, R. (1997). A Model for the Mechanism of Polymerase Translocation 1 1Edited by A. R. Fersht. *J. Mol. Biol.* 265, 8–19. doi:10.1006/jmbi.1996.0707

Guo, X., Myasnikov, A. G., Chen, J., Crucifix, C., Papai, G., Takacs, M., et al. (2018). Structural Basis for NusA Stabilized Transcriptional Pausing. *Mol. Cel.* 69, 816–827. doi:10.1016/j.molcel.2018.02.008

Huang, H., Chopra, R., Verdine, G. L., and Harrison, S. C. (1998). Structure of a Covalently Trapped Catalytic Complex of HIV-1 Reverse Transcriptase: Implications for Drug Resistance. *Science* 282, 1669–1675. doi:10.1126/science.282.5394.1669

Imashimizu, M., Kireeva, M. L., Lubkowska, L., Kashlev, M., and Shimamoto, N. (2019). The Role of Pyrophosphorolysis in the Initiation-To-Elongation Transition by *E. coli* RNA Polymerase. *J. Mol. Biol.* 431, 2528–2542. doi:10.1016/j.jmb.2019.04.020

Jacobs, M., Rodger, A., Bell, D. J., Bhagani, S., Cropley, I., Filipe, A., et al. (2016). Late Ebola Virus Relapse Causing Meningoencephalitis: a Case Report. *The Lancet* 388, 498–503. doi:10.1016/s0140-6736(16)30386-5

Jia, H., and Gong, P. (2019). A Structure-Function Diversity Survey of the RNA-dependent RNA Polymerases from the Positive-Strand RNA Viruses. *Front. Microbiol.* 10, 1945. doi:10.3389/fmicb.2019.01945

Jia, X., Ganter, B., and Meier, C. (2021). Improving Properties of the Nucleobase Analogs T-705/T-1105 as Potential Antiviral. *Annu. Rep. Med. Chem.* 57, 1–47. doi:10.1016/bs.armc.2021.08.002

Jin, Z., Leveque, V., Ma, H., Johnson, K. A., and Klumpp, K. (2013). NTP-mediated Nucleotide Excision Activity of Hepatitis C Virus RNA-dependent RNA Polymerase. *Proc. Natl. Acad. Sci.* 110, E348–E357. doi:10.1073/pnas.1214924110

Jin, Z., Smith, L. K., Rajwanshi, V. K., Kim, B., and Deval, J. (2013). The Ambiguous Base-Pairing and High Substrate Efficiency of T-705 (Favipiravir) Ribofuranosyl 5′-Triphosphate towards Influenza A Virus Polymerase. *PloS one* 8, e68347. doi:10.1371/journal.pone.0068347

Johnson, K. A., and Dangerfield, T. (2021). Mechanisms of Inhibition of Viral RNA Replication by Nucleotide Analogs. *The Enzymes* 49, 39–62. doi:10.1016/bs.enz.2021.07.001

Johnson, R. E., Prakash, S., and Prakash, L. (2000). The Human DINB1 Gene Encodes the DNA Polymerase Poltheta. *Proc. Natl. Acad. Sci.* 97, 3838–3843. doi:10.1073/pnas.97.8.3838

Johnson, S. J., and Beese, L. S. (2004). Structures of Mismatch Replication Errors Observed in a DNA Polymerase. *Cell* 116, 803–816. doi:10.1016/s0092-8674(04)00252-1

Kabinger, F., Stiller, C., Schmitzová, J., Dienemann, C., Kokic, G., Hillen, H. S., et al. (2021). Mechanism of Molnupiravir-Induced SARS-CoV-2 Mutagenesis. *Nat. Struct. Mol. Biol.* 28, 740–746. doi:10.1038/s41594-021-00651-0

Kang, J. Y., Mishanina, T. V., Bellecourt, M. J., Mooney, R. A., Darst, S. A., and Landick, R. (2018). RNA Polymerase Accommodates a Pause RNA Hairpin by Global Conformational Rearrangements that Prolong Pausing. *Mol. Cel.* 69, 802–815. doi:10.1016/j.molcel.2018.01.018

Kassavetis, G. A., and Chamberlin, M. J. (1981). Pausing and Termination of Transcription within the Early Region of Bacteriophage T7 DNA *In Vitro*. *J. Biol. Chem.* 256, 2777–2786. doi:10.1016/s0021-9258(19)69682-1

Kidmose, R. T., Vasiliev, N. N., Chetverin, A. B., Andersen, G. R., and Knudsen, C. R. (2010). Structure of the Q Replicase, an RNA-dependent RNA Polymerase Consisting of Viral and Host Proteins. *Proc. Natl. Acad. Sci.* 107, 10884–10889. doi:10.1073/pnas.1003015107

Kirchdoerfer, R. N., and Ward, A. B. (2019). Structure of the SARS-CoV Nsp12 Polymerase Bound to Nsp7 and Nsp8 Co-factors. *Nat. Commun.* 10, 2342. doi:10.1038/s41467-019-10280-3

Kokic, G., Hillen, H. S., Tegunov, D., Dienemann, C., Seitz, F., Schmitzova, J., et al. (2021). Mechanism of SARS-CoV-2 Polymerase Stalling by Remdesivir. *Nat. Commun.* 12, 279. doi:10.1038/s41467-020-20542-0

Kornberg, R. D. (2007). The Molecular Basis of Eukaryotic Transcription. *Proc. Natl. Acad. Sci.* 104, 12955–12961. doi:10.1073/pnas.0704138104

Krupovic, M., Cvirkaite-Krupovic, V., Iranzo, J., Prangishvili, D., and Koonin, E. V. (2018). Viruses of Archaea: Structural, Functional, Environmental and Evolutionary Genomics. *Virus. Res.* 244, 181–193. doi:10.1016/j.virusres.2017.11.025

Lesburg, C. A., Cable, M. B., Ferrari, E., Hong, Z., Mannarino, A. F., and Weber, P. C. (1999). Crystal Structure of the RNA-dependent RNA Polymerase from Hepatitis C Virus Reveals a Fully Encircled Active Site. *Nat. Struct. Biol.* 6, 937–943. doi:10.1038/13305

Li, Y., Korolev, S., and Waksman, G. (1998). Crystal Structures of Open and Closed Forms of Binary and Ternary Complexes of the Large Fragment of Thermus Aquaticus DNA Polymerase I: Structural Basis for Nucleotide Incorporation. *EMBO J.* 17, 7514–7525. doi:10.1093/emboj/17.24.7514

Liang, B., Li, Z., Jenni, S., Rahmeh, A. A., Morin, B. M., Grant, T., et al. (2015). Structure of the L Protein of Vesicular Stomatitis Virus from Electron Cryomicroscopy. *Cell* 162, 314–327. doi:10.1016/j.cell.2015.06.018

Liu, W., Shi, X., and Gong, P. (2018). A Unique Intra-molecular Fidelity-Modulating Mechanism Identified in a Viral RNA-dependent RNA Polymerase. *Nucleic Acids Res.* 46, 10840–10854. doi:10.1093/nar/gky848

Lu, G., and Gong, P. (2013). Crystal Structure of the Full-Length Japanese Encephalitis Virus NS5 Reveals a Conserved Methyltransferase-Polymerase Interface. *Plos Pathog.* 9, e1003549. doi:10.1371/journal.ppat.1003549

Macdonald, L. E., Durbin, R. K., Dunn, J. J., and McAllister, W. T. (1994). Characterization of Two Types of Termination Signal for Bacteriophage T7 RNA Polymerase. *J. Mol. Biol.* 238, 145–158. doi:10.1006/jmbi.1994.1277

Malone, B., Chen, J., Wang, Q., Llewellyn, E., Choi, Y. J., Olinares, P. D. B., et al. (2021). Structural Basis for Backtracking by the SARS-CoV-2 Replication-Transcription Complex. *Proc. Natl. Acad. Sci. United States America* 118. doi:10.1073/pnas.2102516118

Meyer, P. R., Matsuura, S. E., So, A. G., and Scott, W. A. (1998). Unblocking of Chain-Terminated Primer by HIV-1 Reverse Transcriptase through a

Nucleotide-dependent Mechanism. *Proc. Natl. Acad. Sci.* 95, 13471–13476. doi:10.1073/pnas.95.23.13471

Murphy, M. N., Gong, P., Ralto, K., Manelyte, L., Savery, N. J., and Theis, K. (2009). An N-Terminal Clamp Restrains the Motor Domains of the Bacterial Transcription-Repair Coupling Factor Mfd. *Nucleic Acids Res.* 37, 6042–6053. doi:10.1093/nar/gkp680

Peersen, O. B. (2017). Picornaviral Polymerase Structure, Function, and Fidelity Modulation. *Virus. Res.* 234, 4–20. doi:10.1016/j.virusres.2017.01.026

Pflug, A., Guilligay, D., Reich, S., and Cusack, S. (2014). Structure of Influenza A Polymerase Bound to the Viral RNA Promoter. *Nature* 516, 355–360. doi:10.1038/nature14008

Reed, K. E., and Rice, C. M. (2000). Overview of Hepatitis C Virus Genome Structure, Polyprotein Processing, and Protein Properties. *Curr. Top. Microbiol. Immunol.* 242, 55–84. doi:10.1007/978-3-642-59605-6_4

Reich, S., Guilligay, D., Pflug, A., Malet, H., Berger, I., Crépin, T., et al. (2014). Structural Insight into Cap-Snatching and RNA Synthesis by Influenza Polymerase. *Nature* 516, 361–366. doi:10.1038/nature14009

Roberts, J. W. (2019). Mechanisms of Bacterial Transcription Termination. *J. Mol. Biol.* 431, 4030–4039. doi:10.1016/j.jmb.2019.04.003

Rubin, D., Chan-Tack, K., Farley, J., and Sherwat, A. (2020). FDA Approval of Remdesivir - A Step in the Right Direction. *N. Engl. J. Med.* 383, 2598–2600. doi:10.1056/nejmp2032369

Seifert, M., Bera, S. C., van Nies, P., Kirchdoerfer, R. N., Shannon, A., Le, T. T., et al. (2021). Inhibition of SARS-CoV-2 Polymerase by Nucleotide Analogs from a Single-Molecule Perspective. *eLife* 10. doi:10.7554/eLife.70968

Seley-Radtke, K. L., Thames, J. E., and Waters, C. D., 3rd. (2021). Broad Spectrum Antiviral Nucleosides-Our Best hope for the Future. *Annu. Rep. Med. Chem.* 57, 109–132. doi:10.1016/bs.armc.2021.09.001

Shu, B., and Gong, P. (2016). Structural Basis of Viral RNA-dependent RNA Polymerase Catalysis and Translocation. *Proc. Natl. Acad. Sci. USA* 113, E4005–E4014. doi:10.1073/pnas.1602591113

Smith, E. C., and Denison, M. R. (2013). Coronaviruses as DNA Wannabes: a New Model for the Regulation of RNA Virus Replication Fidelity. *Plos Pathog.* 9, e1003760. doi:10.1371/journal.ppat.1003760

Steitz, T. A., and Steitz, J. A. (1993). A General Two-Metal-Ion Mechanism for Catalytic RNA. *Proc. Natl. Acad. Sci.* 90, 6498–6502. doi:10.1073/pnas.90.14.6498

Subissi, L., Posthuma, C. C., Collet, A., Zevenhoven-Dobbe, J. C., Gorbalenya, A. E., Decroly, E., et al. (2014). One Severe Acute Respiratory Syndrome Coronavirus Protein Complex Integrates Processive RNA Polymerase and Exonuclease Activities. *Proc. Natl. Acad. Sci. USA* 111, E3900–E3909. doi:10.1073/pnas.1323705111

Tchesnokov, E. P., Gordon, C. J., Woolner, E., Kocinkova, D., Perry, J. K., Feng, J. Y., et al. (2020). Template-dependent Inhibition of Coronavirus RNA-dependent RNA Polymerase by Remdesivir Reveals a Second Mechanism of Action. *J. Biol. Chem.* 295, 16156–16165. doi:10.1074/jbc.ac120.015720

Temiakov, D., Patlan, V., Anikin, M., McAllister, W. T., Yokoyama, S., and Vassylyev, D. G. (2004). Structural Basis for Substrate Selection by T7 RNA Polymerase. *Cell* 116, 381–391. doi:10.1016/s0092-8674(04)00059-5

Thompson, A. A., and Peersen, O. B. (2004). Structural Basis for Proteolysis-dependent Activation of the Poliovirus RNA-dependent RNA Polymerase. *Embo J.* 23, 3462–3471. doi:10.1038/sj.emboj.7600357

Tunyasuvunakool, K., Adler, J., Wu, Z., Green, T., Zielinski, M., Žídek, A., et al. (2021). Highly Accurate Protein Structure Prediction for the Human Proteome. *Nature* 596, 590–596. doi:10.1038/s41586-021-03828-1

Vassylyev, D. G., and Artsimovitch, I. (2005). Tracking RNA Polymerase, One Step at a Time. *Cell* 123, 977–979. doi:10.1016/j.cell.2005.11.030

Wandzik, J. M., Kouba, T., Karuppasamy, M., Pflug, A., Drncova, P., Provaznik, J., et al. (2020). A Structure-Based Model for the Complete Transcription Cycle of Influenza Polymerase. *Cell* 181, 877–893. doi:10.1016/j.cell.2020.03.061

Wang, D., Bushnell, D. A., Huang, X., Westover, K. D., Levitt, M., and Kornberg, R. D. (2009). Structural Basis of Transcription: Backtracked RNA Polymerase II at 3.4 Angstrom Resolution. *Science* 324, 1203–1206. doi:10.1126/science.1168729

Wang, D., Bushnell, D. A., Westover, K. D., Kaplan, C. D., and Kornberg, R. D. (2006). Structural Basis of Transcription: Role of the Trigger Loop in Substrate Specificity and Catalysis. *Cell* 127, 941–954. doi:10.1016/j.cell.2006.11.023

Wang, M., Li, R., Shu, B., Jing, X., Ye, H.-Q., and Gong, P. (2020). Stringent Control of the RNA-dependent RNA Polymerase Translocation Revealed by Multiple Intermediate Structures. *Nat. Commun.* 11, 2605. doi:10.1038/s41467-020-16234-4

Wang, Q., Wu, J., Wang, H., Gao, Y., Liu, Q., Mu, A., et al. (2020). Structural Basis for RNA Replication by the SARS-CoV-2 Polymerase. *Cell* 182, 417–428. doi:10.1016/j.cell.2020.05.034

Wolf, Y. I., Kazlauskas, D., Iranzo, J., Lucía-Sanz, A., Kuhn, J. H., Krupovic, M., et al. (2018). Origins and Evolution of the Global RNA Virome. *mBio* 9 (6), e02329-18. doi:10.1128/mBio.02329-18

Wu, J., Wang, H., Liu, Q., Li, R., Gao, Y., Fang, X., et al. (2021). Remdesivir Overcomes the S861 Roadblock in SARS-CoV-2 Polymerase Elongation Complex. *Cel Rep.* 37, 109882. doi:10.1016/j.celrep.2021.109882

Xu, H. T., Hassounah, S. A., Colby-Germinario, S. P., Oliveira, M., Fogarty, C., Quan, Y., et al. (2017). Purification of Zika Virus RNA-dependent RNA Polymerase and its Use to Identify Small-Molecule Zika Inhibitors. *J. Antimicrob. Chemother.* 72, 727–734. doi:10.1093/jac/dkw514

Yan, L., Ge, J., Zheng, L., Zhang, Y., Gao, Y., Wang, T., et al. (2021). Cryo-EM Structure of an Extended SARS-CoV-2 Replication and Transcription Complex Reveals an Intermediate State in Cap Synthesis. *Cell* 184, 184–193. doi:10.1016/j.cell.2020.11.016

Yan, L., Yang, Y., Li, M., Zhang, Y., Zheng, L., Ge, J., et al. (2021). Coupling of N7-Methyltransferase and 3′-5′ Exoribonuclease with SARS-CoV-2 Polymerase Reveals Mechanisms for Capping and Proofreading. *Cell* 184, 3474–3485. doi:10.1016/j.cell.2021.05.033

Yarnell, W. S., and Roberts, J. W. (1999). Mechanism of Intrinsic Transcription Termination and Antitermination. *Science* 284, 611–615. doi:10.1126/science.284.5414.611

Yin, Y. W., and Steitz, T. A. (2004). The Structural Mechanism of Translocation and Helicase Activity in T7 RNA Polymerase. *Cell* 116, 393–404. doi:10.1016/s0092-8674(04)00120-5

Zamyatkin, D. F., Parra, F., Alonso, J. M. M., Harki, D. A., Peterson, B. R., Grochulski, P., et al. (2008). Structural Insights into Mechanisms of Catalysis and Inhibition in Norwalk Virus Polymerase. *J. Biol. Chem.* 283, 7705–7712. doi:10.1074/jbc.m709563200

Zhang, B.-Y., Liu, W., Jia, H., Lu, G., and Gong, P. (2021). An Induced-Fit De Novo Initiation Mechanism Suggested by a Pestivirus RNA-dependent RNA Polymerase. *Nucleic Acids Res.* 49, 8811–8821. doi:10.1093/nar/gkab666

Zhang, Y., Yuan, F., Xin, H., Wu, X., Rajpal, D. K., Yang, D., et al. (2000). Human DNA Polymerase Kappa Synthesizes DNA with Extraordinarily Low Fidelity. *Nucleic Acids Res.* 28, 4147–4156. doi:10.1093/nar/28.21.4147

Zhou, P., Yang, X.-L., Wang, X.-G., Hu, B., Zhang, L., Zhang, W., et al. (2020). A Pneumonia Outbreak Associated with a New Coronavirus of Probable Bat Origin. *Nature* 579, 270–273. doi:10.1038/s41586-020-2012-7

Zhou, Y., Navaroli, D. M., Enuameh, M. S., and Martin, C. T. (2007). Dissociation of Halted T7 RNA Polymerase Elongation Complexes Proceeds via a Forward-Translocation Mechanism. *Proc. Natl. Acad. Sci.* 104, 10352–10357. doi:10.1073/pnas.0606306104

Conflict of Interest: The author declares that the research was conducted in the absence of any commercial or financial relationships that could be construed as a potential conflict of interest.

frontiers in Molecular Biosciences

REVIEW
published: 25 February 2022
doi: 10.3389/fmolb.2022.826593

Conformational Dynamics of DNA Polymerases Revealed at the Single-Molecule Level

*David P. Millar**

Department of Integrative Structural and Computational Biology, The Scripps Research Institute, La Jolla, CA, United States

DNA polymerases are intrinsically dynamic macromolecular machines. The purpose of this review is to describe the single-molecule Förster resonance energy transfer (smFRET) methods that are used to probe the conformational dynamics of DNA polymerases, focusing on *E. coli* DNA polymerase I. The studies reviewed here reveal the conformational dynamics underpinning the nucleotide selection, proofreading and 5′ nuclease activities of Pol I. Moreover, the mechanisms revealed for Pol I are likely employed across the DNA polymerase family. smFRET methods have also been used to examine other aspects of DNA polymerase activity.

Keywords: DNA polymerase, single-molecule FRET, conformational dynamics, DNA replication fidelity, DNA-protein interactions

OPEN ACCESS

Edited by:
Whitney Yin,
University of Texas Medical Branch at Galveston, United States

Reviewed by:
Hengyao Niu,
Indiana University Bloomington, United States
Borja Ibarra,
IMDEA Nanociencia, Spain

***Correspondence:**
David P. Millar
millar@scripps.edu

Specialty section:
This article was submitted to Structural Biology, a section of the Frontiers in Molecular Biosciences

Received: *01 December 2021*
Accepted: *20 January 2022*
Published: *25 February 2022*

Citation:
Millar DP (2022) Conformational Dynamics of DNA Polymerases Revealed at the Single-Molecule Level. Front. Mol. Biosci. 9:826593. doi: 10.3389/fmolb.2022.826593

INTRODUCTION

DNA polymerases are intrinsically dynamic macromolecular machines. During elongation of a nascent DNA strand, a polymerase must select the correct nucleotide substrate, adopt a conformation that promotes catalysis of the phosphoryl transfer reaction, release the pyrophosphate by product and move to the next templating position. This sequence of events likely involves dynamic conformational changes of the polymerase-DNA complex. In addition, many DNA polymerases harbor additional enzymatic activities, such as 3′-5′ exonuclease activity used for proofreading or 5′ nuclease activity used to remove DNA 5′ flaps. The various activities of DNA polymerases must be carefully coordinated to ensure efficient and accurate product formation. Since the respective active sites are widely separated in space, the conversion from one mode of activity to another may involve physical movement of the polymerase on the DNA substrate and/or conformational changes within the polymerase or DNA. While structural studies have provided high resolution snapshots of DNA polymerases in specific functional states (Doublié et al., 1998; Kiefer et al., 1998; Johnson and Beese, 2004; Zahn et al., 2015; Huang et al., 2018; Jain et al., 2018; Jain et al., 2019; Hoitsma et al., 2020), much less is known about the conformational dynamics that underpin DNA polymerase activity.

Experiments performed at the single-molecule level can directly resolve conformational heterogeneity and provide kinetic information without the need to synchronize a population of molecules (Tinoco and Gonzalez, 2011; Monachino et al., 2017; Gruszka, 2021). With these capabilities, single-molecule studies have provided new mechanistic insights across a wide range of biological systems (Hilario and Kowalczykowski, 2010; Pljevaljčić et al., 2012; Hughes et al., 2014; McCluskey et al., 2014; Ordu et al., 2016; Banerjee et al., 2018; Okamoto et al., 2018; Jalihal et al., 2019; Kiss et al., 2020). Single-molecule studies of DNA polymerases and related replication enzymes have also been informative (Liu and Lou, 2017; Mueller et al., 2019; Bocanegra et al., 2021a; Bocanegra et al., 2021b). Observation of polymerase activity on single DNA templates under applied

mechanical force have provided insights into the mechanochemistry of the elongation cycle (Maier et al., 2000; Wuite et al., 2000; Morin et al., 2015), strand displacement activity (Morin et al., 2012a; Morin et al., 2012b; Manosas et al., 2012) and the transition from polymerase activity to 3′-5′ exonuclease activity (Wuite et al., 2000; Ibarra et al., 2009; Hoekstra et al., 2017; Naufer et al., 2017). DNA polymerase activity has also been monitored at the single-molecule level using bioelectronic (Olsen et al., 2013) or nanopore (Cockroft et al., 2008; Lieberman et al., 2010; Olasagasti et al., 2010; Dahl et al., 2012; Lieberman et al., 2012; Lieberman et al., 2013) devices.

Fluorescence-based measurements provide additional insights by revealing conformational changes during polymerase activity. The spectroscopic phenomenon of Förster resonance energy transfer, which probes the distance between donor and acceptor fluorophores, is especially informative when monitored at the single-molecule level (Voith von Voithenberg and Lamb, 2018). Single-molecule Förster resonance energy transfer (smFRET) measurements can readily resolve different conformational states of a DNA polymerase, quantify their relative populations and the rate constants for exchange between them. Importantly, smFRET measurements can detect conformational transitions during a single encounter between a DNA polymerase and a DNA substrate, which can give insights into the mechanism of interconversion between different modes of polymerase activity.

The purpose of this review is to describe the smFRET methods that are used to probe the conformational dynamics of DNA polymerases. The review focuses on *E. coli* DNA polymerase I (Pol I), an A family polymerase, because this polymerase has been extensively studied by smFRET methods. Pol I is an informative model system because it contains template-directed 5′-3′ polymerase (*pol*), 3′-5′ exonuclease (*exo*) and 5′ nuclease (5′ *nuc*) activities in a single 928 aa polypeptide and does not require accessory proteins for proper function. The conformational dynamics underpinning all three activities of Pol I have been investigated by smFRET (Berezhna et al., 2012; Lamichhane et al., 2013; Pauszek et al., 2021). Related smFRET studies of other DNA polymerases are also described. The studies reviewed here provide new mechanistic insights into the biochemical functions of Pol I and highlight the novel information forthcoming from smFRET measurements of DNA polymerases.

smFRET Measurements

For any FRET study, whether performed at the single-molecule or ensemble levels, it is necessary to covalently attach donor and acceptor fluorophores to the biomolecules of interest. In the case of DNA polymerases, one fluorophore can be attached to the DNA substrate and the other to the polymerase. Synthetic DNA oligonucleotides can be used as substrates for the polymerase and these can be readily labeled with fluorophores by incorporating amino-alkyl groups at the 3′ or 5′ ends or an internal base during oligonucleotide synthesis, followed by chemical reaction with succinimidyl ester fluorophore derivatives (Bailey et al., 2004). Site-specific fluorophore labeling of DNA polymerases can be achieved by introducing a single cysteine residue into the desired location, after removal of endogenous cysteines, followed by covalent attachment of maleimide fluorophore derivatives to the cysteine (Berezhna et al., 2012). Hence, to study a given polymerase using smFRET, it is necessary that the polymerase can be mutagenized at specific sites, expressed in reasonable yield (usually in bacteria) and purified to homogeneity. It is important to ensure that neither the protein mutations nor the presence of the fluorophores within the polymerase or DNA substrate perturb the enzymatic activity. An alternative approach is to introduce both donor and acceptor fluorophores into the polymerase. This requires creation of a double cysteine protein mutant, followed by covalent labeling with donor and acceptor (Santoso et al., 2010). Site-specific labeling can be achieved if the two cysteines have different reactivities towards maleimides (Santoso et al., 2010). Otherwise, the doubly labeled polymerase is a statistical mixture of the two possible labeling orientations.

One informative method for smFRET analysis is to attach DNA substrates to a quartz surface and to introduce a polymerase into the surrounding solution. A laser beam impinging on the surface at an angle of incidence beyond the critical angle for total internal reflection creates an evanescent field that penetrates ~ 100–200 nm beyond the surface, allowing for selective excitation of surface-immobilized complexes. The laser is tuned to excite the donor and the emission from both donor and acceptor is recorded over time on a charge coupled device camera. The advantage of this approach is that hundreds of immobilized DNA molecules can be monitored in parallel and encounters between each DNA molecule and a polymerase from solution can be followed for extended periods of time (typically a few hundred seconds). A potential disadvantage is that the proximity of the surface perturbs the interaction between the polymerase and DNA. Accordingly, the quartz surface is generally passivated by a layer of polyethylene glycol (PEG) or similar polymers (Roy et al., 2008). A small fraction of the PEG molecules is biotinylated, enabling streptavidin or neutravidin to be captured on the surface. These multivalent proteins then serve to capture biotinylated DNA substrates on the passivated surface (Roy et al., 2008).

For every immobilized DNA molecule in the imaging field, the FRET efficiency at each time point, $E(t)$, is calculated according to the following formula: $E(t) = I_A(t)/(I_A(t) + I_D(t))$, where $I_D(t)$ and $I_A(t)$ are the corresponding donor and acceptor intensities (after any necessary instrumental corrections). A plot of $E(t)$ versus t, known as a FRET trajectory, is constructed for each immobilized DNA. These trajectories can reveal abrupt changes in FRET efficiency as the polymerase switches between different DNA binding modes or different conformational states. Examples of FRET trajectories are shown in **Figures 2**, **5**, **9**, **10**. Hundreds of individual FRET trajectories are then combined in the form of FRET efficiency histograms (shown in **Figures 2**, **5**, **9**, **10**). These histograms reveal separate peaks (FRET states) corresponding to different DNA binding modes or polymerase conformations, and the areas enclosed by each peak reflect the equilibrium populations of each state. The FRET efficiency for each state is determined by the corresponding donor-acceptor distance, R_{DA}, according to the formula: $E = [1 + (R_{DA}/R_0)^6]^{-1}$, where R_0 is the Förster distance. The point of this analysis is not to determine

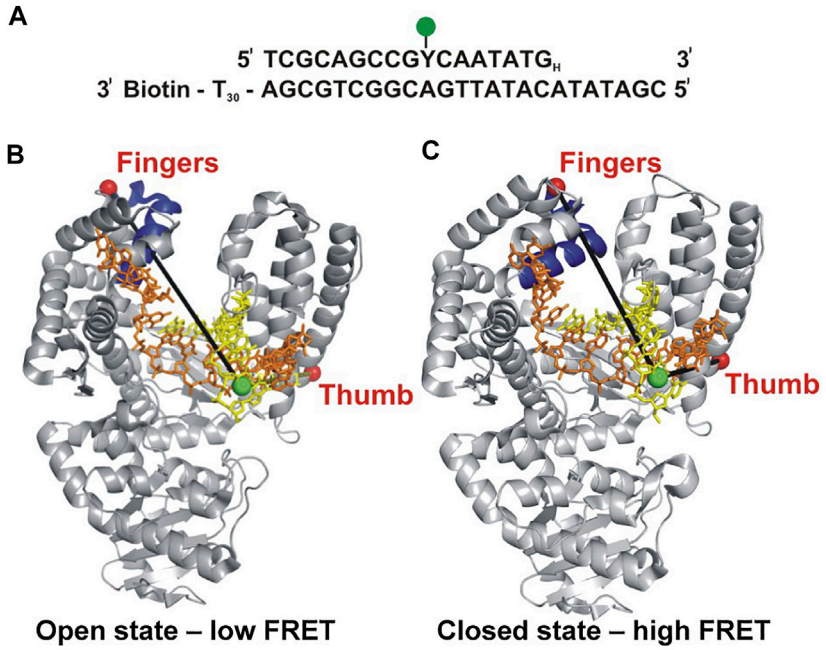

FIGURE 1 | Labeling strategy used to probe the fingers-closure transition in KF. **(A)** Sequence of the primer/template. Y denotes the labeling site for A488 (green) and the H subscript at the 3′ end of the primer denotes a dideoxy modification. The biotin moiety on the template strand is used for surface attachment. **(B)** Crystal structure of the KF homolog *Bst* Pol I in open conformation (PDB code 1L3S). Primer strand is yellow and template strand is orange. **(C)** Crystal structure of *Bst* Pol I in closed conformation (PDB code 1LV5). In both **(B,C)**, the A488 donor is shown as a green sphere and the A594 acceptor attached to the fingers domain as a red sphere. The donor-acceptor distance (black lines) is shorter in the closed conformation than in the open conformation, leading to higher FRET efficiency. For some experiments (not described here), A594 was attached to the thumb domain. Reproduced from reference (Berezhna et al., 2012) with permission.

R_{DA} itself, but rather to resolve different binding modes or polymerase conformations. To do so, the R_{DA} values for each state should be as different as possible, which is dependent on the donor and acceptor labeling positions and the underlying three-dimensional structure of the polymerase-DNA complex. While structural information can be helpful in selecting donor and acceptor labeling sites, these can also be identified by simple trial and error. Another informative statistical method of analysis is to compile two-dimensional plots of transition probability density (TPD) (McKinney et al., 2006). To do so, the final FRET efficiency is plotted versus the initial FRET efficiency for every transition observed in the entire set of FRET trajectories (typically thousands of transitions). These plots reveal prominent off-diagonal cross peaks that reflect how individual FRET states are interconnected. Examples of TPD plots are shown in **Figures 5**, **9**, **10**. Finally, to obtain kinetic information, each FRET trajectory is fitted using Hidden Markov modeling to provide the dwell times spent in one FRET state (state i) before transition to a different FRET state (state j) (McKinney et al., 2006). The dwell times from all trajectories are then compiled in the form of dwell time histograms. These histograms have an exponential shape and can be fitted with a single exponential function to quantify the rate constant for the state-to-state transition, k_{ij}. An example of dwell time analysis is shown in **Figure 6A**. The depth of information available from these smFRET analyses is difficult to obtain using other biophysical or structural methods.

An alternative smFRET method is based on observation of freely diffusing molecules or complexes. In this approach, donor/acceptor-labeled polymerases or polymerase-DNA complexes are observed as they diffuse through the excitation volume of a tightly focused laser beam (tuned to excite the donor) (Santoso et al., 2010). Bursts of emission from both donor and acceptor are recorded on separate avalanche photodiode detectors. The advantage of this approach is that avalanche photodiodes have faster time resolution than charge-coupled device cameras, enabling observation of rapid conformational transitions, although the total observation period is limited by the transit time through the focal region. Another limitation is that molecules or complexes are observed one at a time, rather than in parallel, which reduces the throughput of data acquisition. Details of data acquisition and analysis, with specific reference to DNA polymerases, are described elsewhere (Hohlbein and Kapanidis, 2016). An elaboration of this method is to alternately excite the donor and acceptor with separate lasers, which provides information on both FRET efficiency and the stoichiometry of donor and acceptor labeling (Hohlbein and Kapanidis, 2016).

Role of Polymerase Conformational Dynamics During Nucleotide Selection

DNA replication fidelity begins with the selection of the correct nucleotide substrate during template-directed polymerization of

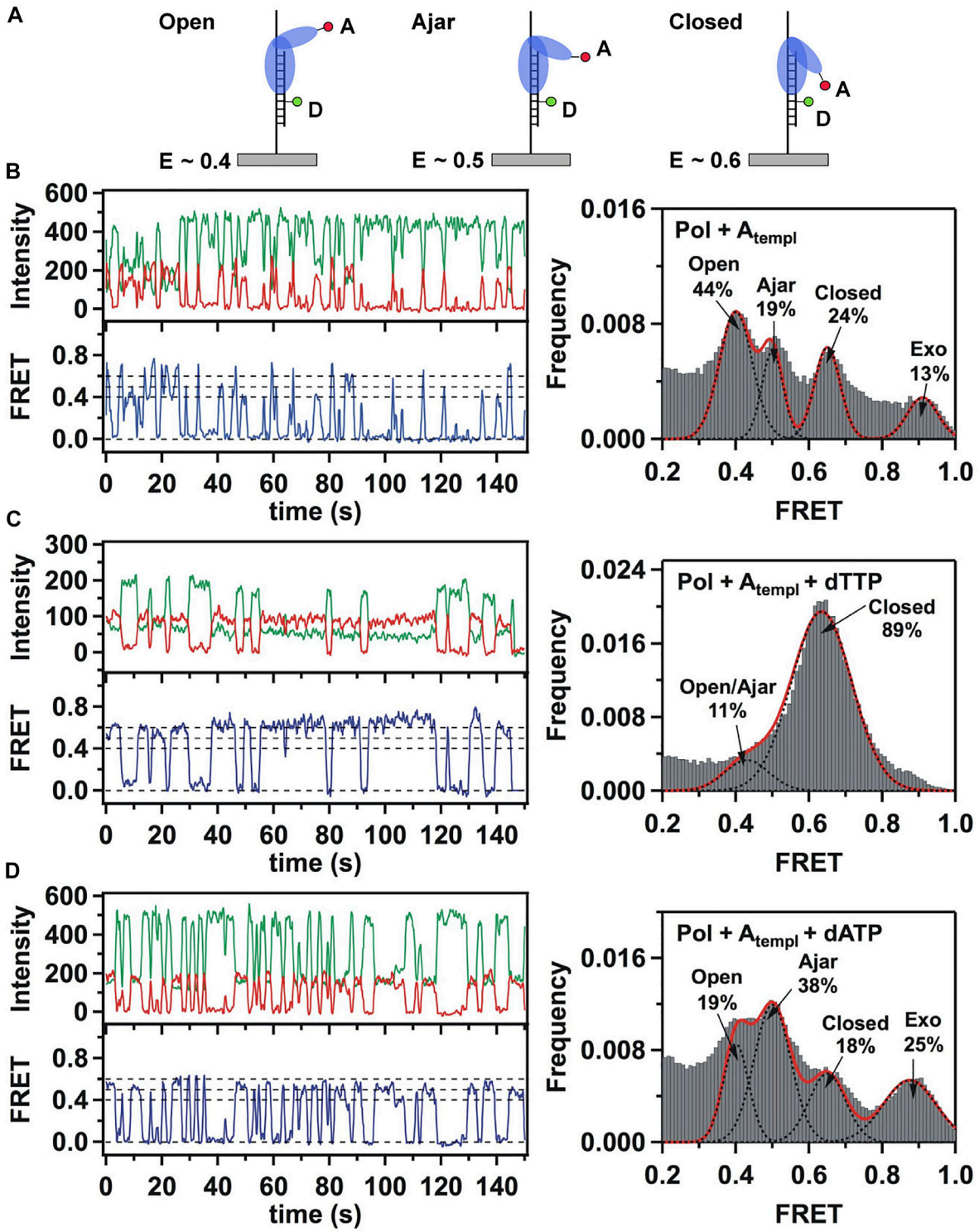

FIGURE 2 | Single-molecule FRET analysis of the fingers closure transition in KF. **(A)** Schematic illustration of the three FRET states associated with different conformations of the fingers domain, with the observed FRET efficiencies indicated. **(B)** smFRET data in the absence of nucleotide substrates. Representative donor intensity (green), acceptor intensity (red) and corresponding FRET efficiency (blue) trajectories are shown on left. The perfect anticorrelation of the donor and acceptor intensity fluctuations is proof that FRET is occurring. The dashed horizontal lines superimposed on the FRET trajectory indicate the FRET efficiencies of the open ($E = 0.4$), ajar ($E = 0.5$) and closed ($E = 0.6$) states. Histogram of FRET efficiencies compiled from multiple traces and fit to four distinct states is shown at right. **(C)** In the presence of the correct dTTP substrate. **(D)** In the presence of the incorrect dATP substrate. Reproduced from reference (Berezhna et al., 2012) with permission.

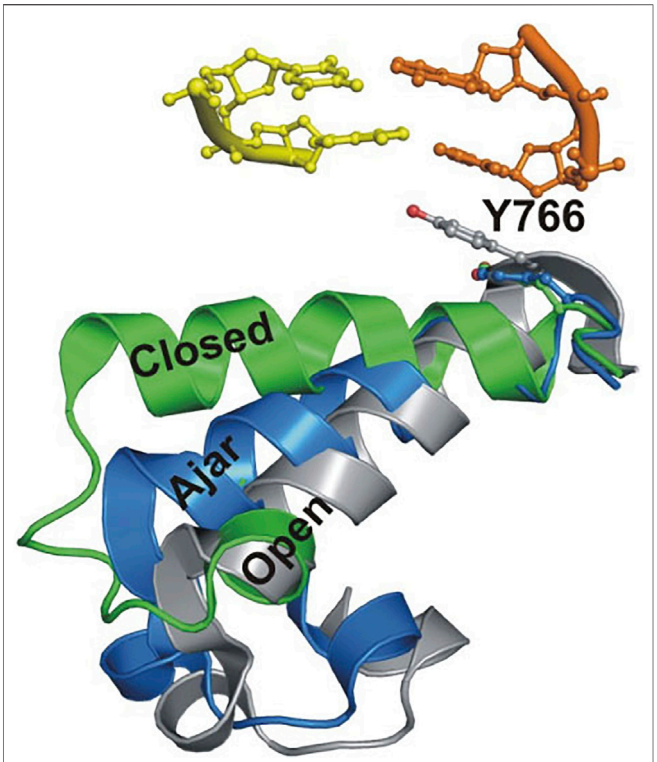

FIGURE 3 | Overlay of crystal structures of *Bst* Pol I reveals three distinct conformations of the O-helix within the fingers domain. Adapted from reference (Berezhna et al., 2012) with permission.

a nascent DNA strand. During each cycle, the polymerase selects the correct dNTP substrate from among the pool of all four possible substrates. While this selection is based on Watson-Crick pairing of the incoming nucleobase with the template base, the observed fidelity of correct nucleotide incorporation significantly exceeds that expected from thermodynamic differences between correct and incorrect base pairs (Kunkel and Bebenek, 2000; Kunkel, 2004), suggesting that the polymerase actively discriminates against incorrect pairings. This discrimination might be linked to conformational changes within the polymerase. X-ray crystallographic studies of DNA polymerases reveal an architecture akin to a human right hand, with thumb, fingers and palm domains (Ollis et al., 1985). In addition, structural studies have also revealed two major polymerase conformations, termed open and closed (Li et al., 1998). In the open conformation, the fingers are retracted away from the DNA substrate, leaving an open cavity that allows for binding of nucleotide substrates, while in the closed conformation the fingers close over the incoming nucleotide.

Berezhna et al. (Berezhna et al., 2012) designed a single-molecule spectroscopic system to detect open and closed conformations in solution and to investigate the possible linkage between nucleotide selection and the conformational dynamics of the polymerase. In this system, a defined oligonucleotide primer/template labeled with Alexa Fluor 488 (A488) at a specific base was immobilized on a quartz surface by biotin-neutravidin attachment (**Figure 1A**). The Klenow fragment (KF) of Pol I, present in solution, was labeled with Alexa Fluor 594 (A594) at a cysteine residue introduced into the fingers domain (at the tip of the O-helix) (**Figure 1B**). KF constitutes the main core of Pol I, but lacks the *5′ nuc* domain, allowing the nucleotide selection step to be decoupled from the *5′ nuc* activity of Pol I. The primer 3′ terminus contained a dideoxy modification, to block covalent incorporation of nucleotide substrates. Accordingly, this system was designed to probe conformational changes of KF that occur after nucleotide binding and precede the chemical step of covalent phosphodiester bond formation. The A488 and A594 fluorophores form a donor/acceptor (D/A) pair for measurement of Förster resonance energy transfer (FRET). The efficiency of FRET is strongly dependent on the D/A distance (Voith von Voithenberg and Lamb, 2018). Based on the expected shortening of the distance, the FRET efficiency should be higher in the closed conformation than in the open conformation (**Figures 1B,C**).

This system was initially used to examine the behavior of the polymerase in the absence of any nucleotide substrates. The polymerase was highly labile under these conditions, transiently binding the immobilized DNA and sampling three distinct FRET states during the brief periods while bound (**Figures 2A,B**). While the low-FRET and high-FRET states were assigned to open and closed conformations, respectively (**Figure 2A**), the observation of an intermediate FRET state was initially unexpected. However, a crystal structure of *Bst* polymerase, a KF homolog, bound to DNA and a mismatched nucleotide revealed a third conformation of the fingers domain, intermediate between open and closed, termed "ajar" (Wu and Beese, 2011) (**Figure 3**). Accordingly, the intermediate FRET state was assigned to an ajar conformation of KF (**Figure 2A**). These observations revealed that KF is intrinsically dynamic in solution, sampling open, ajar and closed conformations, all of which were significantly populated (**Figure 2B**). The results also highlighted the ability of smFRET measurements to resolve conformational heterogeneity of a DNA polymerase.

Strikingly different behavior was observed in the presence of a correct nucleotide substrate (dTTP, complementary to the A templating base). Only the closed conformation was significantly populated, and the residence time of the polymerase on DNA was markedly prolonged, indicating more extensive contacts between DNA and the polymerase (**Figure 2C**). Presumably, the polymerase was poised to incorporate the nucleotide, which was blocked in this study by the dideoxy modification of the primer 3′ terminus. These results revealed that the presence of a correct nucleotide had a significant impact on the local conformational preference of the fingers domain and the global stability of the ternary enzyme-DNA-dNTP complex.

The polymerase was also examined in the presence of an incorrect nucleotide substrate (dATP, mismatched with respect to the A templating base). The polymerase dissociated rapidly after each encounter with the DNA substrate, reminiscent of the binary complex (**Figure 2D**). However, the population of the ajar state was markedly higher than in the binary complex, while the populations of the open and closed states were correspondingly

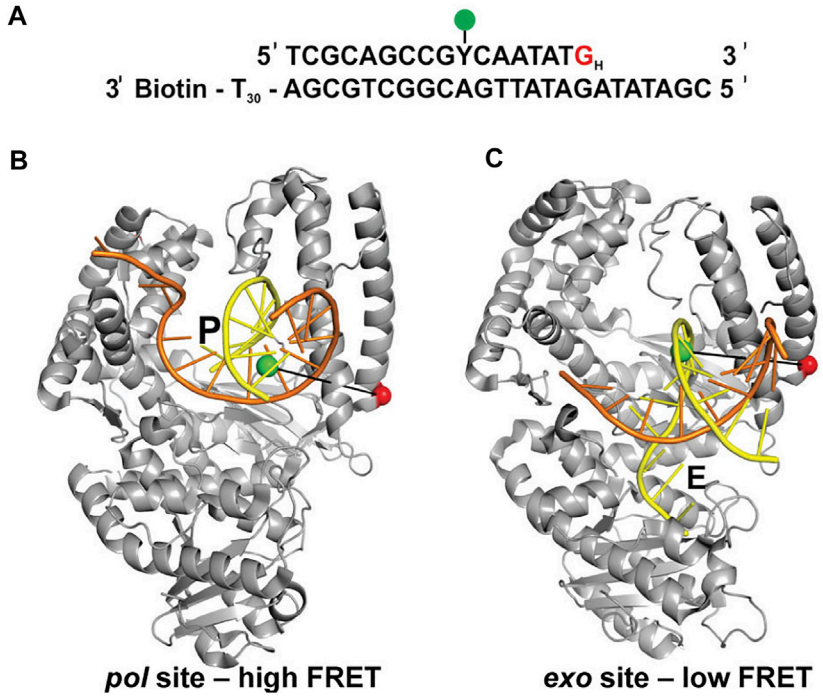

FIGURE 4 | FRET labeling system designed to monitor switching of DNA between *pol* and *exo* sites of KF. **(A)** Sequence of primer/template containing terminal G:G mismatch. **(B)** Crystal structure of *Bst* Pol I with DNA at the *pol* site, P (PDB code 1L3S). Same strand colors as in **Figures 1B,C**. **(C)** Crystal structure of KF with DNA at the *exo* site, E (PDB code 1KLN). In **(B,C)**, the locations of the donor (green) and acceptor (red) are indicated. Different FRET efficiencies are expected for DNA bound to the *pol* site or the *exo* site. Adapted from reference (Lamichhane et al., 2013) with permission.

reduced. Based on these observations, the ajar conformation was proposed to serve as a fidelity checkpoint to examine the identity of an incoming nucleotide substrate. In the presence of a correct nucleotide, the fingers domain rapidly proceeds to the closed conformation and the polymerase remains stably bound to DNA. However, in the presence of an incorrect nucleotide, the fingers domain remains in the ajar conformation and the polymerase rapidly dissociates from the DNA.

Another novel observation of the study by Berezhna et al. (Berezhna et al., 2012) was the appearance of a state with high FRET efficiency, clearly evident in the binary complex (**Figure 2B**). This state was assigned to a subpopulation of KF molecules engaging the immobilized primer/template *via* the *exo* site. This state vanished in the presence of a correct nucleotide (**Figure 2C**), indicating that the polymerase engaged the DNA exclusively *via* the *pol* site, as expected. Surprisingly, the high-FRET state was enhanced in the presence of the incorrect nucleotide substrate (**Figure 2D**), suggesting that the incorrect nucleotide promotes movement of the primer 3′ terminus from the *pol* site to the *exo* site. Shifting the primer terminus out of the *pol* site is an additional mechanism to suppress misincorporation of the incorrect nucleotide. This contribution to polymerase fidelity had not been recognized previously.

The fingers closure transition was also monitored using a complementary smFRET system in which KF was labeled with donor and acceptor in the fingers and thumb domains and freely diffusing polymerase molecules were detected as they passed through the focal volume of a laser (Santoso et al., 2010). This system enabled observation of the apo enzyme, as well as complexes with DNA and nucleotide substrates. Interestingly, the unliganded enzyme was observed to exchange rapidly between low-FRET and high-FRET states, assigned to open and closed conformations, showing that the fingers domain is an intrinsically mobile element of KF. Both open and closed conformations were observed in a binary KF-DNA complex, whereas the closed conformation was preferred in a ternary complex with DNA and a correct dNTP substrate. These observations mirror the results presented above (**Figure 2**). Hence, smFRET analyses of KF employing donor and acceptor within the DNA substrate and polymerase, described above, or both within the polymerase (Santoso et al., 2010; Hohlbein et al., 2013) yield consistent findings.

Doubly labeled KF was also examined in the presence of DNA and an incorrect dNTP (Santoso et al., 2010; Hohlbein et al., 2013). The low-FRET state showed a small shift to higher FRET efficiency, consistent with the formation of a partially closed conformation, presumably the ajar conformation. However, the open and ajar states were not resolved as separate peaks in the FRET histograms, as in **Figure 2**. It appears that the smFRET system described above (**Figures 1**, **2**) is better able to resolve

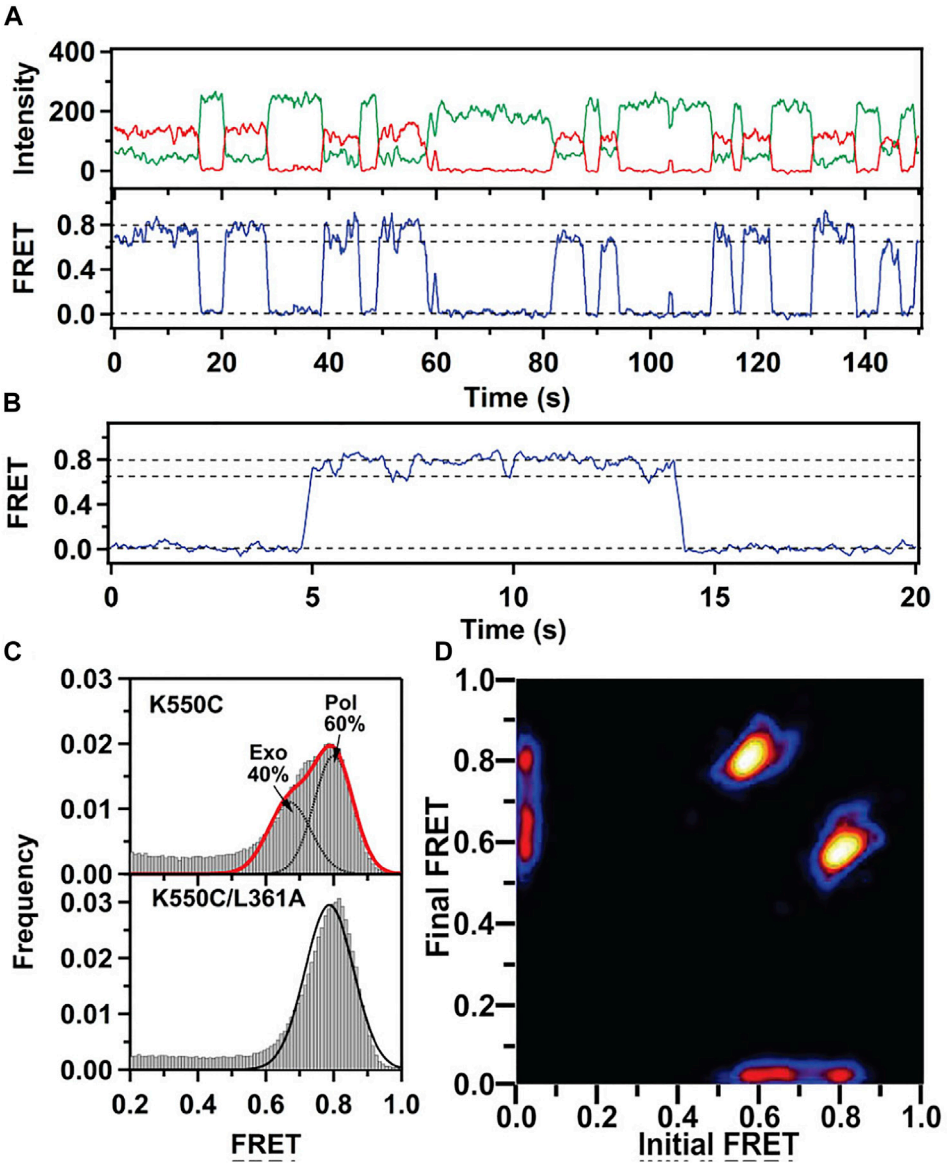

FIGURE 5 | smFRET data for KF interacting with mismatched DNA. **(A)** Representative donor intensity (green), acceptor intensity (red) and FRET efficiency (blue) trajectories. **(B)** Expanded view of a single encounter between KF and DNA. **(C)** FRET efficiency histograms compiled from multiple traces. **(D)** Plot of transition probability density. Reproduced from reference (Lamichhane et al., 2013) with permission.

different conformations of the fingers domain. The diffusion-based smFRET system employing doubly labeled KF was also used to investigate the impact of polymerase mutations (with mutator phenotypes) on nucleotide recognition and the fingers closure transition (Hohlbein et al., 2013).

In a related study, doubly labeled KF was visualized as it interacted with immobilized (unlabeled) DNA primer/templates (Evans et al., 2015). In contrast to diffusion-based smFRET measurements, immobilization of DNA significantly extended the observation time window. This allowed measurement of the rate constants for closure and reopening of the fingers domain, both in the absence and presence of dNTP substrates. These observations provided new information on the pre-chemistry reaction steps in the nucleotide incorporation cycle of KF.

DNA polymerase B1 (PolB1) from *S. solfataricus*, a B family polymerase, has also been investigated using smFRET methods (Maxwell and Suo, 2013). The experimental strategy was similar to that described above for KF, utilizing a FRET donor attached to the primer strand of an immobilized DNA substrate and an acceptor attached to the fingers domain of the polymerase. This system revealed open and closed conformations of the fingers (but not an ajar conformation), as well as a subpopulation of DNA substrates bound at the *exo* site. Notably, the smFRET

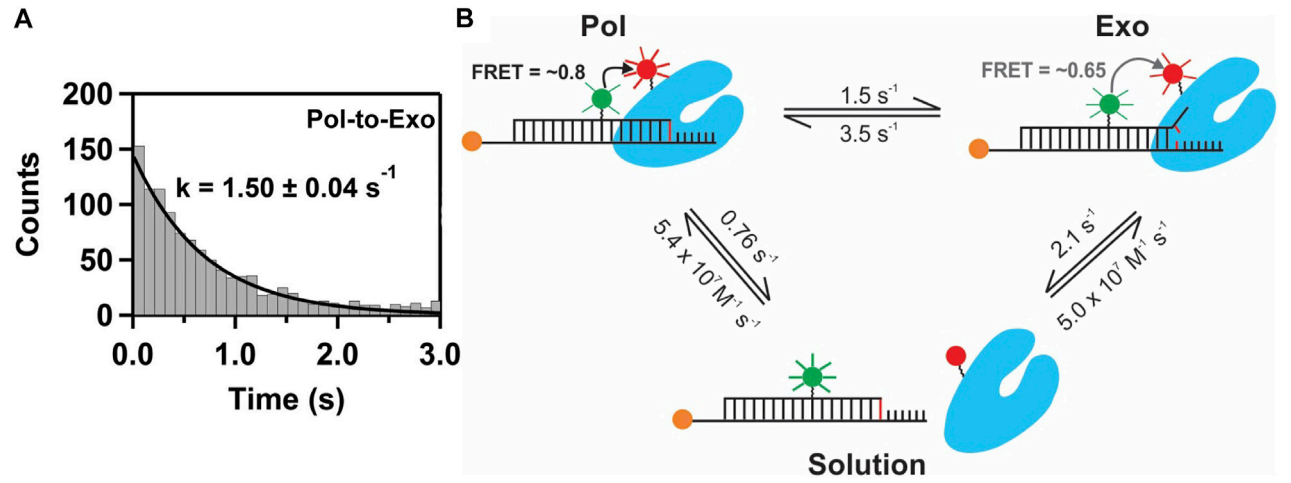

FIGURE 6 | Pathways and rate constants for switching of DNA between *pol* and *exo* sites in KF. **(A)** Dwell time histogram for direct transitions from the *pol* site to the *exo* site. The smooth line is the best fit to a single exponential function, with the rate constant indicated. **(B)** Summary of the two observed transfer pathways. The intramolecular transfer pathway between bound complexes is shown at the top, together with the measured rate constants obtained from dwell time analysis of smFRET trajectories. The intermolecular pathway, involving dissociation from one site and rebinding from solution to the other site, is shown below, together with the respective rate constants.

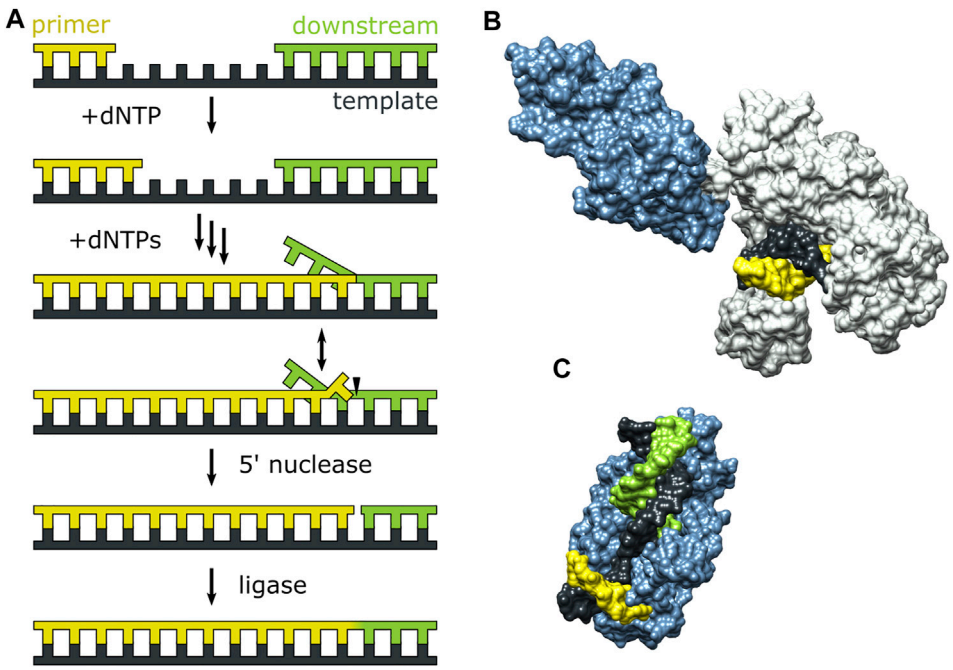

FIGURE 7 | Activities of Pol I and three-dimensional structures of Pol I homologs. **(A)** Processes catalyzed by Pol I during lagging strand DNA synthesis and base excision repair. **(B)** Crystal structure of the Pol I homolog Taq polymerase with primer/template DNA at the *pol* site (PDB code 1TAU). The polymerase core is grey and the *5′ nuc* domain is blue. **(C)** Crystal structure of human FEN1 (homologous to the *5′ nuc* domain of Pol I) bound to a DNA substrate (PDB code 3Q8M). In **(B,C)**, the primer, template and downstream strands are colored as in **(A)**. Reproduced from reference (Pauszek et al., 2021) with permission.

observations revealed transitions among these different states without dissociation from the DNA, as observed with KF (also see next section). Similar smFRET methods were used to monitor the fingers closure transition in DNA polymerase β (an X family polymerase) (Fijen et al., 2020) and Dpo4 polymerase (a Y family polymerase) (Raper and Suo, 2016).

Role of Polymerase Conformational Dynamics During Proofreading

Despite the mechanisms that promote selection of correct nucleotide substrates and prevent misincorporation of incorrect nucleotides, mistakes are still sometimes made. Many DNA polymerases contain a 3′-5′ exonuclease

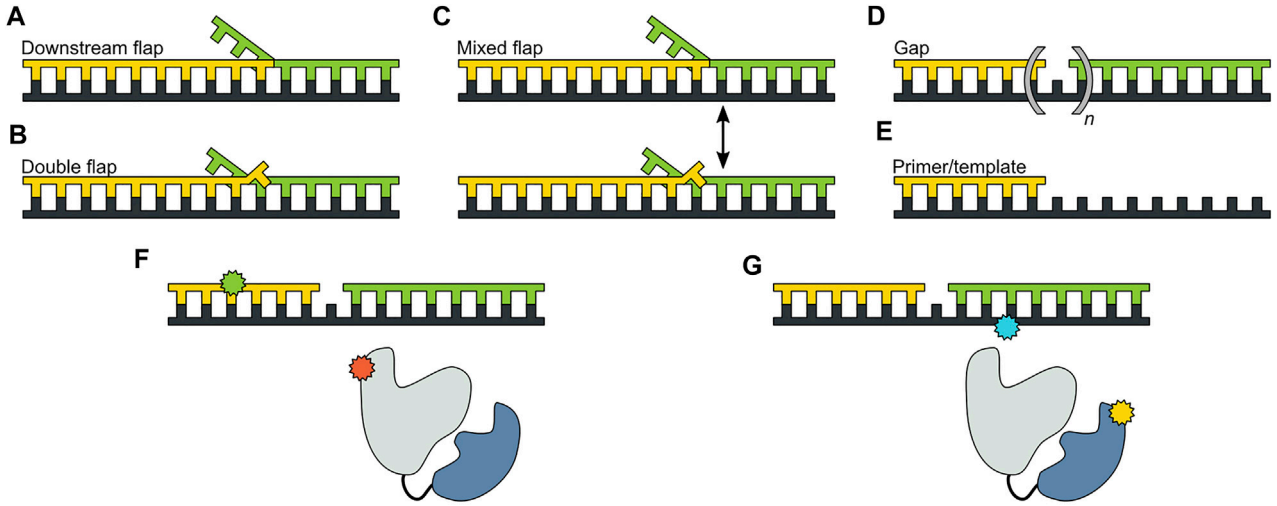

FIGURE 8 | DNA substrates and FRET labeling strategies. **(A)** Substrate containing a 5′ flap on the downstream strand. **(B)** Substrate containing flaps on the primer and downstream strands (double-flap). **(C)** Substrate that exists as a mixture of downstream flap and double-flap forms. **(D)** Substrates containing gaps of various sizes. **(E)** Primer/template substrate, lacking a downstream strand entirely. **(F)** First FRET labeling scheme. Donor is green and acceptor is red. **(G)** Second FRET labeling scheme. Donor is yellow and acceptor is blue. Reproduced from reference (Pauszek et al., 2021) with permission.

activity to remove misincorporated nucleotides (proofreading) (Reha-Krantz, 2010; Bebenek and Ziuzia-Graczyk, 2018). Structural studies of A family (KF) (Freemont et al., 1988), B family (Berman et al., 2007) and C family (*E. coli* pol III) (Fernandez-Leiro et al., 2015; Fernandez-Leiro et al., 2017) polymerases have revealed that the active sites for *pol* activity and *exo* activity are spatially separated in distinct protein domains, indicating that mechanisms must exist to promote movement of a DNA substrate from the *pol* site to the *exo* site during proofreading.

Lamichhane et al. (Lamichhane et al., 2013) developed a smFRET system to monitor switching of DNA between *pol* and *exo* sites in KF. A similar experimental strategy to the assay described in the previous section was employed, featuring an immobilized primer/template labeled with an A488 donor (**Figure 4A**). However, the A594 acceptor was attached to the thumb domain of the polymerase (*via* a K550C mutation), a rigid structural element that provides a static reference point to detect any physical movement relative to the DNA substrate (**Figures 4B,C**). Again, KF was used rather than full length Pol I, since the *pol* and *exo* sites are both contained within the KF portion. Different FRET efficiencies were expected for DNA substrates bound to the *pol* site or the *exo* site (**Figures 4B,C**). To promote occupancy of the *exo* site, the DNA substrate contained a G:G mismatch at the primer 3' terminus (**Figure 4A**), mimicking the product of a misincorporation event.

This system exhibited two distinct FRET states, with FRET efficiencies ~ 0.6 and ~ 0.8, which were assigned to DNA occupying the *exo* site or *pol* site, respectively (**Figure 5A**). These assignments were confirmed using a L361A KF mutant, which is defective in binding DNA at the *exo* site (**Figure 5C**). Importantly, multiple transitions were observed between these FRET states during single encounters between KF and DNA (**Figure 5B**). These direct transitions were also manifested as prominent cross peaks in two-dimensional plots of transition probability density (TPD) (**Figure 5D**). These observations revealed that DNA substrates could transfer reversibly between the *pol* and *exo* sites while remaining associated with the polymerase. This intramolecular transfer mechanism had been inferred from earlier biochemical studies (Joyce, 1989) and was directly revealed by the smFRET results. Moreover, dwell time analysis was used to quantify the rate constants for intramolecular transfer of DNA between the two sites, in either direction (the dwell time histogram for transitions from the *pol* site to the *exo* site is shown in **Figure 6A**). The rate constants for the intramolecular transfer pathway are summarized in **Figure 6B**.

The smFRET results also revealed that KF bound to DNA *via* the *pol* site could dissociate into bulk solution and then rebind DNA *via* the *exo* site (and vice versa). The rate constants for this intermolecular transfer pathway were also determined from dwell time analysis (summarized in **Figure 6B**). During DNA replication *in vivo*, the polymerase is tethered to a replication fork *via* clamp proteins, which would inhibit dissociation of the complex. Intramolecular transfer of DNA is likely to be the relevant pathway during proofreading *in vivo*.

A recent computational study predicted the intramolecular transfer path between *pol* and *exo* sites in *E. coli* Pol III (Dodd et al., 2020). To test the model, the smFRET site switching assay originally developed for KF could be used to quantify how mutations of specific residues lying on the predicted transfer path in Pol III impact the switching kinetics.

Role of Polymerase Conformational Dynamics During 5' Nuclease Activity

Pol I can extend a primer strand in the presence of a downstream strand, resulting in displacement of the

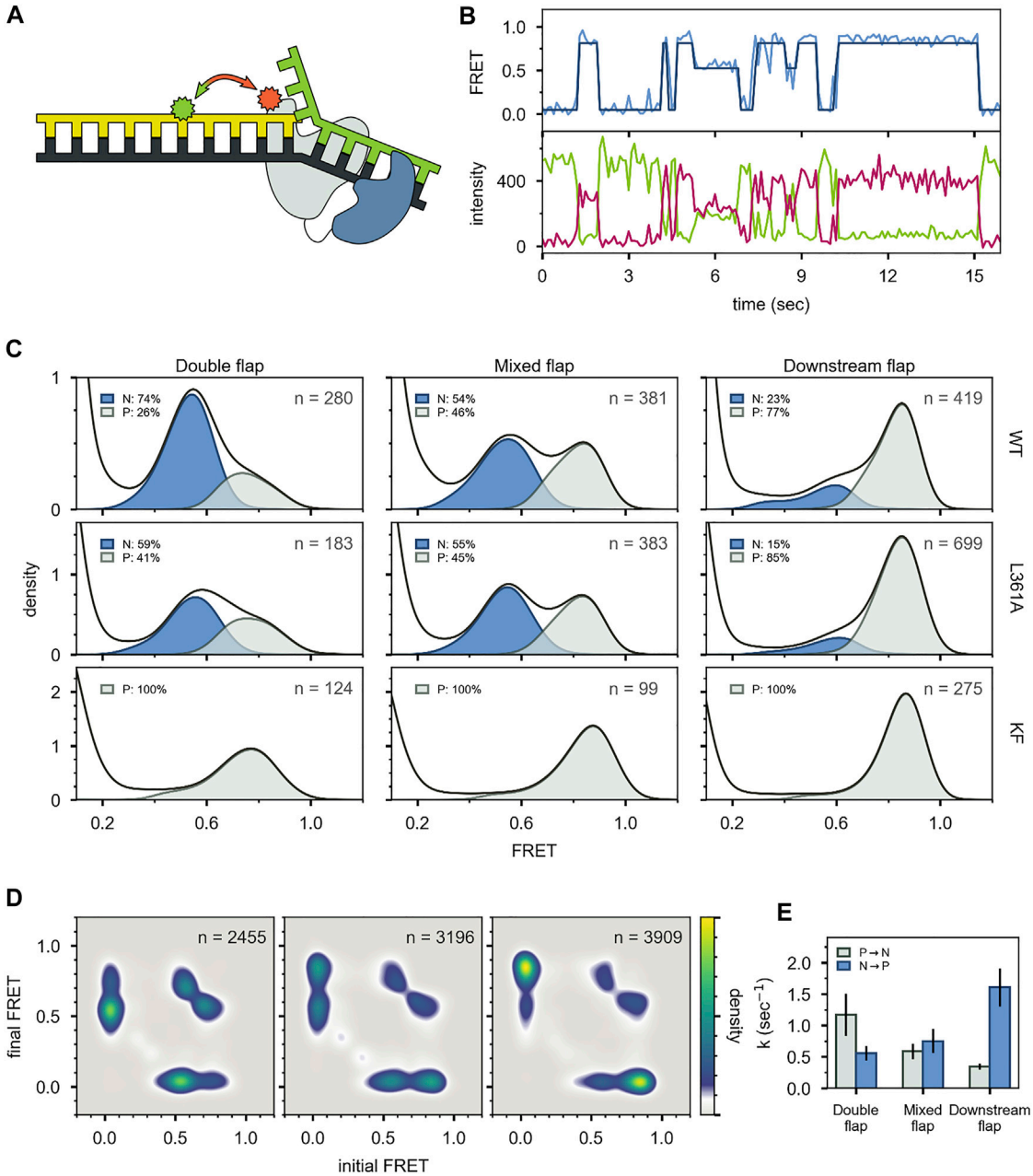

FIGURE 9 | smFRET data for Pol I—DNA complexes obtained using labeling. **(A)** Locations of donor (green) and acceptor (red). Polymerase core is grey and *5′ nuc* domain is blue. **(B)** Donor intensity (green), acceptor intensity (red) and FRET efficiency (blue) trajectories are shown. The black line is a fit from Hidden Markov modeling. **(C)** FRET efficiency histograms compiled from n trajectories, separated into states P and N. **(D)** Transition probability density plots, compiled from n transitions. From left to right: double flap DNA, mixed flap DNA and downstream flap DNA. **(E)** Rate constants for intramolecular transitions between states P and N. Reproduced from reference (Pauszek et al., 2021) with permission.

downstream strand and formation of a 5′ flap (**Figure 7A**). The flap is then cleaved by the 5′ nuclease (*5′ nuc*) activity of Pol I, leaving a nick that can subsequently be sealed by a DNA ligase. The processing steps depicted in **Figure 7A** are carried out by Pol I during lagging strand DNA synthesis (Balakrishnan and Bambara, 2013) and DNA base excision repair (Imai et al., 2007) in *E. coli*. The *5′ nuc* activity is contained in a separate domain that is connected to the main body of the enzyme (the KF portion) by a flexible 16 aa peptide linker (**Figure 7B**). Moreover, the *5′ nuc* domain is homologous to various structure-specific flap endonucleases (**Figure 7C**) (Harrington and Lieber, 1994).

The *pol* and *5′ nuc* activities of Pol I must be carefully coordinated to ensure that the resulting DNA product contains a nick rather than an extended gap or overhanging 5′ strand. However, the physical basis for this coordination is not well

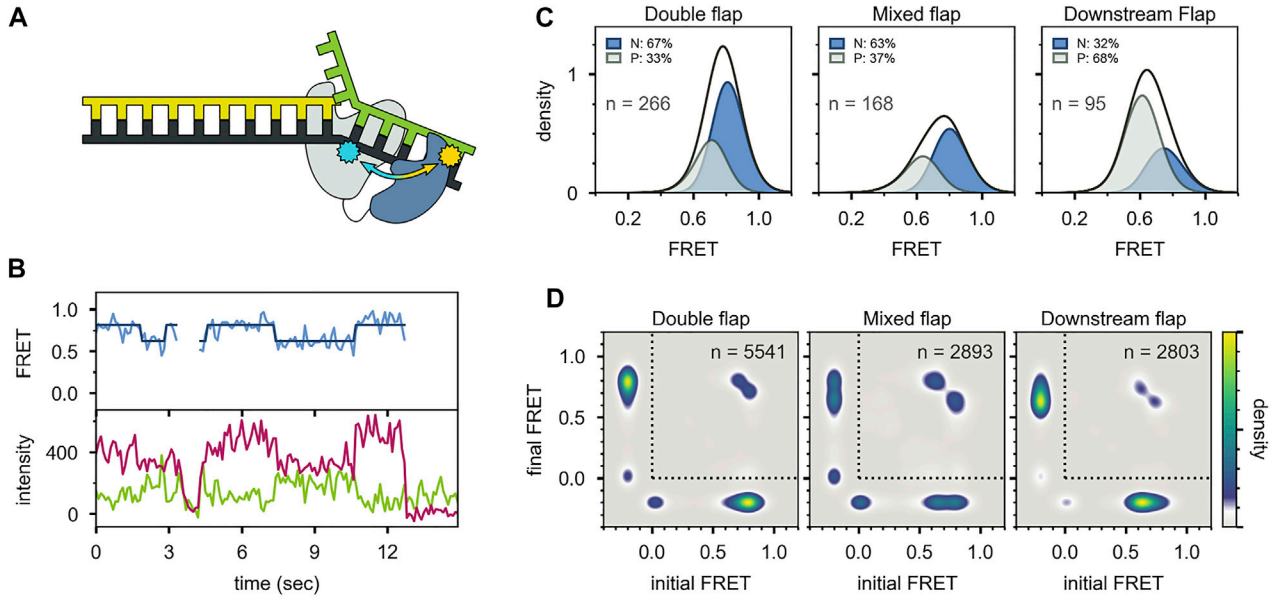

FIGURE 10 | smFRET data for Pol I—DNA complexes obtained using the second labeling scheme. **(A)** Locations of donor (yellow) and acceptor (blue). The polymerase core is grey and *5′ nuc* domain is blue. **(B)** Donor intensity (green), acceptor intensity (red) and FRET efficiency (blue) trajectories are shown. The black line is a fit from Hidden Markov modeling. **(C)** FRET efficiency histograms compiled from n trajectories, separated into states P and N. **(D)** Transition probability density plots, compiled from n transitions. Reproduced from reference (Pauszek et al., 2021) with permission.

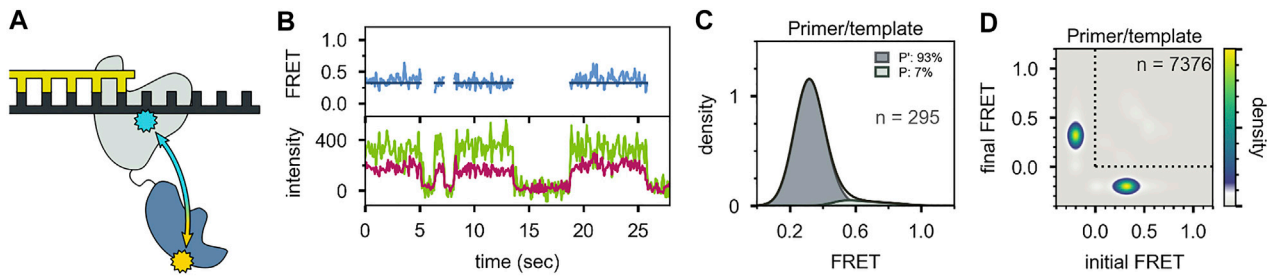

FIGURE 11 | Probing the location of the *5′ nuc* domain in the absence of a downstream DNA strand. **(A)** Schematic representation of donor (yellow) and acceptor (blue) sites. **(B)** Donor intensity (green), acceptor intensity (red) and FRET efficiency (blue) traces are shown. The black line is a fit from Hidden Markov modeling. **(C)** FRET efficiency histogram compiled from n trajectories, separated into states P′ and P. **(D)** Transition probability density plot, compiled from n transitions. Reproduced from reference (Pauszek et al., 2021) with permission.

understood. Pauszek et al. (Pauszek et al., 2021) designed a single-molecule FRET system to monitor the transition from *pol* activity to *5′ nuc* activity in Pol I. A variety of DNA substrates (**Figures 8A–E**) and two complementary labeling schemes were employed (**Figures 8F,G**). The first scheme was identical to that used to monitor *pol* to *exo* site switching in KF (same donor and acceptor sites), except that full length Pol I was employed (**Figure 8F**). This system was designed to monitor any movement of the DNA substrate relative to the enzyme core. The second FRET scheme employed an A488 donor attached to the *5′ nuc* domain of Pol I and an A594 acceptor attached to the template strand downstream of the primer 3′ terminus (**Figure 8G**). This scheme was designed to probe the proximity of the *5’ nuc* domain to the downstream DNA.

For the first labeling scheme (**Figure 9A**), Pol I exhibited two distinct FRET states, ~ 0.6 and ~ 0.8 efficiency, when interacting with any of the flap-containing DNA substrates (**Figures 9B,C**). The population of the 0.6 FRET state was not responsive, or only weakly responsive, to a L361A mutation in Pol I (**Figure 9C**), indicating that this state was not associated with binding of DNA to the *exo* site. In contrast, the 0.6 FRET state was not observed for any of the flap-containing DNAs interacting with KF (**Figure 9C**), which lacks the *5′ nuc* domain entirely. Based on these results, the 0.8 and 0.6 FRET states were assigned to DNA engaging the *pol* site (state P) or the *5′ nuc* site (state N),

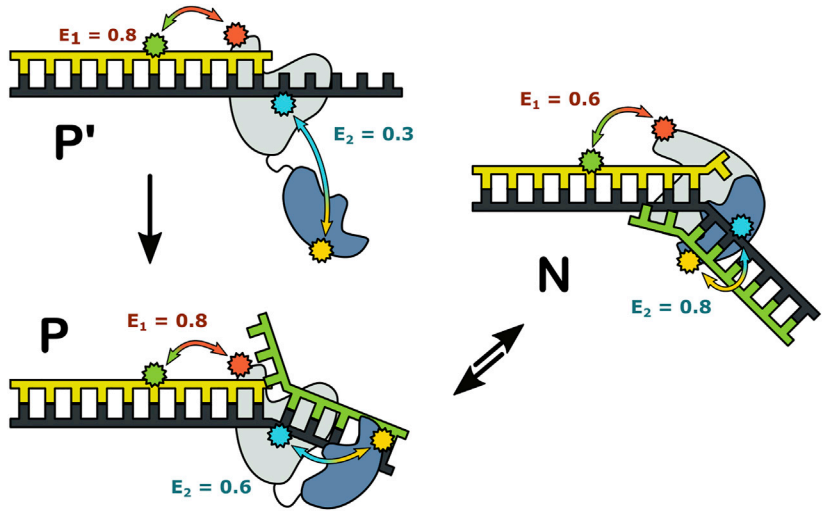

FIGURE 12 | Possible configurations of Pol I—DNA complexes. The FRET efficiencies measured with labeling are denoted E_1 and E_2, respectively. Reproduced from reference (Pauszek et al., 2021) with permission.

respectively. State N was most highly populated with the double-flap DNA (**Figure 9C**), which is the natural substrate for *5′ nuc* activity (blocked here by a D116A mutation).

Two distinct FRET states were also observed with the second labeling scheme (**Figures 10A-C**), which probes the proximity of the *5′ nuc* domain to the downstream DNA. The high-FRET and mid-FRET states were assigned to states N and P, respectively, based on the correspondence in the species populations observed with the two labeling schemes. Hence, the two FRET schemes yield a consistent description of the conformational states populated with flap-containing DNA substrates. Moreover, the results with the second labeling scheme confirmed that the *5′ nuc* domain was in close physical proximity to the downstream DNA in state N. Notably, only a single low-FRET state was observed for a primer/template substrate, indicating that the *5′ nuc* domain was extended away from the DNA (**Figures 11A-D**). Thus, the presence of a downstream strand is necessary to engage the *5′ nuc* domain. This low-FRET state was designated P′ (see below).

For both FRET systems, direct transitions were observed between states P and N during single encounters between Pol I and the flap-containing DNAs (**Figure 9B**, **Figure 10B**). Similarly, prominent cross-peaks were observed in two-dimensional TPD plots (**Figure 9D**, **Figure 10D**). These observations establish that DNA substrates initially engaging the *pol* site can switch to the *5′ nuc* site while remaining associated with Pol I (and vice versa). Hence, transfer of DNA from the *pol* site to the *5′ nuc* site is governed by an intramolecular pathway, as observed for DNA switching between *pol* and *exo* sites. Rate constants for site switching were determined from dwell-time analysis (**Figure 9E**). The double-flap DNA substrate exhibited the fastest transfer from the *pol* site to the *5′ nuc* site and the slowest return to the *pol* site, accounting for the high population of state N (**Figure 9C**).

Together, these observations revealed that three distinct complexes can form during encounters between Pol I and DNA substrates (**Figure 12**). State P′ is formed when the primer 3′ terminus is remote from a downstream strand: the primer terminus is positioned in the *pol* site and the *5′ nuc* domain is extended away from the DNA. State P is formed as the primer 3′ terminus approaches a downstream strand: the primer terminus is still located in the *pol* site, but the *5′ nuc* domain is in proximity to the downstream DNA. State N is formed after the primer 3′ terminus has shifted out of the *pol* site and the *5′ nuc* domain is poised to cleave the downstream strand. Importantly, the smFRET results showed that states P and N can reversibly exchange without dissociation, explaining how the *pol* and *5’ nuc* modes of activity are physically coordinated in Pol I.

Other Applications of smFRET to DNA Polymerases

While the central focus of this review has been on the conformational dynamics underpinning the DNA replication fidelity of Pol I, smFRET methods have also been used to examine other aspects of DNA polymerase function. In an early application, smFRET was used to monitor the movement of KF on a DNA template during DNA synthesis, enabling measurement of primer elongation with single base-pair resolution (Christian et al., 2009). This approach was also used to elucidate the impact of bulky benzopyrene adducts on translesion DNA synthesis by the Y family polymerase Dpo4 (Liyanage et al., 2017).

Craggs et al. studied the structure-specific recognition of gapped DNA substrates by KF (Craggs et al., 2019). A large set of DNA substrates containing donors and acceptors at various sites were examined by smFRET, both in the presence and absence of KF. Using a docking approach based on the resulting network of D/A distances, a solution structure of the gapped DNA bound by KF was established, revealing a sharp bend in the DNA. This comprehensive study exemplified how smFRET data can be combined with structural modeling methods

to provide a detailed structural description of an intrinsically dynamic macromolecular complex. Interestingly, the results also showed that the DNA alone could adopt a similar bent conformation, supporting a model wherein KF recognized a pre-bent DNA conformation.

CONCLUDING REMARKS

The smFRET studies of Pol I, reviewed above, highlight the intrinsically dynamic character of the enzyme. Each of the three biochemical activities is linked to conformational dynamics of the enzyme-DNA complex. Moreover, the results reveal the different physical mechanisms employed in each case: 1) nucleotide selection is coupled to movement of the fingers domain, 2) proofreading involves physical movement of the DNA substrate between separated *pol* and *exo* sites, and 3) the *5′ nuc* activity requires both movement of DNA and a large conformational change of the polymerase (docking of the *5' nuc* domain with the downstream DNA).

The smFRET methods reviewed here can readily resolve different binding modes of a polymerase-DNA complex, quantify their relative populations and the rates of exchange between them. The results also establish whether a polymerase switches from one mode of activity to another during a single encounter between the polymerase and DNA substrate (intramolecular events) or after dissociation and rebinding (intermolecular events). With the ability to label both the DNA substrate and the enzyme at specific locations with donor and acceptor probes, smFRET provides a general tool to probe the conformational dynamics of DNA polymerases in a region-specific manner. Further highlighting the versatility of the method, smFRET can also be used to monitor polymerase-mediated primer extension or to establish structural features of polymerase-DNA complexes. With these wide-ranging capabilities, smFRET is emerging as a powerful adjunct to traditional three-dimensional structural analyses of DNA polymerases.

The smFRET studies of Pol I performed to date were conducted under equilibrium conditions, in which the various enzymatic activities were blocked by enzyme mutations or modifications to the DNA substrate. Future smFRET studies employing fully active Pol I and extendable DNA substrates should reveal the sequence of polymerase conformational changes and DNA movements during each of the DNA processing steps performed by Pol I.

While this review has focused on *E. coli* Pol I, DNA polymerases from other organisms also possess multiple enzymatic activities that must be carefully coordinated to ensure efficient and accurate DNA replication and repair. In many polymerases, including those from eukaryotes, the various enzymatic activities are contained in distinct protein subunits within a multi-protein holoenzyme complex (McHenry, 2011; Burgers and Kunkel, 2017; Raia et al., 2019). The resulting spatial separation of the various active sites poses the same challenge facing Pol I: how to regulate the movement of a DNA substrate between physically remote active sites ? The mechanisms employed by Pol I to coordinate it is three activities, involving intramolecular shuttling of DNA between spatially separated active sites, combined with enzyme conformational changes, are likely employed across the DNA polymerase family. Accordingly, the smFRET methods reviewed here provide general tools to understand the physical basis of functional coordination in multi-functional DNA polymerases.

AUTHOR CONTRIBUTIONS

DM wrote the manuscript.

FUNDING

Research on DNA polymerases in my laboratory has been supported by the National Institute of General Medical Sciences through grant GM044060.

ACKNOWLEDGMENTS

I gratefully acknowledge the colleagues in my laboratory, past and present, who have contributed to the results described in this review: Joshua Gill, Svitlana Berezhna, Rajan Lamichhane, Raymond Pauszek, Arishma Rajnarikar-Singh and Edwin van der Schans. I also thank Silver Jõemetsa for help in preparing some of the figures.

REFERENCES

Bailey, M. F., van der Schans, E. J. C., and Millar, D. P. (2004). Thermodynamic Dissection of the Polymerizing and Editing Modes of a DNA Polymerase. *J. Mol. Biol.* 336 (3), 673–693. doi:10.1016/j.jmb.2003.11.023

Balakrishnan, L., and Bambara, R. A. (2013). Okazaki Fragment Metabolism. *Cold Spring Harb. Perspect. Biol.* 5 (2), a010173. doi:10.1101/cshperspect.a010173

Banerjee, S., Maurya, S., and Roy, R. (2018). Single-molecule Fluorescence Imaging: Generating Insights into Molecular Interactions in Virology. *J. Biosci.* 43 (3), 519–540. doi:10.1007/s12038-018-9769-y

Bebenek, A., and Ziuzia-Graczyk, I. (2018). Fidelity of DNA Replication-A Matter of Proofreading. *Curr. Genet.* 64 (5), 985–996.

Berezhna, S. Y., Gill, J. P., Lamichhane, R., and Millar, D. P. (2012). Single-Molecule Förster Resonance Energy Transfer Reveals an Innate Fidelity Checkpoint in DNA Polymerase I. *J. Am. Chem. Soc.* 134 (27), 11261–11268. doi:10.1021/ja3038273

Berman, A. J., Kamtekar, S., Goodman, J. L., Lázaro, J. M., de Vega, M., Blanco, L., et al. (2007). Structures of Phi29 DNA Polymerase Complexed with Substrate: the Mechanism of Translocation in B-Family Polymerases. *EMBO J.* 26 (14), 3494–3505. doi:10.1038/sj.emboj.7601780

Bocanegra, R., Ismael Plaza, G. A., and Ibarra, B. (2021). DNA Replication Machinery: Insights from *in vitro* Single-Molecule Approaches. *Comput. Struct. Biotechnol. J.* 19, 2057–2069. doi:10.1016/j.csbj.2021.04.013

Bocanegra, R., Plaza G.A., I., and Ibarra, B. (2021). *In Vitro* single-molecule Manipulation Studies of Viral DNA Replication. *Enzymes* 49, 115–148. doi:10.1016/bs.enz.2021.09.001

Burgers, P. M. J., and Kunkel, T. A. (2017). Eukaryotic DNA Replication Fork. *Annu. Rev. Biochem.* 86, 417–438. doi:10.1146/annurev-biochem-061516-044709

Christian, T. D., Romano, L. J., and Rueda, D. (2009). Single-molecule Measurements of Synthesis by DNA Polymerase with Base-Pair Resolution. *Pnas* 106 (50), 21109–21114. doi:10.1073/pnas.0908640106

Cockroft, S. L., Chu, J., Amorin, M., and Ghadiri, M. R. (2008). A Single-Molecule Nanopore Device Detects DNA Polymerase Activity with Single-Nucleotide Resolution. *J. Am. Chem. Soc.* 130 (3), 818–820. doi:10.1021/ja077082c

Craggs, T. D., Sustarsic, M., Plochowietz, A., Mosayebi, M., Kaju, H., Cuthbert, A., et al. (2019). Substrate Conformational Dynamics Facilitate Structure-specific Recognition of Gapped DNA by DNA Polymerase. *Nucleic Acids Res.* 47 (20), 10788–10800. doi:10.1093/nar/gkz797

Dahl, J. M., Mai, A. H., Cherf, G. M., Jetha, N. N., Garalde, D. R., Marziali, A., et al. (2012). Direct Observation of Translocation in Individual DNA Polymerase Complexes. *J. Biol. Chem.* 287 (16), 13407–13421. doi:10.1074/jbc.m111.338418

Dodd, T., Botto, M., Paul, F., Fernandez-Leiro, R., Lamers, M. H., and Ivanov, I. (2020). Polymerization and Editing Modes of a High-Fidelity DNA Polymerase Are Linked by a Well-Defined Path. *Nat. Commun.* 11 (15379), 5379. doi:10.1038/s41467-020-19165-2

Doublié, S., Tabor, S., Long, A. M., Richardson, C. C., and Ellenberger, T. (1998). Crystal Structure of a Bacteriophage T7 DNA Replication Complex at 2.2 Å Resolution. *Nature* 391 (6664), 251–258. doi:10.1038/34593

Evans, G. W., Hohlbein, J., Craggs, T., Aigrain, L., and Kapanidis, A. N. (2015). Real-time Single-Molecule Studies of the Motions of DNA Polymerase Fingers Illuminate DNA Synthesis Mechanisms. *Nucleic Acids Res.* 43 (12), 5998–6008. doi:10.1093/nar/gkv547

Fernandez-Leiro, R., Conrad, J., Scheres, S. H., and Lamers, M. H. (2015). Cryo-EM Structures of the *E. coli* Replicative DNA Polymerase Reveal its Dynamic Interactions with the DNA Sliding Clamp, Exonuclease and τ. *Elife* 4, PMC4703070. doi:10.7554/eLife.11134

Fernandez-Leiro, R., Conrad, J., Yang, J.-C., Freund, S. M. V., Scheres, S. H. W., and Lamers, M. H. (2017). Self-correcting Mismatches during High-Fidelity DNA Replication. *Nat. Struct. Mol. Biol.* 24 (2), 140–143. doi:10.1038/nsmb.3348

Fijen, C., Mahmoud, M. M., Kronenberg, M., Kaup, R., Fontana, M., Towle-Weicksel, J. B., et al. (2020). Using Single-Molecule FRET to Probe the Nucleotide-dependent Conformational Landscape of Polymerase β-DNA Complexes. *J. Biol. Chem.* 295 (27), 9012–9020. doi:10.1074/jbc.ra120.013049

Freemont, P. S., Friedman, J. M., Beese, L. S., Sanderson, M. R., and Steitz, T. A. (1988). Cocrystal Structure of an Editing Complex of Klenow Fragment with DNA. *Proc. Natl. Acad. Sci.* 85 (23), 8924–8928. doi:10.1073/pnas.85.23.8924

Gruszka, D. T. (2021). Biochemistry: One Molecule at a Time. *Essays Biochem.* 65 (1), 1–3. doi:10.1042/ebc20210015

Harrington, J. J., and Lieber, M. R. (1994). The Characterization of a Mammalian DNA Structure-specific Endonuclease. *EMBO J.* 13 (5), 1235–1246. doi:10.1002/j.1460-2075.1994.tb06373.x

Hilario, J., and Kowalczykowski, S. C. (2010). Visualizing Protein-DNA Interactions at the Single-Molecule Level. *Curr. Opin. Chem. Biol.* 14 (1), 15–22. doi:10.1016/j.cbpa.2009.10.035

Hoekstra, T. P., Depken, M., Lin, S.-N., Cabanas-Danés, J., Gross, P., Dame, R. T., et al. (2017). Switching between Exonucleolysis and Replication by T7 DNA Polymerase Ensures High Fidelity. *Biophysical J.* 112 (4), 575–583. doi:10.1016/j.bpj.2016.12.044

Hohlbein, J., Aigrain, L., Craggs, T. D., Bermek, O., Potapova, O., Shoolizadeh, P., et al. (2013). Conformational Landscapes of DNA Polymerase I and Mutator Derivatives Establish Fidelity Checkpoints for Nucleotide Insertion. *Nat. Commun.* 4, 2131. doi:10.1038/ncomms3131

Hohlbein, J., and Kapanidis, A. N. (2016). Probing the Conformational Landscape of DNA Polymerases Using Diffusion-Based Single-Molecule FRET. *Methods Enzymol.* 581, 353–378. doi:10.1016/bs.mie.2016.08.023

Hoitsma, N. M., Whitaker, A. M., Schaich, M. A., Smith, M. R., Fairlamb, M. S., and Freudenthal, B. D. (2020). Structure and Function Relationships in Mammalian DNA Polymerases. *Cell. Mol. Life Sci.* 77 (1), 35–59. doi:10.1007/s00018-019-03368-y

Huang, J., Alnajjar, K. S., Mahmoud, M. M., Eckenroth, B., Doublié, S., and Sweasy, J. B. (2018). The Nature of the DNA Substrate Influences Pre-catalytic Conformational Changes of DNA Polymerase β. *J. Biol. Chem.* 293 (39), 15084–15094. doi:10.1074/jbc.ra118.004564

Hughes, C. D., Simons, M., Mackenzie, C. E., Van Houten, B., and Kad, N. M. (2014). Single Molecule Techniques in DNA Repair: a Primer. *DNA Repair* 20, 2–13. doi:10.1016/j.dnarep.2014.02.003

Ibarra, B., Chemla, Y. R., Plyasunov, S., Smith, S. B., Lázaro, J. M., Salas, M., et al. (2009). Proofreading Dynamics of a Processive DNA Polymerase. *EMBO J.* 28 (18), 2794–2802. doi:10.1038/emboj.2009.219

Imai, M., Tago, Y.-i., Ihara, M., Kawata, M., and Yamamoto, K. (2007). Role of the 5′ → 3′ Exonuclease and Klenow Fragment of *Escherichia coli* DNA Polymerase I in Base Mismatch Repair. *Mol. Genet. Genomics* 278 (2), 211–220. doi:10.1007/s00438-007-0239-8

Jain, R., Aggarwal, A. K., and Rechkoblit, O. (2018). Eukaryotic DNA Polymerases. *Curr. Opin. Struct. Biol.* 53, 77–87. doi:10.1016/j.sbi.2018.06.003

Jain, R., Rice, W. J., Malik, R., Johnson, R. E., Prakash, L., Prakash, S., et al. (2019). Cryo-EM Structure and Dynamics of Eukaryotic DNA Polymerase δ Holoenzyme. *Nat. Struct. Mol. Biol.* 26 (10), 955–962. doi:10.1038/s41594-019-0305-z

Jalihal, A. P., Lund, P. E., and Walter, N. G. (2019). Coming Together: RNAs and Proteins Assemble under the Single-Molecule Fluorescence Microscope. *Cold Spring Harb. Perspect. Biol.* 11 (4), a032441. doi:10.1101/cshperspect.a032441

Johnson, S. J., and Beese, L. S. (2004). Structures of Mismatch Replication Errors Observed in a DNA Polymerase. *Cell* 116 (6), 803–816. doi:10.1016/s0092-8674(04)00252-1

Joyce, C. M. (1989). How DNA Travels between the Separate Polymerase and 3′-5′-Exonuclease Sites of DNA Polymerase I (Klenow Fragment). *J. Biol. Chem.* 264 (18), 10858–10866. doi:10.1016/s0021-9258(18)81699-4

Kiefer, J. R., Mao, C., Braman, J. C., and Beese, L. S. (1998). Visualizing DNA Replication in a Catalytically Active Bacillus DNA Polymerase crystal. *Nature* 391 (6664), 304–307. doi:10.1038/34693

Kiss, B., Mudra, D., Török, G., Mártonfalvi, Z., Csík, G., Herényi, L., et al. (2020). Single-particle Virology. *Biophys. Rev.* 12 (5), 1141–1154. doi:10.1007/s12551-020-00747-9

Kunkel, T. A., and Bebenek, K. (2000). DNA Replication Fidelity. *Annu. Rev. Biochem.* 69, 497–529. doi:10.1146/annurev.biochem.69.1.497

Kunkel, T. A. (2004). DNA Replication Fidelity. *J. Biol. Chem.* 279 (17), 16895–16898. doi:10.1074/jbc.r400006200

Lamichhane, R., Berezhna, S. Y., Gill, J. P., Van der Schans, E., and Millar, D. P. (2013). Dynamics of Site Switching in DNA Polymerase. *J. Am. Chem. Soc.* 135 (12), 4735–4742. doi:10.1021/ja311641b

Li, Y., Korolev, S., and Waksman, G. (1998). Crystal Structures of Open and Closed Forms of Binary and Ternary Complexes of the Large Fragment of Thermus Aquaticus DNA Polymerase I: Structural Basis for Nucleotide Incorporation. *EMBO J.* 17 (24), 7514–7525. doi:10.1093/emboj/17.24.7514

Lieberman, K. R., Cherf, G. M., Doody, M. J., Olasagasti, F., Kolodji, Y., and Akeson, M. (2010). Processive Replication of Single DNA Molecules in a Nanopore Catalyzed by Phi29 DNA Polymerase. *J. Am. Chem. Soc.* 132 (50), 17961–17972. doi:10.1021/ja1087612

Lieberman, K. R., Dahl, J. M., Mai, A. H., Akeson, M., and Wang, H. (2012). Dynamics of the Translocation Step Measured in Individual DNA Polymerase Complexes. *J. Am. Chem. Soc.* 134 (45), 18816–18823. doi:10.1021/ja3090302

Lieberman, K. R., Dahl, J. M., Mai, A. H., Cox, A., Akeson, M., and Wang, H. (2013). Kinetic Mechanism of Translocation and dNTP Binding in Individual DNA Polymerase Complexes. *J. Am. Chem. Soc.* 135 (24), 9149–9155. doi:10.1021/ja403640b

Liu, X. J., and Lou, H. Q. (2017). Single Molecular Biology: Coming of Age in DNA Replication. *Yi Chuan* 39 (9), 771–774. doi:10.16288/j.yczz.17-251

Liyanage, P. S., Walker, A. R., Brenlla, A., Cisneros, G. A., Romano, L. J., and Rueda, D. (2017). Bulky Lesion Bypass Requires Dpo4 Binding in Distinct Conformations. *Sci. Rep.* 7 (117383), 17383. doi:10.1038/s41598-017-17643-0

Maier, B., Bensimon, D., and Croquette, V. (2000). Replication by a Single DNA Polymerase of a Stretched Single-Stranded DNA. *Proc. Natl. Acad. Sci.* 97 (22), 12002–12007. doi:10.1073/pnas.97.22.12002

Manosas, M., Spiering, M. M., Ding, F., Bensimon, D., Allemand, J.-F., Benkovic, S. J., et al. (2012). Mechanism of Strand Displacement Synthesis by DNA Replicative Polymerases. *Nucleic Acids Res.* 40 (13), 6174–6186. doi:10.1093/nar/gks253

Maxwell, B. A., and Suo, Z. (2013). Single-molecule Investigation of Substrate Binding Kinetics and Protein Conformational Dynamics of a B-Family Replicative DNA Polymerase. *J. Biol. Chem.* 288 (16), 11590–11600. doi:10.1074/jbc.m113.459982

McCluskey, K., Shaw, E., Lafontaine, D. A., and Penedo, J. C. (2014). Single-molecule Fluorescence of Nucleic Acids. *Methods Mol. Biol.* 1076, 759–791. doi:10.1007/978-1-62703-649-8_35

McHenry, C. S. (2011). Bacterial Replicases and Related Polymerases. *Curr. Opin. Chem. Biol.* 15 (5), 587–594. doi:10.1016/j.cbpa.2011.07.018

McKinney, S. A., Joo, C., and Ha, T. (2006). Analysis of Single-Molecule FRET Trajectories Using Hidden Markov Modeling. *Biophysical J.* 91 (5), 1941–1951. doi:10.1529/biophysj.106.082487

Monachino, E., Spenkelink, L. M., and van Oijen, A. M. (2017). Watching Cellular Machinery in Action, One Molecule at a Time. *J. Cel. Biol.* 216 (1), 41–51. doi:10.1083/jcb.201610025

Morin, J. A., Cao, F. J., Lazaro, J. M., Arias-Gonzalez, J. R., Valpuesta, J. M., Carrascosa, J. L., et al. (2012). Active DNA Unwinding Dynamics during Processive DNA Replication. *Proc. Natl. Acad. Sci.* 109 (21), 8115–8120. doi:10.1073/pnas.1204759109

Morin, J. A., Cao, F. J., Lázaro, J. M., Arias-Gonzalez, J. R., Valpuesta, J. M., Carrascosa, J. L., et al. (2015). Mechano-chemical Kinetics of DNA Replication: Identification of the Translocation Step of a Replicative DNA Polymerase. *Nucleic Acids Res.* 43 (7), 3643–3652. doi:10.1093/nar/gkv204

Morin, J. A., Cao, F. J., Valpuesta, J. M., Carrascosa, J. L., Salas, M., and Ibarra, B. (2012). Manipulation of Single Polymerase-DNA Complexes: a Mechanical View of DNA Unwinding during Replication. *Cell Cycle* 11 (16), 2967–2968. doi:10.4161/cc.21389

Mueller, S. H., Spenkelink, L. M., and van Oijen, A. M. (2019). When Proteins Play Tag: the Dynamic Nature of the Replisome. *Biophys. Rev.* 641-651, 641–651. doi:10.1007/s12551-019-00569-4

Naufer, M. N., Murison, D. A., Rouzina, I., Beuning, P. J., and Williams, M. C. (2017). Single-molecule Mechanochemical Characterization of *E. coli* Pol III Core Catalytic Activity. *Protein Sci.* 26 (7), 1413–1426. doi:10.1002/pro.3152

Okamoto, K., Hiroshima, M., and Sako, Y. (2018). Single-molecule Fluorescence-Based Analysis of Protein Conformation, Interaction, and Oligomerization in Cellular Systems. *Biophys. Rev.* 10 (2), 317–326. doi:10.1007/s12551-017-0366-3

Olasagasti, F., Lieberman, K. R., Benner, S., Cherf, G. M., Dahl, J. M., Deamer, D. W., et al. (2010). Replication of Individual DNA Molecules under Electronic Control Using a Protein Nanopore. *Nat. Nanotech.* 5 (11), 798–806. doi:10.1038/nnano.2010.177

Ollis, D. L., Brick, P., Hamlin, R., Xuong, N. G., and Steitz, T. A. (1985). Structure of Large Fragment of *Escherichia coli* DNA Polymerase I Complexed with dTMP. *Nature* 313 (6005), 762–766. doi:10.1038/313762a0

Olsen, T. J., Choi, Y., Sims, P. C., Gul, O. T., Corso, B. L., Dong, C., et al. (2013). Electronic Measurements of Single-Molecule Processing by DNA Polymerase I (Klenow Fragment). *J. Am. Chem. Soc.* 135 (21), 7855–7860. doi:10.1021/ja311603r

Ordu, O., Lusser, A., and Dekker, N. H. (2016). Recent Insights from *in vitro* Single-Molecule Studies into Nucleosome Structure and Dynamics. *Biophys. Rev.* 8 (Suppl. 1), 33–49. doi:10.1007/s12551-016-0212-z

Pauszek, R. F., 3rd, Lamichhane, R., Rajkarnikar Singh, A., and Millar, D. P. (2021). Single-molecule View of Coordination in a Multi-Functional DNA Polymerase. *Elife* 10, e6046. doi:10.7554/elife.62046

Pljevaljčić, G., Robertson-Anderson, R., van der Schans, E., and Millar, D. (2012). Analysis of RNA Folding and Ribonucleoprotein Assembly by Single-Molecule Fluorescence Spectroscopy. *Methods Mol. Biol.* 875, 271–295. doi:10.1007/978-1-61779-806-1_15

Raia, P., Delarue, M., and Sauguet, L. (2019). An Updated Structural Classification of Replicative DNA Polymerases. *Biochem. Soc. Trans.* 47 (1), 239–249. doi:10.1042/bst20180579

Raper, A. T., and Suo, Z. (2016). Investigation of Intradomain Motions of a Y-Family DNA Polymerase during Substrate Binding and Catalysis. *Biochemistry* 55 (41), 5832–5844. doi:10.1021/acs.biochem.6b00878

Reha-Krantz, L. J. (2010). DNA Polymerase Proofreading: Multiple Roles Maintain Genome Stability. *Biochim. Biophys. Acta (Bba) - Proteins Proteomics* 1804 (5), 1049–1063. doi:10.1016/j.bbapap.2009.06.012

Roy, R., Hohng, S., and Ha, T. (2008). A Practical Guide to Single-Molecule FRET. *Nat. Methods* 5 (6), 507–516. doi:10.1038/nmeth.1208

Santoso, Y., Joyce, C. M., Potapova, O., Le Reste, L., Hohlbein, J., Torella, J. P., et al. (2010). Conformational Transitions in DNA Polymerase I Revealed by Single-Molecule FRET. *Proc. Natl. Acad. Sci.* 107 (2), 715–720. doi:10.1073/pnas.0910909107

Tinoco, I., Jr., and Gonzalez, R. L., Jr. (2011). Biological Mechanisms, One Molecule at a Time. *Genes Dev.* 25 (12), 1205–1231. doi:10.1101/gad.2050011

Voith von Voithenberg, L., and Lamb, D. C. (2018). Single Pair Förster Resonance Energy Transfer: A Versatile Tool to Investigate Protein Conformational Dynamics. *Bioessays* 40 (3). doi:10.1002/bies.201700078

Wu, E. Y., and Beese, L. S. (2011). The Structure of a High Fidelity DNA Polymerase Bound to a Mismatched Nucleotide Reveals an "ajar" Intermediate Conformation in the Nucleotide Selection Mechanism. *J. Biol. Chem.* 286 (22), 19758–19767. doi:10.1074/jbc.m110.191130

Wuite, G. J. L., Smith, S. B., Young, M., Keller, D., and Bustamante, C. (2000). Single-molecule Studies of the Effect of Template Tension on T7 DNA Polymerase Activity. *Nature* 404 (6773), 103–106. doi:10.1038/35003614

Zahn, K. E., Averill, A. M., Aller, P., Wood, R. D., and Doublié, S. (2015). Human DNA Polymerase θ Grasps the Primer Terminus to Mediate DNA Repair. *Nat. Struct. Mol. Biol.* 22 (4), 304–311. doi:10.1038/nsmb.2993

Conflict of Interest: The author declares that the research was conducted in the absence of any commercial or financial relationships that could be construed as a potential conflict of interest.

frontiers in Molecular Biosciences

ORIGINAL RESEARCH
published: 14 February 2022
doi: 10.3389/fmolb.2022.805187

OPEN ACCESS

Edited by:
Whitney Yin,
University of Texas Medical Branch at Galveston, United States

Reviewed by:
Serdal Kirmizialtin,
New York University Abu Dhabi, United Arab Emirates
David Douglas Boehr,
The Pennsylvania State University (PSU), United States

***Correspondence:**
Karen S. Anderson
karen.anderson@yale.edu

†Present Address:
Kathleen M. Frey,
Department of Pharmaceutical Sciences, Fairleigh Dickinson University School of Pharmacy and Health Sciences, Florham Park, NJ, United States
Albert H. Chan,
National Cancer Institute Cancer Research Technology Program, Frederick National Laboratory for Cancer Research, Frederick, MD, United States
Mariela Bollini,
Laboratorio de Química Medicinal, Centro de Investigaciones en Bionanociencias (CIBION)-Consejo Nacional de Investigaciones Científicas y Técnicas (CONICET), Buenos Aires, Argentina

Specialty section:
This article was submitted to Structural Biology, a section of the journal Frontiers in Molecular Biosciences

Received: 29 October 2021
Accepted: 24 January 2022
Published: 14 February 2022

Citation:
Frey KM, Bertoletti N, Chan AH, Ippolito JA, Bollini M, Spasov KA, Jorgensen WL and Anderson KS (2022) Structural Studies and Structure Activity Relationships for Novel Computationally Designed Non-nucleoside Inhibitors and Their Interactions With HIV-1 Reverse Transcriptase. Front. Mol. Biosci. 9:805187. doi: 10.3389/fmolb.2022.805187

Structural Studies and Structure Activity Relationships for Novel Computationally Designed Non-nucleoside Inhibitors and Their Interactions With HIV-1 Reverse Transcriptase

*Kathleen M. Frey[1†], Nicole Bertoletti[1], Albert H. Chan[2†], Joseph A. Ippolito[2], Mariela Bollini[2†], Krasimir A. Spasov[1], William L. Jorgensen[2] and Karen S. Anderson[1,3]**

[1]Department of Pharmacology, Yale University School of Medicine, New Haven, CT, United States, [2]Department of Chemistry, Yale University, New Haven, CT, United States, [3]Department of Molecular Biophysics and Biochemistry, Yale University School of Medicine, New Haven, CT, United States

Reverse transcriptase (RT) from the human immunodeficiency virus continues to be an attractive drug target for antiretroviral therapy. June 2022 will commemorate the 30th anniversary of the first Human Immunodeficiency Virus (HIV) RT crystal structure complex that was solved with non-nucleoside reverse transcriptase inhibitor nevirapine. The release of this structure opened opportunities for designing many families of non-nucleoside reverse transcriptase inhibitors (NNRTIs). In paying tribute to the first RT-nevirapine structure, we have developed several compound classes targeting the non-nucleoside inhibitor binding pocket of HIV RT. Extensive analysis of crystal structures of RT in complex with the compounds informed iterations of structure-based drug design. Structures of seven additional complexes were determined and analyzed to summarize key interactions with residues in the non-nucleoside inhibitor binding pocket (NNIBP) of RT. Additional insights comparing structures with antiviral data and results from molecular dynamics simulations elucidate key interactions and dynamics between the nucleotide and non-nucleoside binding sites.

Keywords: non-nucleoside reverse transcriptase inhibitors, HIV RT, structural studies, computational chemistry, drug design

INTRODUCTION

The HIV-1 (Human Immunodeficiency Virus) is a member of the retroviral family which contains a single-stranded RNA genome and is the major etiological agent involved in the development of acquired immunodeficiency syndrome or AIDS. The World Health Organization now estimates that in 2019 over 40 million people worldwide were infected. The most recent CDC report estimates that in the US over 1.2 million people are infected including about 13% who are unaware of their infections. Over the past decade, the number of people living with HIV has increased, while the annual number of new infections has remained relatively stable. Still, the pace of new infections, at 50,000 per year, continues at far too high a level, particularly among certain socio-economic groups.

TABLE 1 | Antiviral data and solubility measurements for Compounds 1-4.

Cmpd	EC_{50} WT (μM)	CC_{50} WT (μM)	EC_{50} Y181C (μM)	CC_{50} Y181C (μM)	EC_{50} K103N/Y181C (μM)	CC_{50} K103N/Y181C (μM)	Solubility (μg/ml)
(**1**)	1.1	>100	N/A	>100	N/A	>100	N/D
(**2**)[a]	0.0012	4.5	<0.1	3.4	<0.1	2.4	14.2
(**3**)[b]	0.0011	>100	0.008	>100	0.006	>100	9.1
(**4**)[a]	0.001	10.1	0.00057	8.1	0.039	8.5	8.16

Compd = compound; N/A = not active; N/D = not determined.
[a]*(Lee et al., 2015).*
[b]*(Lee et al., 2014).*

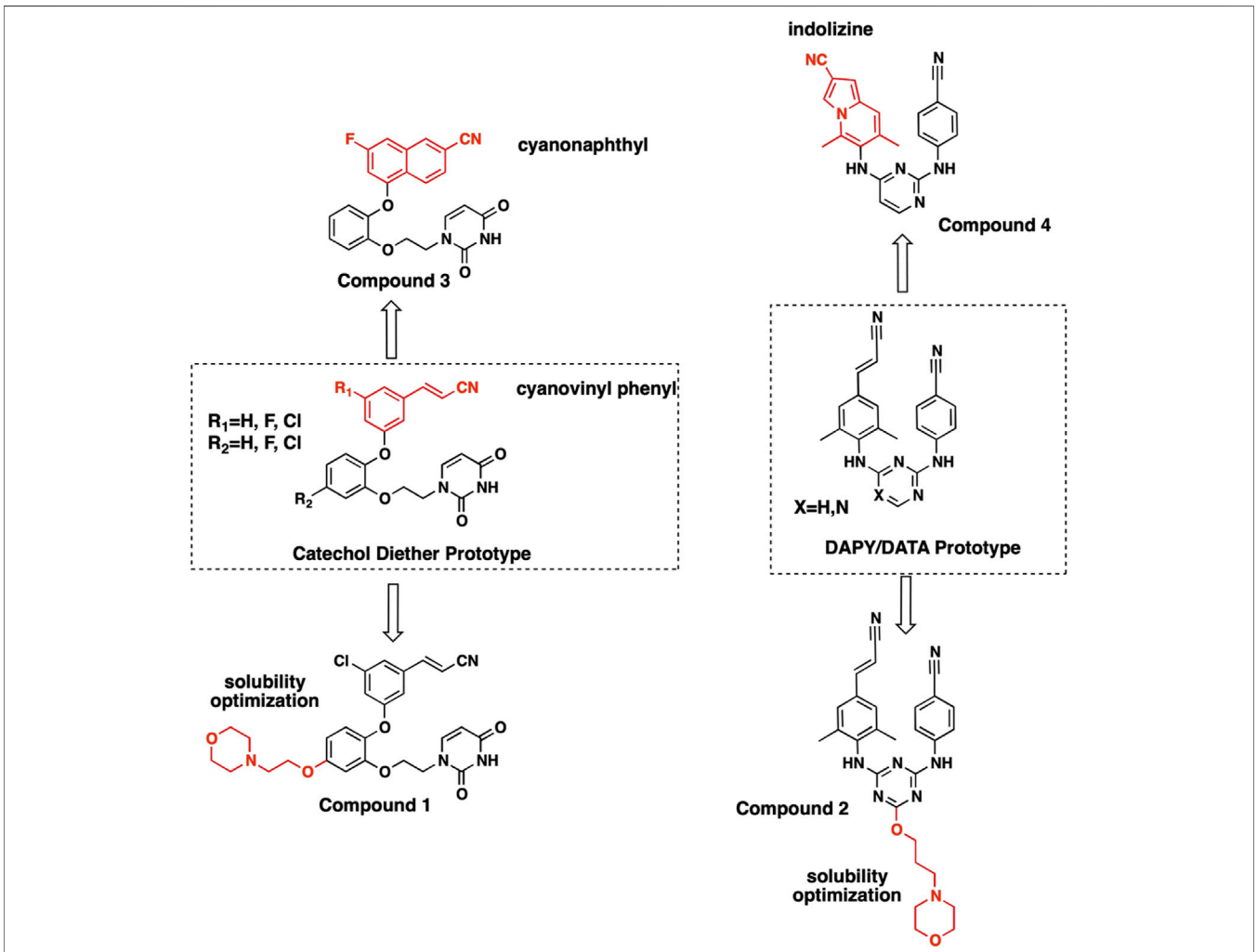

FIGURE 1 | Structures of NNRTI compounds co-crystallized with RT and evaluated for SAR. Synthesis and characterization for compound **1** is provided in Supplementary Material. Synthesis and characterization for compounds 2-4 have been reported previously (Lee et al., 2014; Lee et al., 2015).

With the development of antiretroviral therapy (ART), there has been much needed progress over the past decade. Individuals diagnosed with AIDS no longer face a death sentence, but there continues to be a significant need for new therapeutic strategies, new drugs, and new drug combinations to combat this disease. It is imperative to continue to develop new, effective, and safe antiviral compounds in order to stay in front of the HIV virus with its propensity for rapid mutation and resistance. There are several potential targets in the life cycle of the HIV virus including HIV reverse transcriptase (HIV-RT or RT), HIV protease, and more recently viral entry, attachment, and integration (Richman et al., 2009). Drugs targeting RT remain a cornerstone of AIDS therapy as approximately 90% of conventional therapeutic regimens. The drugs that

TABLE 2 | Data collection and refinement statistics for RT crystal structures in complex with compound **2**.

Structure	RT(WT):2	RT(Y181C):2	RT (K103N/Y181C):2
PDB Code	**7SO1**	**7SO2**	**7SO3**
Data Collection statistics			
Wavelength	1.0	1.0	1.0
Resolution Range	35.58–2.727	42.88–3.089	37.86–2.767
Space Group	C 1 2 1	C 1 2 1	C 1 2 1
Unit Cell: Dimensions, Angles	a = 162.03, b = 73.4, c = 108.525 $\alpha = 90$, $\beta = 100.375$, $\gamma = 90$	a = 161.105, b = 73.101, c = 107.82 $\alpha = 90$, $\beta = 99.629$, $\gamma = 90$	a = 162.597, b = 73.87, c = 108.435 $\alpha = 90$, $\beta = 101.558$, $\gamma = 90$
Unique Reflections	33,088	22,651	31,488
Multiplicity (Redundancy)	3.7	3.6	3.5
Completeness, %	98.18 (90.69)	98.57 (89.51)	97.08 (91.25)
I/sigma	14.9 (2.8)	26.9 (2.2)	25.5 (1.9)
Wilson B-factor	59.87	97.42	73.68
Highest Shell	0.128 (0.296)	0.093 (0.435)	0.113 (0.483)
Refinement Statistics			
R-free	0.2690	0.2879	0.2754
R-work	0.2254	0.2317	0.2291
Average B-factor	70.94	98.19	77.61
RMSD Bonds (Angles)	0.003 (0.70)	0.003 (0.69)	0.004 (0.89)
Ramachandran: Favored, Allowed, Outliers	95.48, 3.79, 0.74	93.97, 5.5, 0.54	97.94, 2.06, 0
Clashscore	4.14	5.24	4.65
Number of Atoms: Protein, Ligands, Solvent	7828, 38, 0	7599, 38, 0	7591, 38, 4

TABLE 3 | Data collection and refinement statistics for RT (WT) crystal structures in complex with compounds 1 and 4, RT (Y181C) with compound 3, and RT (K103N/Y181C) with compound **3**.

Structure	RT(WT):1	RT(WT):4	RT (Y181C):3	RT (K103N/Y181C):3
PDB Code	**7SNP**	**7SNZ**	**7SO4**	**7SO6**
Data Collection Statistics				
Wavelength	1.0	1.0	1.0	1.0
Resolution Range (Highest Shell)	35.597–2.89 (2.95–2.89)	42.830–2.368	37.98–2.946 (3.12–2.946)	41.46–2.793 (2.873–2.793)
Space Group	C 1 2 1	C 1 2 1	C 1 2 1	C 1 2 1
Unit Cell: Dimensions, Angles	a = 224.82, b = 69.048, c = 104.337 $\alpha = 90$, $\beta = 106.292$, $\gamma = 90$	a = 161.909, b = 75.527, c = 108.95 $\alpha = 90$, $\beta = 100.458$, $\gamma = 90$	a = 161.3, b = 73.842, c = 107.063 $\alpha = 90$, $\beta = 100.12$, $\gamma = 90$	a = 161.74, b = 74.17, c = 108.6 $\alpha = 90$, $\beta = 99.369$, $\gamma = 90$
Unique Reflections	34,585	50,672	26,126	31,556
Redundancy (Highest Shell)	3.8 (3.7)	3.7 (3.6)	—	—
Completeness, %	99.43 (99.83)	99.68 (97.39)	98.75 (91.93)	99.31 (94.92)
I/sigma	17.40 (1.9)	25.85 (1.81)	17.82 (2.41)	14.51 (2.62)
Wilson B-factor	83.81	52.40	82.38	74.23
R-merge (Highest Shell)	0.100 (0.588)	0.098 (0.488)	0.053 (0.663)	0.073 (0.571)
Refinement Statistics				
R-free	0.2769	0.2460	0.2716	0.2749
R-work	0.2302	0.2097	0.2284	0.2383
Average B-factor	61.86	59.81	89.17	88.75
RMSD Bonds (Angles)	0.005 (0.95)	0.005 (0.94)	0.002	0.003
Ramachandran: Favored, Allowed, Outliers	94.45, 5.34, 0.21	98.52, 1.27, 0.21	96.87, 3.13, 0	97.46, 2.54, 0
Clashscore	4.14	5.24	3.51	3.98
Number of Atoms: Protein, Ligands, Solvent	7828, 38, 0	7599, 38, 0	7670, 36, 3	7520, 32, 14

target HIV-1 RT are divided into two classes: nucleoside reverse transcriptase inhibitors (NRTIs) and non-nucleoside reverse transcriptase inhibitors (NNRTIs). The rapid development of drug resistance by the error prone RT, off-target side effects, and issues of viral versus host polymerase selectivity continue to necessitate the discovery of more effective NRTIs and NNRTIs with improved safety, pharmacological, and drug resistance profiles.

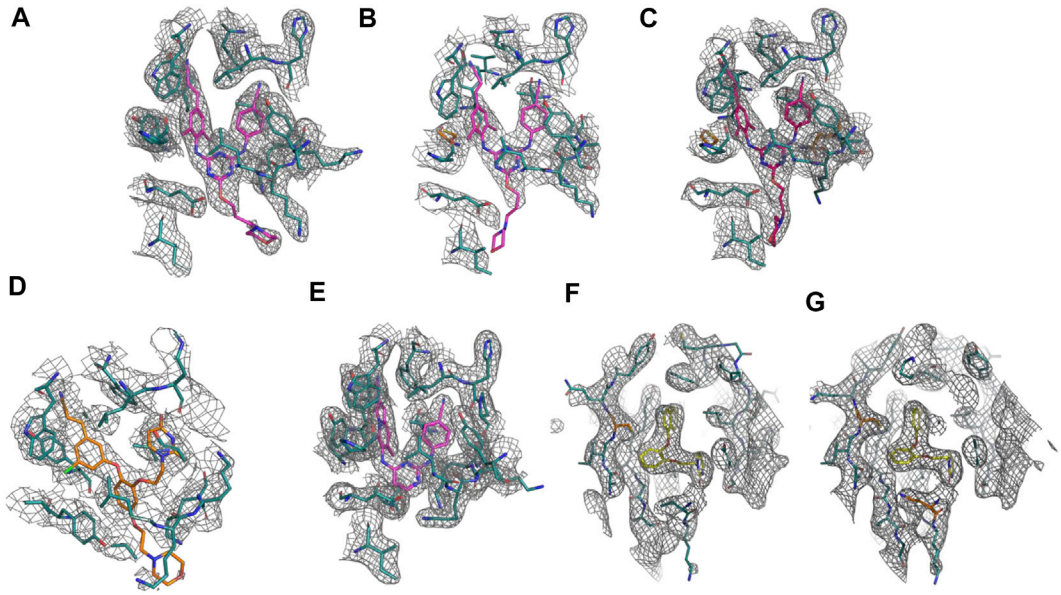

FIGURE 2 | Omit electron density of the non-nucleoside inhibitor binding site for all crystal structure complexes: **(A)** RT (WT):**2**. **(B)** RT (Y181C):**2**. **(C)** RT (K103N/Y181C):**2**. **(D)** RT (WT):**1**. **(E)** RT (WT):**4**. **(F)** RT (Y181C):**3**. **(G)** RT (K103N/Y181C):**3.** Omit electron density maps were generated using simulated annealing omit build in Phenix (Adams et al., 2010).

The first three-dimensional (3D)-structure of RT was solved by the Steitz lab in 1992. This structure was solved in the presence of the NNRTI, nevirapine (Kohlstaedt et al., 1992). The 3-D structure revealed that nevirapine was bound in an allosteric binding pocket 10-Å away from the RT polymerase active site, which is absent in the apo form of RT (Clark et al., 1995; Rodgers et al., 1995). NNRTIs significantly inhibit the catalytic function of RT by binding in the non-nucleoside inhibitor binding pocket (NNIBP). Previous kinetic studies have shown that NNRTIs act as non-competitive inhibitors by slowing the polymerization reaction (Hopkins et al., 1989; Spence et al., 1995b; Rittinger et al., 1995; Nissley et al., 2007).

A major clinical concern in the use of these drugs is the development of resistant strains of HIV harboring mutations in RT (de Bethune, 2010; Iyidogan and Anderson, 2014). For NNRTIs, among the most common resistance mutations are Lys103Asn (K103N) and Tyr181Cys (Y181C), which are observed in 57 and 25% of patients failing treatment (Iyidogan and Anderson, 2014). In particular, Y181C has been a major hurdle in development of NNRTIs (Bollini et al., 2011; Jorgensen et al., 2011; Gubernick et al., 2016); it renders many NNRTIs including nevirapine ineffective. Moreover, nevirapine remains on the World Health Organization (WHO's) Model List of Essential Medicines which is used as a single agent to prevent mother-to-child viral transmission. The double variant Y181C/K103N abrogates efficacy for all NNRTIs except those most recently introduced etravirine, rilpivirine, and doravirine (Janssen et al., 2005; Iyidogan and Anderson, 2014; Martin et al., 2020). More recently, mutations at K101 including K101P have been reported to be problematic with these newer generation NNRTIs including rilpivirine (Balamane et al., 2012). In addition, rilpivirine has very low aqueous solubility and potential cardiotoxicity liabilities due to inhibition of the HERG ion channel that limit dosing regimens (Kudalkar et al., 2018).

Over the past several years, our research has focused on developing improved NNRTIs relative to current FDA approved NNRTIs such as rilpivirine. This includes better pharmacological properties including enhanced aqueous solubility, lack of inhibition on HERG ion channel as well as efficacy on drug resistant HIV variants including Y181C, Y181C/K103N, and K101P. Our strategy combines state-of-the-art technology for *in silico* virtual screening/structure-based drug design, synthetic organic chemistry, mechanistic enzymology and protein crystallography, and pharmacological assays (Kudalkar et al., 2017; Kudalkar et al., 2018). In the current study, we describe the structure activity relationship and structural analysis of some of these NNRTIs and their interactions with HIV-1 RT. Analysis of the crystal structures, paired with antiviral data and molecular dynamics (MD) simulations, elucidate key interactions between the NNRTI and residues in the NNIBP.

MATERIALS AND METHODS

Protein Expression and Purification

RT52A construct expression for RT (WT), RT (Y181C) and RT (K103N/Y181C) were expressed recombinantly in *E. coli* strain BL21(DE3) using methods described previously (Frey et al., 2015). Recombinant RT was purified using cobalt IMAC followed by removal of the N-terminal 6x-histidine tag *via* overnight cleavage with HRV protease. The collected sample

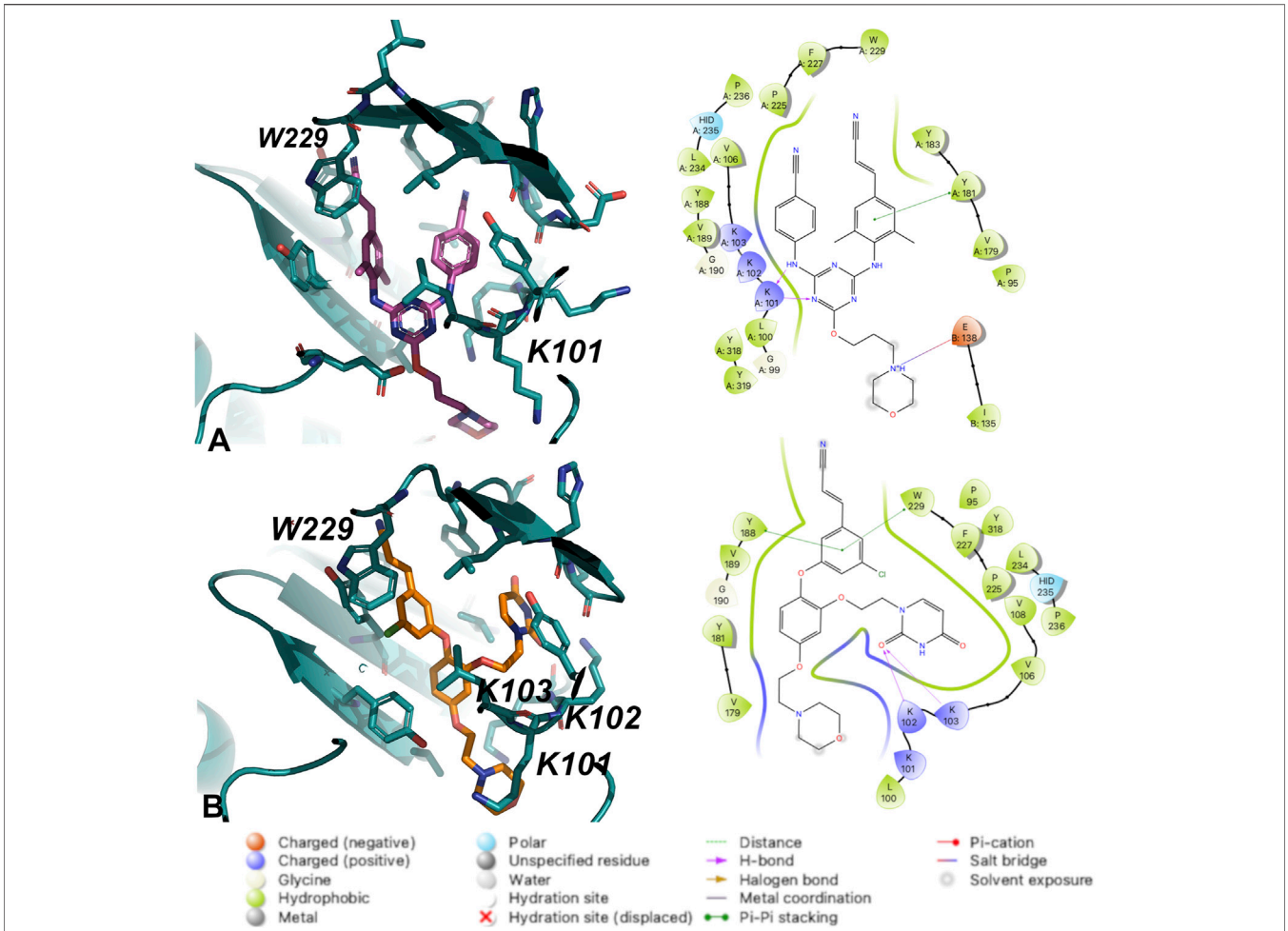

FIGURE 3 | Interactions between **(A)** Compound **2** and **(B)** Compound **1** with residues in the NNIBP of RT (WT). 3D depiction of interactions (left) and 2D schematic diagram of interactions (right). Hydrogen bonds are represented by purple arrows; π-π interactions are represented by green lines between aromatic rings and residues; van der Waals contacts are made between all listed residues within a radius of 4 Å. The key provided specifies residue type, water molecules, and interactions.

was then further purified using ion exchange chromatography. Purified sample was flash frozen with liquid nitrogen until needed for crystallization.

Protein Crystallization, Data Collection, and Refinement

Chemical synthesis for all compounds crystallized with RT enzymes except compound **1** (vide infra) have been reported previously (Frey et al., 2012; Frey et al., 2015). Crystals of RT were prepared using co-crystallization and/or soaking methods described previously. The final optimized condition for crystal growth consisted of 18% (w/v) PEG 8000, 100 mM ammonium sulfate, 15 mM magnesium sulfate, 5 mM spermine, and 50 mM citric acid, pH 7.5. Crystals were transferred to a cryo-solution containing 27% (v/v) ethylene glycol and flash-cooled with liquid nitrogen.

Diffraction datasets for all crystals were collected at Brookhaven NSLS on beamline X29A and APS on beam line 24-ID-E through NE-CAT. Diffraction data was scaled and merged in space group C2 using HKL3000 (Minor et al., 2006). Difference Fourier methods or molecular replacement was used to determined phases using the program Phaser (McCoy et al., 2007). Models for all RT complexes were built into the electron density using program Coot (Emsley et al., 2010) followed by refinement using Phenix Refine (Adams et al., 2010). Several iterations of refinement continued until acceptable R-values and geometric parameters were achieved. All structures were validated using Molprobity and Ramachandran plots (Chen et al., 2010). Structures were analyzed using molecular viewer Pymol (Schrödinger, 2021b). Iterative build omit σ_A-weighted $2mF_0$—F_c electron density maps were generated using Phenix Autobuild (Terwilliger et al., 2008).

Molecular Dynamics Simulation

Crystal structures for compound **1**, compound **2**, RT:dsDNA:dCTP (PDB code: 6P1I), and RT:dsDNA:(-)3TC-TP (PDB code: 6OUN) complexes were used for molecular dynamics (MD) simulations and analysis. All structures were prepared by adding hydrogens, assigning

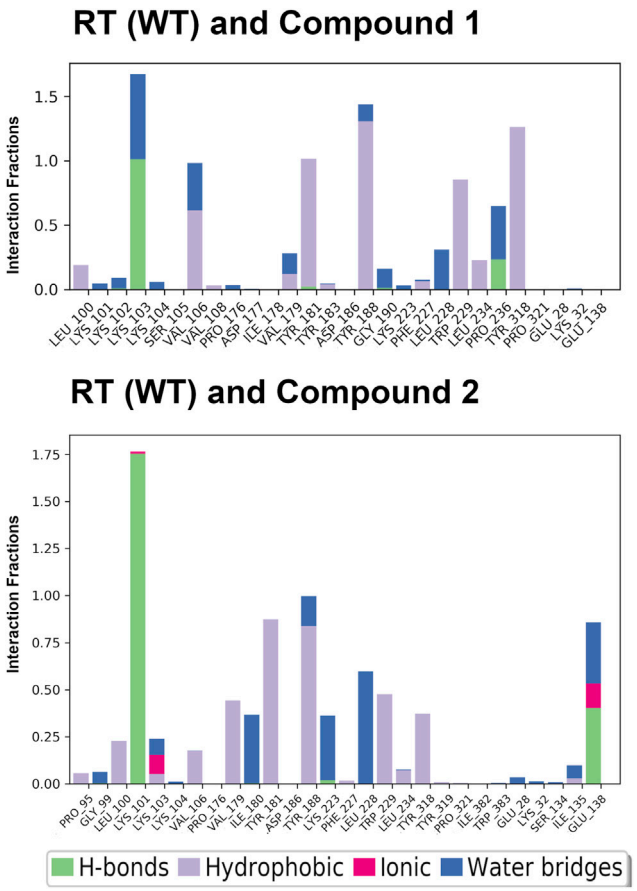

FIGURE 4 | Interaction fractions for RT (WT) and compounds **1** and **2** in the 24 ns simulations. Protein interactions with compounds **1** and **2** were monitored throughout the simulation and are characterized by hydrogen bonds (H-bonds; green); hydrophobic contacts (purple); ionic bonds (pink), and water bridges (blue). Simulation interactions diagrams provided in Supplementary Material (**Supplementary Figures S3, S6**) show % interactions between specific residues and functional groups of the compounds. The interaction fraction describes how long interactions are maintained over the course of the trajectory snapshots. An interaction fraction of 1.0 suggests that this interaction is maintained in the simulation 100% of the time. Interactions fractions >1.0 represent residues capable of making multiple contacts with the compound.

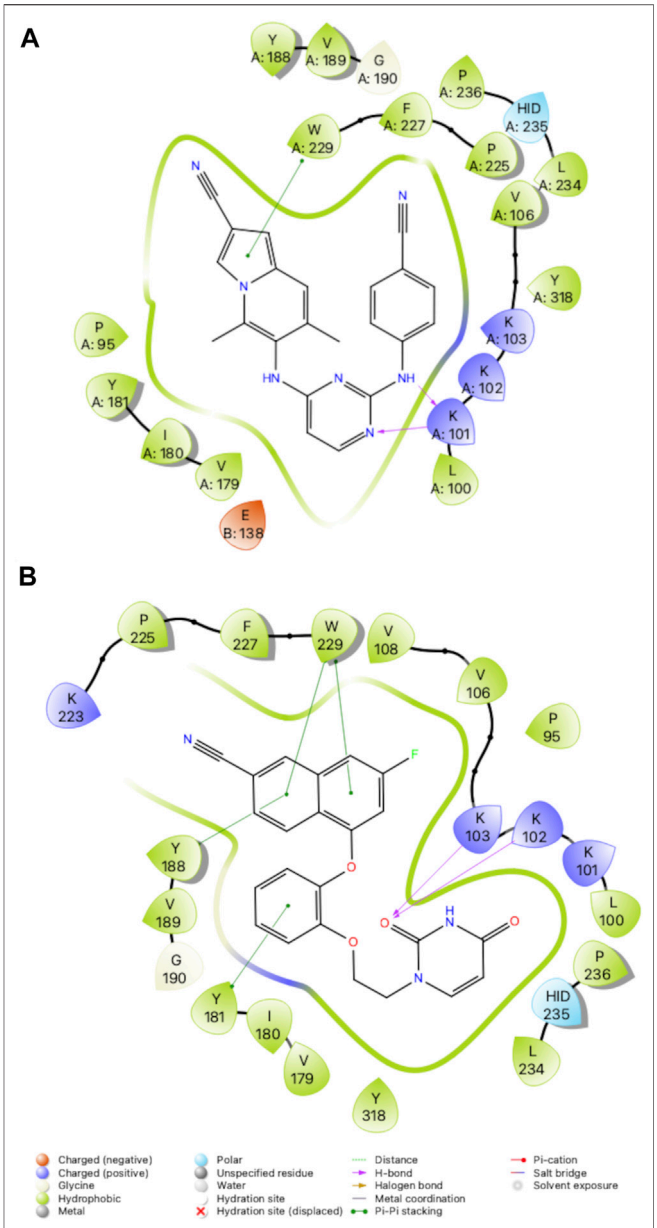

FIGURE 5 | 2D Interaction diagrams for RT complexes with compound **4 (A)** and compound **3 (B)**. Hydrogen bonds are represented by purple arrows; π-π interactions are represented by green lines between aromatic rings and residues; van der Waals contacts are made between all listed residues within a radius of 4 Å. The key provided below specifies residue type, water molecules, and interactions.

charges, capping the termini, and deleting non-interacting water molecules using the Protein Preparation tool in Maestro (Schrödinger, 2021a). The Protein Preparation tool is a collection of programs that prepare biomolecular models for modeling calculations. Prepared models were used to build the system for MD. The models were energy minimized prior to simulation.

Using the System Builder in Desmond (Schrödinger, 2021a), we predefined the solvent model to be TIP4P, calculated the box volume, and then minimized the structure. The system was neutralized by the addition of $Mg2^{+}$ and Cl^{-} ions, simulating a concentration of 0.15 M. The force field applied to each system was OPLS within the System Builder in Desmond. Water molecules and ions around the enzyme were built into the system within the calculated orthorhombic box volume for soluble proteins. The average calculated box volume = 1,337,030 $Å^3$. MD using Desmond (Schrödinger, 2021a) was performed for each model system. The models were relaxed before the simulation. The canonical ensemble or NVT was applied using the Berendsen thermostat (temperature = 300°K) and Berendsen barostat (pressure = 1.01325 bar). Simulation time was set to 24 nanoseconds (ns) to allow for system equilibration. A total of 1000 snapshots (24 picoseconds/interval) were generated for each RT:NNRTI

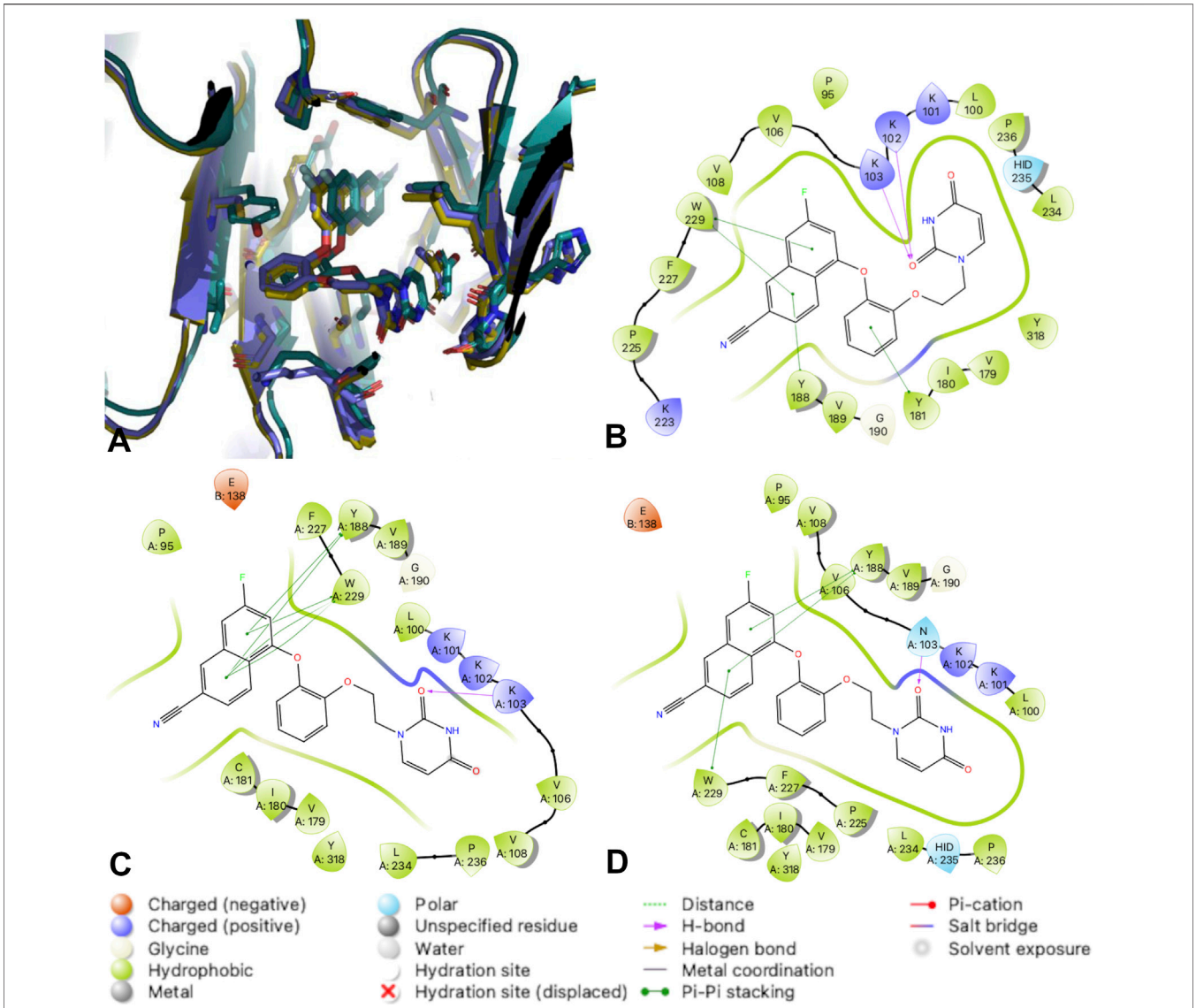

FIGURE 6 | RT complexes with compound 3. **(A)** An overlay of RT (WT) (teal); RT (Y181C) (lavender); and RT (K103N/Y181C) (gold) in complex with compound 3. **(B)** 2D interaction diagram for RT (WT) in complex with compound 3. **(C)** 2D interaction diagram for RT (Y181C) in complex with compound 3. **(D)** 2D interaction diagram for RT (K103N/Y181C) in complex with compound 3. Hydrogen bonds are represented by purple arrows; π-π interactions are represented by green lines between aromatic rings and residues; van der Waals contacts are made between all listed residues within a radius of 4 Å. The key provided specifies residue type, water molecules, and interactions.

complex. Trajectories from each simulation were analyzed using Simulation Interaction Analysis and Simulation Event Analysis programs in Desmond (Schrödinger, 2021a). Simulations were analyzed for equilibration and convergence by examining root mean square deviation (RMSD) versus simulation time plots.

Antiviral Data and Synthesis for Compound 1

The antiviral efficacy of compound **1** was evaluated in MT-2 cells infected with HIV-1 as previously described (Lee et al., 2014; Lee et al., 2015; Kudalkar et al., 2017). Briefly, the antiviral activities against the IIIB strain of HIV-1 were measured using human lymphoid MT-2 T-cells; The antiviral efficacy (EC_{50}) values are obtained as the dose required to achieve 50% protection of the infected cells by the MTT colorimetric method (Pannecouque et al., 2008). Simultaneously, the cytotoxicity (CC_{50}) values for inhibition of growth of MT-2 cells in the absence of virus are determined. The analyses used triplicate samples at each concentration and typically at least two biological replicates. Representative data for compound **1** is shown in (**Supplementary Figure S11**).

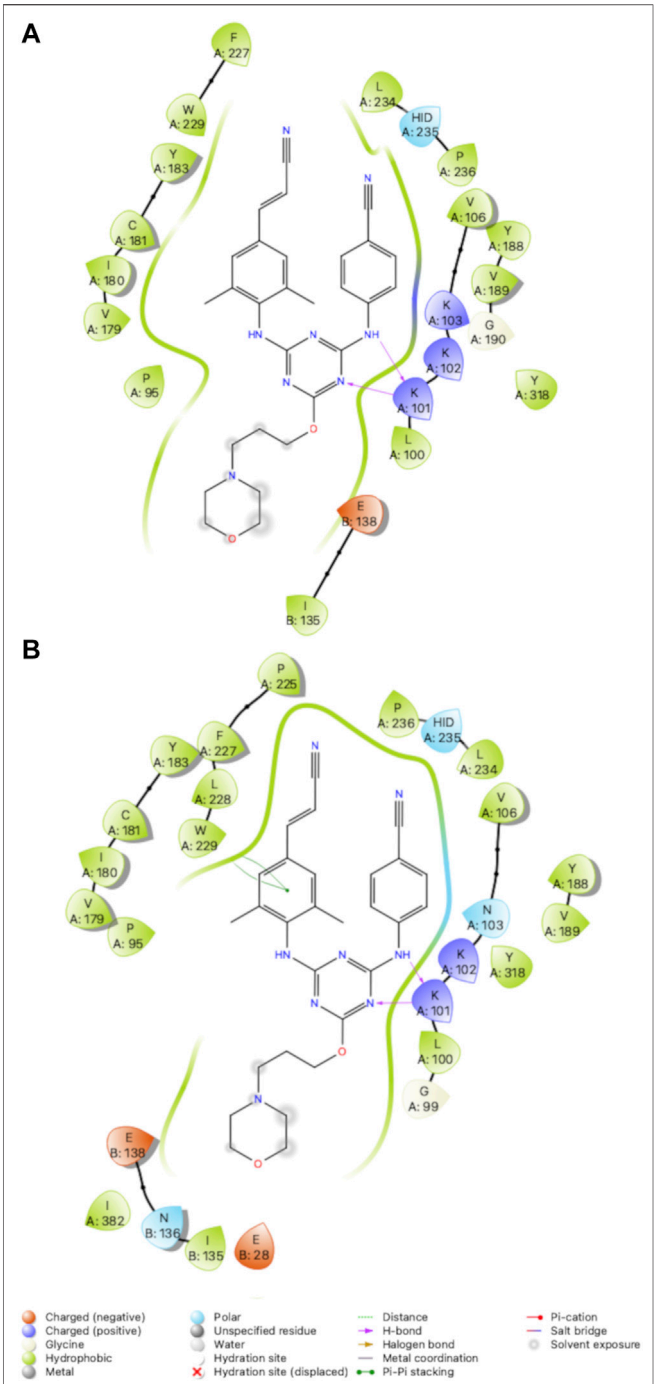

FIGURE 7 | 2D Interaction diagrams for RT (Y181C): Compound **2 (A)** and RT (K103N/Y181C): Compound **2 (B)**. Compound 2 retains hydrogen bonds with K101 and van der Waals contacts with several residues for both variants. Hydrogen bonds are represented by purple arrows; π-π interactions are represented by green lines between aromatic rings and residues; van der Waals contacts are made between all listed residues within a radius of 4 Å. The key provided below specifies residue type, water molecules, and interactions.

The synthesis and characterization data for compound **1** is described in **Supplementary Material**. The synthesis and antiviral activities of compounds **2**-**4** have previously been reported (Lee et al., 2014; Lee et al., 2015). A summary of the antiviral activities and aqueous solubilities is reported in **Table 1**.

RESULTS

For several years, we have been designing NNRTIs targeting variants of RT. **Figure 1** depicts the various compounds designed to target RT and variants. New antiviral data for compound **1** along with 7 new crystal structures help elucidate structure activity relationships (SAR) for major compound classes. The following vignettes summarize our design of these various chemical classes of NNRTIs that possess antiviral activity.

General Structure Details for RT Complexes

We determined crystal structure complexes for wildtype (WT) and variants of RT with various NNRTI compounds. Resolution for the collected crystal structures ranged from 2.368–3.089 Å. Data collection and refinement statistics for all RT complexes are listed in **Tables 2**, **3**. The electron density defines the compounds and all interacting residues for all RT complexes **Figure 2**. The compounds co-crystallized bind the NNIBP causing RT to adopt an "open" conformation commonly observed for RT NNRTI complexes (Das et al., 2008; Lansdon et al., 2010; Frey et al., 2015).

Structure Activity Relationships for Novel NNRTIs

Extensive SAR has been conducted to design novel NNRTIs with improved resistance profiles and optimal physiochemical properties (Bollini et al., 2011; Jorgensen et al., 2011; Lee et al., 2013; Lee et al., 2014; Lee et al., 2015; Chan et al., 2017; Ippolito et al., 2021). Through each iteration of design, new insights were gained regarding key interactions with RT and the NNIBP. The following specific insights led us to develop some of the most potent NNRTIs with improved drug-like properties to date as compared to the current FDA approved NNRTIs as well as others previously published (De Clercq, 1998; De Clercq, 2007; De Clercq, 2010).

DAPY/DATA Versus Catechol Diether

Diarylpyrimidine (DAPY) and diaryltriazine (DATA) SAR led to the development of NNRTIs etravirine and rilpivirine, 2 flexible DAPY NNRTIs that remain potent for RT variants (Das et al., 2008; Lansdon et al., 2010). While the DAPY pharmacophore retained interactions with RT variants, solubility remained a major limitation. The development of the catechol diether system with a terminal uracil resulted in NNRTI compounds with picomolar potency and increased solubility (Bollini et al., 2011). Further optimization focused on improving potency for major RT variants RT (Y181C) and RT (K103N/Y181C) in addition to increasing solubility (Bollini et al., 2011; Bollini et al., 2013a; Bollini et al., 2013b; Frey et al., 2015).

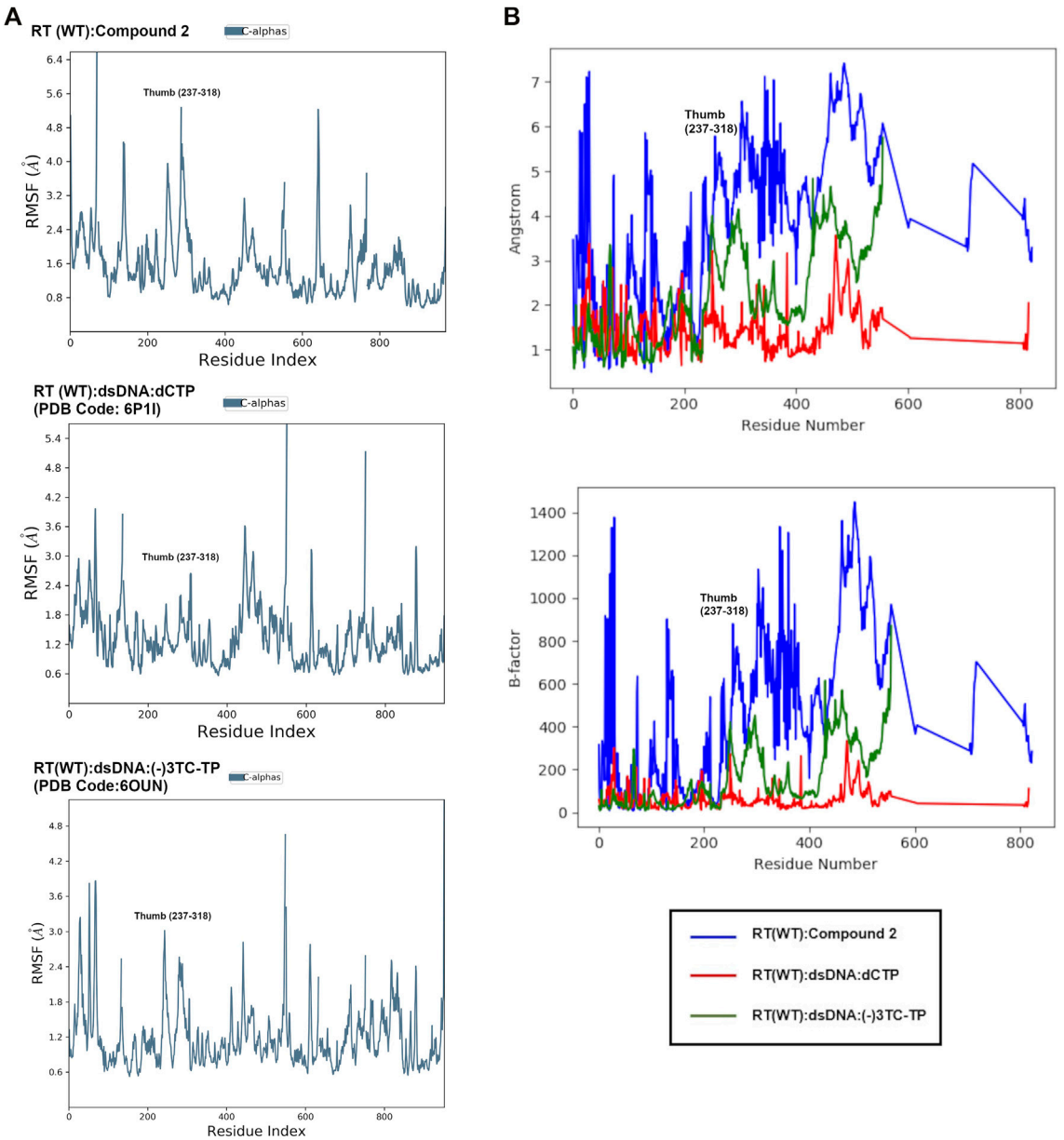

FIGURE 8 | (A): Comparison of root mean square fluctuation (RMSF) values from MD in Å per residue in RT (WT):**2**, RT (WT):dSDNA:dCTP (PDB: 6P1I), and RT (WT):dsDNA:(-)3TC (PDB code: 6OUN). RMSF values in Å were calculated using the RMSF equation in **Supplementary Figure S1** using the initial structure (snapshot or frame 0) as reference. The RMSF values represent the average RMSF for each residue during the 24 ns simulation. **(B)**: Overlay of RMSF values for all 3 complexes in Å and scaled to structure B-factors. A noticeable difference in the thumb region of RT is observed when bound to NNRTI compound 2.

The NNIBP consists of several hydrophobic residues requiring complementary nonpolar NNRTIs. Consequently, solubility for some of the most potent NNRTIs remains a major limitation. In order to improve aqueous solubility, ether-linked morpholine groups were added to DATA and catechol diether systems (Lee et al., 2013). The addition of an ethoxy morpholine to catechol diether compound **1** significantly reduced potency for RT (WT). The attachment of a longer propoxy morpholine to DATA compound **2** retained potency for RT (WT), RT (Y181C), and RT (K103N/Y181C) variants.

Crystal structures for RT (WT) in complex with both **1** and **2** and were determined and analyzed to explain the difference in potency. Compound **2** appears to make several van der Waals contacts with residues in the NNIBP. Compound **2** also hydrogen bonds with K101 *via* the 1) backbone CO and aniline linker; and 2) the backbone NH and the triazine N. Key interactions between RT (WT) and **1** include hydrogen bonds between the uracil carbonyl and 1) the N side chain of K102; and 2) the backbone NH of K103. Additional π-π stacking interactions were observed between Y188 and W229 with compound **1**

along with several van der Waals contacts (**Figure 3**). Based on the analysis from crystal structures, the interactions between compounds **1** and **2** are similar and it remained unclear why **2** retained potency for RT (WT), RT (Y181C) and RT (K103N/Y181C).

The crystal structures could not provide an explanation for why compound **1** has reduced affinity for RT (WT). In order to explore this more, we conducted MD for RT (WT) crystal structures in complex with compound **1** and compound **2**. Results from a 24 ns simulation identified key interactions maintained between ether-linked morpholine compounds **1** and **2**. Compound **2** maintains stronger contacts with K101 and E138 (observed in >100% of snapshots due to multiple bonds with K101), whereas compound **1** only maintains one strong hydrogen bond with K103 **(Figure 4**; **Supplementary Figures S3, S6)**. The propoxy-linked morpholine in compound **2** is longer and makes additional ionic and hydrogen bonds with E138. The ethoxy-linked morpholine in compound **1** does not make any strong contacts with E138 or residues in the binding site. The salt bridge formed between K101 and E138 has been associated with stabilizing NNRTI binding in the NNIBP (Das et al., 2008). In the case of compound **2**, the addition of the propoxy morpholine disrupts the salt bridge interaction but permits an additional contact with E138.

In addition to the stabilizing hydrogen bond, compound **2** maintains more stronger contacts with residues during the simulation **(Figure 4).** Compound **3** makes more van der Waals contacts with hydrophobic residues such as P95, L100, V106, V179, Y181, Y188, W229, L234, Y318, and I135. A π-π interaction between the cyanovinylphenyl of compound 2 and W229 is also apparent.

Cyanovinyl Phenyl to Cyanonaphthyl/Cyanoindolizine

Previous work conducting SAR for DAPYs/DATAs and catechol diether compounds concluded that the CN-vinyl phenyl moiety was important for π-π interaction and van der Waals contacts with aromatic residues Y181, Y188, and W229 (Frey et al., 2012; Frey et al., 2015). Concern for unwanted Michael additions to the cyanovinyl group prompted the design of new derivatives that replaced the CN-vinyl with naphthyl and indolizine aromatics. Replacement of the CN-vinyl phenyl with a CN-naphthyl in the catechol diether series resulted in compounds such as compound **3** (**Figure 2**). The addition of the naphthyl in compound **3** enhances edge-to-face π-π interactions with residues Y188 and W229; each benzene ring in the naphthyl can interact with the residues as opposed to the single phenyl (**Figure 5**). For the DAPY series, replacing the CN-vinyl phenyl with an CN-indolizine in compound **4** increases edge-to-face π-π interaction with W229 (**Figure 5**). The pyrimidine maintains hydrogen bonding with Lys101 and several van der Waals contacts.

Compound **3** also retains potency for RT (Y181C) and RT (K103N/Y181C) variants as shown in the antiviral data (**Table 1**). Analysis of the crystal structures suggest that many key interactions are maintained with residues in the NNIBP (**Figure 6**). Most notably, π-π interactions with residues Y188 and W229 are retained in crystal structures of compound **3** and RT (Y181C) and RT (K103N/Y181C) variants. The key π-π interaction along with the maintained hydrogen bond with K/N103 results in potent nanomolar activity for both variants.

SAR for Variants RT (Y181C) and RT (K103N/Y181C)

Compound **2** has increased solubility compared to other compounds tested (solubility = 14.2 μg/ml and maintains affinity for Y181C and K103N/Y181C variants of RT. **Table 1** reports solubility for compounds **2-4** in addition to antiviral data for variants RT (WT), RT (Y181C) and RT (K103N, Y181C. We compared 3 crystal structures of compound **2** in complex with RT (WT), RT (Y181C), and RT (K103N/Y181C) to examine interactions that promote affinity for Y181C and K103N/Y181C variants. Key interactions such as the 2 hydrogen bonds with K101 are maintained in the RT (Y181C) and RT (K103N/Y181C) crystal structures (**Figure 7**). In both RT (Y181C) and RT (K103N/Y181C) structures, the absence of Y181 causes the DATA scaffold to shift toward aromatic residues Y183, Y188, and W229 to make van der Waals contacts. Antiviral data also complements the analysis from the structures as compound **2** retains nanomolar potency for the virus containing wild-type RT and variants with Y181C and K103N/Y181C mutations (**Table 1**; WT: 0.0012 μM; Y181C: 0.012 μM Y181C/K103N: 0.0013 μM). (Lee et al., 2014; Lee et al., 2015)

MD Simulation to Understand NRTI and NNRTI Effects on Polymerase Activity

NNRTIs have a different mechanism of action than NRTIs that compete with nucleotides for the active site and DNA incorporation. Several kinetic and structural studies have shown that NNRTIs slow the rate of polymerization by causing a conformational change in RT upon binding the allosteric NNIBP (Spence et al., 1995b) Kinetic studies have also shown coordination between the polymerase active site and NNIBP, where NNRTIs enhance the binding of NRTIs (Spence et al., 1995a; Rittinger et al., 1995).

In order to compare the global movement within NRTI/DNA complexes, we conducted additional MD simulations for a catalytic complex of RT bound to a double-stranded DNA primer-template and 1) dCTP (PDB code: 6P1I) and NRTI (-)-3TC (PDB code: 6OUN) (Bertoletti et al., 2019). For the complex with dCTP, we examined root mean square fluctuations (RMSFs) for all residues in RT during the 24 ns simulation. The RMSF values show minimal fluctuations in the catalytic triad (Asp 110, 185, 186), primer grip region (residues 227–235), and thumb subdomain (residues 237–318). The RMSF analysis suggests that regions of RT important for catalysis and DNA binding are stabilized by the primer-template and dCTP in the active site.

In comparison with NNRTIs, we examined the RMSF values for RT (WT) in complex with NNRTI compound 2. RMSF values increase by ~1–2 Å in the thumb region suggesting an increase in residue flexibility (**Figure 8**). Most significantly, RMSF values for the thumb subdomain increases by ~2–5 Å when the NNRTI is bound to RT (WT). Residues in the thumb subdomain appear to

have greater fluctuation when the NNRTI is bound compared to the complex with dsDNA primer-template and dCTP (**Figure 8**).

Interestingly, the thumb subdomain for the (-)-3TC complex are slightly more flexible in the MD simulation, with RMSF values increasing to ~ 1–2 Å in this region when the NRTI is bound **Figure 8**). Some residues that show fluctuation are within the subdomain such as L234, H235, P236, and Y318. Both NRTIs and NNRTIs may increase flexibility in the thumb subdomain and destabilize residues that bind to the primer-template.

DISCUSSION AND CONCLUSION

NNRTIs and NRTIs are commonly used for prevention and treatment of HIV. Structure optimization of NNRTIs is still important for designing new compounds that can overcome physiochemical property and resistance limitations. In our current work, we describe iterations of NNRTI compound optimization guided by crystal structures. We also employed MD simulations to understand the effects of such NNRTIs and NRTIs on RT binding affinity and inhibition of polymerase activity. For all NNRTI complexes examined, the primer grip region is displaced suggesting conformational changes that affect RT polymerase activity. These findings are in accord with our previous kinetic studies to understand how NNRTI binding influences the kinetic reaction pathway (Spence et al., 1995b).

Compound **2** retains affinity for RT (WT), RT (Y181C), and RT (K103N/Y181C) variants. Crystal structures reveal that **2** can maintain most interactions observed in the RT (WT) structure and new interactions with Cys181 of the RT (Y181C) variant are present. The addition of the propoxy linked morpholine also provides potential new interactions while improving solubility. Compounds such as compound **3** and **4** that replace the common cyanovinyl moiety in NNRTIs with CN-naphthyl or CN-indolizine groups also gain additional π- π interactions.

The MD simulations identified structural areas that may be flexible in RT complexes with NNRTIs or DNA/NRTIs. The MD simulations for compound **1** helped identify key reasons why the compound was not effective for RT (WT) compared to compound **2**. The MD simulations also revealed that flexibility of the thumb subdomain is influenced by whether a nucleotide, NNRTI, or NRTI is bound. NNRTIs such as compound **2** appear to increase flexibility of this region in addition to distorting the primer grip and YMDD motif. NRTI (-)-3TC also causes an increase in flexibility within the thumb subdomain. Future work using hydrogen deuterium exchange (HDX) experiments with catalytic complexes can help guide our understanding of how NRTIs and NNRTIs affect polymerase activity alone or synergistically.

DATA AVAILABILITY STATEMENT

The datasets presented in this study can be found in online repositories. The names of the repository/repositories and accession number(s) can be found below: https://www.rcsb.org/ 7SO1 7SNZ 7SNP 7SO3 7SO6 7SO4 7SO2.

AUTHOR CONTRIBUTIONS

KF: Structural data collection, analysis, interpretation; writing original draft; writing-review editing. NB: Structural data interpretation; writing-review editing. JI: Structural data interpretation; writing-review editing. AC: Structural data collection, analysis, interpretation. MB: Compound synthesis and characterization. KS: HIV cell culture assays and interpretation. WJ: Compound synthesis design; data interpretation/conclusions; writing original draft; writing-review editing. KA: Structural data interpretation/conclusions; writing original draft; writing-review editing.

FUNDING

Crystal screening was conducted with support from the Yale Macromolecular X-ray Core Facility (1S10OD018007-01). This research used resources AMX of the National Synchrotron Light Source II, a U.S. Department of Energy (DOE) Office of Science User Facility operated for the DOE Office of Science by Brookhaven National Laboratory under Contract No. DE-SC0012704. The Life Science Biomedical Technology Research resource is primarily supported by the National Institutes of Health, National Institute of General Medical Sciences (NIGMS) through a Center Core P30 Grant (P30GM133893), and by the DOE Office of Biological and Environmental Research (KP1605010). This work is also based upon research conducted at the Northeastern Collaborative Access Team beamlines, which are funded by the National Institute of General Medical Sciences from the National Institutes of Health (P30 GM124165). The Eiger 16M detector on the 24-ID-E beam line is funded by a NIH-ORIP HEI grant (S10OD021527). This research used resources of the Advanced Photon Source; a U.S. Department of Energy (DOE) Office of Science User Facility operated for the DOE Office of Science by Argonne National Laboratory under Contract No. DE-AC02-06CH11357.

ACKNOWLEDGMENTS

Gratitude is expressed to the National Institutes of Health (R01 GM49551, R01 AI155072 to KA and R01 AI44616 to WJ).

SUPPLEMENTARY MATERIAL

The Supplementary Material for this article can be found online at: https://www.frontiersin.org/articles/10.3389/fmolb.2022.805187/full#supplementary-material

REFERENCES

Adams, P. D., Afonine, P. V., Bunkóczi, G., Chen, V. B., Davis, I. W., Echols, N., et al. (2010). PHENIX: a Comprehensive Python-Based System for Macromolecular Structure Solution. *Acta Crystallogr. D Biol. Cryst.* 66 (Pt 2), 213–221. doi:10.1107/S0907444909052925

Balamane, M., Varghese, V., Melikian, G. L., Fessel, W. J., Katzenstein, D. A., and Shafer, R. W. (2012). Panel of Prototypical Recombinant Infectious Molecular Clones Resistant to Nevirapine, Efavirenz, Etravirine, and Rilpivirine. *Antimicrob. Agents Chemother.* 56 (8), 4522–4524. doi:10.1128/AAC.00648-12

Bertoletti, N., Chan, A. H., Schinazi, R. F., Yin, Y. W., and Anderson, K. S. (2019). Structural Insights into the Recognition of Nucleoside Reverse Transcriptase Inhibitors by HIV-1 Reverse Transcriptase: First crystal Structures with Reverse Transcriptase and the Active Triphosphate Forms of Lamivudine and Emtricitabine. *Protein Sci.* 28 (9), 1664–1675. doi:10.1002/pro.3681

Bollini, M., Domaoal, R. A., Thakur, V. V., Gallardo-Macias, R., Spasov, K. A., Anderson, K. S., et al. (2011). Computationally-guided Optimization of a Docking Hit to Yield Catechol Diethers as Potent Anti-HIV Agents. *J. Med. Chem.* 54 (24), 8582–8591. doi:10.1021/jm201134m

Bollini, M., Cisneros, J. A., Spasov, K. A., Anderson, K. S., and Jorgensen, W. L. (2013a). Optimization of Diarylazines as Anti-HIV Agents with Dramatically Enhanced Solubility. *Bioorg. Med. Chem. Lett.* 23 (18), 5213–5216. doi:10.1016/j.bmcl.2013.06.091

Bollini, M., Frey, K. M., Cisneros, J. A., Spasov, K. A., Das, K., Bauman, J. D., et al. (2013b). Extension into the Entrance Channel of HIV-1 Reverse Transcriptase-Crystallography and Enhanced Solubility. *Bioorg. Med. Chem. Lett.* 23 (18), 5209–5212. doi:10.1016/j.bmcl.2013.06.093

Chan, A. H., Lee, W.-G., Spasov, K. A., Cisneros, J. A., Kudalkar, S. N., Petrova, Z. O., et al. (2017). Covalent Inhibitors for Eradication of Drug-Resistant HIV-1 Reverse Transcriptase: From Design to Protein Crystallography. *Proc. Natl. Acad. Sci. USA* 114 (36), 9725–9730. doi:10.1073/pnas.1711463114

Chen, V. B., Arendall, W. B., 3rd, Headd, J. J., Keedy, D. A., Immormino, R. M., Kapral, G. J., et al. (2010). MolProbity: All-Atom Structure Validation for Macromolecular Crystallography. *Acta Crystallogr. D Biol. Cryst.* 66 (Pt 1), 12–21. doi:10.1107/S0907444909042073

Clark, A. D., Jr., Jacobo-Molina, A., Clark, P., Hughes, S. H., and Arnold, E. (1995). [15] Crystallization of Human Immunodeficiency Virus Type 1 Reverse Transcriptase with and without Nucleic Acid Substrates, Inhibitors, and an Antibody Fab Fragment. *Methods Enzymol.* 262, 171–185. doi:10.1016/0076-6879(95)62017-6

Das, K., Bauman, J. D., Clark, A. D., Jr., Frenkel, Y. V., Lewi, P. J., Shatkin, A. J., et al. (2008). High-resolution Structures of HIV-1 Reverse transcriptase/TMC278 Complexes: Strategic Flexibility Explains Potency against Resistance Mutations. *Proc. Natl. Acad. Sci.* 105 (5), 1466–1471. doi:10.1073/pnas.0711209105

de Béthune, M.-P. (2010). Non-nucleoside Reverse Transcriptase Inhibitors (NNRTIs), Their Discovery, Development, and Use in the Treatment of HIV-1 Infection: a Review of the Last 20 Years (1989-2009). *Antiviral Res.* 85 (1), 75–90. doi:10.1016/j.antiviral.2009.09.008

De Clercq, E. (1998). The Role of Non-nucleoside Reverse Transcriptase Inhibitors (NNRTIs) in the Therapy of HIV-1 infection1Presented at the Eleventh International Conference on Antiviral Research, San Diego, CA, 5-10 April 1998.1. *Antiviral Res.* 38, 153–179. doi:10.1016/s0166-3542(98)00025-4

De Clercq, E. (2007). Anti-HIV Drugs. *Verh K Acad. Geneeskd Belg.* 69 (2), 81–104.

De Clercq, E. (2010). Highlights in the Discovery of Antiviral Drugs: A Personal Retrospective. *J. Med. Chem.* 53 (4), 1438–1450. doi:10.1021/jm900932g

Emsley, P., Lohkamp, B., Scott, W. G., and Cowtan, K. (2010). Features and Development ofCoot. *Acta Crystallogr. D Biol. Cryst.* 66 (Pt 4), 486–501. doi:10.1107/S0907444910007493

Frey, K. M., Bollini, M., Mislak, A. C., Cisneros, J. A., Gallardo-Macias, R., Jorgensen, W. L., et al. (2012). Crystal Structures of HIV-1 Reverse Transcriptase with Picomolar Inhibitors Reveal Key Interactions for Drug Design. *J. Am. Chem. Soc.* 134 (48), 19501–19503. doi:10.1021/ja3092642

Frey, K. M., Puleo, D. E., Spasov, K. A., Bollini, M., Jorgensen, W. L., and Anderson, K. S. (2015). Structure-based Evaluation of Non-nucleoside Inhibitors with Improved Potency and Solubility that Target HIV Reverse Transcriptase Variants. *J. Med. Chem.* 58 (6), 2737–2745. doi:10.1021/jm501908a

Gubernick, S. I., Félix, N., Lee, D., Xu, J. J., and Hamad, B. (2016). The HIV Therapy Market. *Nat. Rev. Drug Discov.* 15 (7), 451–452. doi:10.1038/nrd.2016.69

Hopkins, S., Furman, P. A., and Painter, G. R. (1989). Investigation of the Stereochemical Course of DNA Synthesis Catalysed by Human Immunodeficiency Virus Type 1 Reverse Transcriptase. *Biochem. Biophys. Res. Commun.* 163 (1), 106–110. doi:10.1016/0006-291x(89)92105-0

Ippolito, J. A., Niu, H., Bertoletti, N., Carter, Z. J., Jin, S., Spasov, K. A., et al. (2021). Covalent Inhibition of Wild-type HIV-1 Reverse Transcriptase Using a Fluorosulfate Warhead. *ACS Med. Chem. Lett.* 12 (2), 249–255. doi:10.1021/acsmedchemlett.0c00612

Iyidogan, P., and Anderson, K. (2014). Current Perspectives on HIV-1 Antiretroviral Drug Resistance. *Viruses* 6 (10), 4095–4139. doi:10.3390/v6104095

Janssen, P. A. J., Lewi, P. J., Arnold, E., Daeyaert, F., de Jonge, M., Heeres, J., et al. (2005). In Search of a Novel Anti-HIV Drug: Multidisciplinary Coordination in the Discovery of 4-[[4-[[4-[(1e)-2-Cyanoethenyl]-2,6-Dimethylphenyl]amino]-2- Pyrimidinyl]amino]benzonitrile (R278474, Rilpivirine). *J. Med. Chem.* 48 (6), 1901–1909. doi:10.1021/jm040840e

Jorgensen, W. L., Bollini, M., Thakur, V. V., Domaoal, R. A., Spasov, K. A., and Anderson, K. S. (2011). Efficient Discovery of Potent Anti-HIV Agents Targeting the Tyr181Cys Variant of HIV Reverse Transcriptase. *J. Am. Chem. Soc.* 133 (39), 15686–15696. doi:10.1021/ja2058583

Kohlstaedt, L. A., Wang, J., Friedman, J. M., Rice, P. A., and Steitz, T. A. (1992). Crystal Structure at 3.5 Å Resolution of HIV-1 Reverse Transcriptase Complexed with an Inhibitor. *Science* 256, 1783–1790. doi:10.1126/science.1377403

Kudalkar, S. N., Beloor, J., Chan, A. H., Lee, W.-G., Jorgensen, W. L., Kumar, P., et al. (2017). Structural and Preclinical Studies of Computationally Designed Non-Nucleoside Reverse Transcriptase Inhibitors for Treating HIV Infection. *Mol. Pharmacol.* 91 (4), 383–391. doi:10.1124/mol.116.107755

Kudalkar, S. N., Beloor, J., Quijano, E., Spasov, K. A., Lee, W.-G., Cisneros, J. A., et al. (2018). From In Silico Hit to Long-Acting Late-Stage Preclinical Candidate to Combat HIV-1 Infection. *Proc. Natl. Acad. Sci. USA* 115 (4), E802–E811. doi:10.1073/pnas.1717932115

Lansdon, E. B., Brendza, K. M., Hung, M., Wang, R., Mukund, S., Jin, D., et al. (2010). Crystal Structures of HIV-1 Reverse Transcriptase with Etravirine (TMC125) and Rilpivirine (TMC278): Implications for Drug Design. *J. Med. Chem.* 53 (10), 4295–4299. doi:10.1021/jm1002233

Lee, W.-G., Gallardo-Macias, R., Frey, K. M., Spasov, K. A., Bollini, M., Anderson, K. S., et al. (2013). Picomolar Inhibitors of HIV Reverse Transcriptase Featuring Bicyclic Replacement of a Cyanovinylphenyl Group. *J. Am. Chem. Soc.* 135 (44), 16705–16713. doi:10.1021/ja408917n

Lee, W.-G., Frey, K. M., Gallardo-Macias, R., Spasov, K. A., Bollini, M., Anderson, K. S., et al. (2014). Picomolar Inhibitors of HIV-1 Reverse Transcriptase: Design and Crystallography of Naphthyl Phenyl Ethers. *ACS Med. Chem. Lett.* 5 (11), 1259–1262. doi:10.1021/ml5003713

Lee, W.-G., Frey, K. M., Gallardo-Macias, R., Spasov, K. A., Chan, A. H., Anderson, K. S., et al. (2015). Discovery and Crystallography of Bicyclic Arylaminoazines as Potent Inhibitors of HIV-1 Reverse Transcriptase. *Bioorg. Med. Chem. Lett.* 25 (21), 4824–4827. doi:10.1016/j.bmcl.2015.06.074

Martin, E. A., Lai, M.-T., Ngo, W., Feng, M., Graham, D., Hazuda, D. J., et al. (2020). Review of Doravirine Resistance Patterns Identified in Participants during Clinical Development. *J. Acquir Immune Defic. Syndr.* 85 (5), 635–642. doi:10.1097/QAI.0000000000002496

McCoy, A. J., Grosse-Kunstleve, R. W., Adams, P. D., Winn, M. D., Storoni, L. C., and Read, R. J. (2007). Phasercrystallographic Software. *J. Appl. Cryst.* 40 (Pt 4), 658–674. doi:10.1107/S0021889807021206

Minor, W., Cymborowski, M., Otwinowski, Z., and Chruszcz, M. (2006). HKL-3000: the Integration of Data Reduction and Structure Solution - from Diffraction Images to an Initial Model in Minutes. *Acta Crystallogr. D Biol. Cryst.* 62 (Pt 8), 859–866. doi:10.1107/S0907444906019949

Nissley, D. V., Radzio, J., Ambrose, Z., Sheen, C.-W., Hamamouch, N., Moore, K. L., et al. (2007). Characterization of Novel Non-nucleoside Reverse Transcriptase (RT) Inhibitor Resistance Mutations at Residues 132 and 135 in the 51 kDa Subunit of HIV-1 RT. *Biochem. J.* 404 (1), 151–157. doi:10.1042/bj20061814

Pannecouque, C., Daelemans, D., and De Clercq, E. (2008). Tetrazolium-based Colorimetric Assay for the Detection of HIV Replication Inhibitors: Revisited 20 Years Later. *Nat. Protoc.* 3 (3), 427–434. doi:10.1038/nprot.2007.517

Richman, D. D., Margolis, D. M., Delaney, M., Greene, W. C., Hazuda, D., and Pomerantz, R. J. (2009). The challenge of Finding a Cure for HIV Infection. *Science* 323 (5919), 1304–1307. doi:10.1126/science.1165706

Rittinger, K., Divita, G., and Goody, R. S. (1995). Human Immunodeficiency Virus Reverse Transcriptase Substrate-Induced Conformational Changes and the Mechanism of Inhibition by Nonnucleoside Inhibitors. *Proc. Natl. Acad. Sci.* 92 (17), 8046–8049. doi:10.1073/pnas.92.17.8046

Rodgers, D. W., Gamblin, S. J., Harris, B. A., Ray, S., Culp, J. S., Hellmig, B., et al. (1995). The Structure of Unliganded Reverse Transcriptase from the Human Immunodeficiency Virus Type 1. *Proc. Natl. Acad. Sci.* 92 (4), 1222–1226. doi:10.1073/pnas.92.4.1222

Schrödinger (2021a). Desmond Molecular Dynamics System, D. E. Shaw Research. New York, NY: Maestro-Desmond Interoperability Tools.

Schrödinger (2021b). The PyMOL Molecular Graphics System. Version 2.0. Schrödinger, LLC.

Spence, R. A., Kati, W. M., Anderson, K. S., and Johnson, K. A. (1995a). Mechanism of Inhibition of HIV-1 Reverse Transcriptase by Nonnucleoside Inhibitors. *Science* 267 (5200), 988–993. doi:10.1126/science.7532321

Spence, R. A., Kati, W. M., Anderson, K. S., and Johnson, K. A. (1995b). Mechanism of Inhibition of HIV-1 Reverse Transcriptase by Nonnucleoside Inhibitors. *Science* 267 (17), 988–993. doi:10.1126/science.7532321

Terwilliger, T. C., Grosse-Kunstleve, R. W., Afonine, P. V., Moriarty, N. W., Adams, P. D., Read, R. J., et al. (2008). Iterative-build OMIT Maps: Map Improvement by Iterative Model Building and Refinement without Model Bias. *Acta Crystallogr. D Biol. Cryst.* 64 (Pt 5), 515–524. doi:10.1107/S0907444908004319

Conflict of Interest: WJ and KA are listed as the inventors on a patent issued to Yale University on intellectual property associated with some of these compounds (US Patent 9,382,245 (2016)).

The remaining authors declare that the research was conducted in the absence of any commercial or financial relationships that could be construed as a potential conflict of interest.

Publisher's Note: All claims expressed in this article are solely those of the authors and do not necessarily represent those of their affiliated organizations, or those of the publisher, the editors and the reviewers. Any product that may be evaluated in this article, or claim that may be made by its manufacturer, is not guaranteed or endorsed by the publisher.

frontiers in Molecular Biosciences

ORIGINAL RESEARCH
published: 09 March 2022
doi: 10.3389/fmolb.2022.808036

Human Mitochondrial DNA Polymerase Metal Dependent UV Lesion Bypassing Ability

Joon Park[1,2‡], Noe Baruch-Torres[3†‡], Shigenori Iwai[4], Geoffrey K. Herrmann[1,2], Luis G. Brieba[3] and Y. Whitney Yin[1,2]**

[1]Department of Biochemistry and Molecular Biology, University of Texas Medical Branch, Galveston, TX, United States, [2]Sealy Center for Structural Biology and Molecular Biophysics, University of Texas Medical Branch, Galveston, TX, United States, [3]Laboratorio Nacional de Genómica para la Biodiversidad, Centro de Investigación y de Estudios Avanzados del Instituto Politécnico Nacional, Irapuato, Mexico, [4]Division of Chemistry, Graduate School of Engineering Science, Osaka University, Toyonaka, Japan

OPEN ACCESS

Edited by:
Gianluca Molla,
University of Insubria, Italy

Reviewed by:
Sue Cotterill,
St George's University of London, United Kingdom
Joon-Hwa Lee,
Gyeongsang National University, South Korea

***Correspondence:**
Luis G. Brieba
luis.brieba@cinvestav.mx
Y. Whitney Yin
ywyin@utmb.edu

†Present address:
Department of Biochemistry and Molecular Biology, University of Texas Medical Branch, Galveston, TX, United States

‡These authors have contributed equally to this work.

Specialty section:
This article was submitted to Structural Biology, a section of the journal Frontiers in Molecular Biosciences

Received: 02 November 2021
Accepted: 11 January 2022
Published: 09 March 2022

Citation:
Park J, Baruch-Torres N, Iwai S, Herrmann GK, Brieba LG and Yin YW (2022) Human Mitochondrial DNA Polymerase Metal Dependent UV Lesion Bypassing Ability. Front. Mol. Biosci. 9:808036. doi: 10.3389/fmolb.2022.808036

Human mitochondrial DNA contains more UV-induced lesions than the nuclear DNA due to lack of mechanism to remove bulky photoproducts. Human DNA polymerase gamma (Pol γ) is the sole DNA replicase in mitochondria, which contains a polymerase (*pol*) and an exonuclease (*exo*) active site. Previous studies showed that Pol γ only displays UV lesion bypassing when its exonuclease activity is obliterated. To investigate the reaction environment on Pol γ translesion activity, we tested Pol γ DNA activity in the presence of different metal ions. While Pol γ is unable to replicate through UV lesions on DNA templates in the presence of Mg^{2+}, it exhibits robust translesion DNA synthesis (TLS) on cyclobutane pyrimidine dimer (CPD)-containing template when Mg^{2+} was mixed with or completely replaced by Mn^{2+}. Under these conditions, the efficiency of Pol γ′s TLS opposite CPD is near to that on a non-damaged template and is 800-fold higher than that of exonuclease-deficient Pol γ. Interestingly, Pol γ exhibits higher exonuclease activity in the presence of Mn^{2+} than with Mg^{2+}, suggesting Mn^{2+}-stimulated Pol γ TLS is not via suppressing its exonuclease activity. We suggest that Mn^{2+} ion expands Pol γ′s *pol* active site relative to Mg^{2+} so that a UV lesion can be accommodated and blocks the communication between *pol* and *exo* active sites to execute translesion DNA synthesis.

Keywords: mitochondrial DNA, DNA polymerase gamma, UV lesion, metal-dependence, TLS

INTRODUCTION

Ultraviolet (UV) exposure of DNA causes dimerization of two adjacent pyrimidines, forming cyclobutane pyrimidine dimers (CPDs) or (6-4) pyrimidine-pyrimidones ((6-4)PP), which stalls replicating polymerases (Varghese and Wang, 1967a; Varghese and Wang, 1967b; Brash and Haseltine, 1982). Human mitochondria lack nucleotide excision repair or photolyase that removes the photoproducts (Maher et al., 1976; Maher et al., 1979; Maher et al., 1982); therefore, mitochondrial DNA replication machinery would inevitably encounter the UV photoproducts. Increasing sun exposure is correlated to a large spectrum of mitochondrial DNA (mtDNA) deletions in dermis, which, albeit unknown in mechanism, has been used as a biomarker for UV exposure and chronological aging (Birch-Machin et al., 1998; Kawasaki et al., 2000; Ray et al., 2000; Harbottle et al., 2010; Bharti et al., 2014). Deletions and mutations of mtDNA are also associated with skin cancers (Durham et al., 2003; Yang et al., 2004).

TABLE 1 | Sequences of DNA templates and primer.

Name	Sequence
P_N	5′-AGC TAT GAC CAT GAT TAC GAA TTG CTT-3′
T-ND	3′- TCG ATA CTG GTA CTA ATG CTT AAC GAA TTA AGC ACG TCC GTA CCA TCG A-5′
T-CPD	3′- TCG ATA CTG GTA CTA ATG CTT AAC GAA **T<>T_{CPD}**A AGC ACG TCC GTA CCA TCG A-5′
T-(6–4)PP	3′- TCG ATA CTG GTA CTA ATG CTT AAC GAA **T<>T_{6-4}**A AGC ACG TCC GTA CCA TCG A-5′

Human mitochondria DNA is replicated by DNA polymerase gamma (Pol γ), which consists of a catalytic subunit Pol γA and a dimeric accessory subunit Pol γB. Pol γ possesses activities of 5′-3′ polymerization (*pol*) for DNA synthesis, 3′-5′ exonuclease (*exo*) for proofreading, and 5′-deoxyribose phosphate lyase for DNA repair. Pol γB has no intrinsic enzymatic activity, but it accelerates polymerization rate, increases affinity to DNA, and enhances processivity of the holoenzyme (Johnson et al., 2000; Johnson and Johnson, 2001; Lee et al., 2010). Pol γA belongs to the A-family polymerases that are single polypeptide enzymes structurally resembling a right-hand shape and containing fingers, palm, and thumb domains (Steitz, 1999; Garcia-Diaz and Bebenek, 2007; Bębenek and Ziuzia-Graczyk, 2018). Other replicative A-family DNA polymerase members include bacterial DNA polymerase I and phage T7 DNA polymerase.

All known DNA polymerases require divalent metal ions to catalyze DNA synthesis. A general mechanism of two-metal-ion catalysis established a foundation for DNA and RNA polymerases' enzymatic reactions (Steitz and Steitz, 1993). An exonuclease-deficient Pol γ variant was shown to have limited translesion DNA synthesis (TLS) activity on UV lesion-containing DNA in the presence of Mg^{2+}, suggesting that Pol γ possesses intrinsic TLS ability (Kasiviswanathan et al., 2012). Mitochondria are the main storage site of intracellular Mn^{2+} ion (Maynard and Cotzias, 1955; Liccione and Maines, 1988; Gavin et al., 1990; Gavin et al., 1992), which raises an important question on impact of Mn^{2+} or Mg^{2+}/Mn^{2+} mixture on Pol γ mtDNA replication as well as TLS.

We report here studies of the A-family member Pol γ lesion bypassing across UV lesions in the presence of different metal ions. We show that Pol γ is unable to replicate past the CPD- or (6-4)PP-containing DNA template in the presence of Mg^{2+}, but displays efficient TLS ability comparable to that on the non-damaged template in the presence of Mn^{2+} or Mg^{2+}/Mn^{2+} mixture. Mn^{2+} promotes TLS activity without involvement of the polymerase's exonucleolytic activity. The Mn^{2+}-mediated *trans*-UV lesion DNA synthesis appears uniquely to mitochondrial DNA polymerase and is absent in other A-family DNA polymerases tested. These results also give a novel insight into the metal-regulated error recognition and communication between the *pol* and *exo* active sites in Pol γ.

RESULTS

Mn^{2+} Ion Stimulates Robust Translesion DNA Synthesis Across CPD but Not (6-4)PP

DNA templates (49 nt) containing either a CPD (T-CPD) or (6-4)PP (T-(6-4)PP) (**Table 1**) at the 28th position from the 3′-end was synthesized as described in Methods. Pol γ translesion replication was first tested on a 27 nt primer (P_N) annealed to the T-CPD where the 3′- thymine (3′- T) in the CPD serves as the coding base (**Figure 1A**, *lanes* 9–16, **Table 1**). Time-dependent (0–20 min) primer extension assay was conducted in the presence of Mg^{2+}. As a control, a parallel assay was carried out on a non-damaged template (T-ND) with identical sequence except that the CPD is replaced by 2 dT (**Figure 1A**, *lanes* 1–8, **Table 1**). In anticipation of higher polymerase activity on T-ND, the Pol γ concentration was reduced (see Methods). For convenience, only the full-length product formation rate at normalized enzyme concentration was used for rate calculation. Full-length formation rate of Pol γ on T-ND was 4.5 nM/s (**Figure 1C**). However, on T-CPD, the primer was not extended, but instead was degraded to P_{N-1} to P_{N-3} over time (**Figure 1A** *lanes* 9–16).

To evaluate the effect of high Mn^{2+} content in mitochondria on Pol γ activity, we substitute Mg^{2+} with Mn^{2+} and repeated the above experiments. In stark contrast to results with Mg^{2+}, Pol γ exhibited strong TLS across CPD in the presence of Mn^{2+} (**Figure 1B**, *lanes* 9–16). The rates of full-length product formation by Pol γ on T-CPD were calculated to be 0.58 nM/s, which is only 1.7-fold lower than that on T-ND at 1 nM/s (**Figure 1C**). Interestingly, Pol γ is 4.5-fold less efficient on the non-damaged template in the presence of Mn^{2+} than in the presence of Mg^{2+}.

Previous studies showed that exonuclease-deficient (*exo*-) Pol γ displayed limited intrinsic CPD-bypassing ability (Kasiviswanathan et al., 2012). To assess whether Mn^{2+} plays a redundant role with exonuclease activity in Pol γ TLS activity, Pol γ *exo*- (D198A/E200A) (Spelbrink et al., 2000) was analyzed on T-ND and T-CPD. In the presence of Mg^{2+}, Pol γ *exo*- extended a small amount of the primer P_N over the CPD site to full-length product, consistent with the previously reported data (Kasiviswanathan et al., 2012). However, a predominant amount of primer was extended by only a single nucleotide and formed product P_{N+1} (**Figure 2A**, *lanes* 1–8). Accumulation of the P_{N+1} indicates that silencing exonuclease enables the polymerase to synthesize across the 3′-T but not 5′-T of the CPD, suggesting that synthesis using the 5′-T as a coding base is the rate-limiting step of Pol γ TLS.

In the presence of Mn^{2+}, Pol γ *exo*- exhibited significantly elevated TLS activity (**Figure 2B**, *lanes* 9–16). The rate of Pol γ *exo*- full-length product formation on T-CPD was calculated to be 0.81 nM/s with Mn^{2+}, which is more than 800-fold increase than that with Mg^{2+} (0.001 nM/s) and exceeds that of wild-type (0.58 nM/s) (**Figure 2C**), confirming that suppressing *exo* activity indeed increases TLS in the presence of either metal ion. P_{N+1} product was drastically diminished, indicating Mn^{2+} facilitates Pol γ to overcome the energy barrier at the rate-limiting

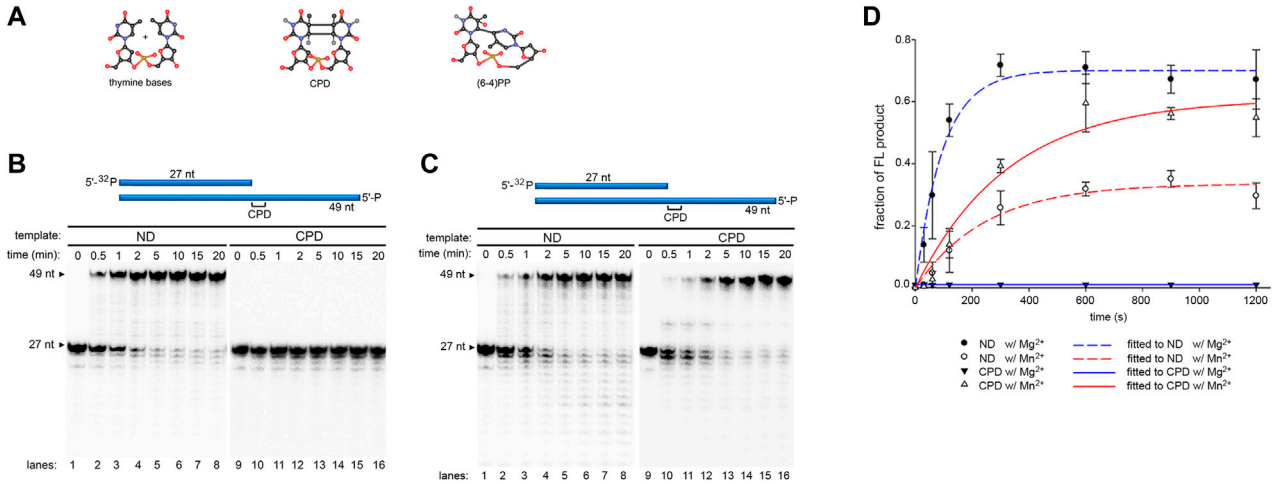

FIGURE 1 | DNA synthesis of wild-type Pol γ on non-damaged and CPD-containing templates in the presence of Mg^{2+} or Mn^{2+}. **(A)** Structure of thymine bases, CPD, and (6-4)PP where nitrogen is represented in blue spheres, oxygen in red spheres, carbon in black spheres, and phosphorus in golden spheres. **(B)** Time-dependent DNA synthesis of wild-type Pol γ on 5′-^{32}P-Primer N (P_N) annealed to a non-damaged template (T-ND) (*lanes* 1–8) or CPD-containing template (T-CPD) (lanes 9–16) in the presence of Mg^{2+}. **(C)** Time-dependent DNA synthesis of wild-type Pol γ on 5′-^{32}P-P_N annealed to T-ND (lanes 1–8) or T-CPD (lanes 9–16) in the presence of Mn^{2+}. **(D)** Quantification of normalized full-length (FL) products from **(B)** and **(C)** over time in seconds. The results are presented as mean and standard deviation from three independent experiments.

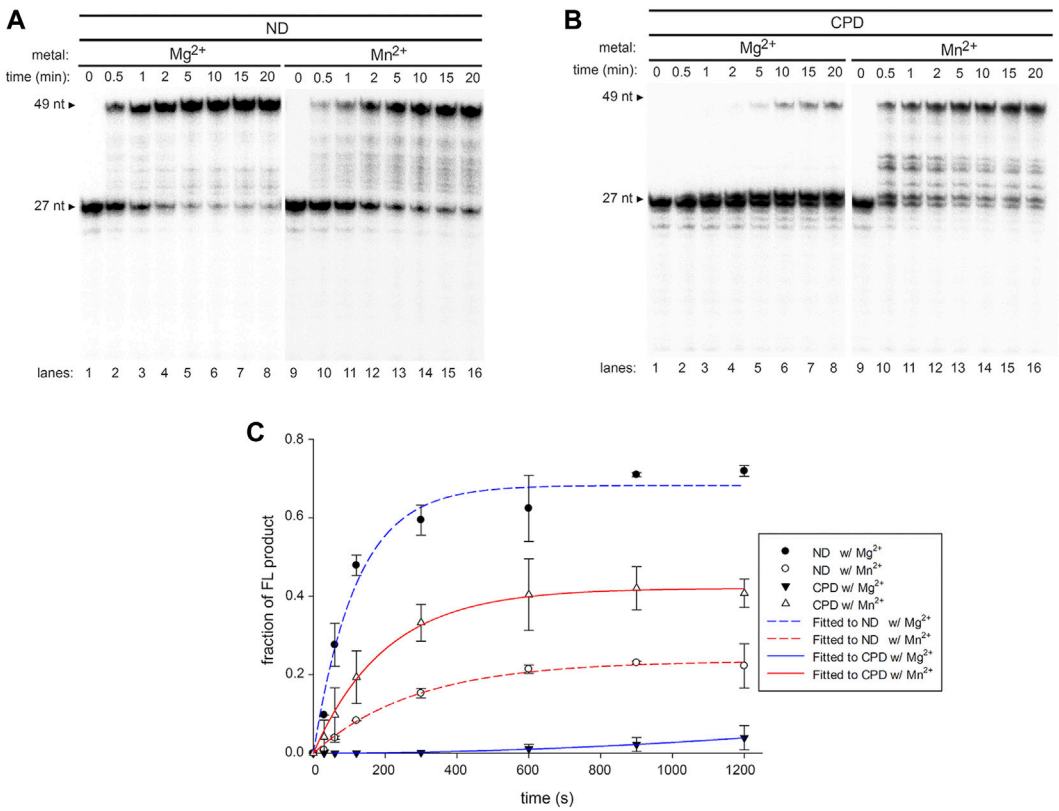

FIGURE 2 | DNA synthesis of exonuclease-deficient Pol γ on non-damaged and CPD-containing templates in the presence of Mg^{2+} or Mn^{2+}. **(A)** Time-dependent DNA synthesis of exonuclease-deficient (*exo*-) Pol γ on 5′-^{32}P-P_N annealed to T-ND in the presence of Mg^{2+} (lanes 1–8) or Mn^{2+} (lanes 9–16) **(B)** Time-dependent DNA synthesis of Pol γ *exo*-on 5′-^{32}P-P_N annealed to T-CPD in the presence of Mg^{2+} (lanes 1–8) or Mn^{2+} (lanes 9–16). **(C)** Quantification of normalized full-length (FL) products from **(A)** and **(B)** over time in seconds. The results are presented as mean and standard deviation from three independent experiments.

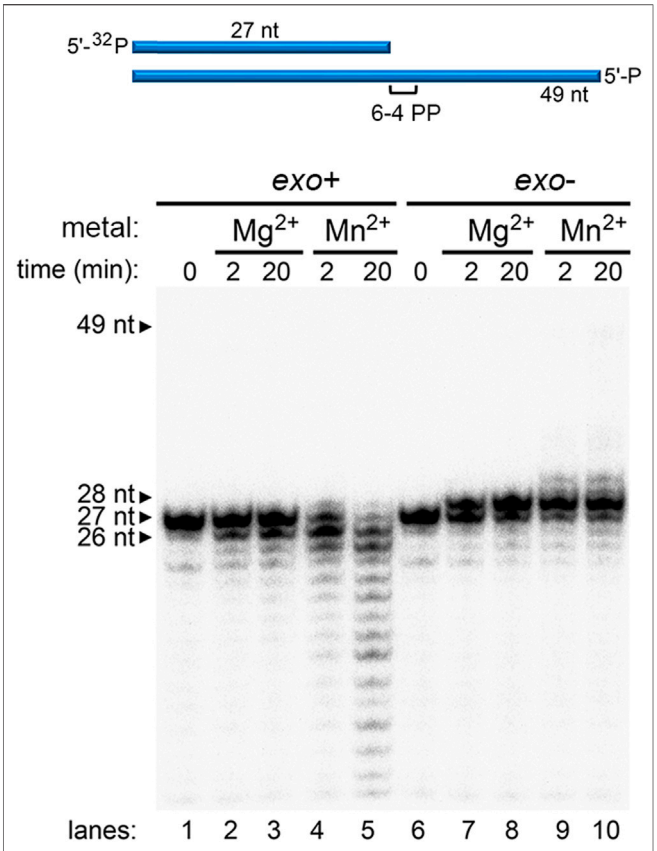

FIGURE 3 | Metal-dependent DNA synthesis of wild-type and exonuclease-deficient Pol γ on a (6-4)PP-containing template. Time-dependent polymerization assay of wild-type Pol γ (*exo+*) on 5′-^{32}P-P_N annealed to T-(6–4)PP in the presence of Mg^{2+} (lanes 2 and 3) or in the presence of Mn^{2+} (lanes 4 and 5) and of Pol γ (*exo-*) on identical DNA substrates in the presence of Mg^{2+} (lanes 7 and 8) or Mn^{2+} (lanes 9 and 10).

step. Similar to wild-type enzyme, Mn^{2+} exhibits inferior activity (eightfold lower) on Pol γ *exo-* synthesis on T-ND than Mg^{2+}.

When translesion synthesis was tested on (6-4)PP lesion containing template, wild-type Pol γ showed no activity in the presence of either Mg^{2+} or Mn^{2+} (**Figure 3**, *lanes* 4 and 5). However, Pol γ *exo-* extended the primer to P_{N+1} with Mg^{2+}, similarly to that on the T-CPD (**Figure 3**, *lanes* 7 and 8). Similarly, no full-length product was formed in the presence of Mn^{2+}, and only P_{N+1} and a small amount of P_{N+2} was formed (**Figure 3**, *lanes* 9–10). Taken together, these results show that exonuclease activity contributes to the Pol γ′s lack of TLS activity, and Mn^{2+} further promotes Pol γ′s TLS ability independent of exonuclease activity.

Mn^{2+} Stimulation of Pol γ TLS Is Independent of Exo Activity

The results thus far showed Mn^{2+} promotes TLS ability to both Pol γ wild-type and *exo-* variant, suggesting Mn^{2+} functions independent of exonuclease activity. To test the conclusion, we tested the *exo* activity of Pol γ with Mn^{2+} and compared it to that with Mg^{2+}. We defined the rate of exonucleolysis as disappearance of the substrate and exonuclease events following the initial reaction were discounted, thus it is an underestimate of the actual rate. The rate of exonucleolysis of Pol γ on single-stranded DNA P_N is 12.6 min^{-1} with Mn^{2+}, sevenfold faster than that of Mg^{2+} at 1.8 min^{-1} (**Figures 4A,C**). Pol γ *exo* activity was also assayed on duplex P_N/T-ND (**Figure 4B**). The excision rate of the duplex P_N/T-ND in the presence of Mn^{2+} is at 3.9 min^{-1}, which is about eightfold higher than Mg^{2+} at 0.5 min^{-1} (**Figure 4C**). Our results are consistent with a previous report where Mn^{2+} stimulates porcine liver Pol γ excision of terminal mismatch (Longley and Mosbaugh, 1991). As Mn^{2+} increased *exo* activity of Pol γ on P_N/N-ND, which is free of error, it suggests that primer is sent more frequently from the *pol* to the *exo* site. As suppressing *exo* activity as well as addition of Mn^{2+} that increases *exo* activity both promote Pol γ′s TLS, we predict that Mn^{2+} must reduce error recognition ability of reading correct Watson-Crick base pairing geometry, which in turn promotes erroneous shuttling of the primer strand to the *exo* site.

Pol γ CPD Bypassing Activity in the Presence of Metal Ions Mixture

We show that Mg^{2+} and Mn^{2+} play opposite roles on Pol γ TLS. Since both ions are present in mitochondria, we tested the effects of metal ion mixture. Pol γ′s translesion synthesis assays were carried out at a fixed, near physiological concentration of one metal ion and varying the concentrations of the other. Specifically, Mg^{2+} was kept constant at 1.0 mM, and Mn^{2+} varied from 0.1 to 10 mM (**Figure 6A**); Mn^{2+} was kept constant at 0.4 mM, and Mg^{2+} varied from 0.1 to 10 mM (**Figure 6C**). Titrations of a single metal were also performed (**Figure 5**). As each dNTP is capable of binding to one of either metal ion and with higher affinity to Mn^{2+}, the precise concentrations of free Mg^{2+} and Mn^{2+} ions for catalysis cannot be accurately calculated, but, in the presence of a total 0.8 mM dNTPs, it should be significantly lower than the initial concentrations.

In the presence of Mg^{2+} alone, Pol γ showed no TLS activity on CPD at any concentration tested (**Figure 5C**, lanes 1-9, **5D**), whereas, in the presence of Mn^{2+} alone, it produced full-length (FL) TLS product from 0.025 to 10 mM (**Figure 5C**, lanes 10–18, **5D**).

The TLS activity with mixed metal ions differs from that with a single metal ion alone. For example, assays with constant 1.0 mM Mg^{2+} and increasing Mn^{2+}, Pol γ began to show TLS activity at 0.1 mM Mn^{2+} (**Figure 6A**, lane 10–18, **6B**). Nonetheless, different from Pol γ producing 97% FL product with 0.1 mM Mn^{2+} on T-ND (**Figure 5B**), it only produced 5% FL TLS product with 0.1 mM Mn^{2+}/ 1.0 mM Mg^{2+} on T-CPD (**Figure 6B**); the polymerase produced 95% FL product with 0.2 mM Mn^{2+} alone on T-ND (**Figure 5B**) but no activity with 1.0 mM Mg^{2+} on T-CPD (**Figure 5C**, lanes1-9), yet producing 12% FL TLS product with metal mixture (**Figure 6B**). These results suggest that Pol γ′s metal binding sites are unlikely occupied by the same metal ion. We thus hypothesize that both metals are bound to the polymerase simultaneously.

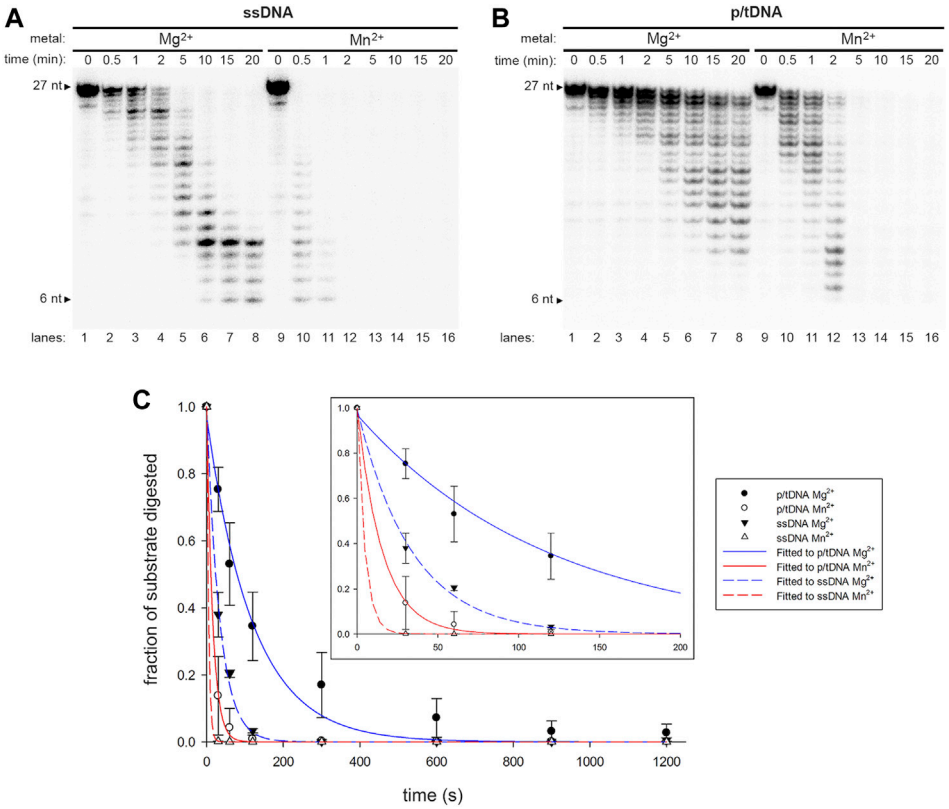

FIGURE 4 | Metal-regulated exonuclease activity of wild-type Pol γ. **(A)** Exonuclease assay of Pol γ on a single-stranded DNA, 5′-^{32}P-P_N, in the presence of Mg^{2+} (lanes 1–8) or in the presence of Mn^{2+} (lanes 9–16). **(B)** Exonuclease assay Pol γ on primer/template, 5′-^{32}P-P_N/T-ND, in the presence of Mg^{2+} (lanes 1–8) or in the presence of Mn^{2+} (lanes 9–16) **(C)**. Quantification of normalized fraction of substrate remaining in **(A)** and **(B)** over time in seconds shown. The results are presented as mean and standard deviation from three independent experiments. Shorter time points (0–200 s) are shown as an inset.

A similar conclusion can be drawn from assays with fixed Mn^{2+} and varying Mg^{2+}. In the presence of 0.4 mM Mn^{2+} and substoichiometric (0.1–0.3 mM), equimolar (0.4–0.5 mM) to slightly excess stoichiometric among Mg^{2+} (1.0 mM), Pol γ generated 35–40% FL TLS product (**Figure 6C**, lanes 10–17, **6D**). Even with the addition of 25-fold excess, 10 mM Mg^{2+}, Pol γ still displays 10% of TLS activity (**Figure 6C**, lane 18, **6D**), suggesting high probability of Pol γ binding to both metal ions.

We should note that under the reaction condition Pol γ TLS activity was observed (0.2 mM Mn^{2+} and 1.0 mM Mg^{2+}, **Figure 6A**, lane 13), and assume dNTPs exhibit equal affinity to Mg^{2+} and Mn^{2+} ions and ignore metal binding to DNA, the free Mn^{2+} ions available for Pol γ catalysis is ~67 μM $\{0.2 - 0.8*[^{0.2}/_{(1+0.2)}]\}$ (mM), below the reported physiological concentration of Mn^{2+} in mitochondria (Corkey et al., 1986; Romani, 2011).

Mn^{2+} Does Not Stimulate Translesion Synthesis in Other Family A Polymerases

Previous studies show that Mn^{2+} does not stimulate TLS activity in other A-family DNA polymerase members, such as *E. coli* Pol I and Klenow Fragment (Moore et al., 1981; Rabkin et al., 1983). To further evaluate the uniqueness of Mn^{2+} activity on Pol γ, we analyzed Mn^{2+} function on another A-family member, T7 DNA polymerase (T7 DNAP), a structural homolog of Pol γ. Neither Mg^{2+} nor Mn^{2+} enables wild-type T7 DNAP to bypass CPD (**Figures 7A,B**, *lanes* 8–14), while both metals support activity on T-ND (**Figures 7A,B** *lanes* 1–7). Similar to Pol γ, T7 DNAP exonuclease activity appeared to be higher in the presence of Mn^{2+} than Mg^{2+}. The results suggest Mn^{2+} exclusively stimulates Pol γ′s TLS activity among replicative A-family polymerases.

DISCUSSION

Perhaps due to lack of UV lesion repair mechanism, mtDNA bares more pyrimidine dimers than chromosomal DNA (Birch-Machin et al., 2013). Nuclear DNA polymerases assume distinct functions in replication or lesion bypassing, but mitochondrial DNA polymerase, Pol γ, is the sole replicase responsible for synthesis on normal as well as lesion-containing mtDNA. Thus, the mitochondrial replicase will unavoidably encounter these bulky photoproducts during mtDNA replication. We present here studies of Pol γ replicating on CPD- and (6-4)PP-containing DNA templates. We showed that Pol γ exerts

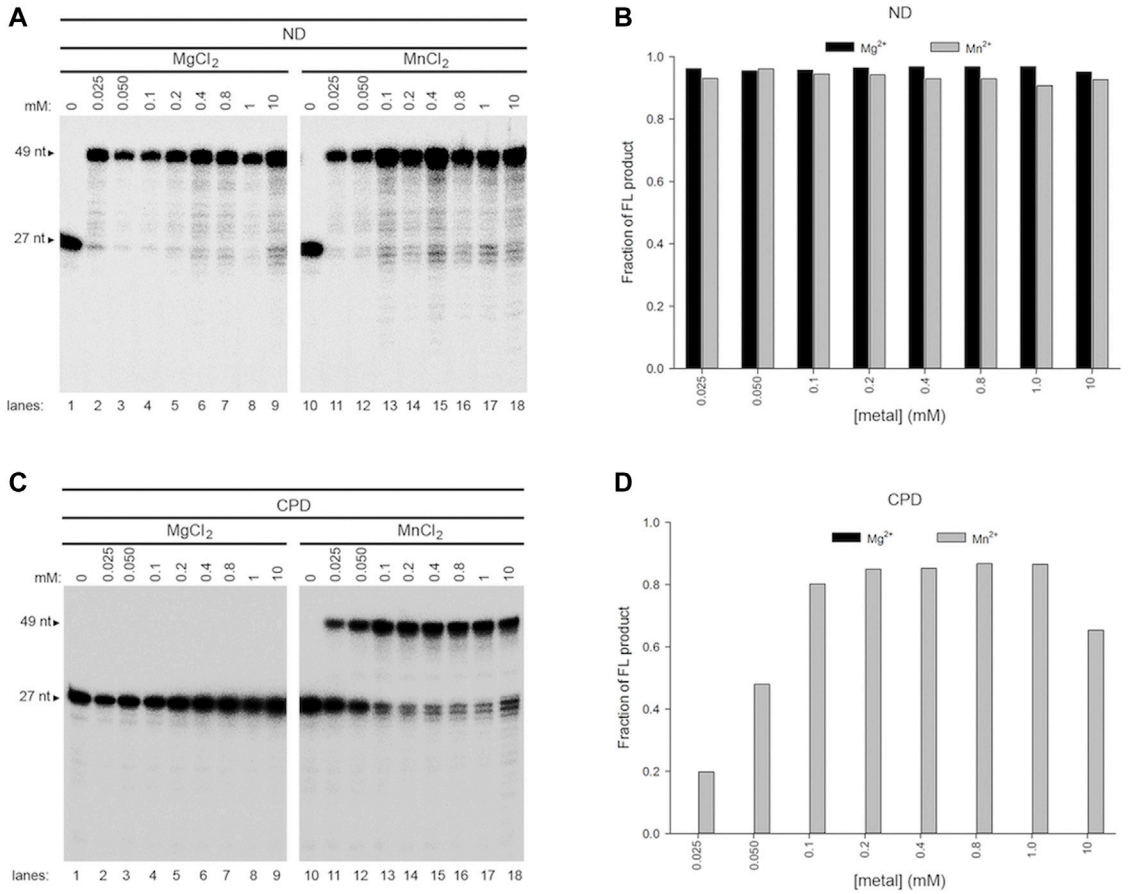

FIGURE 5 | Effect of a single metal ion on wild-type Pol γ DNA activity on non-damaged and CPD-containing templates. **(A)** Wild-type Pol **γ** primer extension on T-ND annealed to 5′-^{32}P-PN in the presence of Mg^{2+}(lanes 1–9) or Mn^{2+} (lanes 10-18). **(B)** Quantification of the full-length product on T-ND vs. a gradient of Mg^{2+} or Mn^{2+} shown in **(A)**. **(C)** Wild-type Pol **γ** primer extension on T-CPD annealed to 5′-^{32}P-PN in the presence of Mg^{2+} (lanes 1–9) or Mn^{2+} (lanes 10-18). **(D)** Quantification of the full-length product on T-CPD vs. a gradient of Mg^{2+} or Mn^{2+} shown in **(C)**.

robust metal dependent activity on lesioned templates under physiological concentrations of Mg^{2+} and Mn^{2+} mixture or Mn^{2+} alone. The metal dependent UV dimer bypassing under a wide range of Mg^{2+} and Mn^{2+} concentrations is unique to Pol γ and has not been found in other A-family DNA polymerases.

Pol γ May Bind to Both Mg^{2+} and Mn^{2+} in Mitochondria

Manganese is an essential element for biological functions and many ubiquitous enzymatic reactions in mitochondria. Mn^{2+} is rapidly transported into mitochondria via the uniporter with activated Ca^{2+} but slowly exported (Chance, 1965; Gavin et al., 1992), thus the organelle concentration is higher than that in cytosol. Mitochondrial concentration of Mn^{2+} is reported at 0.1–0.35 mM with an upper limit of ~1 mM in brain, heart, and liver (Konji et al., 1985; Gunter et al., 2004), and a concentration of Mg^{2+} was 0.37–0.95 mM with upper limit of ~1.5 mM in the heart (Corkey et al., 1986; Romani, 2011). We showed that, under the sub-stoichiometric concentrations of Mg^{2+}/Mn^{2+}, Pol γ displayed significant *trans*-CPD synthesis ability and presented features of binding to both metal ions. Based on these results, we hypothesize that Pol γ could bind to both metals *in vivo* and is therefore capable of replicating on non-damaged and CPD-containing templates. At very low Mg^{2+} or Mn^{2+} concentration, Pol γ is still able to replicate on both non-damaged and CPD-containing templates. Although the exact affinities of Mg^{2+} and Mn^{2+} to Pol γ are not known, it must be higher than the affinities toward dNTPs. Mg^{2+} or Mn^{2+} will first bind to metal A site in Pol γ, then Pol γ will selectively recruit incoming nucleotide pre-bound to metal ion, or metal B site. This feature of Pol γ partially compensates for lack of UV-lesion repair mechanism and TLS polymerase in mitochondria.

It is interesting to speculate Pol γ replication fidelity in the presence of Mg^{2+}/Mn^{2+} mixture. At a high concentration of Mn^{2+} (above mM), many DNA polymerases become mutagenic and exhibit elevated replication errors with Mg^{2+} (Sirover and Loeb, 1976). A simplistic hypothesis would be that Mn^{2+} suppresses the proofreading exonuclease activity in DNA polymerases. However, others (Longley and Mosbaugh, 1991) and we show

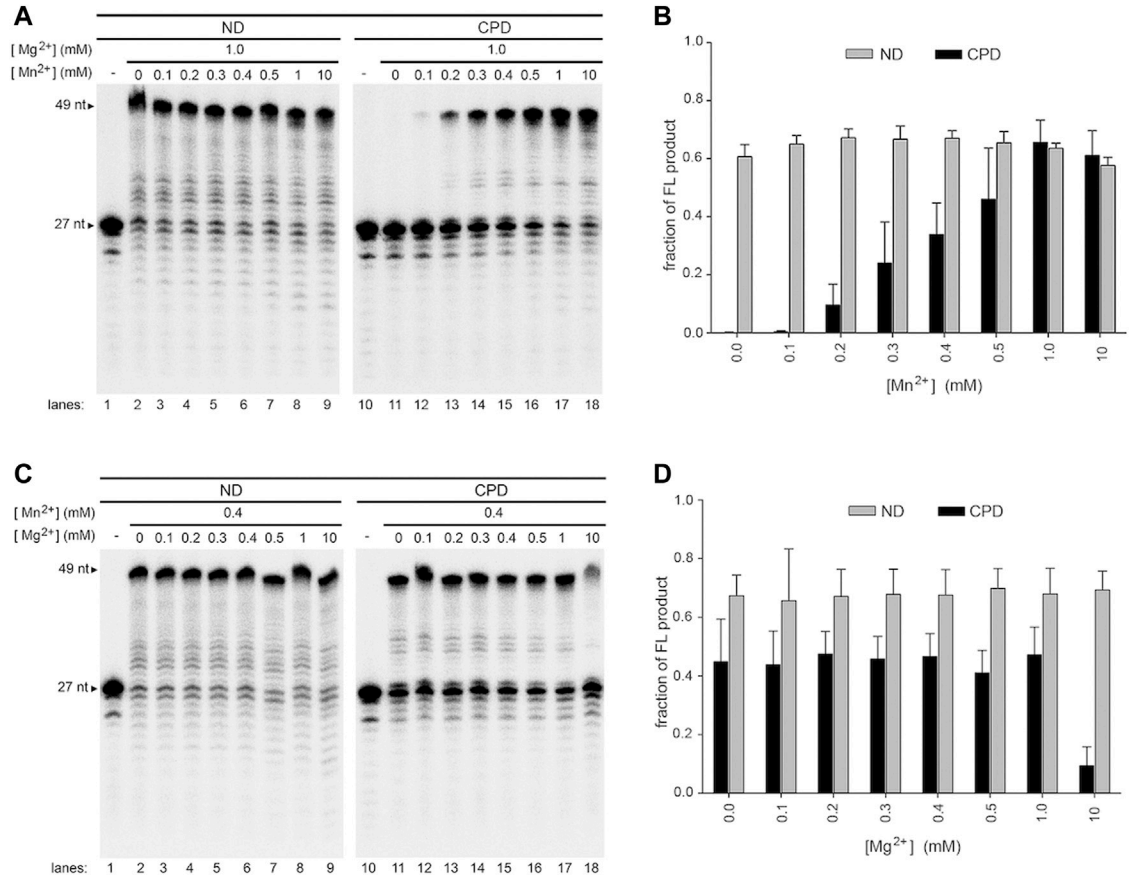

FIGURE 6 | Effect of mixed metal ions on wild-type Pol γ DNA synthesis on non-damaged and CPD-containing templates in a mixture of Mg^{2+} and Mn^{2+}. **(A)** Wild-type Pol γ primer extension on T-ND (lanes 1–9) or T-CPD (lanes 10–18) annealed to the 5′-^{32}P-P_N at a constant concentration of Mg^{2+} and varied concentrations of Mn^{2+}. **(B)** Quantification of the full-length product vs. concentration of Mn^{2+} shown in **(A)**. **(C)** Wild-type Pol γ primer extension on T-ND (lanes 1–9) or T-CPD (lanes 10–18) annealed to the 5′-^{32}P-P_N at constant concentration of Mn^{2+} and varied concentrations of Mg^{2+}. **(D)** Quantification of the full-length product vs. concentration of Mg^{2+} shown in **(C)**.

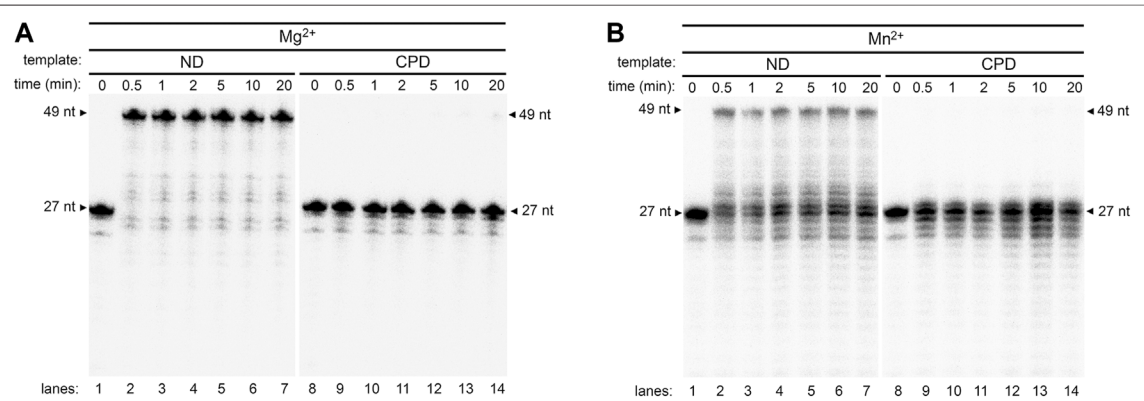

FIGURE 7 | Evaluation of wild-type T7 polymerase activity on a non-damaged and CPD substrates in the presence of Mg^{2+} or Mn^{2+}. **(A)** Time course activity assay of wild-type T7 DNA polymerase on T-ND (lanes 1–8) and on T-CPD (lanes 9–16) annealed to 5′- ^{32}P-P_N in the presence of Mg^{2+}. **(B)** Time course activity assay of wild-type T7 DNA polymerase on T-ND (lanes 1–8) and on T-CPD (lanes 9–16) annealed to 5′-^{32}P-P_N in the presence of Mn^{2+}.

here that Pol γ displayed increased *exo* activity in the presence of Mn^{2+} relative to that of Mg^{2+}. Thus, high concentrations in Mn^{2+}-induced replication errors are not by direct inhibition of *exo* activity, rather by hindrance of error recognition. Nevertheless, at low concentrations of Mn^{2+}, DNA polymerases can replicate accurately. For example, at 2 μM free Mn^{2+} concentration, *E. coli* Pol I was shown to synthesize DNA with similar error frequency as with Mg^{2+} (Beckman et al., 1985). We predict Pol γ would also replicate with high fidelity at a physiological concentration of Mn^{2+} and Mg^{2+}. Needless to say, the hypothesis should be rigorously tested experimentally in future investigations. Lack of TLS activity on (6-4)PP-containing template by Pol γ suggests two possible outcomes: there may be another TLS polymerase that can overcome this UV lesion, or the damaged mtDNA is eliminated by a mitochondrial degradation mechanism as observed in *C. elegans* and primary human fibroblasts upon UV radiation damage (Bess et al., 2012; Bess et al., 2013).

Selective Stimulation of CPD Bypassing Among Pol I Family Members

Pol γ is the only A-family polymerase found to have an intrinsic TLS activity across UV lesions as a wild-type enzyme. Studies from the Copeland and Meyer groups showed that silencing Pol γ′s exonuclease activity led to limited CPD bypassing activity, despite the diminished activity for wild-type enzymes (Miller and Grollman, 1997; Kasiviswanathan et al., 2012). We show that the TLS activities of both wild-type and exonuclease-deficient Pol γ are greatly stimulated by the presence of Mn^{2+}. Additionally, plant and yeast mitochondrial DNA polymerases also exhibited TLS activity similar to human Pol γ (unpublished results). However, such activities are not found in other replicative A-family DNA polymerases. *E. coli* Pol I and Klenow Fragment lack intrinsic TLS activity and only insert one nucleotide against 3′-T in the CPD in presence of Mn^{2+} (Moore et al., 1981; Rabkin et al., 1983; Smith et al., 1998). We showed here that wild-type T7 DNAP does not display Mn^{2+}-stimulated TLS activity. The Mn^{2+}-stimulated TLS activity appears to be reserved only to mitochondrial DNA polymerases, perhaps to take advantage of higher Mn^{2+} concentration in the mitochondria.

Nevertheless, Mn^{2+}-dependent activity is observed in certain TLS polymerases (Putrament et al., 1975; Kunkel and Loeb, 1979; Goodman et al., 1983). For example, Dpo4 bypasses abasic sites and CPD much more efficiently with Mn^{2+} than with Mg^{2+} (Vaisman et al., 2005), and DNA polymerase ι bypasses abasic sites, benzopyrenes, CPD, and (6-4)PP only in the presence of Mn^{2+} (Frank and Woodgate, 2007). In addition, PrimPol bypasses more lesions when bound to Mn^{2+} relative to Mg^{2+} (Tokarsky et al., 2017; Makarova et al., 2018).

Manganese Ion Likely Alters Pol γ′s Pol Active Site Structure

A distinct structural difference between high fidelity DNA polymerase such as Pol γ and bona fide TLS polymerases such as Pol η is the *pol* active site conformation and polymerase-enforced template DNA conformation. Crystal structures of Pol γ showed that Pol γ belongs to the A-family polymerases with characteristic fingers, thumb, and palm domains (Lee et al., 2009). Upon binding to a correct incoming nucleotide, the fingers domain undergoes large open-closed conformational changes to align the γ-phosphate of dNTP, 3′-OH of the primer, and catalytic metal ions for optimal catalysis for phosphodiester bond formation (Lee et al., 2009; Szymanski et al., 2015; Sohl et al., 2015). Significantly, the template bends 90° at the coding base (*n*) and downstream neighboring residue (*n+1*) (**Figure 8**, right). DNA template bending in Pol γ is accomplished by the helices O and O1 in the finger domain. Such template strand bending is thought to prevent template 'slippage' and ensuring replication fidelity. A non-bendable dimer is deterred from entering the *pol* site and stalls replication (Li et al., 2004). Indeed, the structure of T7 DNA polymerase, a Pol γ homolog, complexed with CPD lesion (Li et al., 2004) shows that after incorporating a nucleotide opposing the 3′-T of CPD, base pairing with the 5′-T of CPD is severely crooked, preventing replication at the *n+1* position.

Contrary to the closed *pol* site in high-fidelity polymerases ternary conformation, the *pol* active site is more open in Y-family TLS polymerases Pol *η*. Structure of DNA polymerase *η* (Pol η) complexed with a CPD-containing template and primer duplex reveals that the bulky CPD can be easily accommodated in the *pol* site due to the preformed, spacious *pol* active site and highly mobile little-fingers and thumb domains, shared features in Y-family DNA polymerases (**Figure 8**, left) (Yang and Woodgate, 2007; Biertümpfel et al., 2010). Unlike replicative DNA polymerases, the fingers subdomain in Y-family DNA polymerases does not go through large conformational changes. Rather, the enzyme is already poised for DNA synthesis even in the absence of incoming nucleotides. Little-finger and thumb domains go through the largest conformational changes and seem to confer specific TLS activities (Boudsocq et al., 2004; Yang and Woodgate, 2007).

To provide a structural interpretation for Pol γ metal-dependent TLS activity, we composited a ternary complex of Pol γ, primer/CPD-template, and an incoming nucleotide by docking CPD-containing substrate from T7 DNA polymerase complex (PDB: 1SL2) onto Pol γ ternary complex (PDB: 4ZTZ) after superposition on the two *pol* active sites (**Figure 8**, middle). The resulting complex showed that the CPD would sterically clash with the O1 helix fingers domain severely if no conformational change occurs. For Pol γ to accommodate the bulky CPD, the fingers domain would have to adopt a more open configuration resembling the Pol γ-DNA binary complex. In addition, Mn^{2+} may also enlarge the *pol* site in a way that no longer bends the template strand, allowing the bulky thymine dimers to enter effortlessly. We thus hypothesize that Mn^{2+} may alter Pol γ structure from high-fidelity configuration to that of TLS polymerases. Under this idea, when Pol γ replicates on a non-damaged DNA, the catalytic site is not challenged for which a catalytic site reshaping is not needed (**Figure 9A**). But on a CPD-containing substrate, due to its volume, Pol γ′s catalytic site is reshaped in the presence of Mn^{2+} or a mixture with Mg^{2+} (**Figure 9B**). More studies should be addressed to better understand this mechanism.

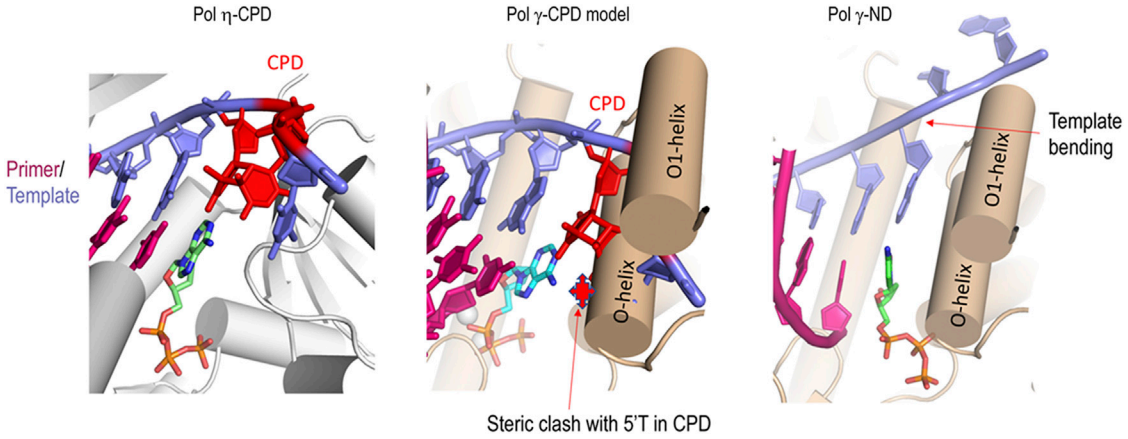

FIGURE 8 | Comparison of *pol* site conformation of Pol η and Pol γ. Left, Pol *η* ternary complex with CPD (red)-containing template (blue) and primer (magenta) and incoming nucleotide (green) (PDB: 3MR3). Middle, modeled Pol γ-CPD containing primer/template DNA showing the CPD (red) steric clashes with the O helices. Right, Pol γ ternary complex with primer/template and incoming nucleotide showing the bending of the template by O- and O1-helix.

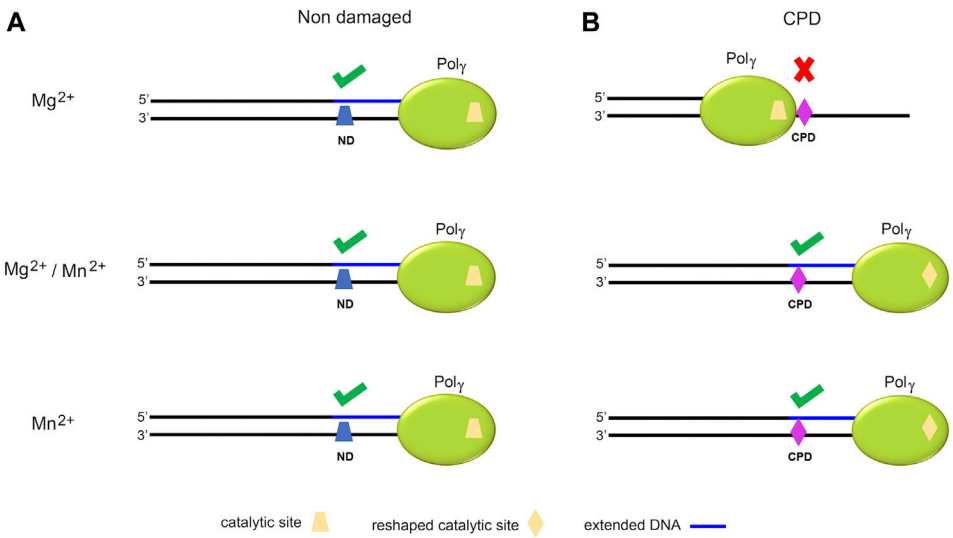

FIGURE 9 | Schematic model of the hypothetical function of Mg^{2+} and Mn^{2+} in reshaping Pol γ's active site. Illustration of Pol γ (green) on an ND- (blue trapezoid) or CPD-containing template (violet rhomboid). **(A)** Representation of DNA replication by Pol γ on an ND-containing substrate in the presence of Mg^{2+}, Mg^{2+}/Mn^{2+}, or Mn^{2+} showing full extension in all cases without significant changes in the catalytic site (yellow trapezoid). **(B)** Representation of DNA replication by Pol γ on a CPD-containing template illustrating a change of the Pol γ's catalytic site (yellow trapezoid) in the presence of Mn^{2+} upon encountering CPD to trigger TLS activity.

Pol ι, another Y-family DNA polymerase, has better TLS activity across UV lesions in the presence of Mn^{2+} compared to Mg^{2+} (Frank and Woodgate, 2007). The mechanism behind Mn^{2+}-mediated TLS in Pol ι is not by large conformational changes of protein. Crystal structures of Pol ι do not display noticeable overall structural changes in the presence of Mn^{2+} compared to Mg^{2+} except for small changes near divalent cations in the active site (Choi et al., 2016). Mn^{2+} supports more optimal octahedral coordination compared to Mg^{2+}, explaining the higher activity and fidelity in presence of Mn^{2+}. In addition, Pol ι does not go through large conformational change upon dNTP binding like replicative DNA polymerases do, which gives molecular explanation behind its ability to tolerate bulkier lesions in its wide and rigid active site (Nair et al., 2006). For replicative polymerases like Pol γ, finger domain movement upon dNTP binding is essential. It is possible that Mn^{2+} binding induces sufficient structural changes to accommodate CPD.

Mn^{2+}-induced conformational changes are seen in other polymerases. The *pol* active site of Pol *η* widens when bound to Mn^{2+} relative to being bound to Mg^{2+} and Ca^{2+} (Yang and

Woodgate, 2007; Ling et al., 2003; Rechkoblit et al., 2006; Weng et al., 2018). The proteolysis pattern for a catalytic subunit of herpes simplex virus DNA polymerase (UL30) bound to platinated DNA differs in the presence of Mn^{2+} than in the presence of Mg^{2+}, implying that UL30 undergoes conformational changes between Mn^{2+} to Mg^{2+} bound states (Villani et al., 2002). If Mn^{2+} actually alters Pol γ *pol* site and the fingers domain resemble that in Pol η, Pol γ would be able to accommodate the rigid thymine dimer in the enlarged *pol* site and to incorporate incoming nucleotide opposite to the dimer without stringent geometry check for W-C base pairing complementarity. Crystal structures of RB69 DNA polymerase, replicative B-family DNA polymerase, in the presence of Mg^{2+} or Mn^{2+} do not display significant conformational changes (Xia et al., 2011). It is likely the same for Pol γ when it is replicating on T-ND. However, when Pol γ is challenged with bulky lesion like CPD, the Mn^{2+}-mediated flexibility in the *pol* site may allow enlargement to accommodate CPD (**Figure 8**). Currently, structural studies revealed only two catalytic metal ions in the *pol* site; however, EPR study of *E. coli* Pol I showed at least 25 Mn^{2+} binding sites were present (Slater et al., 1972). Whether the catalytic metal ions or additional metal ions are involved in reshaping the *pol* site warrants further investigation.

METHODS

Proteins Preparation

His-tagged Pol γA and Pol γB subunits were expressed in Sf9 insect cells and *E. coli* Rosetta (DE3) cells, respectively, and purified as previously described (Lee et al., 2009). Wild-type Pol γA subunit and exonuclease-deficient (*exo*-) variant containing double mutation D198A/E200A lack N-terminal 25 residues (the putative mitochondrial localization sequence) as well as 10 of the 13 sequential glutamines (residues 43–52). Briefly, both Pol γA wild-type and exonuclease deficient variant were purified sequentially using TALON (Cytiva, Marlborough, MA) and gel filtration column Superdex 200. Pol γB subunit lacking N-terminal 25 residues was purified using Ni-NTA (Qiagen, Germantown, MD) and Mono S affinity chromatography. Purified Pol γA and Pol γB were complexed at 1:2 M ratio, respectively, then applied to a gel filtration column Superdex 200. After gel filtration, pure fractions were pooled and concentrated in a buffer containing 20 mM HEPES (pH 7.5), 140 mM KCl, 5% glycerol, 1 mM EDTA (pH 8,0), and 10 mM BME. Fractions were aliquoted and stored at −80°C.

Wild-type T7 DNA polymerase bound to thioredoxin was purchased from New England Biolab (Ipswich, MA). Concentrations of the proteins were determined on the NanoDrop™ spectrophotometer (Thermo Scientific, Waltham, MA) based on the absorbance at 280 nm. All experiments reported in this study were carried out with the same batch purified proteins. The protein concentrations are determined by A280 absorption and specific extinction coefficients, not active site concentration. The active site concentrations of purified Pol γ are routinely measured to be 80–84%.

DNA Substrates

All oligonucleotides are synthesized by Integrated DNA Technologies (Morrisville, NC) except for templates containing CPD and (6-4)PP (**Table 1**). The oligonucleotides containing the CPD and the (6-4)PP were synthesized as described previously (Murata et al., 1990; Iwai et al., 1996). Complementary oligonucleotides were mixed in solution containing 50 mM Tris (pH 7.8), 50 mM NaCl, and 1 mM EDTA (pH 8), then were annealed by heating at 95°C for 5 min followed by slowly cooling to room temperature overnight. For all activity assays, 5′-end of the primer strands were labeled using T4 polynucleotide kinase (New England Biolab, Ipswich, MA) using γ-^{32}P-ATP (PerkinElmer, Waltham, MA).

Polymerase Activity Assays

Three primer/template duplexes were formed by primer P_N (27 nt) annealed to a 49 nt non-damaged template (T-ND), a CPD-containing template (T-CPD), or a (6-4)PP-containing template (T-(6–4)PP) (**Table 1**). For UV product-containing DNA, 200 nM wild-type or exonuclease-deficient Pol γ was pre-incubated with 1000 nM P_N/T-CPD or P_N/T-(6–4)PP in Buffer N (25 mM HEPES pH 7.5, 140 mM KCl, 1 mM EDTA, 5% glycerol, and 100 μg/ml BSA) at 37°C for 5 min. For T-ND, 100 nM wild-type or exonuclease-deficient Polγ was preincubated with 1000 nM P_N/T-ND in Buffer N. The reaction was started by the addition of equal volume of Buffer C (Buffer N supplemented with 400 μM dNTP mix and 40 mM $MgCl_2$ or $MnCl_2$) to a final concentration of 200 μM dNTP mix and 20 mM $MgCl_2$ or $MnCl_2$. Reaction was quenched at the indicated times by adding ninefold excess of Buffer Q (80% Formamide, 50 mM EDTA pH 8, 0.1% SDS, 5% glycerol, and 0.02% bromophenol blue). Quenched samples were heated at 95°C for 5 min and resolved on a 23% polyacrylamide gel containing 7 M urea. Gels were soaked in solution containing 50% methanol and 20% glycerol prior to drying overnight under vacuum at 50°C. Gels were exposed on a phosphor screen, which was imaged using Amersham Typhoon RGB scanner (Cytiva, Marlborough, MA). The intensities of bands were quantified using ImageQuant TL 8.2 (Cytiva, Marlborough, MA). Graphs were plotted using the mean and standard deviation in SigmaPlot 14 (Systat Software, San Jose, CA). To obtain the rate of full-length product formation, we used the following equation: $rate = \frac{I_{FL}}{I_0}$, where I_{FL} is the intensity of the full-length product band at 120 s, and I_0 is the intensity of the original substrate band at 0 s. We normalized the enzyme concentration as polymerase activity assays on T-CPD contained 100 nM Pol γ whereas polymerase activity assays on T-ND contained 50 nM Pol γ.

For polymerase activity assays using wild-type T7 DNA polymerase, a total of 400 nM T7 DNA polymerase was pre-incubated with 200 nM of P_N/T-ND or P_N/T-CPD in Buffer N at 37°C for 5 min. The reaction was started by addition of equal volume of Buffer C to a final concentration of 200 μM dNTP mix and 20 mM $MgCl_2$ or $MnCl_2$. Quench step, electrophoresis, and autoradiography were carried out identically to polymerase activity assays using P_N.

Exonuclease Assays

A total of 400 nM Polγ was pre-incubated with 1000 nM single stranded primer P_N or duplex P_N/T-ND in Buffer N, and the reaction was started by addition of an equal volume of Buffer C without dNTPs to a final concentration of 20 mM $MgCl_2$ or $MnCl_2$. Quench step, electrophoresis, autoradiography, and quantification were carried out identically to polymerase activity assays. The experimental data were fitted to an equation $y = Ae^{-kt}$, where A is the amplitude and k is the rate of excision. Graphs were plotted using the mean and standard deviation in SigmaPlot 14 (Systat Software, San Jose, CA).

Polymerase Assays With Mixed Metal Ions

For polymerase assay using mixed metal ions, 1000 nM wild-type Polγ was pre-incubated with 1000 nM P_N/T-ND or P_N/T-CPD in Buffer N at 37°C for 5 min. The reaction was started by addition of an equal volume of Buffer C to final concentrations of either constant 1 mM $MgCl_2$ and varied $MnCl_2$ (0.1, 0.2, 0.3 0.4, 0.5, 1, and 10 mM) concentrations, or constant 0.4 mM $MnCl_2$ and varied $MgCl_2$ (0.1, 0.2, 0.4, 0.4, 0.5, 1, and 10 mM) concentrations. Reaction was quenched 5 min after adding ninefold excess of Buffer Q. Electrophoresis, autoradiography, and quantification were carried out identically to polymerase activity assays.

Polymerase Assays With Single Metal Ions

For polymerase assay using single metal ions, 200 nM wild-type Polγ was pre-incubated with 200 nM P_N/T-ND or P_N/T-CPD in Buffer N at 37°C for 5 min. Reaction was started by addition of an equal volume of Buffer C containing $MgCl_2$ or $MnCl_2$ (0.025, 0.05, 0.1 0.2, 0.4, 0.8, 1.0, and 10 mM). Reaction was quenched 5 min after adding ninefold excess of Buffer Q. Electrophoresis, autoradiography, and quantification were carried out identically to polymerase activity assays.

Experimental Replicas

Experiments with corresponding graphs containing error bars were repeated three times. The rest of the experiments with corresponding graphs not containing error bars were repeated twice.

DATA AVAILABILITY STATEMENT

The data supporting the conclusions of this article will be made available by the corresponding authors, without undue reservation.

AUTHOR CONTRIBUTIONS

JP, NB-T, LB, and YWY designed experiments, JP, NB-T, SI, and GH executed the experiments, JP and NB-T wrote the first draft, and all authors contributed to the final manuscript.

FUNDING

The work is supported in parts by grants from NIH to YWY and SJT (R01AI134611 and R01NS095747), the James W. McLaughlin Fellowship Fund to JP, and an endowment from the Sealy and Smith Foundation to the Sealy Center for Structural Biology and Molecular Biophysics at UTMB.

ACKNOWLEDGMENTS

We thank Satya Prakash and Louise Prakash for helpful discussion.

REFERENCES

Bębenek, A., and Ziuzia-Graczyk, I. (2018). Fidelity of DNA Replication-A Matter of Proofreading. *Curr. Genet.* 64, 985–996. doi:10.1007/s00294-018-0820-1

Beckman, R. A., Mildvan, A. S., and Loeb, L. A. (1985). On the Fidelity of DNA Replication: Manganese Mutagenesis *In Vitro*. *Biochemistry* 24, 5810–5817. doi:10.1021/bi00342a019

Bess, A. S., Crocker, T. L., Ryde, I. T., and Meyer, J. N. (2012). Mitochondrial Dynamics and Autophagy Aid in Removal of Persistent Mitochondrial DNA Damage in *Caenorhabditis elegans*. *Nucleic Acids Res.* 40, 7916–7931. doi:10.1093/nar/gks532

Bess, A. S., Ryde, I. T., Hinton, D. E., and Meyer, J. N. (2013). UVC-induced Mitochondrial Degradation via Autophagy Correlates with mtDNA Damage Removal in Primary Human Fibroblasts. *J. Biochem. Mol. Toxicol.* 27, 28–41. doi:10.1002/jbt.21440

Bharti, S. K., Sommers, J. A., Zhou, J., Kaplan, D. L., Spelbrink, J. N., Mergny, J.-L., et al. (2014). DNA Sequences Proximal to Human Mitochondrial DNA Deletion Breakpoints Prevalent in Human Disease Form G-Quadruplexes, a Class of DNA Structures Inefficiently Unwound by the Mitochondrial Replicative Twinkle Helicase. *J. Biol. Chem.* 289, 29975–29993. doi:10.1074/jbc.m114.567073

Biertümpfel, C., Zhao, Y., Kondo, Y., Ramón-Maiques, S., Gregory, M., Lee, J. Y., et al. (2010). Structure and Mechanism of Human DNA Polymerase η. *Nature* 465, 1044–1048. doi:10.1038/nature09196

Birch-Machin, M. A., Russell, E. V., and Latimer, J. A. (2013). Mitochondrial DNA Damage as a Biomarker for Ultraviolet Radiation Exposure and Oxidative Stress. *Br. J. Dermatol.* 169, 9–14. doi:10.1111/bjd.12207

Birch-Machin, M. A., Tindall, M., Turner, R., Haldane, F., and Rees, J. L. (1998). Mitochondrial DNA Deletions in Human Skin Reflect Photo- rather Than Chronologic Aging. *J. Invest. Dermatol.* 110, 149–152. doi:10.1046/j.1523-1747.1998.00099.x

Boudsocq, F., Kokoska, R. J., Plosky, B. S., Vaisman, A., Ling, H., Kunkel, T. A., et al. (2004). Investigating the Role of the Little finger Domain of Y-Family DNA Polymerases in Low Fidelity Synthesis and Translesion Replication. *J. Biol. Chem.* 279, 32932–32940. doi:10.1074/jbc.m405249200

Brash, D. E., and Haseltine, W. A. (1982). UV-induced Mutation Hotspots Occur at DNA Damage Hotspots. *Nature* 298, 189–192. doi:10.1038/298189a0

Chance, B. (1965). The Energy-Linked Reaction of Calcium with Mitochondria. *J. Biol. Chem.* 240, 2729–2748. doi:10.1016/s0021-9258(18)97387-4

Choi, J.-Y., Patra, A., Yeom, M., Lee, Y.-S., Zhang, Q., Egli, M., et al. (2016). Kinetic and Structural Impact of Metal Ions and Genetic Variations on Human DNA Polymerase ι. *J. Biol. Chem.* 291, 21063–21073. doi:10.1074/jbc.m116.748285

Corkey, B. E., Duszynski, J., Rich, T. L., Matschinsky, B., and Williamson, J. R. (1986). Regulation of Free and Bound Magnesium in Rat Hepatocytes and Isolated Mitochondria. *J. Biol. Chem.* 261, 2567–2574. doi:10.1016/s0021-9258(17)35825-8

Durham, S. E., Krishnan, K. J., Betts, J., and Birch-Machin, M. A. (2003). Mitochondrial DNA Damage in Non-melanoma Skin Cancer. *Br. J. Cancer* 88, 90–95. doi:10.1038/sj.bjc.6600773

Frank, E. G., and Woodgate, R. (2007). Increased Catalytic Activity and Altered Fidelity of Human DNA Polymerase ι in the Presence of Manganese. *J. Biol. Chem.* 282, 24689–24696. doi:10.1074/jbc.m702159200

Garcia-Diaz, M., and Bebenek, K. (2007). Multiple Functions of DNA Polymerases. *Crit. Rev. Plant Sci.* 26, 105–122. doi:10.1080/07352680701252817

Gavin, C. E., Gunter, K. K., and Gunter, T. E. (1990). Manganese and Calcium Efflux Kinetics in Brain Mitochondria. Relevance to Manganese Toxicity. *Biochem. J.* 266, 329–334. doi:10.1042/bj2660329

Gavin, C. E., Gunter, K. K., and Gunter, T. E. (1992). Mn2+ Sequestration by Mitochondria and Inhibition of Oxidative Phosphorylation. *Toxicol. Appl. Pharmacol.* 115, 1–5. doi:10.1016/0041-008x(92)90360-5

Goodman, M. F., Keener, S., Guidotti, S., and Branscomb, E. W. (1983). On the Enzymatic Basis for Mutagenesis by Manganese. *J. Biol. Chem.* 258, 3469–3475. doi:10.1016/s0021-9258(18)32685-1

Gunter, T. E., Miller, L. M., Gavin, C. E., Eliseev, R., Salter, J., Buntinas, L., et al. (2004). Determination of the Oxidation States of Manganese in Brain, Liver, and Heart Mitochondria. *J. Neurochem.* 88, 266–280. doi:10.1046/j.1471-4159.2003.02122.x

Harbottle, A., Maki, J., Reguly, B., Wittock, R., Robinson, K., Parr, R., et al. (2010). Real-time Polymerase Chain Reaction Analysis of a 3895-bp Mitochondrial DNA Deletion in Epithelial Swabs and its Use as a Quantitative Marker for Sunlight Exposure in Human Skin. *Br. J. Dermatol.* 163, 1291–1295. doi:10.1111/j.1365-2133.2010.10001.x

Iwai, S., Shimizu, M., Kamiya, H., and Ohtsuka, E. (1996). Synthesis of a Phosphoramidite Coupling Unit of the Pyrimidine (6-4) Pyrimidone Photoproduct and its Incorporation into Oligodeoxynucleotides. *J. Am. Chem. Soc.* 118, 7642–7643. doi:10.1021/ja9603158

Johnson, A. A., and Johnson, K. A. (2001). Exonuclease Proofreading by Human Mitochondrial DNA Polymerase. *J. Biol. Chem.* 276, 38097–38107. doi:10.1074/jbc.m106046200

Johnson, A. A., Tsai, Y.-c., Graves, S. W., and Johnson, K. A. (2000). Human Mitochondrial DNA Polymerase Holoenzyme: Reconstitution and Characterization. *Biochemistry* 39, 1702–1708. doi:10.1021/bi992104w

Kasiviswanathan, R., Gustafson, M. A., Copeland, W. C., and Meyer, J. N. (2012). Human Mitochondrial DNA Polymerase γ Exhibits Potential for Bypass and Mutagenesis at UV-Induced Cyclobutane Thymine Dimers. *J. Biol. Chem.* 287, 9222–9229. doi:10.1074/jbc.m111.306852

Kawasaki, K., Suzuki, T., Ueda, M., Ichihashi, M., Reguer, G., and Yamasaki, H. (2000). CC to TT Mutation in the Mitochondrial DNA of normal Skin: Relationship to Ultraviolet Light Exposure. *Mutat. Research/Genetic Toxicol. Environ. Mutagenesis* 468, 35–43. doi:10.1016/s1383-5718(00)00038-3

Konji, V., Montag, A., Sandri, G., Nordenbrand, K., and Ernster, L. (1985). Transport of Ca2+ and Mn2+ by Mitochondria from Rat Liver, Heart and Brain. *Biochimie* 67, 1241–1250. doi:10.1016/s0300-9084(85)80133-4

Kunkel, T. A., and Loeb, L. A. (1979). On the Fidelity of DNA Replication. Effect of Divalent Metal Ion Activators and Deoxyrionucleoside Triphosphate Pools on *In Vitro* Mutagenesis. *J. Biol. Chem.* 254, 5718–5725. doi:10.1016/s0021-9258(18)50474-9

Lee, Y.-S., Kennedy, W. D., and Yin, Y. W. (2009). Structural Insight into Processive Human Mitochondrial DNA Synthesis and Disease-Related Polymerase Mutations. *Cell* 139, 312–324. doi:10.1016/j.cell.2009.07.050

Lee, Y.-S., Lee, S., Demeler, B., Molineux, I. J., Johnson, K. A., and Yin, Y. W. (2010). Each Monomer of the Dimeric Accessory Protein for Human Mitochondrial DNA Polymerase Has a Distinct Role in Conferring Processivity. *J. Biol. Chem.* 285, 1490–1499. doi:10.1074/jbc.m109.062752

Li, Y., Dutta, S., Doublié, S., Bdour, H. M. d., Taylor, J.-S., and Ellenberger, T. (2004). Nucleotide Insertion Opposite a Cis-Syn Thymine Dimer by a Replicative DNA Polymerase from Bacteriophage T7. *Nat. Struct. Mol. Biol.* 11, 784–790. doi:10.1038/nsmb792

Liccione, J. J., and Maines, M. D. (1988). Selective Vulnerability of Glutathione Metabolism and Cellular Defense Mechanisms in Rat Striatum to Manganese. *J. Pharmacol. Exp. Ther.* 247, 156–161.

Ling, H., Boudsocq, F., Plosky, B. S., Woodgate, R., and Yang, W. (2003). Replication of a Cis-Syn Thymine Dimer at Atomic Resolution. *Nature* 424, 1083–1087. doi:10.1038/nature01919

Longley, M. J., and Mosbaugh, D. W. (1991). Properties of the 3' to 5' Exonuclease Associated with Porcine Liver DNA Polymerase Gamma. Substrate Specificity, Product Analysis, Inhibition, and Kinetics of Terminal Excision. *J. Biol. Chem.* 266, 24702–24711. doi:10.1016/s0021-9258(18)54287-3

Maher, V. M., Dorney, D. J., Mendrala, A. L., Konze-Thomas, B., and McCormick, J. J. (1979). DNA Excision-Repair Processes in Human Cells Can Eliminate the Cytotoxic and Mutagenic Consequences of Ultraviolet Irradiation. *Mutat. Research/Fundamental Mol. Mech. Mutagenesis* 62, 311–323. doi:10.1016/0027-5107(79)90087-3

Maher, V. M., Ouellette, L. M., Curren, R. D., and McCormick, J. J. (1976). Frequency of Ultraviolet Light-Induced Mutations Is Higher in Xeroderma Pigmentosum Variant Cells Than in normal Human Cells. *Nature* 261, 593–595. doi:10.1038/261593a0

Maher, V. M., Rowan, L. A., Silinskas, K. C., Kateley, S. A., and McCormick, J. J. (1982). Frequency of UV-Induced Neoplastic Transformation of Diploid Human Fibroblasts Is Higher in Xeroderma Pigmentosum Cells Than in normal Cells. *Proc. Natl. Acad. Sci.* 79, 2613–2617. doi:10.1073/pnas.79.8.2613

Makarova, A. V., Boldinova, E. O., Belousova, E. A., and Lavrik, O. I. (2018). *In Vitro* lesion Bypass by Human PrimPol. *DNA Repair* 70, 18–24. doi:10.1016/j.dnarep.2018.07.009

Maynard, L. S., and Cotzias, G. C. (1955). The Partition of Manganese Among Organs and Intracellular Organelles of the Rat. *J. Biol. Chem.* 214, 489–495. doi:10.1016/s0021-9258(18)70986-1

Miller, H., and Grollman, A. P. (1997). Kinetics of DNA Polymerase I (Klenow Fragment Exo-) Activity on Damaged DNA Templates: Effect of Proximal and Distal Template Damage on DNA Synthesis. *Biochemistry* 36, 15336–15342. doi:10.1021/bi971927n

Moore, P. D., Bose, K. K., Rabkin, S. D., and Strauss, B. S. (1981). Sites of Termination of *In Vitro* DNA Synthesis on Ultraviolet- and N-Acetylaminofluorene-Treated Phi X174 Templates by Prokaryotic and Eukaryotic DNA Polymerases. *Proc. Natl. Acad. Sci.* 78, 110–114. doi:10.1073/pnas.78.1.110

Murata, T., Iwai, S., and Ohtsuka, E. (1990). Synthesis and Characterization of a Substrate for T4 Endonuclease V Containing a Phosphorodithioate Linkage at the Thymine Dimer Site. *Nucl. Acids Res.* 18, 7279–7286. doi:10.1093/nar/18.24.7279

Nair, D. T., Johnson, R. E., Prakash, L., Prakash, S., and Aggarwal, A. K. (2006). An Incoming Nucleotide Imposes an Anti to Syn Conformational Change on the Templating Purine in the Human DNA Polymerase-ι Active Site. *Structure* 14, 749–755. doi:10.1016/j.str.2006.01.010

Putrament, A., Baranowska, H., Ejchart, A., and Prazmo, W. (1975). Manganese Mutagenesis in Yeast. A Practical Application of Manganese for the Induction of Mitochondrial Antibiotic-Resistant Mutations. *J. Gen. Microbiol.* 90, 265–270. doi:10.1099/00221287-90-2-265

Rabkin, S. D., Moore, P. D., and Strauss, B. S. (1983). *In Vitro* bypass of UV-Induced Lesions by *Escherichia coli* DNA Polymerase I: Specificity of Nucleotide Incorporation. *Proc. Natl. Acad. Sci.* 80, 1541–1545. doi:10.1073/pnas.80.6.1541

Ray, A. J., Turner, R., Nikaido, O., Rees, J. L., and Birch-Machin, M. A. (2000). The Spectrum of Mitochondrial DNA Deletions Is a Ubiquitous Marker of Ultraviolet Radiation Exposure in Human Skin. *J. Invest. Dermatol.* 115, 674–679. doi:10.1046/j.1523-1747.2000.00092.x

Rechkoblit, O., Malinina, L., Cheng, Y., Kuryavyi, V., Broyde, S., Geacintov, N. E., et al. (2006). Stepwise Translocation of Dpo4 Polymerase during Error-free Bypass of an oxoG Lesion. *Plos Biol.* 4, e11. doi:10.1371/journal.pbio.0040011

Romani, A. M. P. (2011). Cellular Magnesium Homeostasis. *Arch. Biochem. Biophys.* 512, 1–23. doi:10.1016/j.abb.2011.05.010

Sirover, M. A., and Loeb, L. A. (1976). Infidelity of DNA Synthesis *In Vitro*: Screening for Potential Metal Mutagens or Carcinogens. *Science* 194, 1434–1436. doi:10.1126/science.1006310

Slater, J. P., Tamir, I., Loeb, L. A., and Mildvan, A. S. (1972). The Mechanism of *Escherichia coli* Deoxyribonucleic Acid Polymerase I. *J. Biol. Chem.* 247, 6784–6794. doi:10.1016/s0021-9258(19)44655-3

Smith, C. A., Baeten, J., and Taylor, J.-S. (1998). The Ability of a Variety of Polymerases to Synthesize Past Site-specific Cis-Syn, Trans-syn-II, (6-4), and Dewar Photoproducts of Thymidylyl-(3′→5′)-Thymidine. *J. Biol. Chem.* 273, 21933–21940. doi:10.1074/jbc.273.34.21933

Sohl, C. D., Szymanski, M. R., Mislak, A. C., Shumate, C. K., Amiralaei, S., Schinazi, R. F., et al. (2015). Probing the Structural and Molecular Basis of Nucleotide Selectivity by Human Mitochondrial DNA Polymerase γ. *Proc. Natl. Acad. Sci. USA* 112, 8596–8601. doi:10.1073/pnas.1421733112

Spelbrink, J. N., Toivonen, J. M., Hakkaart, G. A. J., Kurkela, J. M., Cooper, H. M., Lehtinen, S. K., et al. (2000). *In Vivo* functional Analysis of the Human Mitochondrial DNA Polymerase POLG Expressed in Cultured Human Cells. *J. Biol. Chem.* 275, 24818–24828. doi:10.1074/jbc.m000559200

Steitz, T. A. (1999). DNA Polymerases: DNA Polymerases: Structural Diversity and Common Mechanisms. *J. Biol. Chem.* 274, 17395–17398. doi:10.1074/jbc.274.25.17395

Steitz, T. A., and Steitz, J. A. (1993). A General Two-Metal-Ion Mechanism for Catalytic RNA. *Proc. Natl. Acad. Sci.* 90, 6498–6502. doi:10.1073/pnas.90.14.6498

Szymanski, M. R., Kuznetsov, V. B., Shumate, C., Meng, Q., Lee, Y. S., Patel, G., et al. (2015). Structural Basis for Processivity and Antiviral Drug Toxicity in Human Mitochondrial DNA Replicase. *EMBO J.* 34, 1959–1970. doi:10.15252/embj.201591520

Tokarsky, E. J., Wallenmeyer, P. C., Phi, K. K., and Suo, Z. (2017). Significant Impact of Divalent Metal Ions on the Fidelity, Sugar Selectivity, and Drug Incorporation Efficiency of Human PrimPol. *DNA Repair* 49, 51–59. doi:10.1016/j.dnarep.2016.11.003

Vaisman, A., Ling, H., Woodgate, R., and Yang, W. (2005). Fidelity of Dpo4: Effect of Metal Ions, Nucleotide Selection and Pyrophosphorolysis. *EMBO J.* 24, 2957–2967. doi:10.1038/sj.emboj.7600786

Varghese, A. J., and Wang, S. Y. (1967a). cis-syn Thymine Homodimer from Ultraviolet Irradiated Calf Thymus DNA. *Nature* 213, 909–910. doi:10.1038/213909a0

Varghese, A. J., and Wang, S. Y. (1967b). Ultraviolet Irradiation of DNA *In Vitro* and *In Vivo* Produces a Third Thymine-Derived Product. *Science* 156, 955–957. doi:10.1126/science.156.3777.955

Villani, G., Tanguy Le Gac, N., Wasungu, L., Burnouf, D., Fuchs, R. P., and Boehmer, P. E. (2002). Effect of Manganese on *In Vitro* Replication of Damaged DNA Catalyzed by the Herpes Simplex Virus Type-1 DNA Polymerase. *Nucleic Acids Res.* 30, 3323–3332. doi:10.1093/nar/gkf463

Weng, P. J., Gao, Y., Gregory, M. T., Wang, P., Wang, Y., and Yang, W. (2018). Bypassing a 8,5′-Cyclo-2′-Deoxyadenosine Lesion by Human DNA Polymerase η at Atomic Resolution. *Proc. Natl. Acad. Sci. USA* 115, 10660–10665. doi:10.1073/pnas.1812856115

Xia, S., Wang, M., Blaha, G., Konigsberg, W. H., and Wang, J. (2011). Structural Insights into Complete Metal Ion Coordination from Ternary Complexes of B Family RB69 DNA Polymerase. *Biochemistry* 50, 9114–9124. doi:10.1021/bi201260h

Yang, J. H., Lee, H. C., Chung, J. G., and Wei, Y. H. (2004). Mitochondrial DNA Mutations in Light-Associated Skin Tumors. *Anticancer Res.* 24, 1753–1758.

Yang, W., and Woodgate, R. (2007). What a Difference a Decade Makes: Insights into Translesion DNA Synthesis. *Proc. Natl. Acad. Sci.* 104, 15591–15598. doi:10.1073/pnas.0704219104

Conflict of Interest: The authors declare that the research was conducted in the absence of any commercial or financial relationships that could be construed as a potential conflict of interest.

Publisher's Note: All claims expressed in this article are solely those of the authors and do not necessarily represent those of their affiliated organizations, or those of the publisher, the editors, and the reviewers. Any product that may be evaluated in this article, or claim that may be made by its manufacturer, is not guaranteed or endorsed by the publisher.

frontiers in Molecular Biosciences

ORIGINAL RESEARCH
published: 03 November 2021
doi: 10.3389/fmolb.2021.778400

Identification and Characterization of Thermostable Y-Family DNA Polymerases η, ι, κ and Rev1 From a Lower Eukaryote, *Thermomyces lanuginosus*

Alexandra Vaisman[1†§], *John P. McDonald*[1†§], *Mallory R. Smith*[1†], *Sender L. Aspelund*[1†‡], *Thomas C. Evans Jr*[2†] *and Roger Woodgate*[1*†]

[1]*Laboratory of Genomic Integrity, National Institute of Child Health and Human Development, National Institutes of Health, Bethesda, MD, United States,* [2]*New England Biolabs Incorporated, Ipswich, MA, United States*

Y-family DNA polymerases (pols) consist of six phylogenetically separate subfamilies; two UmuC (polV) branches, DinB (pol IV, Dpo4, polκ), Rad30A/POLH (polη), and Rad30B/POLI (polι) and Rev1. Of these subfamilies, DinB orthologs are found in all three domains of life; eubacteria, archaea, and eukarya. UmuC orthologs are identified only in bacteria, whilst Rev1 and Rad30A/B orthologs are only detected in eukaryotes. Within eukaryotes, a wide array of evolutionary diversity exists. Humans possess all four Y-family pols (pols η, ι, κ, and Rev1), *Schizosaccharomyces pombe* has three Y-family pols (pols η, κ, and Rev1), and *Saccharomyces cerevisiae* only has polη and Rev1. Here, we report the cloning, expression, and biochemical characterization of the four Y-family pols from the lower eukaryotic thermophilic fungi, *Thermomyces lanuginosus*. Apart from the expected increased thermostability of the *T. lanuginosus* Y-family pols, their major biochemical properties are very similar to properties of their human counterparts. In particular, both Rad30B homologs (*T. lanuginosus* and human polι) exhibit remarkably low fidelity during DNA synthesis that is template sequence dependent. It was previously hypothesized that higher organisms had acquired this property during eukaryotic evolution, but these observations imply that polι originated earlier than previously known, suggesting a critical cellular function in both lower and higher eukaryotes.

Keywords: thermostable fungi, Y-family DNA polymerases, phylogenetic analysis, translesion DNA synthesis, DNA polymerase eta (polη), DNA polymerase iota (polι), DNA polymerase kappa (polκ), Rev1

OPEN ACCESS

Edited by:
Janice Pata,
Wadsworth Center, United States

Reviewed by:
Penny J. Beuning,
Northeastern University, United States
Pierre Barraud,
Expression Génétique Microbienne, France

****Correspondence:***
Roger Woodgate
woodgate@mail.nih.gov

†ORCID:
Alexandra Vaisman
orcid.org0000-0002-2521-1467
John P. McDonald
orcid.org/0000-0003-2482-148X
Mallory R. Smith
orcid.org/0000-0003-1450-7825
Sender L. Aspelund
orcid.org/0000-0003-0726-4028
Thomas C. Evans Jr
orcid.org/0000-0001-5406-0146
Roger Woodgate
orcid.org/0000-0002-2521-1467

‡Present address:
Sender L. Aspelund,
Novavax, Inc., Gaithersburg, MD 20878, United States

§The authors share first authorship

Specialty section:
This article was submitted to Structural Biology, a section of the journal Frontiers in Molecular Biosciences

Received: *16 September 2021*
Accepted: *19 October 2021*
Published: *03 November 2021*

Citation:
Vaisman A, McDonald JP, Smith MR, Aspelund SL, Evans TC and Woodgate R (2021) Identification and Characterization of Thermostable Y-Family DNA Polymerases η, ι, κ and Rev1 From a Lower Eukaryote, Thermomyces lanuginosus. *Front. Mol. Biosci. 8:778400. doi: 10.3389/fmolb.2021.778400*

INTRODUCTION

The Y-family DNA polymerases are responsible for copying damaged DNA during DNA replication in a process called translesion synthesis (TLS) (Sale et al., 2012). These enzymes are highly specialized in order to accommodate different structural DNA distortions caused by a wide variety of DNA lesions. The Y-family is divided into six phylogenetically distinct subfamilies: two UmuC (polV)

Abbreviations: Pols, polymerases; TLS, translesion synthesis; CPD, cyclobutane pyrimidine dimer; BPDE, benzo[*a*] pyrene diol epoxide; *S. cerevisiae*, *Saccharomyces cerevisiae*; *T. lanuginosus*, *Thermomyces lanuginosus*; *S. pombe*, *Schizosaccharomyces pombe*.

branches; Rad30A/POLH (polη); Rad30B/POLI (polι); and DinB (pol IV, Dpo4, polκ); and Rev1 (Ohmori et al., 2001). Across the different domains of life, Y-family polymerase subfamilies are found in various combinations. For example, UmuC orthologs are only detected in Gram-positive and Gram-negative bacteria, whereas Rev1 and Rad30A/B orthologs are only detected in eukaryotes. The DinB subfamily is the most evolutionarily conserved, having members scattered throughout all three domains of life from unicellular bacteria to humans. However, differences in the distribution of Y-family DNA pols are present within each kingdom. For example, the eukaryote *Saccharomyces cerevisiae* (*S. cerevisiae*) contains neither a *POLK* nor a *POLI* gene. Indeed, it was originally assumed that polι was expressed only in higher eukaryotes. However, next generation whole genome sequencing has revealed that polι orthologs are actually distributed throughout the whole Eukaryota domain. One example is the thermophilic fungus, *Thermomyces lanuginosus* (*T. lanuginosus*) which possesses all four eukaryotic Y-family subfamilies much like humans, in contrast to its fungal relatives, *S. cerevisiae* and *Schizosaccharomyces pombe* (*S. pombe*). Is there logic in such seemingly random distribution of polι? Using phylogenetic analysis and comparing the biochemical characterization of Y-family pols from different species, we hoped to shed some light on this question.

The Y-family DNA pols are classically described as specializing in TLS activity that arises from their capacious active sites that accommodate DNA lesions which would otherwise obstruct the processive confined active sites of A- and B-family replicative pols (Sale et al., 2012). Each Y-family polymerase is tailored to process different lesions, leaving behind unique errors after gaining access to the replication fork (Yang and Gao, 2018). Polymerases belonging to the same subfamily often specialize in targeting the same type of DNA lesions. For example, DinB/polκ orthologs are very adept at bypassing minor groove DNA adducts (*e.g.,* N^2-dG adducts) (Liu et al., 2014; Basu et al., 2017; Jha and Ling, 2018; Stern et al., 2019). Although, the archaeal ortholog, Dpo4, is notably less efficient at bypassing bulky aromatic lesions than its eukaryotic ortholog polκ (Avkin et al., 2004; Ling et al., 2004b; Choi et al., 2006). Along with a common preference for bulky aromatics, DinB pols also share a propensity for template slippage that increases deletion events in the mutation spectra (Kokoska et al., 2002).

Eukaryotic Rad30 orthologs polη and polι are similar in sequence but exhibit very different TLS properties. Human and *S. cerevisiae* polη are exceptionally efficient at bypassing a thymine-thymine cyclobutane pyrimidine dimer (CPD) (Johnson et al., 2000c; Masutani et al., 2000; McCulloch et al., 2004). Although polι can insert nucleotides opposite CPDs, the efficiency is substantially lower than polη-catalyzed TLS (Tissier et al., 2000a; Vaisman et al., 2003). Polι also has a unique feature; it misincorporates dG opposite dT, 3- to 10-fold more frequently than the correct base dA (Johnson et al., 2000b; Tissier et al., 2000b; Zhang et al., 2000c; McIntyre, 2020). These dG:dT misinsertions arise from polι′s remarkably large aliphatic side chains in the finger domain, unlike any other Y-family pols (Kirouac and Ling, 2009; Makarova and Kulbachinskiy, 2012). Despite the extremely low fidelity of polι on a template dT, it is moderately accurate when incorporating opposite other target bases. The highest fidelity is found opposite the template A, where polι inserts the correct base dT with error rate of 10^{-4} (Johnson et al., 2000b; Tissier et al., 2000b; Zhang et al., 2000c).

The unique feature of eukaryotic Rev1 orthologs is their efficiency at bypassing both damaged guanines and abasic sites using a deoxycytidyl transferase mechanism that limits Rev1 to exclusively incorporate dC (Nelson et al., 1996). This is achieved by displacing the DNA lesion from the active site entirely and instead using a protein sidechain (R324 in *S. cerevisiae* and R357 in *H. sapiens*) as the "template" which base pairs solely with dC (Nair et al., 2005, 2011; Weaver et al., 2020).

In this manuscript, we describe the identification, purification and characterization of thermostable eukaryotic orthologs of polη, polι, polκ, and Rev1 from a thermophilic, multicellular fungal species, *T. lanuginosus*. Biochemical characterization of TLS DNA pols η, ι, κ, and Rev1 include determination of the enzyme's fidelity, processivity, thermostability, metal ion requirements, and TLS specificity during bypass of CPDs, abasic sites, and benzo[*a*] pyrene diol epoxide (BPDE) adducts. Our findings serve as basis for comparative analysis of the properties of proteins from different species, thus providing an important insight into the functional evolution of the Y-family polymerases.

MATERIALS AND METHODS

Bacterial Plasmids

Plasmids used in this study are described in **Table 1**. Where noted, bacteria were grown on LB agar plates containing 20 μg/ml chloramphenicol; 25 μg/ml zeocin; 30 μg/ml kanamycin; 20 μg/ml spectinomycin; or 100 μg/ml ampicillin.

Identification and Cloning of Y-Family Orthologs From *T. lanuginosus*

At the onset of this investigation, the complete genomic sequence of *T. lanuginosus* was not yet available. Therefore, in order to identify and clone the various Y-family polymerase orthologs from *T. lanuginosus*, we used several PCR-based procedures. Initially, we employed a degenerate PCR approach by first generating protein homology comparisons for known fungal polη, polι, polκ, and Rev1 proteins. Regions of conserved amino acid stretches within these four polymerase families were identified and degenerate PCR primers were designed based on selected conserved amino acid regions. Purified *T. lanuginosus* genomic DNA was purchased from DSMZ (Leibniz Institute DSMZ-German Collection of Microorganisms and Cell Cultures GmbH) (DSM 10635). PCR and nested-PCR were performed utilizing this *T. lanuginosus* genomic DNA and amplicons of gene segments encoding these four Y-family polymerases were cloned and sequenced. Based on the cloned DNA sequences that encoded regions of the Y-family polymerase genes, gene-specific PCR primers were designed. Additional PCR reactions were performed either using

TABLE 1 | Plasmids used in this study.

Plasmid	Relevant characteristics	Source or reference
pGEM-T	TA PCR cloning vector	Promega
pET22b+	Protein expression vector	EMD Millipore
pJM871	Low copy expression vector	Frank et al. (2012)
pJM574	*T. lanuginosus POLH* in pGEM-T	This study
pJM676	*T. lanuginosus POLK* in pGEM-T	This study
pJM861	*T. lanuginosus REV1* in pGEM-T	This study
pUC57_Ec_CO_TI iota	*T. lanuginosus POLI* in pUC57	Genscript
pJM596	*T. lanuginosus POLH* expression vector (pET22b)	This study
pJM682	*T. lanuginosus POLK* expression vector (pET22b)	This study
pJM863	*T. lanuginosus REV1* expression vector (pET22b)	This study
pJM966	*T. lanuginosus POLI* expression vector (pJM871)	This study

genomic DNA or DNA from a *T. lanuginosus* cDNA library, kindly provided by the Fungal Genomics Project at Concordia University (Adrian Tsang; Director of the Center for Functional and Structural Genomics). PCR techniques employed included RACE PCR (cDNA library), Flanking-sequence PCR (Sorensen et al., 1993) utilizing degenerate biotinylated primers and overlapping exon PCR (genomic DNA). Full-length genes were amplified with gene-specific primers with the addition of an *Nde*I site at the 5′ end and either a *Bam*HI or *Bgl*II (*POLK*) site at the 3′ end and cloned into pGEM vectors for sequencing. The *POLH*, *POLK* and *REV1* genes were subcloned into the *Nde*I to *Bam*HI sites of pET22b+ for protein expression. An *E. coli* codon optimized version of the *POLI* gene was subsequently synthesized by Genscript (Piscataway, NJ) and cloned into the pJM871 low expression vector (Frank et al., 2012) from *Nde*I to *Bam*HI.

Subsequently, the full *T. lanuginosus* SSBP genomic sequence was published and released (https://mycocosm.jgi.doe.gov/Thelan1/Thelan1.home.html) (McHunu et al., 2013) (GenBank assembly accession GCA_000315315935.1), and we were able to confirm that our clones do indeed encode the *T. lanuginosus* polη, polι, polκ, and Rev1 proteins. The *POLH* gene is encoded on contig00146 (Genbank accession ANHP01000280) from nucleotide 84213–86129. The *POLI* gene is encoded on contig00250 (Genbank accession ANHP01000232) from nucleotide 126087–127864 with two introns. The *POLK* gene is encoded on contig00025 (Genbank accession ANHP01000258) from nucleotide 58089–60067 with one intron. The Rev1 gene is encoded on contig00203 (Genbank accession ANHP01000194) from nucleotide 112065–115607 with one intron. The Joint Genome Institute MycoCosm database designations for theses proteins is as follows: polη – jgi|Thelan1|4409|TLAN_03021-R0; polι – jgi|Thelan1|3308|TLAN_02476-R0; polκ – jgi |Thelan1| 3900|TLAN_01802-R0; Rev1 – jgi|Thelan1|3900|TLAN_ 01802-R0.

Phylogenetic Tree Construction

A multiple sequence alignment of the newly described *T. lanuginosus* polι protein and polι proteins from various other organisms was performed using the ClustalW algorithm in MacVector (version 15.5.4). Known polι protein sequences were obtained from Genbank protein records or identified by BLAST homology searches of Genbank genomic sequence records. Genbank accession numbers are indicated within the legend of **Figure 1**. The alignment was exported from MacVector in the Nexus sequence file format. This Nexus file was imported into the SplitsTree4 (version 4.14.4) and an unrooted phylogenetic tree was generated by setting the distance method to BioNJ.

Purification of the *T. lanuginosus* DNA Polη

E.coli strain RW644 [F^- *dcm ompT hsdS*(rB^- mB^-) *gal* λ(DE3) Δ*umuDC596*::*ermGT* Δ*dinB61*::*ble* Δ*araD-polB*::Ω Δ(*gpt-proA*)62] harboring pJM596 was grown overnight in 20 ml LB media containing 100 μg/ml ampicillin at 37°C. The overnight culture was then transferred into 1L fresh LB-ampicillin and grown at 37°C until an OD_{600} ~0.5. At this point, IPTG was added to a final concentration of 1 mM to induce expression of *T. lanuginosus* DNA polη and grown for an additional 2 h before cells were harvested by centrifugation. The cell pellet was resuspended in 15 ml lysis buffer (50 mM Tris pH 8.0, 150 mM NaCl, 10 mM β-mercaptoethanol), sonicated, and cleared by ultracentrifugation at 45,000 rpm in a Beckman 50.2 Ti rotor for 45 min. Ammonium sulfate (45% saturation, 0.27 g/ml) was slowly added to the cleared lysate and stirred at 4°C for 30 min. Precipitated proteins were harvested by centrifugation and the resulting pellet resuspended in a buffer "A" (50 mM Tris pH 8.0, 20 mM NaCl, 10 mM β-mercaptoethanol, 20% v/v glycerol) and dialyzed overnight at 4°C against 1L of the same buffer. The dialyzed protein suspension was applied to a 5 ml HiTrap DEAE FF column (Cytiva, cat#17515401) and bound proteins were eluted with a 20–500 mM linear gradient of NaCl. Fractions containing polη were pooled and dialyzed against buffer "B" (10 mM sodium phosphate, pH 7.0,10 mM β-mercaptoethanol, 20% v/v glycerol) and applied to a 5 ml Bio-Scale™ Mini CHT™ Type II cartridge (BioRad, cat#7324332) and eluted with a 10–300 mM linear gradient of sodium phosphate in buffer B. Peak polη-containing fractions were pooled, aliquoted and stored at −80°C.

Purification of the *T. lanuginosus* DNA Polκ-

T. lanuginosus DNA polκ was expressed in RW644 harboring pJM682 and purified using the same protocol as described above for polη.

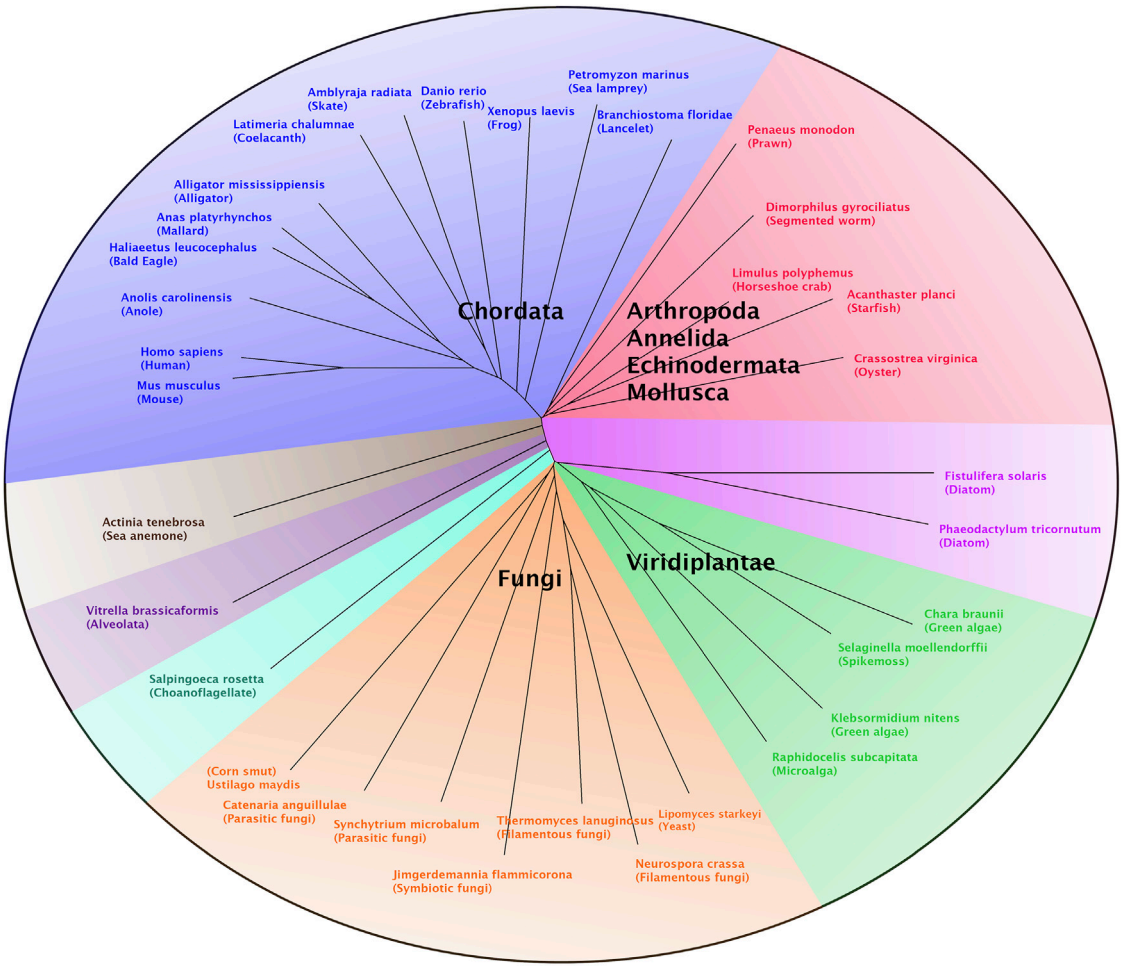

FIGURE 1 | Phylogenetic analysis of polι. A multiple sequence alignment of polι proteins from a broad range of eukaryotic organisms, including *T. lanuginosus* polι and human polι, was performed using the ClustalW algorithm in MacVector (version 15.5.4). This alignment was exported from MacVector as a Nexus file which was then imported into SplitsTree4 (version 4.14.4) to generate an unrooted phylogenetic tree by setting the distance method to BioNJ. Most of the polι proteins cluster into several groups comprised of chordates (blue), lower animals (red), lower plants (green), fungi (orange) and diatoms (pink). Polι protein sequences for each organism were obtained from the following Genbank sequence files: *Acanthaster planci* (XP_022107640), *Actinia tenebrosa* (XP_031566011), *Alligator mississippiensis* (XP_006269716), *Amblyraja radiata* (XP_032889300), *Anas platyrhynchos* (XP_027302772), *Anolis carolinensis* (XP_016850726), *Branchiostoma floridae* (XP_035668094), *Catenaria anguillulae* (ORZ32752), *Chara braunii* (GBG75489), *Crassostrea virginica* (XP_022331447), *Danio rerio* (NP_001017834), *Dimorphilus gyrociliatus* (CAD5123533), *Fistulifera solaris* (GAX13589), *Haliaeetus leucocephalus* (XP_010581340), *Homo sapiens* (NP_001338561), *Jimgerdemannia flammicorona* (RUP43481), *Klebsormidium nitens* (GAQ87748), *Latimeria chalumnae* (XP_005994715), *Limulus polyphemus* (XP_022236329), *Lipomyces starkeyi* (ODQ70434), *Mus musculus* (NP_036102), *Neurospora crassa* (CAD70389), *Penaeus monodon* (XP_037797824), *Petromyzon marinus* (XP_032824552), *Phaeodactylum tricornutum* (XP_002178064), *Raphidocelis subcapitata* (GBF90329), *Salpingoeca rosetta* (XP_004998634), *Selaginella moellendorffii* (XP_024528028), *Synchytrium microbalum* (XP_031023241), *T. lanuginosus* (this study and ANHP01000232), *Ustilago maydis* (XP_011387208), *Vitrella brassicaformis* (CEL97102) and *Xenopus laevis* (XP_018100075).

Purification of the *T. lanuginosus* DNA Polι

Our attempts to purify untagged *T. lanuginosus* polι using the above protocol for polη and polκ proved to be unsuccessful. We therefore decided to purify an N-terminal His-tagged version of *T. lanuginosus* polι. To do so, plasmid pJM966 was introduced into the *E.coli* SHuffle® T7 Express strain [F' *lac, pro, lacI*^{q}/Δ(*ara-leu*)*7697 araD139 fhuA2 lacZ*::T7 gene1 Δ(*phoA*)PvuII *phoR ahpC galE galK* λ*att*::pNEB3-r1-cDsbC (Spec^{R}, *lacI*^{q}) *ΔtrxB rpsL150*(Str^{R}) Δ*gor* Δ(m*alF*)3] (New England Biolabs, cat#C3029J). Expression, cell harvest, lysis, and clearance were performed as described above for polη and polκ and the cleared lysate was dialyzed overnight at 4°C against 1L of buffer "C" (20 mM Sodium Phosphate, pH 7.5, 500 mM NaCl, 20 mM imidazole, 10 mM β-mercaptoethanol, 10% v/v glycerol) The dialysed lysate was applied to a 5 ml HisTrap HP column (Cytiva, cat#17524701) and eluted with a linear 20 mM to 1 M imidazole gradient. Fractions containing polι were pooled and dialyzed against 1L of buffer "D" (10 mM Sodium Phosphate, pH 7.5, 300 mM NaCl, 10 mM β-mercaptoethanol, 20% v/v glycerol) and applied to a 5 ml Bio-Scale™ Mini CHT™ Type II cartridge

(BioRad, cat#7324332) and eluted with a 10–300 mM linear gradient of sodium phosphate. Peak polι-containing fractions were pooled, aliquoted and stored at −80°C.

Purification of *T. lanuginosus* Rev1

RW644 harboring pRARE2 (expressing tRNAs for seven rare codons; AGA, AGG, AUA, CUA, GGA, CCC, and CGG) was transformed with pJM863. The strain was grown overnight in 60 ml LB media containing 100 μg/ml ampicillin at 37°C. The overnight culture was then transferred into 3L fresh LB-ampicillin (1.5 L each in 2 x 4L flasks) and grown at 37 °C until an OD_{600} ~0.5. At this point, IPTG was added to a final concentration of 1 mM to induce expression of *T. lanuginosus* Rev1 and grown for an additional 2 h before cells were harvested by centrifugation. The cell pellet was resuspended in 60 ml lysis buffer (50 mM Tris pH 7.5, 0.5 mM EDTA, 1 mM DTT, 20% glycerol), sonicated, and cleared by ultracentrifugation at 45,000 rpm in a Beckman 50.2 Ti rotor for 45 min. Ammonium sulfate (35% saturation, 0.2 g/ml) was slowly added to the cleared lysate and stirred at 4°C for 30 min. Precipitated proteins were harvested by centrifugation and the resulting pellet resuspended in a buffer "E" (10 mM Sodium phosphate pH 7.0, 25 mM NaCl) and dialyzed overnight against 2L of the same buffer at 4°C. The dialysed lysate was applied to a 20 ml HiPrep Heparin FF 16/10 column (Cytiva, cat#28936549) and eluted with a 25–400 mM NaCl linear gradient. Fractions containing Rev1 were pooled and applied to a HiPrep 16/60 Sephacryl S-200 HR size exclusion column (Cytiva, Cat#17116601) equilibrated in Phosphate Buffered Saline (PBS, pH6.8). Rev1 containing fractions were pooled and applied to a 5 ml Phosphocellulose P11 column (Whatman), equilibrated with buffer "F" (20 mM KPO_4 pH 7.0, 100 μM EDTA, 10% glycerol, 1 mM DTT, and 100 mM KCl) and eluted with a 200–800 mM KCl linear gradient. Rev1-containing fractions were pooled, concentrated, and aliquoted for storage at −80°C.

DNA Templates

Undamaged synthetic oligonucleotide primers and an 48 bp abasic site-containing template were synthesized by Lofstrand Laboratories (Gaithersburg, MD) using standard technique and PAGE purified. A synthetic abasic site, dSpacer, was purchased from Glen Research (Sterling, VA) and incorporated into the oligonucleotide template using standard techniques by Lofstrand Laboratories. The 7.2 kb M13mp18 circular template was purchased from New England Biolabs (Ipswich, MA). The *cis-syn* CPD containing oligonucleotide was synthesized by TriLink BioTechnologies (San Diego, CA) and has been described previously (Boudsocq et al., 2004). The synthesis of a template with BPDE-dA adduct was described previously (Frank et al., 2002). The sequence of each primer-template pair is given in the legend of the respective figures. Radiolabeled primers were labeled with [γ-^{32}P]ATP using T4 polynucleotide kinase by Lofstrand Laboratories (Gaithersburg, MD). The fluorescent primer containing a 5′-Fluorescein (6-FAM), 5′-6FAM-ATGGTACGGACGTGCTT-3′, was synthesized by Lofstrand Laboratories. The template strand complementary to the fluorescent primer used in **Figure 7B–D** had the following sequence: 5′-ATTAACGAATGAAGCACGTCCGTACCATCG-3′, whereby the underlined base indicates the identity of the templating base. For **Figure 7E**, the sequences of the three template strands used to investigate damaged and undamaged bypass were also complementary to the fluorescent primer and are as follows: dG: 5′-ATTAACGAATGAAGCACGTCCGTACC ATCG-3'; abasic site (X): 5′-ATTAACGAATXAAGCACG TCCGTACCATCG-3'; and CPD: 5′-TCGATACTGGTA CTAATGATTAACGAATTAAGCACGTCCGTACCATCG-3'. All primers were annealed to the unlabeled templates at a ratio of 1:2 by heating the primer and template together at 95°C in annealing buffer (0.1 M Tris-HCl, pH 8.0, 10 mg/ml BSA, 14.2 mM β-mercaptoethanol) and allowing the mixture to slowly cool to room temperature.

Radiolabeled *in vitro* Primer Extension

Standard 10 μl reactions contained 50 mM Tris-HCl, pH 7.5, 100 μM each dNTP, 10 mM DTT, 10 nM primer-template DNA, unless specified otherwise in the legend, and supplemented with 4 mM $MgCl_2$ for pols η- and κ-catalyzed reactions and 4 mM $MnCl_2$ for polι-catalyzed reactions. Reactions were carried out at 37°C for 10 min except in thermostability and processivity experiments, where the temperature and duration varied as noted in the figure legends. Reactions were terminated by the addition of 10 μl of 95% Formamide, 17.5 mM EDTA, 0.025% Xylene cyanol, and 0.025% Bromophenol blue, heated at 95°C for 5 min, and briefly chilled on ice. Aliquots containing 5 μl of the samples were separated on 15% 8 M Urea polyacrylamide gels and visualized by PhosphorImager analysis.

6-FAM *in vitro* Primer Extension

For *in vitro* polymerase assays with *T. lanuginosus* Rev1, 12 μl reactions containing 50 mM Tris-HCl, pH 7.5, 10% glycerol w/v, 1 mM β-mercaptoethanol, 100 nM primer-template DNA, 5 nM *T. lanuginosus* Rev1, and 5 mM $MgCl_2$ (with the exception of the Me^{2+} activation experiment) were initiated with 100 μM dNTP. Reactions were carried out at 37°C for 10 min except in the thermostability and processivity experiments, where the temperature and duration of experiments varied, respectively, as detailed in the figure legends. Reactions were terminated by the addition of 12 μl of 10 M Urea, 100 mM EDTA, 0.2% Xylene cyanol, and 0.02% Bromophenol blue, heated at 95°C for 5 min. Aliquots containing 12 μl of the samples were separated on 22% 8 M Urea polyacrylamide gels (Triple Wide Mini-Vertical gel system, C.B.S. Scientific) and visualized using 5′-fluorescein (6-FAM) fluorescence with a Typhoon FLA 7000 (GE Healthcare).

RESULTS AND DISCUSSION

Identification of Y-Family Polymerases in *T. lanuginosus*

Based on previous investigations and observations, it has been noted that the genomes of higher eukaryotes, such as humans and

mice, possess genes for the four known eukaryotic Y-family pols, whereas, the model organism *S. cerevisiae* only possesses genes for two of the eukaryotic Y-family pols, *RAD30* and *REV1*. Based on this observation, it has been suggested the genes encoding the closely related polη and polι proteins are paralogs of each other that diverged during evolution sometime after the origination of fungi. However, BLAST homology searches revealed that the genomes of filamentous fungi such as *Neurospora crassa* and *Aspergillus nidulans* and even the corn smut *Ustilago maydis* harbor a *POLI* gene, indicating to us that the genetic and biochemical characteristics of translesion synthesis in some "higher" fungi could be quite akin to that in higher eukaryotes such as humans. This notion of conserved functionality provided the impetus to embark on our efforts to identify and clone the four eukaryotic Y-family pols from the fungi, *T. lanuginosus*. Since *T. lanuginosus* is thermophilic, we reasoned the Y-family pols from this organism would exhibit enhanced stability during purification and biochemical analysis (see below).

In order to identify and clone the *T. lanuginosus* Y-family pols, protein sequence similarity comparisons were performed using known polη, polι, polκ, and Rev1 protein sequences, including other fungal sequences. Initially, degenerate PCR primers were designed based on highly conserved regions of protein homology between the various proteins within the four Y-family polymerase groups. Degenerate PCR was performed using *T. lanuginosus* genomic DNA and amplicons were cloned and sequenced. Subsequently, sequence of cloned regions of the Y-family polymerase genes were used to design gene-specific primers. A combination of various PCR techniques was then employed, for example degenerate PCR, nested PCR, RACE PCR, over-lapping exon PCR and flanking-sequence PCR using either genomic DNA or cDNA library DNA, to generate full-length sequences of each of the *T. lanuginosus POLH, POLI, POLK* and *REV1* genes. Full-length genes were then subcloned into protein expression vectors to facilitate purification of the four Y-family DNA pols. After we completed cloning the Y-family pol genes, the *T. lanuginosus* genome was sequenced and published allowing us to confirm that our cloned sequences do indeed encode the correct *T. lanuginosus* proteins. Sequence comparisons between *T. lanuginosus* and human Y-family pols reveal modest similarities that are higher than those observed between *S.cerevisiae* and human homologs. *T. lanuginosus* and human polη have 22% identical and 15% similar residues (compare to *S. cerevisiae* versus human at 16% identical and 15% similar residues). *T. lanuginosus* and human Rev1 have 24% identical and 15% similar residues (compare to *S. cerevisiae* versus human at 16% identical and 16% similar residues). Additionally, *T. lanuginosus* and human polκ have 20% identical and 14% similar residues, and *T. lanuginosus* and human polι have 24% identical and 16% similar residues.

Phylogenetic analysis of the Y-Family Polymerase poli

The observation that the four eukaryotic Y-family pols are present in many filamentous fungi suggested to us that the divergence of *POLI* and *POLH* is even more ancient than the divergence of the fungi and metazoan (animals) groups. This supposition prompted us to perform a more in-depth phylogenetic analysis on the origins of the polι protein. We executed an exhaustive search for polι protein sequences within the Genbank database, including the fungi and metazoan groups, all other groups with clades containing various "lower" eukaryotes, and the plant kingdom. Although the *POLI* gene was absent from many "lower" or "simpler" eukaryotic organisms than fungi, as well as higher plants, we did find several examples of lower eukaryotes and simpler plants that do in fact encode a *POLI* gene.

A ClustalW alignment was performed using a group of sequenced *POLI* genes from organisms that include simple eukaryotes, lower plants, fungi and metazoans, all of which also possess genes for *POLH*, *POLK* and *REV1*. The unrooted phylogenetic tree of this alignment (**Figure 1**) reveals that the polι proteins cluster, for the most part, within several groups that include a chordate group, a lower animal grouping, including arthropods, annelids, echinoderms and mollusks, a fungi group, and a lower plant group. Polι proteins from other organisms that did not fit into these groups include a protein from a sea anemone (a Cnidarian), two proteins from diatom organisms and proteins from an Alveolate and a Choanoflagellate, which are examples of very simple single-celled eukaryotes. Interestingly, our analysis further supports the perception that the *POLI* gene is quite commonly found in fungal species, including some yeasts, and even other lower eukaryotic organisms and therefore substantiates our supposition that the evolutionary "split" between *POLH* and *POLI* may have preceded the emergence of fungi.

During this phylogenetic analysis of polι, one particularly noteworthy and unexpected observation was that *POLI* genes were quite frequently identified in some organisms within a particular group and absent in other organisms within that group. This finding holds true from the simplest eukaryotes to higher eukaryotes. For example, many protists do not possess a *POLI* gene such as Metamonads (*e.g.,* diplomonads, *i.e., Giardia lamblia* and parabasalids, *i.e., Trichomonas vaginalis*), Euglenozoans (*e.g.,* trypanosomatids, *i.e., Trypanosoma brucei* and *Leishmania donovani*) and Amoebozoans (*e.g., Entamoeba histolytica*). While other groups of protists do have a *POLI* gene such as Heteroloboseas (*e.g., Naegleria gruberi*) and Alveolates [*e.g., Vitrella brassicaformis* (Colpodellida clade)]. In direct contrast, other species of Alveolates in the Apicomplexans clade (*e.g., Cryptosporidium parvum*) and the Ciliophorans clade (ciliates) (*e.g., Paramecium tetraurelia*) do not have a *POLI* gene. In addition, some Stramenopiles have a *POLI* gene (*e.g.,* diatoms, *i.e., Phaeodactylum tricornutum* and *Fistulifera solaris*) and some do not (*e.g.,* diatoms, *i.e., Thalassiosira oceanica* and *e.g.,* water mould, *i.e., Saprolegnia parasitica*). Thus, it seems the presence, or absence, of a *POLI* gene in the genome of any specific organism is quite indiscriminate.

This unpredictable "hit or miss" trait of *POLI* holds true in plants, fungi, and metazoans as well. For example, we found *POLI* genes in the genomes of lower plant forms such as microalga,

green algae, and spikemoss but were unable to find *POLI* genes in any higher vascular plants. A similar situation exists in fungi. No *POLI* genes were found in lower fungal forms such as Microsporidia and Glomeromycota. Likewise, in Saccharomycotina (true yeasts) (e.g., *S. cerevisiae*) no *POLI* genes were found. Some fungi in the Taphrinomycotina subphylum, such as *Saitoella complicate*, have *POLI* genes, while the closely related fission yeasts, *Schizosaccharomyces* species, do not. Furthermore, *POLI* genes were found in other yeast forms (*e.g.,* Lipomyces starkeyi), filamentous fungi, parasitic, and symbiotic fungi, and corn smut (**Figure 1**). However, we found no *POLI* genes in Basidiomycota which include club fungi and mushrooms.

Although most organisms within the various groups of animals, from the Choanoflagellates (considered to be the closest living relatives of the animals) up to the mammals, possess a *POLI* gene, we found it remarkable that there are numerous examples of higher eukaryotes organisms that do not possess a *POLI* gene. For example, we found no *POLI* genes in most Platyzoa (*i.e.,* Platyhelminthes, *e.g.,* flat worms), Rotifera (i.e., wheel animals), and Annelids (i.e., segmented worms), with the notable exception of *Dimorphilus gyrociliatus* which does harbor a *POLI* gene (**Figure 1**). While, many types of Mollusks do possess *POLI* genes, we found no *POLI* gene in octopi. Apparently, Arthopods such as spiders, scorpions, sea spiders, centipedes, millipedes and tardigrades (water bears) do not have *POLI*, but horseshoe crabs do. With a few exceptions, the majority of crustaceans and insects have *POLI*. Lastly, we found that the vast majority of chordates from the lancelet to humans do indeed possess a *POLI* gene (**Figure 1**). However, there are some extraordinary exceptions. We found that the tunicates (sea squirts), which are lower chordates, lack a *POLI* gene. Thus far, only a single fish species, *Esox lucius* (northern pike), was identified as lacking *POLI*. While alligators possess a *POLI* gene, the Australian saltwater crocodile (*Crocodylus porosus*) and the gharial (*Gavialis gangeticus*) both lack *POLI*. Most astoundingly, the majority of bird species, including Galliformes (*e.g.,* chickens, turkeys, grouse, quail, partridges and pheasants), Bucerotiformes (hornbills), Upupiformes (hoopoes) and the vast majority of Passeriformes (*e.g.,* sparrow, finch, tit, crow, canary, rifleman, and starlings) which includes more than half of all bird species, lack a *POLI* gene.

This phylogenetic analysis provides a "snapshot" of the evolution of *POLI* at this given moment in time. At some time in the past, the polη and polι paralogs diverged from one another due to a need to have two biochemically distinct translesion synthesis polymerases. The biochemical properties of both human polη and polι are well characterized. However, unlike polη which is defective in the human *Xeroderma Pigmentosum* Variant syndrome (Masutani et al., 1999), the cellular function of polι remains enigmatic (McIntyre, 2020; Vaisman and Woodgate, 2020). Therefore, the evolutionary pressure that led to this division of polη and polι remains a mystery. Perhaps this seemingly arbitrary "hit or miss" distribution of *POLI* genes in eukaryotic organisms can provide clues as to the cellular functioning of polι. Evaluation of the biological and biochemical translesion synthesis properties of polη and polι from closely related lower eukaryotes, one of which possesses a *POLI* gene and the other that does not, may provide hints as to when, and why, these two paralogs diverged and the cellular functions of polι.

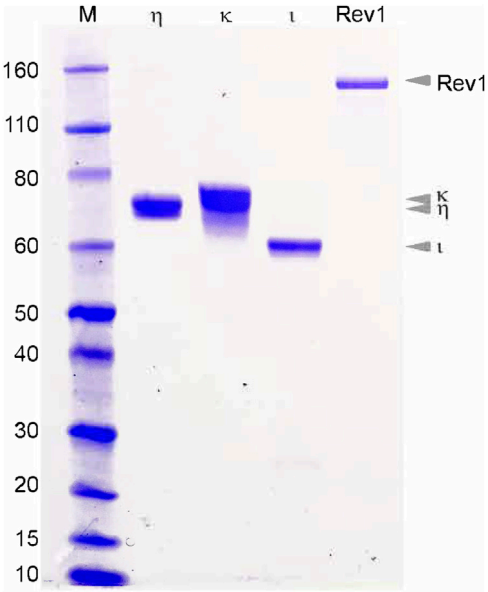

FIGURE 2 | Purified *T. languinosus* polymerases η, κ, ι and Rev1. Two to five μg of the final purified polymerases were separated on a 12% SDS-PAGE gel. Visual analysis suggests each polymerase is greater than 95% pure.

Expression and Purification of *T. lanuginosus* Polymerases η, ι, κ, and Rev1

All four Y-family pols from *T. lanuginosus* were expressed in *E. coli*, but their expression levels, solubility, and ease of purification varied. Both pols η and κ were well-expressed in *E. coli* and readily purified by conventional protocols including ammonium sulfate precipitation and ion-exchange chromatography (**Figure 2**). Rev1 was initially poorly expressed (unpublished observations), but expression increased dramatically in the presence of the pRARE2 plasmid coding for rare *E.coli* tRNAs. *T. lanuginosus* Rev1 was also purified by conventional methods including ammonium sulfate precipitation, size-exclusion and ion-exchange chromatography (**Figure 2**). *T. lanuginosus* polι was the most problematic of the four Y-family polymerases to purify, requiring codon optimization for *E.coli* expression and the addition of an N-terminal Histidine tag. Subsequently, the protein was purified by affinity- and ion exchange-chromatography (**Figure 2**). Once the polymerases were purified to >95% homogeneity, they were characterized for metal ion requirement, ability to bypass lesions, fidelity, thermostability, and processivity.

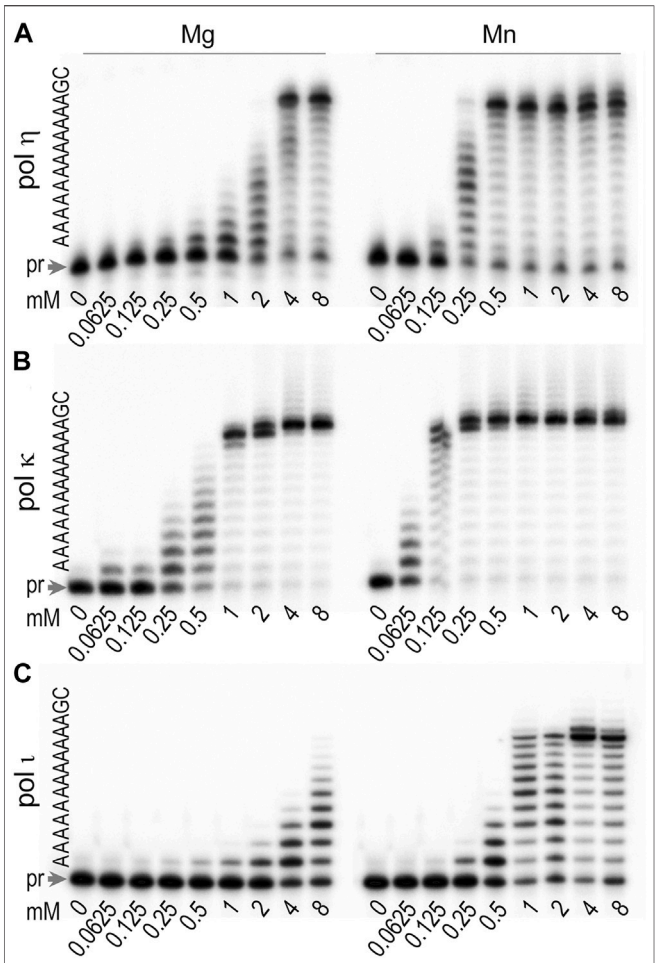

FIGURE 3 | Determination of metal ion requirements (type and concentration) for optimal activity of **(A)** polη **(B)** polκ, and **(C)** polι. The extension of ^{32}P-labeled primer 5′-CGATGGTACGGACGTGCTT-3′ hybridized to a template 3′-GCTACCATGCCTGCACGAAAAAAAAAA AAGC-5′ was carried out for 10 min at 37°C in the presence of 100 μM dNTPs mixture and with increasing concentrations of $MgCl_2$ or $MnCl_2$, ranging from 0.0625 to 8 mM. Concentrations of enzymes were 0.17 pM for polη, 0.32 pM for polκ, and 0.15 pM for polι. The sequence of the template immediately downstream of the primer (pr) is shown on the left-hand side of each gel pair.

Activation of *T. lanuginosus* Polymerases η, κ, ι by Mn^{2+} and Mg^{2+}

DNA polymerases are known to require divalent cations to catalyze the nucleotidyl transfer reaction (Bessman et al., 1958; Mildvan and Loeb, 1979; Loeb and Kunkel, 1982; Vashishtha et al., 2016). Although it is generally believed that Mg^{2+} is the activating co-factor *in vivo* due to its cellular abundance, other divalent metal cations such as Mn^{2+}, Co^{2+}, Ni^{2+}, Zn^{2+} have the ability to substitute for Mg^{2+} under certain conditions (Mildvan and Loeb, 1979; Loeb and Kunkel, 1982). Different metal co-factors can affect the activity and fidelity of DNA polymerases, promote TLS, and in the case of X-family enzymes, increase polymerization efficiency (Martin et al., 2013). In rare cases, Mn^{2+} appears to serve as a natural metal activator of DNA polymerases. This has been shown for X-family polymerases λ and μ and Y-family polι which exhibit great preference for Mn^{2+} over Mg^{2+} as the activating metal ion (Dominguez et al., 2000; Frank and Woodgate, 2007; Garcia-Diaz et al., 2007). In particular, human polι was inhibited by $MgCl_2$ present at physiological concentrations and exhibited peak activity at low $MnCl_2$ levels (0.05–0.25 mM). Furthermore, at optimal concentrations, Mn^{2+} ions improved the fidelity of polι-catalyzed nucleotide incorporation opposite template dT.

We were interested in determining the optimal concentration and type of divalent metal ion that is required for activation of *T. lanuginosus* pols η, κ, and ι. We assessed the primer extension activity of these polymerases in the presence of Mg^{2+} and Mn^{2+} at concentrations ranging from 62.5 μM to 8 mM (**Figure 3**).

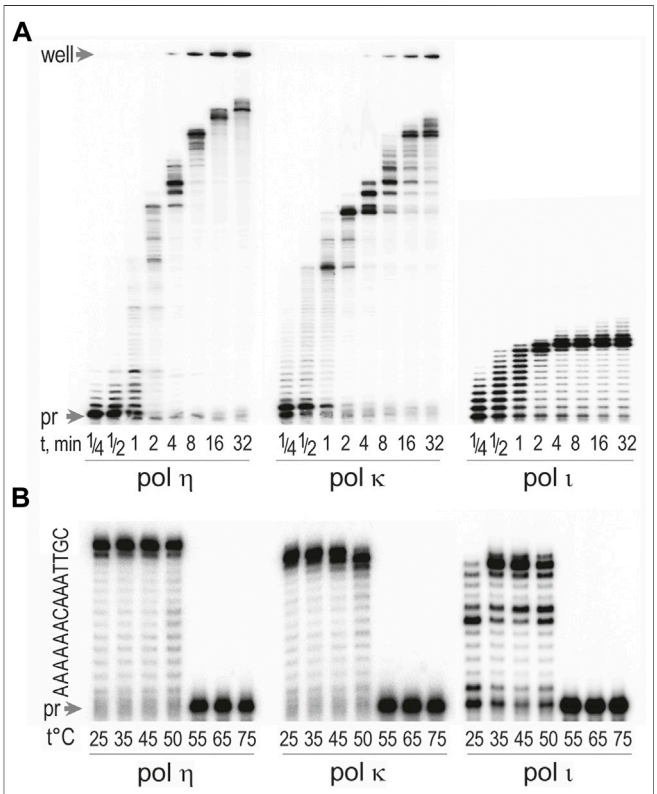

FIGURE 4 | Thermostability and processivity of *Thermomyces lanuginosus* pols η, κ, and ι. Concentrations of enzymes were 0.17 pM for pol η, 0.32 pM for pol κ, and 0.15 pM for pol ι. **(A)** Processivity of pols η, κ, and ι were assayed in reactions containing 100 μM dNTPs and 4 mM $MnCl_2$ for polι or $MgCl_2$ for polη and polκ. Extension of ^{32}P labeled primer 5′ TATTTA TCCCAATCCAAATAAGAAACGA-3′ hybridized to the circular single-stranded 7.2 kb M13mp18 bacteriophage was at 37°C for various times ranging from 0.25 to 32 min. Reactions containing 100 μM dNTPs and 4 mM $MnCl_2$ for reactions with polι and $MgCl_2$ for reactions with polη and polκ. (**B**) Thermostability was assayed by primer extension reactions using DNA template generated by annealing of a^{32}P-labeled primer 5′-TATTTATCCCAA TCCAAATAAGAAACGA-3′ with an undamaged DNA template 5′-CGTTAA ACAAAAAATCGTTTCTTATTTGGATTGGGATAAATA-3′. Reactions were carried out for 10 min at various temperatures ranging from 25 to 75°C and contained 100 μM dNTPs and 4 mM Mn^{2+} to activate polι or Mg^{2+} to activate polη and polκ.

Polη exhibited greatest activity in reactions with 4–8 mM Mg^{2+} and 0.5–8 mM Mn^{2+} (**Figure 3A**). Reactions catalyzed by polκ were most efficient at 1–8 mM Mg^{2+} and 0.25–8 mM Mn^{2+} (**Figure 3C**). Polι was most active in the presence of ~4 mM Mn^{2+} (**Figure 3B**).

As shown in **Figure 3**, Mn^{2+} appears to be a more conducive co-factor than Mg^{2+} in reactions with all three *T. lanuginosus* pols, as they all were active over a wider range of Mn^{2+} and exhibited greater activity at the same concentration of Mn^{2+} vs. Mg^{2+}. However, there are some interesting differences seen between the reported metal ion requirements for human and *T. lanuginosus* polι. Human polι exhibits highest activity at 0.05–0.2 mM $MnCl_2$ (Frank and Woodgate, 2007), whereas *T. lanuginosus* enzyme required much higher concentrations of Mn^{2+} with a sharp peak of activity at ~4 mM $MnCl_2$. In contrast, while human polι was inhibited by $MgCl_2$ at concentrations >1 mM, *T. lanuginosus* polι required at least 0.5 mM Mg^{2+} and its activity gradually increased with concentrations up to 8 mM.

Because Mn^{2+} is generally known to decrease replication fidelity, we used 4 mM Mg^{2+} for the subsequent studies with polη and polκ. In contrast, further characterization of polι was performed in the presence of 4 mM Mn^{2+}.

Processivity of *T. lanuginosus* Polymerases η, ι and κ

We next examined the processivity of *T. lanuginosus* pols η, ι, and κ (**Figure 4A**). As with the human enzymes, *T. lanuginosus* polη and polκ were much more processive than polι and incorporated ~6 and ~35 bases, respectively, in a single binding event after only 1 min. In contrast, polι incorporated ~10–11 bases in a distributive manner. It then exhibited a strong pause after encountering two adjacent template dTs located 11 and 12 nucleotides from the 5′ end of the primer. Presumably this is due to misincorporation of dG opposite the dTs and its subsequent poor extension (Vaisman et al., 2001). These results indicate that the processivity of *T. lanuginosus* pols η, ι, and κ are therefore similar to their human counterparts (Washington et al., 1999; Ohashi et al., 2000a; Tissier et al., 2000b).

Thermostability of *T. lanuginosus* Polymerases

T. lanuginosus is a thermophilic fungus with a natural habitat of growing in organic soils, *e.g.,* decomposing vegetable matter, composts, and animal excrements, at an optimal temperature between 48 and 52°C (Tsiklinsky, 1899; Maheshwari et al., 2000; Singh et al., 2003).The ability of this fungus to live in such an environment suggests that its proteins possess enhanced thermostability (Maheshwari et al., 2000). We therefore examined the optimum temperature for the *T. lanuginosus* pols η, κ, and ι by incubating primer extension reactions at temperatures ranging between 25 and 75°C. All three polymerases exhibited robust activity between 25 and 50°C, but there was sharp decline in activity at temperatures greater than 50°C (**Figure 4B**).

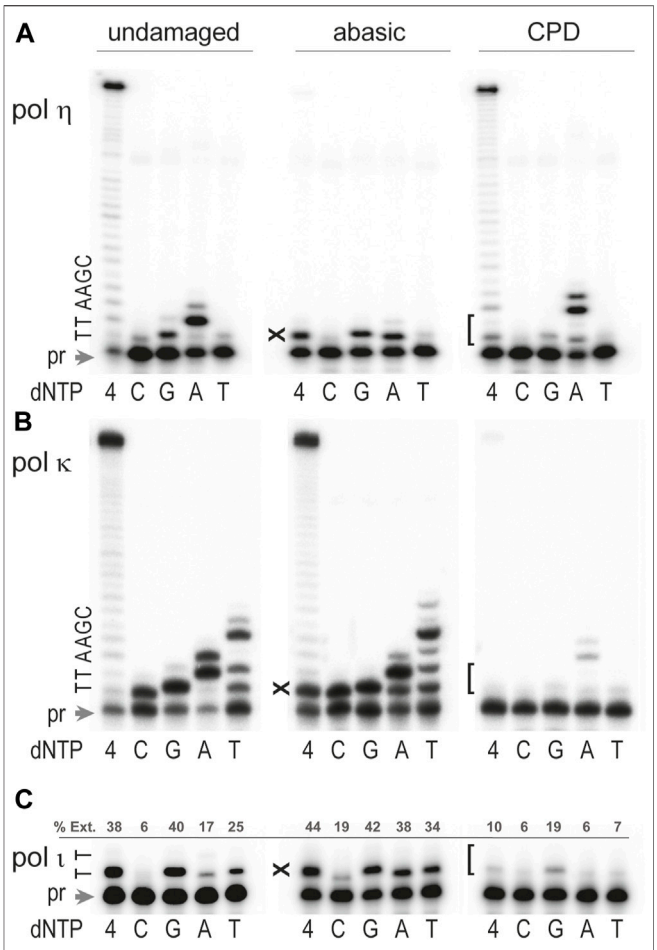

FIGURE 5 | Bypass of abasic and CPD site by *Thermomyces lanuginosus* polymerases. The ability to bypass abasic site and CPD by **(A)** polη, **(B)** polκ, and **(C)** polι was assayed by measuring extension of ^{32}P labeled primer 5′-CGATGGTACGGACGTGCTT-3′ hybridized to the undamaged or damaged DNA template. 5′-TCGATACTGGTACTAATGATTAACGAA-**TN**-AAGCACGTCCGTACCATCG-3′. The underlined bold TN sequence stands for the undamaged TT, TT-CPD, or TX, where X is an abasic site, pr is unextended primer. Reactions contained 100 μM each individual nucleotide (dC, dG, dA, dT) or mixture of all four dNTPs as indicated in the Figure, and 4 mM Mn^{2+} for reactions catalyzed by polι or Mg^{2+} for reactions with polη and polκ. Primer extension reactions were carried out at 37°C for 10 min. Concentrations of enzymes were 0.17 pM for pol η, 0.32 pM for polκ, and 0.15 pM for polι. The sequence of the template immediately downstream of the primer (pr) is shown on the left-hand side of each gel pair. "X" denotes the position of the abasic site and "[" indicates position of the T-T CPD. For panel C, primer extension (%Ext.) was quantified using ImageJ software and reported as the percentage of product density relative to total density for each reaction.

Polη, Polι, and polκ-dependent Lesion Bypass Past Abasic Sites, CPDs, and benzo [*a*] Pyrene Adducts

The Y-family polymerases are best characterized by their ability to catalyze translesion replication past a variety of DNA lesions, in a manner distinct from the cell's conventional replicases (Sale et al., 2012; Vaisman and Woodgate, 2017). We were therefore

interested in assessing the ability and fidelity of *T. lanuginosus* pols η, κ, ι and to carry out translesion synthesis across a *cis-syn* CPD, an abasic site, and a benzo[*a*]pyrene adduct.

Apurinic/apyrimidinic (or abasic) sites are generated as a result of spontaneous or enzymatically-induced base loss and are considered the most frequent form of DNA damage (Lindahl, 1993; Boiteux and Guillet, 2004). An estimated 10,000 abasic sites occur per human cell per day under physiological conditions (Loeb, 1989). It is therefore not surprising that the ability of polη to copy DNA templates containing this noninstructional lesion has been extensively investigated. What is surprising, is that studies performed by various groups with human and *S. cerevisiae* polη produced conflicting results, ranging from those stating that "hPolη has the highest abasic lesion bypass efficiency" among human Y-family DNA pols and "is a major pol involved in abasic site bypass" (Choi et al., 2010; Sherrer et al., 2011; Patra et al., 2015; Thompson and Cortez, 2020) to those which dismiss human, or *S. cerevisiae* polη, as contributing to *in vivo* abasic site bypass because of "negligible nucleotide insertion opposite the abasic site and primer extension past the lesion" (Haracska et al., 2001; Pages et al., 2008). Somewhere in between these polar extremes are studies suggesting that polη catalyzes insertion and/or extension steps of abasic site bypass efficiently enough to ensure its involvement in TLS *in vivo*, but not as a major player (Zhang et al., 2000a; Masutani et al., 2000; Zhao et al., 2004; Sherrer et al., 2011).

We show here that the efficiency and fidelity of *T. lanuginosus* polη during TLS of abasic sites is reminiscent of properties of human and yeast polη uncovered in the third group of studies described above (Zhang et al., 2000a; Masutani et al., 2000; Zhao et al., 2004). In particular, in standing-start primer extensions *T. lanuginosus* polη inserted dA and dG opposite the abasic site with moderate efficiency, but further primer elongation was largely obstructed (**Figure 5A**). However, minuscule extension of the primer with terminal dA opposite the abasic site occurred by incorporation of an additional dA when the base 5′ to the abasic site was dT (**Figure 5A**, incorporation of dA). It should be noted that base selectivity of polη on the template with an abasic site is similar to its moderate fidelity on the undamaged DNA. As shown in **Figure 5A**, polη preferentially incorporates a correct dA opposite the undamaged dT although substantial misinsertion of dG and low level of dC and dT misincorporation can also be seen.

As with polη, there is no consensus regarding the ability of the DinB orthologs (polκ) to utilize DNA templates containing abasic sites (Strauss, 1991; Ohashi et al., 2000b; Zhang et al., 2000b; Boudsocq et al., 2001; Gerlach et al., 2001; Choi et al., 2010; Sherrer et al., 2011), which is at least partly explained by the strong effect of the surrounding sequence context on the bypass mechanism, base selectivity, and efficiency of insertion and extension steps of TLS. Thus, it has been shown that human polκ tolerates an abasic site much better when the next (5′) template base is dT, and the nucleotide preferentially incorporated opposite the lesion is dA. Furthermore, when primer/template slippage is possible, bypass often occurs through a stabilized misalignment mechanism leading to 1– or 2-base deletions (Boudsocq et al., 2001; Ling et al., 2004a). Similarly, *T. lanuginosus* polκ-catalyzed TLS of the abasic site was quite efficient when the 5′ template was dT and dA was preferentially incorporated opposite the lesion, although the other three nucleotides were also inserted at substantial levels (**Figure 5B**). The low fidelity of polκ during abasic site bypass is very similar to its highly error-prone nucleotide incorporation on undamaged DNA. The fact that the major product of *T. lanuginosus* polκ primer extension reactions in the presence of dT was generated by addition of four nucleotides is consistent with the aforementioned human polκ template-slippage mechanism (Mukherjee et al., 2013). Therefore, the resulting main product would contain two mismatches and total primer elongation by four bases because the DNA template used in the current study has two dA's next to dT. When the DNA template was not susceptible to primer/template slippage (reactions with dC, dG, and dA) only one wrong nucleotide was incorporated opposite the abasic site.

Human polι has the capacity to insert deoxynucleotides opposite an abasic site, however further extension is limited (Zhang et al., 2000c; Vaisman et al., 2002; Nair et al., 2009; Choi et al., 2010; Sherrer et al., 2011). *T. lanuginosus* polι behaved in a similar manner, *i.e.,* a single nucleotide was readily inserted opposite the abasic site with no indication of further extension (**Figure 5C**). Furthermore, akin to human polι, *T. lanuginosus* polι incorporates dG, dA, and dT with similar efficiency. Interestingly, when undamaged templates were used, *T. lanuginosus* polι was even more inaccurate than the human polymerase, *i.e.,* not only dG, but also dT, was inserted opposite template dT more often than the correct dA (**Figure 5C**).

The most common ultraviolet light photoproduct is a *cis-syn* cyclobutane pyrimidine dimer (CPD). Unlike the ambiguity of TLS of an abasic site, there is no question as to which TLS polymerase bypasses a CPD most efficiently. Indeed, it is well established that polη can bypass a CPD with the same efficiency and accuracy as undamaged template dT's (Johnson et al., 2000c; Masutani et al., 2000; McCulloch et al., 2004). Most other pols halt synthesis either immediately before the lesion, or opposite the first template dT of the CPD, as their active site is unable to accommodate the covalently joined dT's of the CPD. Similar to human and *S. cerevisiae* polη, *T. lanuginosus* polη efficiently bypassed the CPD lesion (**Figure 5A**). Like polymerases purified from other species, *T. lanuginosus* polη was even more accurate while inserting nucleotides opposite the damaged bases than on undamaged DNA templates (**Figure 5A**).

The pols in the DinB branch of the Y-family (polκ) are unable to replicate past UV-induced *cis-syn* CPD dimers (Johnson et al., 2000a; Ohashi et al., 2000b; Zhang et al., 2000b) with the one reported exception of archaeal *Sulfolobus solfataricus* Dpo4, whose properties resemble eukaryotic polη (Boudsocq et al., 2001). Interestingly, the ability of *T. lanuginosus* polκ to copy a CPD-containing template resembles the behavior of its human orthologs rather than the thermophilic archaeal enzyme, *i.e., T. lanuginosus* polκ was virtually blocked by the CPD lesion in reactions with all four dNTPs although a very low level of the

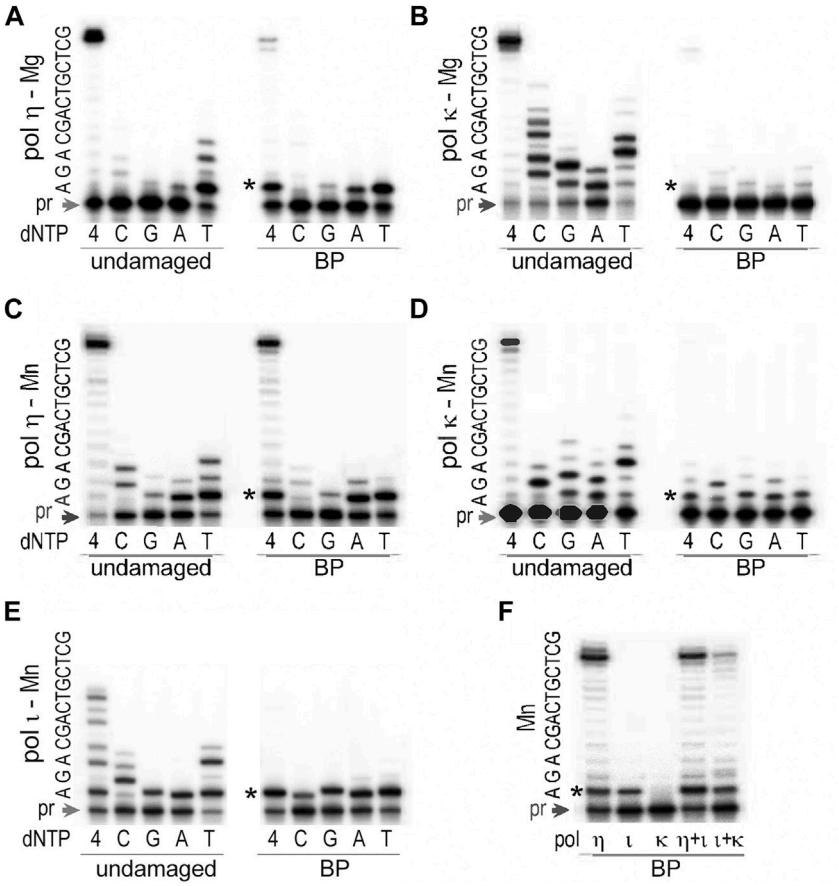

FIGURE 6 | TLS past *trans*-*S*-BPDE-dA by *T. lanuginosus* pols. The ability to bypass BPDE-dA was assayed for **(A)** polη in presence of 4 mM Mg^{2+}, **(B)** polκ in presence of 4 mM Mg^{2+}, **(C)** polη in presence of 4 mM Mn^{2+}, **(D)** polκ in presence of 4 mM Mn^{2+}, **(E)** polι in presence of 4 mM Mn^{2+}, and **(F)** individual, or mixture of various pols in 4 mM Mn^{2+}. The substrate used in these assays was made by annealing of the ^{32}P labeled primer 5′-CACTGCAGACTCTAAA-3′ and either an undamaged or BPDE-containing template 5′- GCTCGTCAGCAG**A**TTTAGAGTCTGCAGTG-3′, where the underlined bold A stands for the undamaged, or BPDE-modified dA. Reactions contained 100 μM each individual nucleotide (dC, dG, dA, dT) or mixture of all four dNTPs as indicated in the figure and were carried out at 37°C for 10 min. Concentrations of enzymes were 0.17 pM for polη, 0.32 pM for polκ, and 0.15 pM for polι. The sequence of the template immediately downstream of the primer (pr) is shown on the left-hand side of each gel pair. The star (*) indicates position of the adduct.

correct incorporation of two dAs opposite the damaged bases was detected in reactions where only dATP was present (**Figure 5B**).

It has been reported that human polι can bypass a CPD. Depending on the sequence context, it incorporates anywhere between 1–5 nucleotides, albeit with low efficiency (Tissier et al., 2000a; Vaisman et al., 2003). *T. lanuginosus* polι was much less efficient compared to the human enzyme. In fact, CPD bypass was barely detectible (**Figure 5C**). As with undamaged template dT, the preferred nucleotide inserted opposite the 3′-dT of the CPD was dG (**Figure 5C**).

Benzopyrene diol epoxides (BPDEs) are the highly carcinogenic metabolites of the environmental pollutant benzo [*a*]pyrene, found in tobacco smoke and automobile exhaust. In mammalian cells, various BPDE stereoisomers covalently bind to DNA forming adducts at the N^2 and N^6 position of guanine and adenine, respectively. Previous studies demonstrated that efficiency and fidelity of TLS past BPDE by different pols not only depends on the DNA base to which the adduct is linked, but is also often modulated by the stereochemistry of the adduct (Zhang et al., 2002a; Chiapperino et al., 2002; Frank et al., 2002; Rechkoblit et al., 2002; Suzuki et al., 2002; Jia et al., 2008). For example, in general, human polκ is almost completely stalled by BPDE-dA adducts. Under similar reaction conditions, it accurately and efficiently bypasses most of the BPDE-dG stereoisomers (Zhang et al., 2002a; Rechkoblit et al., 2002; Suzuki et al., 2002; Jia et al., 2008), although the *cis*-*S*-BPDE-dG represents a significant block for the polymerase (Suzuki et al., 2002). In contrast, polι is much more efficient and accurate while incorporating nucleotides opposite BPDE-dA than opposite BPDE-dG (Frank et al., 2002). Furthermore, independent of adduct stereochemistry, the correct dT is inserted by polι equally efficiently opposite various BPDE-dA isomers. On the other hand, the ability of human polη to replicate past the BPDE is strongly affected by the adduct conformation and damaged base, *i.e.,* it readily traverses through the *trans*-*S*-BPDE-dA, but not through the isomeric *trans*-*R*- adduct, or through the BPDE-

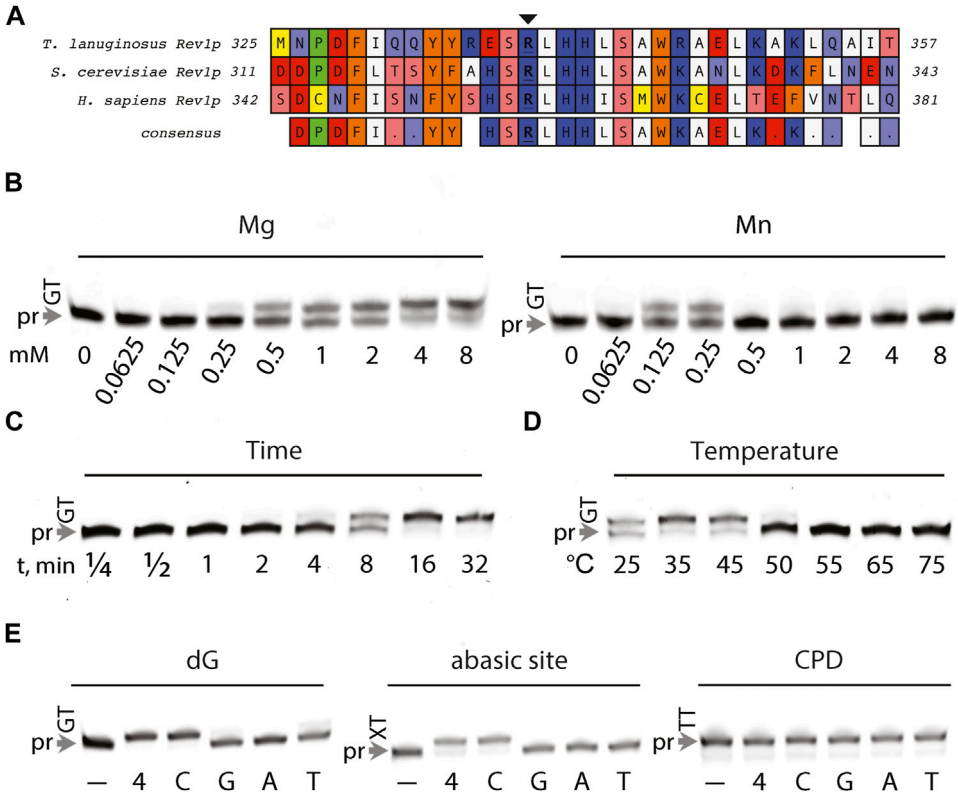

FIGURE 7 | Characterization of DNA synthesis by *T. lanuginosis* Rev1. **(A)** Sequence alignment between REV1 orthologs (*Thermomyces lanuginosus, Saccharomyces cerevisiae, and Homo sapiens*), illustrating the conserved arginine residue (indicated with an arrow) required for protein-templated DNA synthesis **(B)** Serial 1:1 dilutions of Mg^{2+} and Mn^{2+} metal ions present within 6-FAM primer extension reactions, starting at 8 mM Me^{2+}. **(C)** Processivity was qualitatively assessed by varying the duration (minutes) of 6-FAM primer extension reactions. **(D)** Thermostability was evaluated by monitoring DNA synthesis activity at varied temperature (25–75°C). **(E)** Lesion bypass activity for undamaged (dG), abasic site, and CPD template base/lesion identities was examined in the presence of either none (–), 100 μM dNTPs (4), 100 μM dCTP (C), 100 μM dGTP (G), 100 μM dATP (A), 100 μM dTTP (T).

dG isomers (Chiapperino et al., 2002; Rechkoblit et al., 2002). In the current study with *T. lanuginosus* pols, we used DNA templates with a *trans*-*S*-BPDE-dA adduct. Reactions with polη and polκ contained Mg^{2+} or Mn^{2+}, whereas polι was tested only in the presence of Mn^{2+}.

Similar to the human enzyme, *T. lanuginosus* polη was quite efficient, but rather inaccurate, while incorporating nucleotides opposite the *trans*-*S*-BPDE-dA (**Figures 6A,C**) especially when reactions were carried out in the presence of Mn^{2+} which significantly boosted TLS efficiency without noticeably reducing fidelity (**Figure 6C**). Nucleotide incorporation opposite the lesion by polι was at least as efficient as by polη (**Figure 6E**), but it was less accurate and further primer extension was inhibited (**Figure 6E**). We have previously found that fidelity of human polι was influenced by the local sequence context of the BPDE-dA lesion (Frank et al., 2002), and when the template bases 5′ to the lesion were GAC, uncharacteristically accurate insertion of dT opposite the BPDE-dA was observed. In contrast, it appears that on the same template, *T. lanuginosus* polι keeps its general unfaithful nature. Finally, *T. lanuginosus* polκ when activated by Mg^{2+} barely showed any activity on the BPDE-dA-adducted DNA (**Figure 6B**). However, when Mg^{2+} was substituted by an equimolar concentration of Mn^{2+} (**Figure 6D**), *T. lanuginosus* polκ was able to utilize this template adding 1–2 nucleotides to the primer. Incorporation of all four nucleotides in the presence of 4 mM Mn^{2+}occurred with similar efficiency, making synthesis by polκ highly error-prone (**Figure 6D**).

While polκ itself was incapable of extending primers by more than one nucleotide after insertion opposite the BPDE-dA even in the presence of Mn^{2+}, it was able to assist polι to bypass the lesion and elongate primers to the end of the template (**Figure 6F**). Nevertheless, TLS catalyzed by the combined action of polι and polκ was still less efficient than by polη alone (**Figure 6F**).

Characterization of *T. lanuginosus* Rev1

S. cerevisiae and human Rev1 function as a dCMP transferase, incorporating strictly dCMP opposite abasic sites and dG-lesions (Nelson et al., 1996; Lin et al., 1999; Masuda et al., 2001). dCMP transferase activity is instructed by Rev1's conserved active site side chain arginine residue *via* a protein-templated mechanism (Nair et al., 2005; Weaver et al., 2020). We hypothesized that the conservation of the functional arginine and Rev1 consensus sequence (**Figure 7A**)

would make *T. lanuginosis* Rev1 a bonafide dCMP transferase. Therefore, the DNA synthesis activity of *T. lanuginosus* Rev1 was characterized *in vitro* opposite damaged and undamaged DNA. We found that *T. lanuginosus* Rev1 could utilize both Mn^{2+} and Mg^{2+}, but reasoned that Mg^{2+} was a more likely candidate for physiological utilization given its wider efficacy in comparison to Mn^{2+} (**Figure 7B**). Similar to the activities of *S. cerevisiae* and human Rev1, DNA synthesis by *T. lanuginosus* Rev1 was not processive, whereby it inserted only once opposite a templating dG and stalled at the following dT base (**Figure 7C**). As expected, *T. lanuginosus* Rev1 had a similar thermostability to the other *T. lanuginosus* Y-family pols (**Figure 7D**). The well-characterized dCMP transferase activity of Rev1 ortholog was evaluated opposite undamaged, as well as abasic site- and CPD-containing templates (**Figure 7E**). The ability for *T. lanuginosus* Rev1 to perform DNA synthesis was efficient only in the presence of dCMP opposite undamaged, or abasic site templates, akin to *S. cerevisiae* and human REV1 (Zhang et al., 2002b; Nair et al., 2011; Weerasooriya et al., 2014). In summary, we found that the DNA synthesis properties of *T. lanuginosus* Rev1 are comparable with its higher eukaryotic ortholog.

CONCLUDING REMARKS

In this paper, we describe the cloning, purification, and biochemical characterization of Y-family pols from the thermophilic fungus *T. lanuginosus*. *T. lanuginosis* contains all four eukaryotic Y-family orthologs that each generally demonstrate biochemical properties similar to the properties of higher eukaryotic orthologs with the exception of the expected thermostability of the *T. lanuginosis* Y-family polymerases. Interestingly, while *T. lanuginosis* polι exhibited biochemical properties akin to the human enzyme, its metal ion requirement was significantly different. Whereas human polι is activated by very low levels of Mn^{2+} (250 μM) and inhibited by high levels of Mg^{2+} (>1 mM) (Frank and Woodgate, 2007), *T. lanuginosis* polι required 4–8 mM Mn^{2+} or Mg^{2+} respectively, for maximal activity *in vitro*.

The conservation of Y-family polymerase activities between lower and higher eukaryotic organisms suggests that TLS activity may be more essential to cellular viability than previously appreciated. Further structure-function studies of these polymerases, as well as identification and characterization of other Y-family orthologs from yet unsequenced species would help clarify the seemingly random ortholog dispersion among eukaryotes and how their presence/absence might provide evolutionary advantages in the face of different environmental stressors.

DATA AVAILABILITY STATEMENT

The raw data supporting the conclusions of this article will be made available by the authors, without undue reservation.

AUTHOR CONTRIBUTIONS

Conceptualization: JM and RW. Data curation: AV, JM, MS, and SA. Formal analysis: AV, JM, and MS. Funding acquisition: RW. Investigation: AV, JM, MS, and SA. Visualization: AV, JM, and MS. Writing-original draft, Review and editing: AV, JM, MS, SA, TE, and RW.

FUNDING

Funding for this work was provided by the National Institute of Child Health and Human Development/National Institutes of Health Intramural Research Program (RW).

ACKNOWLEDGMENTS

We would like to thank Dominic Quiros (NIH) for assistance with the early exploratory phase of Rev1 purification. We also thank Francine B. Perler for her work on purifying *T. lanuginosus* polι.

REFERENCES

Avkin, S., Goldsmith, M., Velasco-Miguel, S., Geacintov, N., Friedberg, E. C., and Livneh, Z. (2004). Quantitative Analysis of Translesion DNA Synthesis across a Benzo[*a*]pyrene-Guanine Adduct in Mammalian Cells. *J. Biol. Chem.* 279, 53298–53305. doi:10.1074/jbc.M409155200

Basu, A. K., Pande, P., and Bose, A. (2017). Translesion Synthesis of 2′-Deoxyguanosine Lesions by Eukaryotic DNA Polymerases. *Chem. Res. Toxicol.* 30, 61–72. doi:10.1021/acs.chemrestox.6b00285

Bessman, M. J., Lehman, I. R., Simms, E. S., and Kornberg, A. (1958). Enzymatic Synthesis of Deoxyribonucleic Acid. II. General Properties of the Reaction. *J. Biol. Chem.* 233, 171–177. doi:10.1016/s0021-9258(19)68049-x

Boiteux, S., and Guillet, M. (2004). Abasic Sites in DNA: Repair and Biological Consequences in *Saccharomyces cerevisiae*. *DNA Repair* 3, 1–12. doi:10.1016/j.dnarep.2003.10.002

Boudsocq, F., Iwai, S., Hanaoka, F., and Woodgate, R. (2001). *Sulfolobus solfataricus* P2 DNA Polymerase IV (Dpo4): an Archaeal DinB-like DNA Polymerase with Lesion-Bypass Properties Akin to Eukaryotic Polη. *Nucleic Acids Res.* 29, 4607–4616. doi:10.1093/nar/29.22.4607

Boudsocq, F., Kokoska, R. J., Plosky, B. S., Vaisman, A., Ling, H., Kunkel, T. A., et al. (2004). Investigating the Role of the Little Finger Domain of Y-Family DNA Polymerases in Low Fidelity Synthesis and Translesion Replication. *J. Biol. Chem.* 279, 32932–32940. doi:10.1074/jbc.m405249200

Chiapperino, D., Kroth, H., Kramarczuk, I. H., Sayer, J. M., Masutani, C., Hanaoka, F., et al. (2002). Preferential Misincorporation of Purine Nucleotides by Human DNA Polymerase η Opposite Benzo[a]pyrene 7,8-Diol 9,10-Epoxide Deoxyguanosine Adducts. *J. Biol. Chem.* 277, 11765–11771. doi:10.1074/jbc.m112139200

Choi, J.-Y., Angel, K. C., and Guengerich, F. P. (2006). Translesion Synthesis across Bulky N^2-Alkyl Guanine DNA Adducts by Human DNA Polymerase κ. *J. Biol. Chem.* 281, 21062–21072. doi:10.1074/jbc.M602246200

Choi, J.-Y., Lim, S., Kim, E.-J., Jo, A., and Guengerich, F. P. (2010). Translesion Synthesis across Abasic Lesions by Human B-Family and Y-Family DNA Polymerases α, δ, η, ι, κ, and REV1. *J. Mol. Biol.* 404, 34–44. doi:10.1016/j.jmb.2010.09.015

Dominguez, O., Ruiz, J. F., Lain De Lera, T., Garcia-Diaz, M., Gonzalez, M. A., Kirchhoff, T., et al. (2000). DNA Polymerase Mu (Pol μ), Homologous to TdT, Could Act as a DNA Mutator in Eukaryotic Cells. *EMBO J.* 19, 1731–1742. doi:10.1093/emboj/19.7.1731

Frank, E. G., and Woodgate, R. (2007). Increased Catalytic Activity and Altered Fidelity of Human DNA Polymerase ι in the Presence of Manganese. *J. Biol. Chem.* 282, 24689–24696. doi:10.1074/jbc.m702159200

Frank, E. G., Sayer, J. M., Kroth, H., Ohashi, E., Ohmori, H., Jerina, D. M., et al. (2002). Translesion Replication of Benzo[a]pyrene and Benzo[*c*]phenanthrene Diol Epoxide Adducts of Deoxyadenosine and Deoxyguanosine by Human DNA Polymerase ι. *Nucleic Acids Res.* 30, 5284–5292. doi:10.1093/nar/gkf643

Frank, E. G., McDonald, J. P., Karata, K., Huston, D., and Woodgate, R. (2012). A Strategy for the Expression of Recombinant Proteins Traditionally Hard to Purify. *Anal. Biochem.* 429, 132–139. doi:10.1016/j.ab.2012.07.016

Garcia-Diaz, M., Bebenek, K., Krahn, J. M., Pedersen, L. C., and Kunkel, T. A. (2007). Role of the Catalytic Metal during Polymerization by DNA Polymerase λ. *DNA Repair* 6, 1333–1340. doi:10.1016/j.dnarep.2007.03.005

Gerlach, V. L., Feaver, W. J., Fischhaber, P. L., and Friedberg, E. C. (2001). Purification and Characterization of Polκ, a DNA Polymerase Encoded by the Human *DINB1* Gene. *J. Biol. Chem.* 276, 92–98. doi:10.1074/jbc.m004413200

Haracska, L., Washington, M. T., Prakash, S., and Prakash, L. (2001). Inefficient Bypass of an Abasic Site by DNA Polymerase η. *J. Biol. Chem.* 276, 6861–6866. doi:10.1074/jbc.m008021200

Jha, V., and Ling, H. (2018). Structural Basis for Human DNA Polymerase κ to Bypass Cisplatin Intrastrand Cross-Link (Pt-GG) Lesion as an Efficient and Accurate Extender. *J. Mol. Biol.* 430, 1577–1589. doi:10.1016/j.jmb.2018.04.023

Jia, L., Geacintov, N. E., and Broyde, S. (2008). The N-Clasp of Human DNA Polymerase κ Promotes Blockage or Error-free Bypass of Adenine- or Guanine-Benzo[a]pyrenyl Lesions. *Nucleic Acids Res.* 36, 6571–6584. doi:10.1093/nar/gkn719

Johnson, R. E., Prakash, S., and Prakash, L. (2000a). The Human *DINB1* Gene Encodes the DNA Polymerase Polθ. *Proc. Natl. Acad. Sci.* 97, 3838–3843. doi:10.1073/pnas.97.8.3838

Johnson, R. E., Washington, M. T., Haracska, L., Prakash, S., and Prakash, L. (2000b). Eukaryotic Polymerases ι and ζ Act Sequentially to Bypass DNA Lesions. *Nature* 406, 1015–1019. doi:10.1038/35023030

Johnson, R. E., Washington, M. T., Prakash, S., and Prakash, L. (2000c). Fidelity of Human DNA Polymerase η. *J. Biol. Chem.* 275, 7447–7450. doi:10.1074/jbc.275.11.7447

Kirouac, K. N., and Ling, H. (2009). Structural Basis of Error-Prone Replication and Stalling at a Thymine Base by Human DNA Polymerase ι. *EMBO J.* 28, 1644–1654. doi:10.1038/emboj.2009.122

Kokoska, R. J., Bebenek, K., Boudsocq, F., Woodgate, R., and Kunkel, T. A. (2002). Low Fidelity DNA Synthesis by a Y Family DNA Polymerase Due to Misalignment in the Active Site. *J. Biol. Chem.* 277, 19633–19638. doi:10.1074/jbc.m202021200

Lin, W., Xin, H., Zhang, Y., Wu, X., Yuan, F., and Wang, Z. (1999). The Human *REV1* Gene Codes for a DNA Template-dependent dCMP Transferase. *Nucleic Acids Res.* 27, 4468–4475. doi:10.1093/nar/27.22.4468

Lindahl, T. (1993). Instability and Decay of the Primary Structure of DNA. *Nature* 362, 709–715. doi:10.1038/362709a0

Ling, H., Boudsocq, F., Woodgate, R., and Yang, W. (2004a). Snapshots of Replication through an Abasic Lesion. *Mol. Cel* 13, 751–762. doi:10.1016/s1097-2765(04)00101-7

Ling, H., Sayer, J. M., Plosky, B. S., Yagi, H., Boudsocq, F., Woodgate, R., et al. (2004b). Crystal Structure of a Benzo[*a*]pyrene Diol Epoxide Adduct in a Ternary Complex with a DNA Polymerase. *Proc. Natl. Acad. Sci.* 101, 2265–2269. doi:10.1073/pnas.0308332100

Liu, Y., Yang, Y., Tang, T.-S., Zhang, H., Wang, Z., Friedberg, E., et al. (2014). Variants of Mouse DNA Polymerase κ Reveal a Mechanism of Efficient and Accurate Translesion Synthesis Past a Benzo[*a*]pyrene dG Adduct. *Proc. Natl. Acad. Sci. USA* 111, 1789–1794. doi:10.1073/pnas.1324168111

Loeb, L. A., and Kunkel, T. A. (1982). Fidelity of DNA Synthesis. *Annu. Rev. Biochem.* 51, 429–457. doi:10.1146/annurev.bi.51.070182.002241

Loeb, L. A. (1989). Endogenous Carcinogenesis: Molecular Oncology into the Twenty-First Century--Presidential Address. *Cancer Res.* 49, 5489–5496.

Maheshwari, R., Bharadwaj, G., and Bhat, M. K. (2000). Thermophilic Fungi: Their Physiology and Enzymes. *Microbiol. Mol. Biol. Rev.* 64, 461–488. doi:10.1128/MMBR.64.3.461-488.2000

Makarova, A. V., and Kulbachinskiy, A. V. (2012). Structure of Human DNA Polymerase ι and the Mechanism of DNA Synthesis. *Biochem. Mosc.* 77, 547–561. doi:10.1134/S0006297912060016

Martin, M. J., Garcia-Ortiz, M. V., Esteban, V., and Blanco, L. (2013). Ribonucleotides and Manganese Ions Improve Non-Homologous End Joining by Human Polμ. *Nucleic Acids Res.* 41, 2428–2436. doi:10.1093/nar/gks1444

Masuda, Y., Takahashi, M., Tsunekuni, N., Minami, T., Sumii, M., Miyagawa, K., et al. (2001). Deoxycytidyl Transferase Activity of the Human REV1 Protein Is Closely Associated with the Conserved Polymerase Domain. *J. Biol. Chem.* 276, 15051–15058. doi:10.1074/jbc.m008082200

Masutani, C., Kusumoto, R., Yamada, A., Dohmae, N., Yokoi, M., Yuasa, M., et al. (1999). The XPV (Xeroderma Pigmentosum Variant) Gene Encodes Human DNA Polymerase η. *Nature* 399, 700–704. doi:10.1038/21447

Masutani, C., Kusumoto, R., Iwai, S., and Hanaoka, F. (2000). Mechanisms of Accurate Translesion Synthesis by Human DNA Polymerase η. *EMBO J.* 19, 3100–3109. doi:10.1093/emboj/19.12.3100

McCulloch, S. D., Kokoska, R. J., Masutani, C., Iwai, S., Hanaoka, F., and Kunkel, T. A. (2004). Preferential *Cis-Syn* Thymine Dimer Bypass by DNA Polymerase η Occurs with Biased Fidelity. *Nature* 428, 97–100. doi:10.1038/nature02352

McHunu, N. P., Permaul, K., Abdul Rahman, A. Y., Saito, J. A., Singh, S., and Alam, M. (2013). Xylanase Superproducer: Genome Sequence of a Compost-Loving Thermophilic Fungus, *Thermomyces Lanuginosus* Strain SSBP. *Genome Announc* 1, e00388–13. doi:10.1128/genomeA.00388-13

McIntyre, J. (2020). Polymerase ι - an Odd Sibling Among Y Family Polymerases. *DNA Repair* 86, 102753. doi:10.1016/j.dnarep.2019.102753

Mildvan, A. S., Loeb, L. A., and Wu, C.-W. (1979). The Role of Metal Ions in the Mechanisms of DNA and RNA Polymerase. *CRC Crit. Rev. Biochem.* 6, 219–244. doi:10.3109/10409237909102564

Mukherjee, P., Lahiri, I., and Pata, J. D. (2013). Human Polymerase κ Uses a Template-Slippage Deletion Mechanism, but Can Realign the Slipped Strands to Favour Base Substitution Mutations over Deletions. *Nucleic Acids Res.* 41, 5024–5035. doi:10.1093/nar/gkt179

Nair, D. T., Johnson, R. E., Prakash, L., Prakash, S., and Aggarwal, A. K. (2005). Rev1 Employs a Novel Mechanism of DNA Synthesis Using a Protein Template. *Science* 309, 2219–2222. doi:10.1126/science.1116336

Nair, D. T., Johnson, R. E., Prakash, L., Prakash, S., and Aggarwal, A. K. (2009). DNA Synthesis across an Abasic Lesion by Human DNA Polymerase ι. *Structure* 17, 530–537. doi:10.1016/j.str.2009.02.015

Nair, D. T., Johnson, R. E., Prakash, L., Prakash, S., and Aggarwal, A. K. (2011). DNA Synthesis across an Abasic Lesion by Yeast REV1 DNA Polymerase. *J. Mol. Biol.* 406, 18–28. doi:10.1016/j.jmb.2010.12.016

Nelson, J. R., Lawrence, C. W., and Hinkle, D. C. (1996). Deoxycytidyl Transferase Activity of Yeast REV1 Protein. *Nature* 382, 729–731. doi:10.1038/382729a0

Ohashi, E., Bebenek, K., Matsuda, T., Feaver, W. J., Gerlach, V. L., Friedberg, E. C., et al. (2000a). Fidelity and Processivity of DNA Synthesis by DNA Polymerase κ, the Product of the Human *DINB1* Gene. *J. Biol. Chem.* 275, 39678–39684. doi:10.1074/jbc.M005309200

Ohashi, E., Ogi, T., Kusumoto, R., Iwai, S., Masutani, C., Hanaoka, F., et al. (2000b). Error-Prone Bypass of Certain DNA Lesions by the Human DNA Polymerase Kappa. *Genes Dev.* 14, 1589–1594. doi:10.1101/gad.14.13.1589

Ohmori, H., Friedberg, E. C., Fuchs, R. P. P., Goodman, M. F., Hanaoka, F., Hinkle, D., et al. (2001). The Y-Family of DNA Polymerases. *Mol. Cel* 8, 7–8. doi:10.1016/s1097-2765(01)00278-7

Pages, V., Johnson, R. E., Prakash, L., and Prakash, S. (2008). Mutational Specificity and Genetic Control of Replicative Bypass of an Abasic Site in Yeast. *Proc. Natl. Acad. Sci.* 105, 1170–1175. doi:10.1073/pnas.0711227105

Patra, A., Zhang, Q., Lei, L., Su, Y., Egli, M., and Guengerich, F. P. (2015). Structural and Kinetic Analysis of Nucleoside Triphosphate Incorporation Opposite an Abasic Site by Human Translesion DNA Polymerase η. *J. Biol. Chem.* 290, 8028–8038. doi:10.1074/jbc.M115.637561

Rechkoblit, O., Zhang, Y., Guo, D., Wang, Z., Amin, S., Krzeminsky, J., et al. (2002). trans-Lesion Synthesis Past Bulky Benzo[*a*]pyrene Diol Epoxide N^2-dG and N6-dA Lesions Catalyzed by DNA Bypass Polymerases. *J. Biol. Chem.* 277, 30488–30494. doi:10.1074/jbc.m201167200

Sale, J. E., Lehmann, A. R., and Woodgate, R. (2012). Y-family DNA Polymerases and Their Role in Tolerance of Cellular DNA Damage. *Nat. Rev. Mol. Cel Biol* 13, 141–152. doi:10.1038/nrm3289

Sherrer, S. M., Fiala, K. A., Fowler, J. D., Newmister, S. A., Pryor, J. M., and Suo, Z. (2011). Quantitative Analysis of the Efficiency and Mutagenic Spectra of Abasic Lesion Bypass Catalyzed by Human Y-Family DNA Polymerases. *Nucleic Acids Res.* 39, 609–622. doi:10.1093/nar/gkq719

Singh, S., Madlala, A. M., and Prior, B. A. (2003). *Thermomyces Lanuginosus*: Properties of Strains and Their Hemicellulases. *FEMS Microbiol. Rev.* 27, 3–16. doi:10.1016/S0168-6445(03)00018-4

Sørensen, A. B., Duch, M., Jørgensen, P., and Pedersen, F. S. (1993). Amplification and Sequence Analysis of DNA Flanking Integrated Proviruses by a Simple Two-step Polymerase Chain Reaction Method. *J. Virol.* 67, 7118–7124. doi:10.1128/JVI.67.12.7118-7124.1993

Stern, H. R., Sefcikova, J., Chaparro, V. E., and Beuning, P. J. (2019). Mammalian DNA Polymerase κ Activity and Specificity. *Molecules* 24, 2805. doi:10.3390/molecules24152805

Strauss, B. S. (1991). The 'A Rule' of Mutagen Specificity: A Consequence of DNA Polymerase Bypass of Non-instructional Lesions? *BioEssays* 13, 79–84. doi:10.1002/bies.950130206

Suzuki, N., Ohashi, E., Kolbanovskiy, A., Geacintov, N. E., Grollman, A. P., Ohmori, H., et al. (2002). Translesion Synthesis by Human DNA Polymerase κ on a DNA Template Containing a Single Stereoisomer of dG-(+)- or dG-(−)-Anti-N^2-BPDE (7,8-Dihydroxy-Anti-9,10-Epoxy-7,8,9,10-Tetrahydrobenzo[*a*]pyrene). *Biochemistry* 41, 6100–6106. doi:10.1021/bi020049c

Thompson, P. S., and Cortez, D. (2020). New Insights into Abasic Site Repair and Tolerance. *DNA Repair* 90, 102866. doi:10.1016/j.dnarep.2020.102866

Tissier, A., Frank, E. G., McDonald, J. P., Iwai, S., Hanaoka, F., and Woodgate, R. (2000a). Misinsertion and Bypass of Thymine-Thymine Dimers by Human DNA Polymerase ι. *EMBO J.* 19, 5259–5266. doi:10.1093/emboj/19.19.5259

Tissier, A., McDonald, J. P., Frank, E. G., and Woodgate, R. (2000b). Polι, a Remarkably Error-Prone Human DNA Polymerase. *Genes Dev.* 14, 1642–1650. doi:10.1101/gad.14.13.1642

Tsiklinsky, P. (1899). *Sur les Mucedinees Thermophiles*. Paris: Libraires de L'academie de Medecine, 500–504.

Vaisman, A., and Woodgate, R. (2017). Translesion DNA Polymerases in Eukaryotes: what Makes Them Tick? *Crit. Rev. Biochem. Mol. Biol.* 52, 274–303. doi:10.1080/10409238.2017.1291576

Vaisman, A., and Woodgate, R. (2020). Mysterious and Fascinating: DNA Polymerase ι Remains Enigmatic 20 Years after its Discovery. *DNA Repair* 93, 102914. doi:10.1016/j.dnarep.2020.102914

Vaisman, A., Tissier, A., Frank, E. G., Goodman, M. F., and Woodgate, R. (2001). Human DNA Polymerase ι Promiscuous Mismatch Extension. *J. Biol. Chem.* 276, 30615–30622. doi:10.1074/jbc.m102694200

Vaisman, A., Frank, E. G., McDonald, J. P., Tissier, A., and Woodgate, R. (2002). Polι-Dependent Lesion Bypass *In Vitro*. *Mutat. Res./Fundam. Mol. Mech. Mutagen.* 510, 9–22. doi:10.1016/s0027-5107(02)00248-8

Vaisman, A., Frank, E. G., Iwai, S., Ohashi, E., Ohmori, H., Hanaoka, F., et al. (2003). Sequence Context-dependent Replication of DNA Templates Containing UV-Induced Lesions by Human DNA Polymerase ι. *DNA Repair* 2, 991–1006. doi:10.1016/s1568-7864(03)00094-6

Vashishtha, A. K., Wang, J., and Konigsberg, W. H. (2016). Different Divalent Cations Alter the Kinetics and Fidelity of DNA Polymerases. *J. Biol. Chem.* 291, 20869–20875. doi:10.1074/jbc.R116.742494

Washington, M. T., Johnson, R. E., Prakash, S., and Prakash, L. (1999). Fidelity and Processivity of *Saccharomyces cerevisiae* DNA Polymerase η. *J. Biol. Chem.* 274, 36835–36838. doi:10.1074/jbc.274.52.36835

Weaver, T. M., Cortez, L. M., Khoang, T. H., Washington, M. T., Agarwal, P. K., and Freudenthal, B. D. (2020). Visualizing Rev1 Catalyze Protein-Template DNA Synthesis. *Proc. Natl. Acad. Sci. USA* 117, 25494–25504. doi:10.1073/pnas.2010484117

Weerasooriya, S., Jasti, V. P., and Basu, A. K. (2014). Replicative Bypass of Abasic Site in *Escherichia coli* and Human Cells: Similarities and Differences. *PLoS One* 9, e107915. doi:10.1371/journal.pone.0107915

Yang, W., and Gao, Y. (2018). Translesion and Repair DNA Polymerases: Diverse Structure and Mechanism. *Annu. Rev. Biochem.* 87, 239–261. doi:10.1146/annurev-biochem-062917-012405

Zhang, Y., Yuan, F., Wu, X., Rechkoblit, O., Taylor, J. S., Geacintov, N. E., et al. (2000a). Error-prone Lesion Bypass by Human DNA Polymeraseη. *Nucleic Acids Res.* 28, 4717–4724. doi:10.1093/nar/28.23.4717

Zhang, Y., Yuan, F., Wu, X., Wang, M., Rechkoblit, O., Taylor, J. S., et al. (2000b). Error-free and Error-Prone Lesion Bypass by Human DNA Polymerase κ *In Vitro*. *Nucleic Acids Res.* 28, 4138–4146. doi:10.1093/nar/28.21.4138

Zhang, Y., Yuan, F., Wu, X., and Wang, Z. (2000c). Preferential Incorporation of G Opposite Template T by the Low-Fidelity Human DNA Polymerase ι. *Mol. Cel Biol* 20, 7099–7108. doi:10.1128/mcb.20.19.7099-7108.2000

Zhang, Y., Wu, X., Guo, D., Rechkoblit, O., and Wang, Z. (2002a). Activities of Human DNA Polymerase κ in Response to the Major Benzo[a]pyrene DNA Adduct: Error-free Lesion Bypass and Extension Synthesis from Opposite the Lesion. *DNA Repair* 1, 559–569. doi:10.1016/s1568-7864(02)00055-1

Zhang, Y., Wu, X., Rechkoblit, O., Geacintov, N. E., Taylor, J. S., and Wang, Z. (2002b). Response of Human REV1 to Different DNA Damage: Preferential dCMP Insertion Opposite the Lesion. *Nucleic Acids Res.* 30, 1630–1638. doi:10.1093/nar/30.7.1630

Zhao, B., Xie, Z., Shen, H., and Wang, Z. (2004). Role of DNA Polymerase in the Bypass of Abasic Sites in Yeast Cells. *Nucleic Acids Res.* 32, 3984–3994. doi:10.1093/nar/gkh710

Conflict of Interest: TE is employed by New England Biolabs, Inc., a company that commercializes enzyme reagents, including DNA polymerases.

The remaining authors declare that the research was conducted in the absence of any commercial or financial relationships that could be construed as a potential conflict of interest.

Publisher's Note: All claims expressed in this article are solely those of the authors and do not necessarily represent those of their affiliated organizations, or those of the publisher, the editors and the reviewers. Any product that may be evaluated in this article, or claim that may be made by its manufacturer, is not guaranteed or endorsed by the publisher.

frontiers in Molecular Biosciences

CORRECTION
published: 15 December 2021
doi: 10.3389/fmolb.2021.819157

OPEN ACCESS

Approved by:
Frontiers Editorial Office,
Frontiers Media SA, Switzerland

***Correspondence:**
Roger Woodgate
woodgate@nih.gov

[§]These authors share first authorship

[†]ORCID:
Alexandra Vaisman
orcid.org/0000-0002-2521-1467
John P. McDonald
orcid.org/0000-0003-2482-148X
Mallory R. Smith
orcid.org/0000-0003-1450-7825
Sender L. Aspelund
orcid.org/0000-0003-0726-4028
Thomas C. Evans Jr.
orcid.org/0000-0001-5406-0146
Roger Woodgate
orcid.org/0000-0002-2521-1467

[‡]Present address:
Sender L. Aspelund,
Novavax, Inc., Gaithersburg, MD,
United States

Specialty section:
This article was submitted to
Structural Biology,
a section of the journal
Frontiers in Molecular Biosciences

Received: 20 November 2021
Accepted: 22 November 2021
Published: 15 December 2021

Citation:
Vaisman A, McDonald JP, Smith MR,
Aspelund SL, Evans TC and
Woodgate R (2021) Corrigendum:
Identification and Characterization of
Thermostable Y-Family DNA
Polymerases η, ι, κ and Rev1 From a
Lower Eukaryote,
Thermomyces lanuginosus.
Front. Mol. Biosci. 8:819157.
doi: 10.3389/fmolb.2021.819157

Corrigendum: Identification and Characterization of Thermostable Y-Family DNA Polymerases η, ι, κ and Rev1 From a Lower Eukaryote, *Thermomyces lanuginosus*

Alexandra Vaisman[1†§], John P. McDonald[1†§], Mallory R. Smith[1†], Sender L. Aspelund[1†‡], Thomas C. Evans Jr[2†] and Roger Woodgate[1†]*

[1]Laboratory of Genomic Integrity, National Institute of Child Health and Human Development, National Institutes of Health, 9800 Medical Center Drive, Bethesda, MD, United States, [2]New England Biolabs Incorporated, Ipswich, MA, United States

Keywords: thermostable fungi, Y-family DNA polymerases, phylogenetic analysis, translesion DNA synthesis, DNA polymerase η, DNA polymerase ι, DNA polymerase κ, REV1

A Corrigendum on

Identification and Characterization of Thermostable Y-Family DNA Polymerases η, ι, κ and Rev1 From a Lower Eukaryote, *Thermomyces lanuginosus*
by Vaisman A, McDonald JP, Smith MR, Aspelund SL, Evans TC and Woodgate R (2021). Front. Mol. Biosci. 8:778400. doi: 10.3389/fmolb.2021.778400

In the original article, there was a formatting issue in **Figure 6** as published. This occurred when the image was converted from a PC generated pdf to an Apple Macintosh generated tif for publication. The corrected **Figure 6** appears below.

The authors apologize for this error and state that this does not change the scientific conclusions of the article in any way. The original article has been updated.

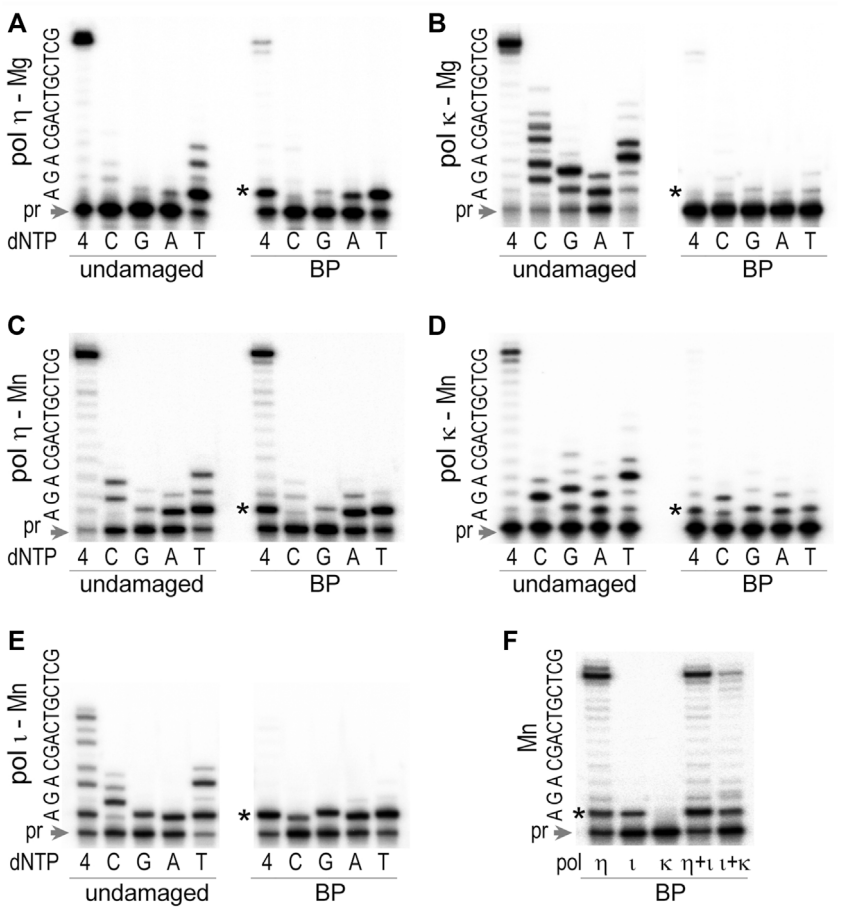

FIGURE 6 | TLS past *trans-S*-BPDE-dA by *T. lanuginosus* pols. The ability to bypass BPDE-dA was assayed for **(A)** polη in thepresence of 4 mM Mg^{2+}, **(B)** polκ in the presence of 4 mM Mg^{2+}, **(C)** polη in the presence of 4 mM Mn^{2+}, **(D)** polκ in the presence of 4 mM Mn^{2+}, **(E)** polι in the presence of 4 mM Mn^{2+}, and **(F)** individual, or a mixture of various pols in 4 mM Mn^{2+}. The substrate used in these assays was made by annealing of the ^{32}P labeled primer 5′-CACTGCAGACTCTAAA-3′ and either an undamaged or BPDE-containing template 5′- GCTCGTCAGCAG**A**TTTAGAGTCTGCAGTG-3′, where the underlined bold A stands for the undamaged, or BPDE modified dA. Reactions contained 100 μM each of individual nucleotide (dC, dG, dA, and dT) or a mixture of all four dNTPs as indicated in the figure and were carried out at 37°C for 10 min. Concentrations of enzymes were 0.17 pM for polη, 0.32 pM for polκ, and 0.15 pM for polι. The sequence of the template immediately downstream of the primer (pr) is shown on the left-hand side of each gel pair. The star (*) indicates the position of the adduct.

frontiers in Molecular Biosciences

ORIGINAL RESEARCH
published: 18 November 2021
doi: 10.3389/fmolb.2021.704813

Structure of New Binary and Ternary DNA Polymerase Complexes From Bacteriophage RB69

Jongseo Park[1,2†], *Hyung-Seop Youn*[1,2,3†], *Jun Yop An*[1,2,4], *Youngjin Lee*[1,2,5], *Soo Hyun Eom*[1,2,6*] and *Jimin Wang*[2,7*]

[1]School of Life Sciences, Gwangju Institute of Science and Technology (GIST), Gwangju, South Korea, [2]Steitz Center for Structural Biology, GIST, Gwangju, South Korea, [3]BIO R&D Center, Ingredient Business Unit, Daesang Corporation, Gyeonggi-do, Korea, [4]Virocure Inc., Seoul, Korea, [5]Metabolic Regulation Research Center, Korea Research Institute of Bioscience and Biotechnology (KRIBB), Daejeon, Korea, [6]Department of Chemistry, GIST, Gwangju, Korea, [7]Department of Molecular Biophysics and Biochemistry, New Haven, CT, United States

OPEN ACCESS

Edited by:
Indrajit Lahiri,
Indian Institute of Science Education and Research Mohali, India

Reviewed by:
Antonio Chaves-Sanjuan,
University of Milan, Italy
David Douglas Boehr,
The Pennsylvania State University (PSU), United States

***Correspondence:**
Jimin Wang
jimin.wang@yale.edu
Soo Hyun Eom
eom@gist.ac.kr

†These authors have contributed equally to this work

Specialty section:
This article was submitted to Structural Biology, a section of the journal Frontiers in Molecular Biosciences

Received: 03 May 2021
Accepted: 30 September 2021
Published: 18 November 2021

Citation:
Park J, Youn H-S An JY, Lee Y, Eom SH and Wang J (2021) Structure of New Binary and Ternary DNA Polymerase Complexes From Bacteriophage RB69. Front. Mol. Biosci. 8:704813. doi: 10.3389/fmolb.2021.704813

DNA polymerase plays a critical role in passing the genetic information of any living organism to its offspring. DNA polymerase from enterobacteria phage RB69 (RB69pol) has both polymerization and exonuclease activities and has been extensively studied as a model system for B-family DNA polymerases. Many binary and ternary complex structures of RB69pol are known, and they all contain a single polymerase-primer/template (P/T) DNA complex. Here, we report a crystal structure of the exonuclease-deficient RB69pol with the P/T duplex in a dimeric form at a resolution of 2.2 Å. The structure includes one new closed ternary complex with a single divalent metal ion bound and one new open binary complex in the pre-insertion state with a vacant dNTP-binding pocket. These complexes suggest that initial binding of the correct dNTP in the open state is much weaker than expected and that initial binding of the second divalent metal ion in the closed state is also much weaker than measured. Additional conformational changes are required to convert these complexes to high-affinity states. Thus, the measured affinities for the correct incoming dNTP and divalent metal ions are average values from many conformationally distinctive states. Our structure provides new insights into the order of the complex assembly involving two divalent metal ions. The biological relevance of specific interactions observed between one RB69pol and the P/T duplex bound to the second RB69pol observed within this dimeric complex is discussed.

Keywords: RB69 DNA polymerase, crystal structure, open binary complex, closed ternary complex, single-divalent metal ion–containing complex, replisomal complex

INTRODUCTION

DNA replication at the replication fork is the semi-discontinuous process; one strand is the leading strand, and the other strand is the lagging strand (Hamdan et al., 2009; Yao and O'Donnell, 2008). In the presence of externally supplied primers, a minimal T4 replication model containing only two polymerases (pols), a lagging strand polymerase and a leading polymerase, is capable of forming trombone loops mimicking these in the holo-assembly at the replication fork (Alberts et al., 1983; Noble et al., 2015; Benkovic and Spiering, 2017). However, direct pol–pol interactions are relatively weak (Salinas and Benkovic, 2000), suggesting that coordination of DNA synthesis of both strands may be mediated by other replisomal proteins or/and by a DNA

duplex. This study provides evidence for such coordination *via* a primer/template (P/T) DNA duplex.

DNA polymerases are very dynamic, undergo many conformational changes with correct incoming dNTPs, and transverse various distinctive functional states such as pre-insertion or post-insertion (which can be in pre-translocation or post-translocation) according to their interactions with both dNTPs and the P/T duplex (Franklin et al., 2001; Berman et al., 2007). The DNA polymerase from RB69 phage (RB69pol) belongs to the B-family pols and shares a high degree of similarity with human pols (Wang et al., 1997). It contains two activities (polymerase and exonuclease) and is a classic model for studying DNA replication (Wang et al., 1997; Alberts, 2003). RB69pol has been extensively studied both structurally and biochemically with respect to its domain architecture, substrate binding, nucleotide incorporation, and metal coordination in both polymerizing and editing modes (Wang et al., 1997; Shamoo and Steitz, 1999; Franklin et al., 2001; Hogg et al., 2004; Aller et al., 2007; Hogg et al., 2007; Zahn et al., 2007; Hogg et al., 2010; Aller et al., 2011; Xia et al., 2011a; Zahn et al., 2011a; Xia et al., 2011b; Zahn et al., 2011b; Xia et al., 2012b; Xia et al., 2013b). RB69pol has the following distinct domains: the N-terminal, Exonuclease, Palm, Fingers, and Thumb domains, and a functionally important tail for the assembly of the holo-enzyme at the replication fork.

DNA synthesis by DNA pols is catalyzed by two divalent metal ions, A and B (Steitz, 1999). Metal ion A generates the attacking hydroxyl anion of the 3′-nucleotide of the primer strand (*pt*O3′) as a general base, and metal ion B stabilizes the leaving pyrophosphate as an acid in the transition state (TS). Upon binding of correct incoming dNTPs, a large conformational change occurs to close down the fingers domain and to bury the reactants inside the pol for catalysis (Franklin et al., 2001). The apparent binding affinities for both Watson–Crick base-paired dNTPs and divalent metal ions are very high (apparent K_d ~50 μM) (Xia et al., 2013a). These apparent values are averaged from many conformational steps. Within the closed ternary complex, many additional hydrogen bonds (with residues of Arg482, Lys660, and Asn564) are formed that are not present in the initial binding of the dNTP in the open complex. Therefore, initial binding would be expected to be much weaker than the final binding step immediately before chemistry, implying that the actual binding affinity of the final substrate complex near the TS could be much higher than the measured average values. The assembly of the replication complex clearly involves many steps, not all of which have been fully characterized structurally, including the initial binding of the first divalent metal ion followed by the second metal ion which is dehydrated inside the closed complex because metal ion B has no water ligand in the final substrate complex. In this study, we capture two new intermediates in a single dimeric structure, one corresponding to an open complex with a vacant dNTP-binding site where the apparent binding affinity of the dNTP in this specific conformational state is likely to be very low, and the second corresponding to a one-metal ion bound closed ternary complex where the binding affinity of the second divalent metal ion should also be very low. Additional conformational changes are required to convert these low-affinity complexes to high-affinity states. Intermediate structures between the classic open binary complex and the fully closed ternary complex have already been reported for other DNA pols, for example, an "ajar" intermediate (Wu and Beese, 2011). Nevertheless, how these intermediates are correlated with the base selectivity of nucleotide incorporation by DNA pols remains poorly understood.

MATERIALS AND METHODS

Protein Overexpression and Purification

The exonuclease-deficient (*exo*$^-$ with the mutations of D222A and D327A) RB69pol variant gene was a gift from Professor William H. Konigsberg (Yale University, New Haven, CT, United States) and amplified by PCR using a 2,720 thermal cycler (Applied Biosystems). PCR was run in ThermoPol buffer (New England Biolabs) using *Pfu* DNA polymerase (New England Biolabs). The forward and reverse primers of RB69pol RB69pol (5′-CGC GGA TCC ATG AAA GAA TTT TAC TTA AC-3′ and 5′-CCG CTC GAG TCA AAA ATC GAA CAT ATC G-3′) were designed from the nucleotide sequences in GenBank, accession numbers AAP75958.1. The amplified genes and the modified pET28b expression vector were digested using BamHI and XhoI and then ligated into the expression vector, which was used to transform *Escherichia coli* strain BL21 (DE3). The transformed BL21 (DE3) cells were grown overnight at 37°C in 50 ml Luria-Bertani broth containing 50 μg/ml kanamycin (Duchefa Biochemie). Cells were resuspended in 4 L of the same media and grown at 37°C to an OD_{600} of 0.4–0.6. His_6-tagged recombinant protein was then induced using 0.5 mM isopropyl-β-D-thiogalactoside (Pharmacia) and incubated for 16 h at 20°C. After incubation, cells of 11.7 g were obtained, which contained the overexpressed RB69pol *exo*$^-$. Cells were resuspended in lysis buffer [50 mM sodium phosphate (pH 8.0), 300 mM NaCl, 5 mM imidazole, and 10% (*v*/*v*) glycerol]. The lysate was then produced using an ultrasonic processor (Sonics) and cleared by centrifugation at 1,593 *g* for 1 h. The His_6-tagged recombinant protein was purified with Ni-NTA chelating agarose resin (Peptron, Korea) by washing with lysis buffer and eluting with 50 mM sodium phosphate (pH 8.0), 300 mM NaCl, and 150 mM imidazole. Tobacco etch virus protease was added into the eluted protein and incubated for 12 h at 4°C to remove the N-terminal His_6-tag. The protein was further loaded onto a Superdex 200 16/60 column (GE Healthcare) that was pre-equilibrated in 10 mM Tris-HCl (pH 8.0), 50 mM NaCl, 5 mM dithiothreitol (DTT), and 5% glycerol. Fractions containing the RB69pol were pooled and concentrated to 25.8 mg/ml.

Crystallization

To form a 15-base paired P/T duplex, the primer (5′-GGAGCGGAC TGCTTAC-3′) and the template (5′-TCAAGTAAGCAGTCCGCT C-3′) were purchased (Cosmogenetech, Korea) and annealed after mixing in a 1:1 ratio. This P/T duplex was two base pairs longer than one used in an initial study of a single-pol replicating complex of RB69pol (Franklin et al., 2001). RB69pol was then mixed with the P/T duplex at a 1:1.2 stoichiometry to form the RB69pol-P/T complex in 10 mM Tris-HCl (pH 8.0), 50 mM NaCl, 10 mM $CaCl_2$, 5 mM dithiothreitol (DTT), and 5% glycerol, followed by the addition of 1 mM 2′-deoxyuridine-5'-(α,β-imido) triphosphate (dUpNpp, Jena Bioscience), which was a non-hydrolyzable analog of dTTP, for incubation for 12 h at 4°C. The formed complex was initially

TABLE 1 | Data processing and model refinement statistics (PDB ID 7f4y).

Data processing statistics	
X-ray source	PF-NW12A
Wavelength (Å)	1.0000
Space group	$P3_221$
Unit cell parameters	$a = b = 164.44$ Å, $c = 165.60$ Å, $\alpha = \beta = 90^\circ$, $\gamma = 120^\circ$
Resolution (Å)	65.41–2.20 (2.24–2.20)
Total partial observations	1,635,833
Unique reflections	130,936
Completeness (%)	100.0 (100.0)
R_{merge}[a]	0.13 (1.86)
R_{PIM}[b]	0.04 (0.56)
$CC_{1/2}$[c]	0.99 (0.54)
Multiplicity	12.4 (12.0)
$I/\sigma(I)$	11.2 (1.8)
Refinement statistics	
Resolution (Å)	50.–2.2
Overall R_{work} (%)	19.3
Overall R_{free} (%)[d]	24.5
R.M.S.D. from ideal geometry	
R.M.S.D. bond lengths (Å)	0.012
R.M.S.D. bond angles (°)	1.55
Mean B-factor (Å^2)	52.7
Ramachandran statistics	
Most favored (%)	95.2
Generously allowed (%)	4.8
Disallowed (%)	0.0

Values in parentheses are for the highest resolution shell. [a] $R_{merge} = \sum_{hkl} \sum_i |I_i(hkl) - \langle I(hkl)\rangle| / \sum_{hkl} \sum_i I_i(hkl)$, *where* $I_i(hkl)$ *is the intensity of the ith observation of reflection* hkl, *and* $\langle I(hkl)\rangle$ *is an average intensity of reflection (*hkl*).* [b] R_{PIM} *is redundancy-corrected merging R-factor.* [c] $CC_{1/2}$ *is Pearson correlation coefficient.* [d] R_{free} *calculated with 5% cross-validation set.*

screened for crystallization using the sitting-drop vapor-diffusion method in a 96-well INTELLI-PLATE (Art Robbins, Inc.). The final crystallization conditions were obtained *via* optimization from the initial crystallization setup performed using *Natrix* HT (Hampton Research). Crystals were grown at 21°C in 2 µl of the drop containing equal volumes of the protein/DNA solution and the reservoir solution, which was composed of 50 mM sodium cacodylate (pH 5.0), 2–7% (*v*/*v*) isopropanol, 5 mM $MgCl_2$, 2 mM NaCl, and 12 mM spermine. The crystals were cryo-protected by transferring them to the reservoir solution supplemented with 30% (*v*/*v*) polyethylene glycol 400 (PEG 400) and flash-frozen in liquid nitrogen for data collection.

Structure Determination

A complete data set was collected at a resolution of 2.2 Å at 100 K at BL-NW12A of the Photon Factory, Japan. Data were indexed and initially processed using the *HKL-2000* package (Otwinowski and Minor, 1997) and then reprocessed using *iMOSFLM* (Battye et al., 2011) and merged using *AIMLIESS* in the *CCP4i* package (Battye et al., 2011). The crystals of the RB69pol-P/T complexes belonged to the $P3_221$ space group and had the unit-cell dimensions of $a = b = 164.44$ Å, $c = 165.60$ Å, $\alpha = \beta = 90^\circ$, $\gamma = 120^\circ$. Assuming one dimeric RB69pol-P/T DNA complex molecule was in an asymmetric unit, the Matthews coefficient was 2.23 Å^3/Da, which corresponded to a solvent content of 45% (Matthews, 1968). Initial molecular replacement calculations were performed using *Phaser* in the *CCP4* suite (McCoy et al., 2007) using search models derived from the previously reported structure (PDB ID 3nci) after the P/T duplex, the C-terminal tail, and the Fingers domain were removed (Franklin et al., 2001). Afterward, the P/T duplex, the Fingers, the C-terminal tail, dUpNpp, and Ca^{2+} were manually built using *Coot* (Emsley et al., 2010), followed by automated water picking with *ARP/wARP* (Langer et al., 2008). Several steps of manual rebuilding and refinement of this structure were performed using *Coot* and *Refmac5* (Murshudov et al., 2011); the final crystallographic *R* value was 19.3% (R_{free} = 24.5%). The statistics for data collection and refinement are summarized in **Table 1**.

Structural Analysis

All structural figures were generated using *PyMOL* version 2.4.0 (Schrödinger LLC). Multiple sequence alignment (see Supporting Materials) was performed using *Clustal X* and visualized using *JalView* (Jeanmougin et al., 1998; Waterhouse et al., 2009). The σ_A-weighed $2F_o$-F_c map was calculated using *phenix.maps* and *phenix.mtz2map* in the CCP4 format (Liebschner et al., 2019). The *PDBePISA* web server was used for the interface analysis (Krissinel and Henrick, 2004).

RESULTS AND DISCUSSION

The Crystal Structure of the Two Polymerase Complexes From Bacteriophage RB69

We crystallized the exonuclease-deficient RB69pol complex with the P/T duplex and determined its structure at a resolution of 2.2 Å with a free R-factor of about 24.5% (PDB ID 7f4y) (**Table 1**). Two RB69pol-

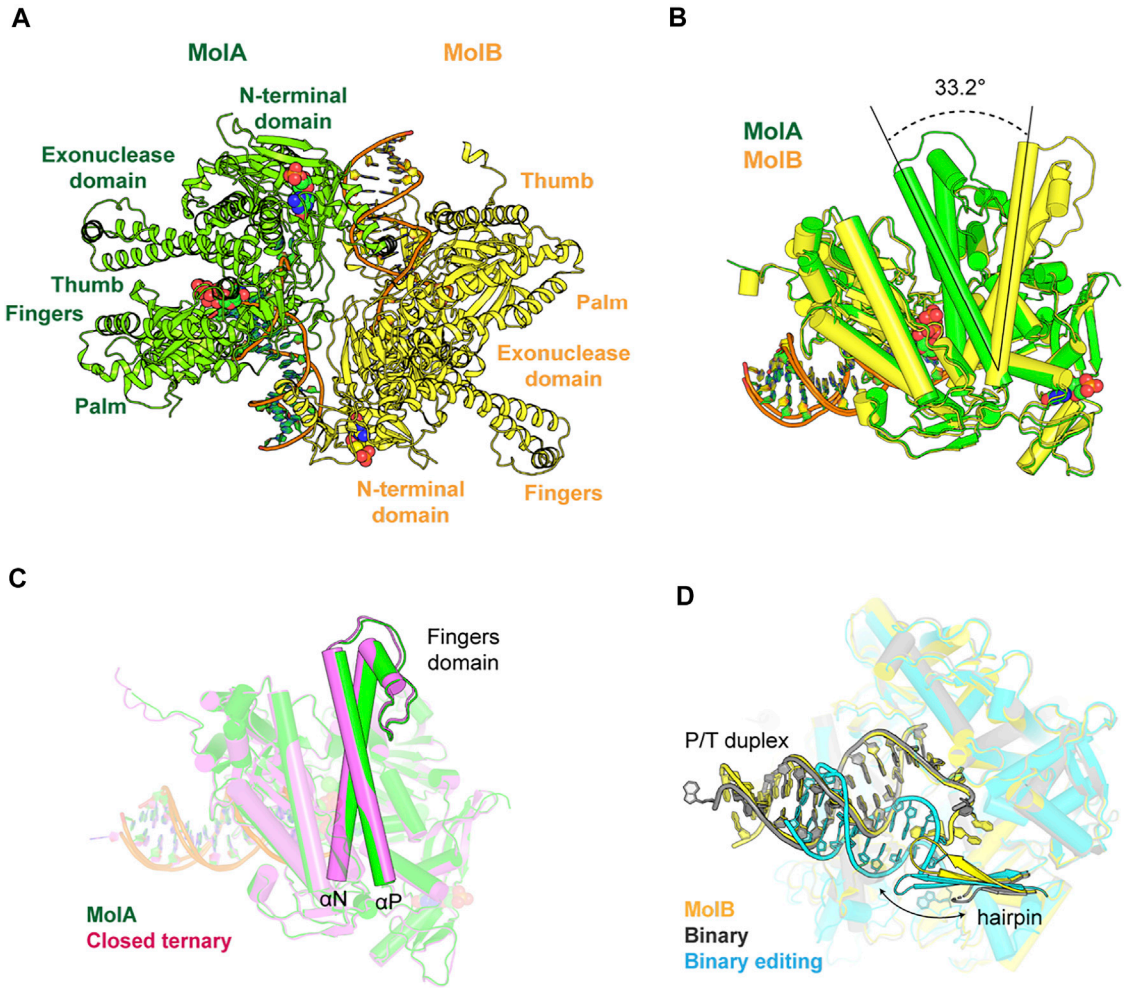

FIGURE 1 | Overall structure of RB69pol-DNA complexes. **(A)** Structures of the ternary complex (MolA, green) and the binary complex (MolB, yellow). Nucleotide molecules are shown as cartoons and spheres. **(B)** Superimposition of ternary and binary complexes and the conformational change of the Fingers domain is shown as the two-sided dashed line. **(C)** Same conformation of the Fingers domains of MolA (green) and a closed ternary complex reported previously (magenta, PDB ID 1ig9). **(D)** Different topologies of the P/T duplex and hairpins of MolB (yellow) and other binary complexes (PDB ID 3l8b, 1clq).

P/T complexes are present in one asymmetric unit (**Figure 1A**). The N-terminal domain (NTD) of RB69pol and the part of the P/T duplex away from the active site participate in the dimerization of the two complexes. One RB69pol-P/T complex (MolA) is identified as a new closed ternary complex with dUpNpp, which was similar to many other known ternary complexes of this enzyme. However, this complex contained only one divalent metal ion. The other complex (MolB) is identified as a new open binary RB69pol-P/T complex in the pre-insertion state but without dUpNpp bound and with a vacant dNTP-binding pocket. The major differences of the two complexes are rotations (approximately 33.2°) of the Fingers domain, as previously reported (**Figure 1B**) (Franklin et al., 2001).

A New Closed Ternary Complex With Single Divalent Metal Ion Bound

In the MolA structure, the nascent Watson–Crick base pair dA/dUpNpp was well defined in electron density maps, as were all the 5' overhanging nucleotide residues of the template strand (**Figure 2A**). The conformation of the Fingers domain in this structure was essentially the same as the one in the closed ternary complex reported previously with a root mean square deviation of 0.34 Å for all Cα coordinates (**Figure 1C**) (Franklin et al., 2001), representing a closed ternary complex before chemistry. Although the crystals were grown in the presence of 10 mM $CaCl_2$, the standard cryoprotectant solution commonly used for the RB69pol-P/T complex crystals replaced 10 mM Ca^{2+} ions with 5 mM Mg^{2+} ions, which could eliminate any weakly bound divalent metal ion. Indeed, we observed that it had only a single Ca^{2+} ion bound at the B site but no Ca^{2+} ion at the A site. Thus, there was a significant difference between this complex and the previously reported structures that often contained two catalytic divalent metal ions at both the B and A sites (Franklin et al., 2001; Xia et al., 2012a; Xia et al., 2013a). This observation suggests that the binding affinity of the divalent metal ion at the A site should be much weaker in this specific conformation than the affinity

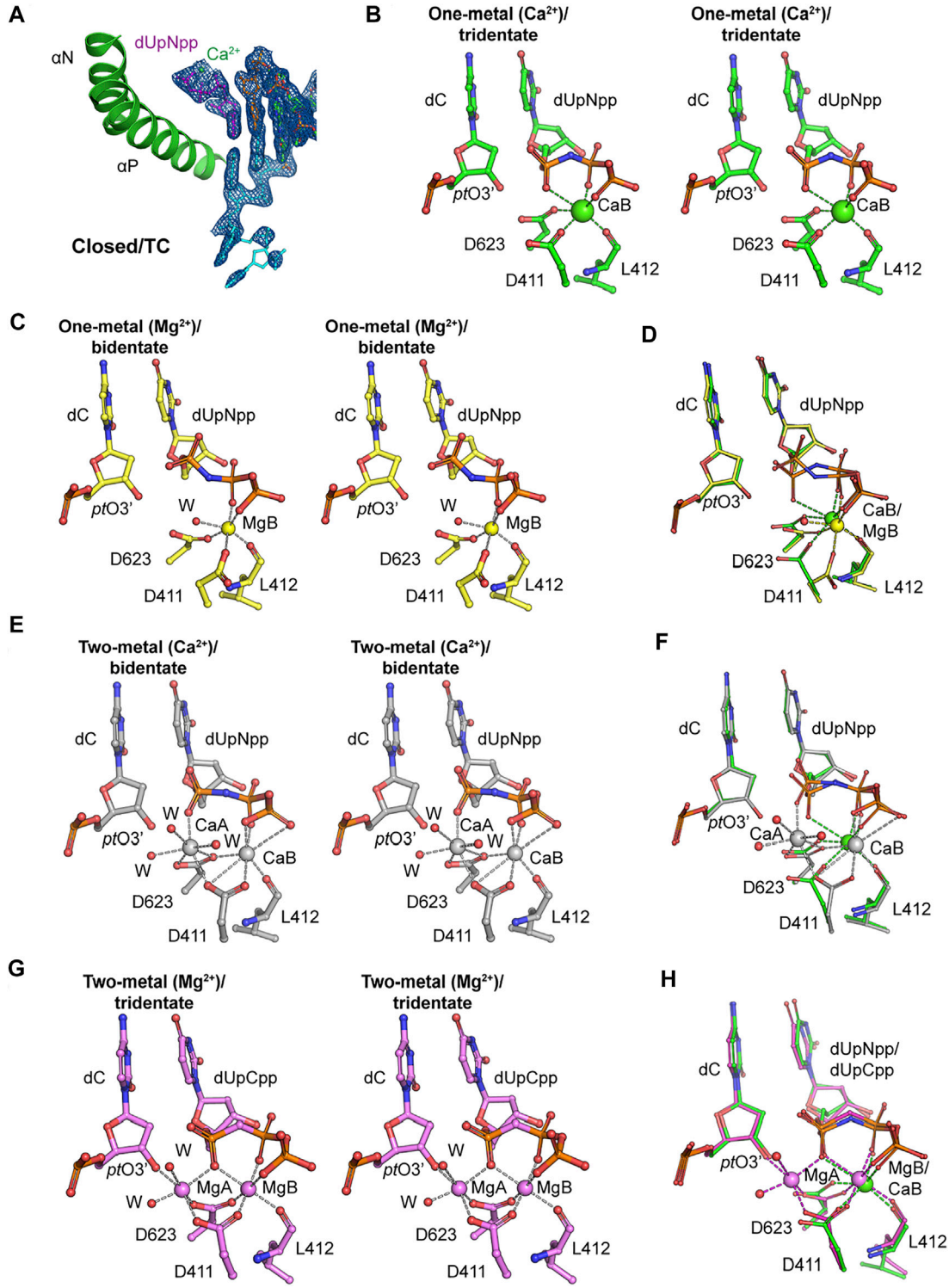

FIGURE 2 | Metal coordination in the closed ternary complexes. **(A)** Closed ternary complex (MolA) containing one divalent metal ion bound to the triphosphate moiety instead of the two observed previously. Incoming dNTP (dUpNpp), primer, and template are in magenta, orange, and cyan, respectively. The σ_A-weighted $2F_{obs}$-F_{calc} electron density maps are contoured at 1.5 σ. **(B)** Stereodiagram of tridentate Ca^{2+} coordination in the one–metal ion replication complex (MolA) with octahedral geometry. The Ca^{2+} ion is in green, and Ca^{2+} coordination is marked with dashed lines. **(C)** Stereodiagram of bidentate Mg^{2+} coordination in the one–metal ion replication complex (PDB ID 3si6) with octahedral geometry. The Mg^{2+} ion is in yellow, and Mg^{2+} coordination is marked with dashed lines. **(D)** Superimposed representation of Ca^{2+} or Mg^{2+} coordination complexes of the one–metal ion with tridentate coordination (MolA, green) and with bidentate coordination (yellow). The

(*Continued*)

FIGURE 2 | metal coordination is in green or yellow in tridentate or bidentate coordination complexes, respectively. **(E)** Stereodiagram of bidentate Ca^{2+} coordination in the two–metal ion replication complex (PDB ID 3uiq) with pentagonal bipyramidal geometries for sites A (CaA) and B (CaB), and CaA does not bind to *pt* O 3'. Ca^{2+} ions and water molecules are in gray and red, respectively. **(F)** Superimposed representation of Ca^{2+} coordination complexes of the one–metal ion with tridentate coordination (MolA, green) and two–metal ion with bidentate coordination (gray). The Ca^{2+} coordination is in green or gray in one–metal ion or two–metal ion replication complexes, respectively. **(G)** Stereodiagram of tridentate Mg^{2+} coordination in the two–metal ion replication complex (PDB ID 3spy) with octahedral geometries for sites A (MgA) and B (MgB), and the MgA interacts with *pt* O 3'. Mg^{2+} ions and water molecules are in magenta and red, respectively. **(H)** Superimposed representation of metal coordination complexes of a Ca^{2+}-bound one–metal ion with tridentate coordination (MolA, green) and Mg^{2+} bound two–metal ion with bidentate coordination (magenta). The metal coordination is in green or magenta in Ca^{2+}-bound one–metal ion or Mg^{2+}-bound two–metal ion replication complexes, respectively.

observed in the previous monomeric RB69pol-P/T complex and the measured average value in steady-state kinetics (Xia et al., 2013a).

This structure adds to a new variation on the closed ternary complexes of RB69pol with respect to both the number of divalent metal ions and the conformations of the triphosphate moiety of incoming dNTP. Similar to the classic ternary complex, the B site in MolA of this structure was coordinated by the catalytic carboxylates Asp411 and Asp623 and by the backbone carbonyl of Leu412; in turn, it binds the triphosphate moiety of incoming dNTP with α,β,γ-tridentate coordination (**Figure 2B**). Previously, a single Mg^{2+} ion bound in the closed ternary complex at the B site was reported, which forms a β,γ-bidentate coordination (**Figure 2C**) (PDB ID 3si6) (Xia et al., 2011a). Comparison of these two structures suggests that a conversion of the bidentate to tridentate coordination is likely to be a necessary step because Mg^{2+} ions can typically neutralize only two negative charges of two phosphate groups by forming only the bidentate coordination of the triphosphate moiety of a free dNTP in solution, but not with three phosphates simultaneously (**Figure 2D**). This conversion requires complete dehydration of the B metal ion so that it can be fully buried inside the complex. When the non-exchangeable Rh^{3+}/dNTP complex was used in kinetical studies, this step would be kinetically invisible because these studies revealed only the kinetic properties of the binding of the A metal ion (Bakhtina et al., 2005; Lee et al., 2009; Wang et al., 2009).

Another conformation of β,γ,-bidentate Ca^{2+} coordination was observed previously in an RB69pol ternary complex (**Figure 2E**) (PDB ID 3uiq) (Xia et al., 2012b). However, that complex had two Ca^{2+} ions bound, one at each of the B and A metal ions (**Figures 2E,F**). Therefore, the order of the bidentate-to-tridentate conversion and the binding of metal ion A (the second site) may be stochastically independent processes, providing a mechanism of allostery and regulation of binding affinities on the kinetic pathway of dNMP incorporation. Both processes should be essential for catalysis because with β,γ,-bidentate coordination to metal ion B (the first site), the α-phosphate of the triphosphate moiety of the incoming dNTP would be free to move in an arc, and because without the binding of metal ion A, the 3′-hydroxyl of the terminal nucleotide of the primer strand (*pt*O3′) could not be brought close enough to the freely moving α-phosphate of the dNTP. In the catalytically competent complex of RB69pol (Xia et al., 2011a), metal ion A binds both the α-phosphate of dNTP and the *pt*O3', bringing them closer together for chemistry (**Figure 2G**) (PDB ID 3spy) (Xia et al., 2011a).

Without considering the stochastic kinetic schemes discussed above, kinetic studies may not be sufficient to explain the kinetic behaviors of nucleotide selectivity for dNMP incorporation by DNA pols. In fact, allosteric regulation of binding affinities of metal ions in the two metal-ion sites and the conformational changes associated may play important roles in base selectivity. With the correct incoming dNTP, these two processes are likely to be highly cooperative, that is, the binding of the second divalent metal ion could accelerate the bidentate-to-tridentate conversion of the triphosphate moiety of the incoming dNTP. Simultaneously, this conversion could also stabilize the binding of the second divalent metal ion. However, with an incorrect incoming dNTP, these two processes may not be cooperative, that is, the binding of the second divalent metal ion may prevent the bidentate-to-tridentate conversion by transiently stabilizing the bidentate conformation of the incorrect dNTP, which would eventually be rejected. Simultaneously, the bidentate-to-tridentate conversion may destabilize the binding of the second divalent metal ion because distorted Watson–Crick base-pairing geometry could prevent the tridentate moiety from properly fitting into its putative binding pocket when both metal ions are present. Without both metal ions, chemistry cannot occur, and the incorrect dNTP would eventually be rejected. Based on this analysis, we conclude that our new closed ternary complex of MolA is not the catalytically competent complex but rather a complex on its way to formation of the pre-chemistry ternary complex immediately before catalysis (**Figure 2H**).

New Open Binary Complex

In the open binary complex of MolB, the penultimate base pair was also well defined in electron density maps alongside all the 5' overhanging nucleotide residues of the template strand (**Figure 3A**). In this binary complex, the P/T duplex was completely superimposable with the closed ternary complex, representing a pre-insertion complex where the nascent base pair–binding pocket was partially formed and ready for binding of the next incoming dNTP. However, the next templating base was well ordered but remained in a non-stacking geometry with the proceeding base pair. The base of this nucleotide formed hydrogen bond interactions with the enzyme through ordered water molecules and remained highly hydrated, as seen in **Supplementary Figure S1**.

This open complex differed from all the previously reported binary complexes that had non–Watson–Crick geometry for the nascent base pair or non-stackable templating nucleotide residues (**Figure 1D**) (Shamoo and Steitz, 1999; Aller et al., 2010). It also differed from the conformation of the apo structure (PDB ID 1ih7) (Franklin et al., 2001). In this binary complex, there was only one ordered water molecule placed between the Asn564 and the Tyr567 backbone in the kinked

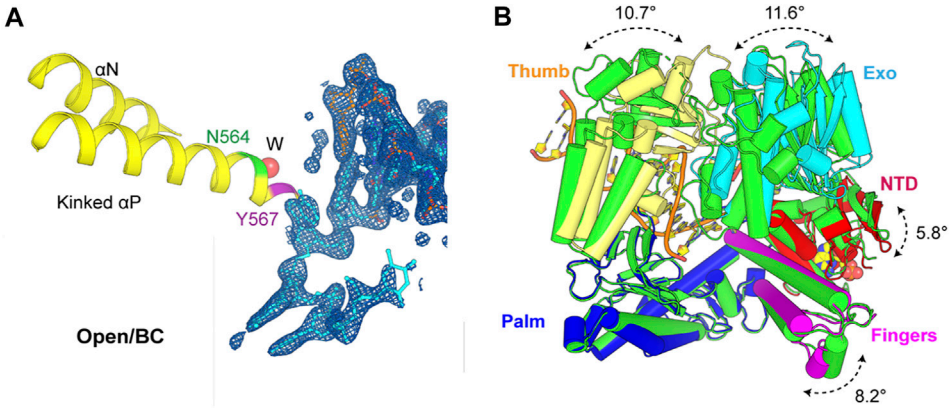

FIGURE 3 | Active site of the open binary complex (MolB) and overall structure comparison with apo structure reported previously. **(A)** Open binary complex (MolB) containing a vacant dNTP-binding site with one ordered water molecule (W) inserted into the backbone of the kinked helix *p* instead of the two observed in the apo structure. Asn564 and Tyr567 are in green and magenta, respectively. The $2F_{obs}$-F_{calc} electron density maps are contoured at 1.5 σ. **(B)** Exo (cyan), Thumb (yellow), Fingers (magenta), and NT (red) domains rotate relative to the Palm (blue) domain from this binary complex compared to the apo (green) structure by 11.6°, 10.7°, 8.2°, and 5.8°, respectively.

helix *p*, whereas there were two ordered water molecules observed in the open conformation of the apo form. The Exo, Thumb, Fingers, and N-terminal domains (NTD) rotated relative to the Palm domain from this binary complex compared to the apo structure by 11.6°, 10.7°, 8.2°, and 5.8°, respectively (**Figure 3B**). Collectively, the open binary complex showed not only a difference in the rotation of the Fingers domain but also in the rotation of the template base opposite the incoming dNTP compared to the closed ternary complex. This new open complex adopted a pre-insertion form, which was not observed previously.

Unique Nucleotide Binding Pocket and Conformational Change by GMP at the N-Terminal Domains

There was a conserved small cavity in the NTDs of each RB69pol that tightly bound GMP (**Figure 4**). The surface area buried between the bound GMP and RB69pol was ~331 Å^2. This binding involved eight hydrogen bonds with the Tyr49/Asp95 side chains and the backbones of Met85/Lys378/Ile380 and one salt-bridge interaction with the Lys48 side chains. This nucleotide most likely came from copurification because it was never added during purification.

The binding of GMP at this location was also observed previously in the apo structure of RB69pol and the key interaction pattern was conserved with those of our new structure, but it was not present in the isolated NTD/Exo domain structure of T4 DNA polymerase (T4pol) (Wang et al., 1997; Wang et al., 1996). In all previous P/T ternary complexes of RB69pol, this pocket was occupied by the overhanging 5′-dG template nucleotide of a neighboring molecule (**Supplementary Figure S2**) (Franklin et al., 2001; Aller et al., 2007). Comparison of the RB69pol/T4pol structures with and without GMP (namely, in the truncated T4 exonuclease domain) revealed a large GMP-dependent NTD conformational change, including the re-orientation of helix αA by 90° (**Supplementary Figure S3**).

GMP-Dependent Conformations of N-Terminal Domains for Formation of the Two-P/T Two-Pol Complex

Each NTD of two RB69pol molecules interacted with the part of the P/T duplex away from the pol active site (**Figure 5**). This interaction included the Asp13, Arg66, Lys73, and Lys247 side chains. Among them, Arg66 was highly conserved and protruded into the minor groove of the P/T duplex bound in the second opposing RB69pol complex within the dimer (**Supplementary Figure S4**). As the two complexes were in two different conformations, inter-complex interactions were also slightly different in interface areas buried between the NTD of MolA and the P/T duplex of MolB (385.5 Å^2) and between the NTD of MolB and the P/T duplex of MolA (291.6 Å^2). It appears that the interactions of the closed RB69pol with the P/T duplex of the open complex were stronger than those of the open RB69pol with the P/T duplex of the closed RB69pol complex (**Figures 5A,B**).

Given the observation that the conformation of the NTD was GMP-dependent, we investigated how this might affect the formation of the dimeric complex. Using computer modeling, we observed that only the GMP-bound conformation could form this dimer and that the conformation of the NTD without GMP could result in severe stereochemical clashes in this dimer (**Supplementary Figure S3**). Interestingly, the RB69pol NTD had the common βαββαβ topology found in many oligonucleotide-binding and RNA-binding proteins (Burd and Dreyfuss, 1994; Liu et al., 2006). Assembly and disassembly of a minimal replication complex containing both leading and lagging replication complexes were extensively studied in the T4 system, including the use of the two-hybrid system (Salinas and Benkovic, 2000; Benkovic and Spiering, 2017). Given the sequence identity of 61% between RB69pol and T4pol, it is likely that the

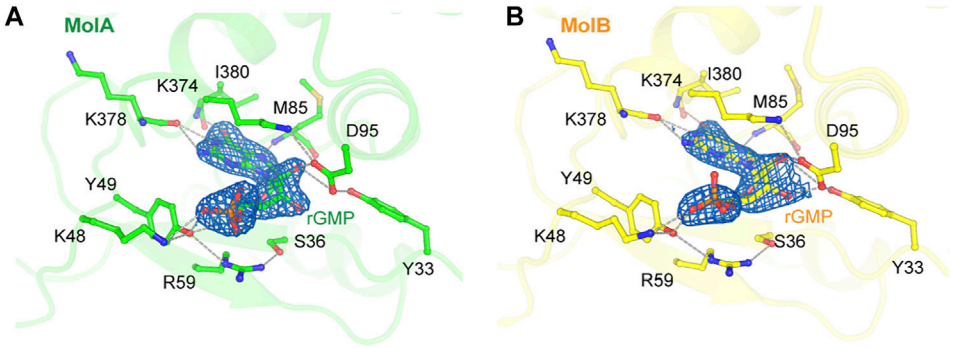

FIGURE 4 | Nucleotide binding site in the N-terminal domains of MolA **(A)** and MolB **(B)**. The σ_A-weighted $2F_{obs}$-F_{calc} electron density maps are contoured at 1.5 σ. Hydrogen bonds are displayed as dashed lines.

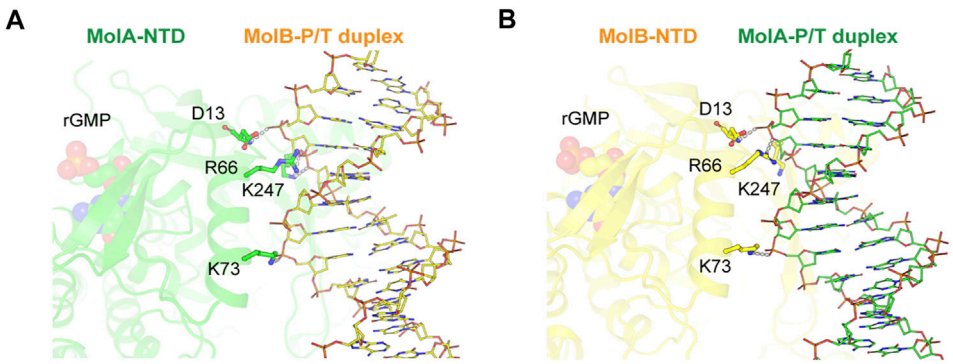

FIGURE 5 | Inter-complex interaction between ternary (MolA, green) and binary (MolB, yellow) complexes. Detailed views of interactions for the NTD (MolA) with the P/T duplex (MolB) **(A)** and the NTD (MolB) with the P/T duplex (MolA) **(B)** complexes. Nucleotides (rGMP) bound to the N-terminal domain and DNA helices are shown as spheres and sticks, respectively. Hydrogen bonds between the N-terminal domain in one subunit and the DNA strand in the other subunit are displayed as dashed lines.

dimerization observed here is relevant in both systems, but how it is controlled by the binding and release of GMP in this pocket requires additional studies.

Implications of New Conformations on the Dynamics of DNA Pols and on Base Selectivity

It was unexpected that a partially open P/T complex of RB69pol was captured under the conditions favorable for formation of the closed replication complex. On the other hand, the lengths of the P/T duplex used in earlier studies were too short, so they may have precluded the formation of this dimeric complex. In fact, the optimized length of the P/T duplex used in kinetic studies and then in earlier crystallization attempts consisted of 13 base pairs because longer P/T duplexes gave complex kinetic results, likely involving two DNA pol complexes binding at both ends of the same DNA duplex (Franklin et al., 2001). Therefore, the dimeric complex with the longer 16-base pair P/T duplex reported here might be more biologically relevant. The structures of both conformations simultaneously captured in our dimeric complex represent the new stable intermediates that were not previously known, and they are clearly involved in forming the catalytically competent complex (**Supplementary Figure S5**). Our observation also indicated that the fractions of these two conformations of P/T complexes in the population in solution were significant and that they should have similar free energies. Our findings remind us of the fact that other stable intermediates may also exist but remain hidden from us but may be kinetically important for base selectivity.

Our new partially open complex provides new insights into the initial steps in the assembly of the replication complex (**Supplementary Figure S5**). An initial Watson–Crick base pair is formed between the templating base and the incoming dNTP while the templating nucleobase remains partially hydrated and the Fingers domain remains open and is gradually converted to the partially closed state. Continuous closing of the Fingers domain requires cooperation of binding of two divalent metal ions as discussed above. Simultaneously, dehydration of the nascent base pair occurred alongside closing motions of RB69pol and stacking interactions of base pairs. With the correct incoming dNTP, this process

can be cooperatively completed. However, with an incorrect incoming dNTP, full dehydration of the incorrect base pair would be blocked and the binding of two divalent metal ions cannot be accomplished. As a result, an incorrect dNTP would be rejected.

DATA AVAILABILITY STATEMENT

The dataset presented in in this study can be found in online repository RCSB PDB with the accession number 7f4y (https://www.rcsb.org/structure/7F4Y).

AUTHOR CONTRIBUTIONS

H-SY and JP have done crystallographic analysis. H-SY and JP prepared the figures. JYA and YL have done biochemical analysis. JW and SHE designed experiments and have done some crystallographic analysis and wrote the article with input from H-SY and JP.

ACKNOWLEDGMENTS

This work was partially supported by the "GIST Research Institute (GRI) IIBR" grant funded by GIST in 2021 and the National Research Foundation (NRF) of the Korean government (NRF-2021R1A2C1006267). The X-ray diffraction data and coordinates for the two-pol complex structure are available from the PDB (PDB ID 7f4y). The authors thank the late Professor T. A. Steitz for advice and suggestions during the course of this study and Professor W. H. Konigsberg for plasmid gifts and comments on this manuscript. The authors also thank the staff at beamlines NW-12A of the Photon Factory (Tsukuba, Japan) for their kind help with data collection.

SUPPLEMENTARY MATERIAL

The Supplementary Material for this article can be found online at: https://www.frontiersin.org/articles/10.3389/fmolb.2021.704813/full#supplementary-material

REFERENCES

Alberts, B. M., Barry, J., Bedinger, P., Formosa, T., Jongeneel, C. V., and Kreuzer, K. N. (1983). Studies on DNA Replication in the Bacteriophage T4 a--.Gif System. *Cold Spring Harbor Symp. Quant. Biol.* 47, 655–668. doi:10.1101/sqb.1983.047.01.077

Alberts, B. (2003). DNA Replication and Recombination. *Nature* 421, 431–435. doi:10.1038/nature01407

Aller, P., Rould, M. A., Hogg, M., Wallace, S. S., and Doublié, S. (2007). A Structural Rationale for Stalling of a Replicative DNA Polymerase at the Most Common Oxidative Thymine Lesion, Thymine Glycol. *Pnas* 104, 814–818. doi:10.1073/pnas.0606648104

Aller, P., Ye, Y., Wallace, S. S., Burrows, C. J., and Doublié, S. (2010). Crystal Structure of a Replicative DNA Polymerase Bound to the Oxidized Guanine Lesion Guanidinohydantoin ,. *Biochemistry* 49, 2502–2509. doi:10.1021/bi902195p

Aller, P., Duclos, S., Wallace, S. S., and Doublié, S. (2011). A Crystallographic Study of the Role of Sequence Context in Thymine Glycol Bypass by a Replicative DNA Polymerase Serendipitously Sheds Light on the Exonuclease Complex. *J. Mol. Biol.* 412, 22–34. doi:10.1016/j.jmb.2011.07.007

Bakhtina, M., Lee, S., Wang, Y., Dunlap, C., Lamarche, B., and Tsai, M.-D. (2005). Use of Viscogens, dNTPαS, and Rhodium(III) as Probes in Stopped-Flow Experiments to Obtain New Evidence for the Mechanism of Catalysis by DNA Polymerase β,. *Biochemistry* 44, 5177–5187. doi:10.1021/bi047664w

Battye, T. G. G., Kontogiannis, L., Johnson, O., Powell, H. R., and Leslie, A. G. W. (2011). iMOSFLM: a New Graphical Interface for Diffraction-Image Processing withMOSFLM. *Acta Crystallogr. D Biol. Cryst.* 67, 271–281. doi:10.1107/s0907444910048675

Benkovic, S. J., and Spiering, M. M. (2017). Understanding DNA Replication by the Bacteriophage T4 Replisome. *J. Biol. Chem.* 292, 18434–18442. doi:10.1074/jbc.r117.811208

Berman, A. J., Kamtekar, S., Goodman, J. L., Lázaro, J. M., de Vega, M., Blanco, L., et al. (2007). Structures of Phi29 DNA Polymerase Complexed with Substrate: the Mechanism of Translocation in B-Family Polymerases. *EMBO J.* 26, 3494–3505. doi:10.1038/sj.emboj.7601780

Burd, C., and Dreyfuss, G. (1994). Conserved Structures and Diversity of Functions of RNA-Binding Proteins. *Science* 265, 615–621. doi:10.1126/science.8036511

Emsley, P., Lohkamp, B., Scott, W. G., and Cowtan, K. (2010). Features and Development ofCoot. *Acta Crystallogr. D Biol. Cryst.* 66, 486–501. doi:10.1107/s0907444910007493

Franklin, M. C., Wang, J., and Steitz, T. A. (2001). Structure of the Replicating Complex of a Pol α Family DNA Polymerase. *Cell* 105, 657–667. doi:10.1016/s0092-8674(01)00367-1

Hamdan, S. M., Loparo, J. J., Takahashi, M., Richardson, C. C., and van Oijen, A. M. (2009). Dynamics of DNA Replication Loops Reveal Temporal Control of Lagging-Strand Synthesis. *Nature* 457, 336–339. doi:10.1038/nature07512

Hogg, M., Wallace, S. S., and Doublié, S. (2004). Crystallographic Snapshots of a Replicative DNA Polymerase Encountering an Abasic Site. *EMBO J.* 23, 1483–1493. doi:10.1038/sj.emboj.7600150

Hogg, M., Aller, P., Konigsberg, W., Wallace, S. S., and Doublié, S. (2007). Structural and Biochemical Investigation of the Role in Proofreading of a β Hairpin Loop Found in the Exonuclease Domain of a Replicative DNA Polymerase of the B Family. *J. Biol. Chem.* 282, 1432–1444. doi:10.1074/jbc.m605675200

Hogg, M., Rudnicki, J., Midkiff, J., Reha-Krantz, L., Doublié, S., and Wallace, S. S. (2010). Kinetics of Mismatch Formation Opposite Lesions by the Replicative DNA Polymerase from Bacteriophage RB69. *Biochemistry* 49, 2317–2325. doi:10.1021/bi901488d

Jeanmougin, F., Thompson, J. D., Gouy, M., Higgins, D. G., and Gibson, T. J. (1998). Multiple Sequence Alignment with Clustal X. *Trends Biochem. Sci.* 23, 403–405. doi:10.1016/s0968-0004(98)01285-7

Krissinel, E., and Henrick, K. (2004). Secondary-structure Matching (SSM), a New Tool for Fast Protein Structure Alignment in Three Dimensions. *Acta Crystallogr. D Biol. Cryst.* 60, 2256–2268. doi:10.1107/s0907444904026460

Langer, G., Cohen, S. X., Lamzin, V. S., and Perrakis, A. (2008). Automated Macromolecular Model Building for X-ray Crystallography Using ARP/wARP Version 7. *Nat. Protoc.* 3, 1171–1179. doi:10.1038/nprot.2008.91

Lee, H. R., Wang, M., and Konigsberg, W. (2009). The Reopening Rate of the Fingers Domain Is a Determinant of Base Selectivity for RB69 DNA Polymerase. *Biochemistry* 48, 2087–2098. doi:10.1021/bi8016284

Liebschner, D., Afonine, P. V., Baker, M. L., Bunkóczi, G., Chen, V. B., Croll, T. I., et al. (2019). Macromolecular Structure Determination Using X-Rays, Neutrons and Electrons: Recent Developments in Phenix. *Acta Cryst. Sect D Struct. Biol.* 75, 861–877. doi:10.1107/s2059798319011471

Liu, S., Knafels, J. D., Chang, J. S., Waszak, G. A., Baldwin, E. T., Deibel, M. R., Jr., et al. (2006). Crystal Structure of the Herpes Simplex Virus 1 DNA Polymerase. *J. Biol. Chem.* 281, 18193–18200. doi:10.1074/jbc.m602414200

Matthews, B. W. (1968). Solvent Content of Protein Crystals. *J. Mol. Biol.* 33, 491–497. doi:10.1016/0022-2836(68)90205-2

McCoy, A. J., Grosse-Kunstleve, R. W., Adams, P. D., Winn, M. D., Storoni, L. C., and Read, R. J. (2007). Phasercrystallographic Software. *J. Appl. Cryst.* 40, 658–674. doi:10.1107/s0021889807021206

Murshudov, G. N., Skubák, P., Lebedev, A. A., Pannu, N. S., Steiner, R. A., Nicholls, R. A., et al. (2011). REFMAC5 for the Refinement of Macromolecular crystal Structures. *Acta Crystallogr. D Biol. Cryst.* 67, 355–367. doi:10.1107/s0907444911001314

Noble, E., Spiering, M., and Benkovic, S. (2015). Coordinated DNA Replication by the Bacteriophage T4 Replisome. *Viruses* 7, 3186–3200. doi:10.3390/v7062766

Otwinowski, Z., and Minor, W. (1997). [20] Processing of X-ray Diffraction Data Collected in Oscillation Mode. *Methods Enzymol.* 276, 307–326. doi:10.1016/s0076-6879(97)76066-x

Salinas, F., and Benkovic, S. J. (2000). Characterization of Bacteriophage T4-Coordinated Leading- and Lagging-Strand Synthesis on a Minicircle Substrate. *Proc. Natl. Acad. Sci.* 97, 7196–7201. doi:10.1073/pnas.97.13.7196

Shamoo, Y., and Steitz, T. A. (1999). Building a Replisome from Interacting Pieces. *Cell* 99, 155–166. doi:10.1016/s0092-8674(00)81647-5

Steitz, T. A. (1999). DNA Polymerases: Structural Diversity and Common Mechanisms. *J. Biol. Chem.* 274, 17395–17398. doi:10.1074/jbc.274.25.17395

Wang, J., Yu, P., Lin, T. C., Konigsberg, W. H., and Steitz, T. A. (1996). Crystal Structures of an NH2-terminal Fragment of T4 DNA Polymerase and its Complexes with Single-Stranded DNA and with Divalent Metal Ions. *Biochemistry* 35, 8110–8119. doi:10.1021/bi960178r

Wang, J., Sattar, A. K. M. A., Wang, C. C., Karam, J. D., Konigsberg, W. H., and Steitz, T. A. (1997). Crystal Structure of a Pol α Family Replication DNA Polymerase from Bacteriophage RB69. *Cell* 89, 1087–1099. doi:10.1016/s0092-8674(00)80296-2

Wang, M., Lee, H. R., and Konigsberg, W. (2009). Effect of A and B Metal Ion Site Occupancy on Conformational Changes in an RB69 DNA Polymerase Ternary Complex. *Biochemistry* 48, 2075–2086. doi:10.1021/bi801627h

Waterhouse, A. M., Procter, J. B., Martin, D. M. A., Clamp, M., and Barton, G. J. (2009). Jalview Version 2--a Multiple Sequence Alignment Editor and Analysis Workbench. *Bioinformatics* 25, 1189–1191. doi:10.1093/bioinformatics/btp033

Wu, E. Y., and Beese, L. S. (2011). The Structure of a High Fidelity DNA Polymerase Bound to a Mismatched Nucleotide Reveals an "ajar" Intermediate Conformation in the Nucleotide Selection Mechanism. *J. Biol. Chem.* 286, 19758–19767. doi:10.1074/jbc.m110.191130

Xia, S., Wang, M., Blaha, G., Konigsberg, W. H., and Wang, J. (2011a). Structural Insights into Complete Metal Ion Coordination from Ternary Complexes of B Family RB69 DNA Polymerase. *Biochemistry* 50, 9114–9124. doi:10.1021/bi201260h

Xia, S., Wang, M., Lee, H. R., Sinha, A., Blaha, G., Christian, T., et al. (2011b). Variation in Mutation Rates Caused by RB69pol Fidelity Mutants Can Be Rationalized on the Basis of Their Kinetic Behavior and crystal Structures. *J. Mol. Biol.* 406, 558–570. doi:10.1016/j.jmb.2010.12.033

Xia, S., Christian, T. D., Wang, J., and Konigsberg, W. H. (2012a). Probing Minor Groove Hydrogen Bonding Interactions between RB69 DNA Polymerase and DNA. *Biochemistry* 51, 4343–4353. doi:10.1021/bi300416z

Xia, S., Eom, S. H., Konigsberg, W. H., and Wang, J. (2012b). Bidentate and Tridentate Metal-Ion Coordination States within Ternary Complexes of RB69 DNA Polymerase. *Protein Sci.* 21, 447–451. doi:10.1002/pro.2026

Xia, S., Wang, J., and Konigsberg, W. H. (2013a). DNA Mismatch Synthesis Complexes Provide Insights into Base Selectivity of a B Family DNA Polymerase. *J. Am. Chem. Soc.* 135, 193–202. doi:10.1021/ja3079048

Xia, S., Wood, M., Bradley, M. J., De La Cruz, E. M., and Konigsberg, W. H. (2013b). Alteration in the Cavity Size Adjacent to the Active Site of RB69 DNA Polymerase Changes its Conformational Dynamics. *Nucleic Acids Res.* 41, 9077–9089. doi:10.1093/nar/gkt674

Yao, N. Y., and O'Donnell, M. (2008). Replisome Dynamics and Use of DNA Trombone Loops to Bypass Replication Blocks. *Mol. Biosyst.* 4, 1075–1084. doi:10.1039/b811097b

Zahn, K. E., Belrhali, H., Wallace, S. S., and Doublié, S. (2007). Caught Bending the A-Rule: crystal Structures of Translesion DNA Synthesis with a Non-natural Nucleotide. *Biochemistry* 46, 10551–10561. doi:10.1021/bi7008807

Zahn, K. E., Averill, A., Wallace, S. S., and Doublié, S. (2011a). The Miscoding Potential of 5-hydroxycytosine Arises Due to Template Instability in the Replicative Polymerase Active Site. *Biochemistry* 50, 10350–10358. doi:10.1021/bi201219s

Zahn, K. E., Tchesnokov, E. P., Götte, M., and Doublié, S. (2011b). Phosphonoformic Acid Inhibits Viral Replication by Trapping the Closed Form of the DNA Polymerase. *J. Biol. Chem.* 286, 25246–25255. doi:10.1074/jbc.m111.248864

Conflict of Interest: H-SY was employed by Daesang Corporation. JYA was employed by Virocure Inc.

The remaining authors declare that the research was conducted in the absence of any commercial or financial relationships that could be construed as a potential conflict of interest.

Publisher's Note: All claims expressed in this article are solely those of the authors and do not necessarily represent those of their affiliated organizations, or those of the publisher, the editors, and the reviewers. Any product that may be evaluated in this article, or claim that may be made by its manufacturer, is not guaranteed or endorsed by the publisher.

Advantages of publishing in Frontiers

OPEN ACCESS
Articles are free to read for greatest visibility and readership

FAST PUBLICATION
Around 90 days from submission to decision

HIGH QUALITY PEER-REVIEW
Rigorous, collaborative, and constructive peer-review

TRANSPARENT PEER-REVIEW
Editors and reviewers acknowledged by name on published articles

Frontiers
Avenue du Tribunal-Fédéral 34
1005 Lausanne | Switzerland

Visit us: www.frontiersin.org
Contact us: frontiersin.org/about/contact

REPRODUCIBILITY OF RESEARCH
Support open data and methods to enhance research reproducibility

DIGITAL PUBLISHING
Articles designed for optimal readership across devices

FOLLOW US
@frontiersin

IMPACT METRICS
Advanced article metrics track visibility across digital media

EXTENSIVE PROMOTION
Marketing and promotion of impactful research

LOOP RESEARCH NETWORK
Our network increases your article's readership